SCIENCE OF CLIMATE CHANGE

Volume 6.1
2026

https://scienceofclimatechange.org

Published by: SCC Publishing (Org. no. 935 567 653)

ISSN 2703-9080 (print)   ISNN 2703-9072 (online)

Science of Climate Change (SCC)

AN OPEN ACCESS JOURNAL

Advancing scientific understanding of the Earth's climate system and its governing processes through rigorous research and open scientific dialogue.

OPEN ACCESS
All published content is freely accessible worldwide immediately upon publication — no subscription barriers.

PEER REVIEWED
Rigorous and constructive peer review by experts ensures high scientific standards.

INDEPENDENT
Editorial independence and a commitment to open scientific inquiry and debate.

NOT-FOR-PROFIT
Operated under a not-for-profit framework supported by moderate article processing charges.

A BROAD AND INTEGRATED SCOPE

SCC welcomes contributions from a wide range of climate-related disciplines, including:

Atmospheric Sciences and Climate Dynamics
Radiative transfer, circulation, clouds, aerosols, and atmospheric variability.

Solar and Astronomical Influences on Climate
Solar variability, solar–terrestrial interactions, cosmic rays, orbital and planetary influences, volcanism, and paleoclimate drivers.

Meteorology and Weather–Climate Interactions
Large-scale and mesoscale processes, extreme weather, precipitation variability, heatwaves, and climate linkages.

Hydrology and Hydroclimatology
Hydrological cycle, droughts and floods, soil moisture, water balance, and hydroclimatic variability.

Land–Atmosphere Coupling and Vegetation–Climate Interactions
Evapotranspiration, land use, ecosystems, and biosphere–atmosphere exchange.

Oceanic and Cryospheric Climate Processes
Ocean circulation, sea-ice, glaciers, cryosphere interactions, and ocean–atmosphere exchanges.

Climate Data Analysis and Modeling
Statistics, data analysis, model evaluation, uncertainty quantification, and climate inference.

Earth–System Modelling and Climate Informatics
Coupled modelling, data-driven methods, remote sensing, and integrative Earth-system approaches.

ABOUT SCC

Science of Climate Change (SCC) is an independent, peer-reviewed, open-access scholarly journal dedicated to advancing scientific understanding of the Earth's climate system and its governing processes.

Established in 2021, SCC has developed into an international publication published by the SCC Publishing Association since 2025.

SCC provides a platform for original research articles, review papers, methodological studies, data analyses, and scholarly discussion addressing climate variability and change across spatial and temporal scales.

The journal promotes open scientific discourse by welcoming a diversity of scientifically reasoned perspectives and by encouraging critical examination of current assumptions and explanations.

FOR AUTHORS

- Original research, reviews, data papers, methodology, and discussions.
- Constructive peer review focused on scientific quality and clarity.
- Global visibility and impact through open access.
- Simple submission process and dedicated editorial support.

JOIN THE GLOBAL CLIMATE SCIENCE COMMUNITY

SCC is committed to advancing knowledge of the climate system through high-quality research, interdisciplinary collaboration, and open exchange.

Submit your work and be part of the conversation.

SCIENCE OF CLIMATE CHANGE
SCIENCE • OPENNESS • UNDERSTANDING

Website
www.scienceofclimatechange.org

Email
editor@scienceofclimatechange.org

Publisher
SCC Publishing Association

Address
Michelets vei 8 B
1366 Lysaker, Norway

ISSN
2703-9072

Established
2021

Science of Climate Change
Volume 6.1

June 2026

ISSN 2703 9072

https://doi.org/10.53234/scc202603/01

SCC Publishing, Michelets vei 8 B, 1366 Lysaker, Norway

Org. no 935 567 653

Table of Contents

Preface

On 1 January 2026, I assumed the position of Editor-in-Chief of *Science of Climate Change*, succeeding Professor Hermann Harde. It is a great honour, as well as a considerable responsibility, to continue the work of those who established and developed the journal and to guide it through the next stage of its scientific and institutional development.

Science of Climate Change is an independent, peer-reviewed and fully open-access scholarly journal devoted to advancing scientific understanding of the Earth's climate system and its governing processes. It welcomes original research articles, review papers, methodological studies, data analyses, essays, commentaries and scholarly discussion covering climate variability and change across different spatial and temporal scales. Its scope extends across atmospheric sciences, meteorology, hydrology and water resources, land-atmosphere interactions, oceanic and cryospheric processes, paleoclimate, remote sensing, climate-data analysis, Earth-system modelling, and solar and astronomical influences on climate.

The establishment and subsequent progress of the journal have depended on the commitment of several editors and many supporting colleagues. The origins of SCC can be traced to 2020, when Professor Nils-Axel Mörner accepted the role of Chief Editor during the journal's initial formation. Regrettably, he passed away before the publication of the first issue. Geir Hasnes subsequently undertook the demanding work of leading the journal through its founding phase, and the first issue appeared in August 2021.

Professor Jan-Erik Solheim served as Chief Editor from October 2022 through the end of 2023 and made a major contribution to the journal's early development, publication programme and international outreach. His contribution did not end with his term as Chief Editor. He continues to support Science of Climate Change actively through his participation in the Extended Board, his scientific advice, his engagement with authors and contributors, and his assistance with the journal's editorial and organisational activities. His continuing commitment, experience and close association with the journal remain highly valuable to its present operation and future development.

From 2024 until the end of 2025, Professor Hermann Harde served as Editor-in-Chief. I wish to express my sincere appreciation for his outstanding scientific, editorial and organisational contribution. Through his sustained commitment, meticulous editorial work and close involvement in the review and production processes, he played a decisive role in consolidating the journal's scientific identity, maintaining its publication programme and strengthening its international profile. The orderly transfer of editorial responsibility provided a strong foundation upon which the journal can continue to develop.

The institutional development of SCC also represents an important achievement. The journal has been published since the beginning of 2025 by the SCC Publishing Association, strengthening its status as an independently operating, not-for-profit scientific publication. Its open-access model ensures that all published contributions are immediately and freely available to readers worldwide, while moderate publication charges support editorial administration, peer-review coordination and digital dissemination. This progress would not have been possible without the dedicated contribution of Stein Storlie Bergsmark, who currently chairs the SCC Publishing Association. His organisational work, institutional support and continuing engagement have been essential to the operation, stability and development of the journal.

I also wish to acknowledge the substantial contribution of the Co-Editors as their scientific expertise, editorial judgement and willingness to coordinate peer review have been indispensable to maintaining the quality and continuity of the journal. I am particularly pleased that Professor Hermann Harde will continue contributing to SCC as a Co-Editor, allowing the journal to benefit from his extensive editorial experience.

Special recognition is due to Jan Guttulsrud, the SCC Secretary, for his dependable administrative assistance and his contribution to the journal's day-to-day operation.

Finally, I wish to thank all authors who have entrusted their research and ideas to *Science of Climate Change*. Since its establishment, the journal has published original research articles, review papers, essays, discussion and debate papers, commentaries, conference proceedings, book reviews and other scholarly contributions. The diversity of these publications reflects both the breadth of climate science and the journal's commitment to substantive scientific discussion.

As Editor-in-Chief, my objective is to preserve SCC's intellectual independence while further strengthening its scientific standards, peer-review procedures, editorial transparency and international visibility. The journal will continue to welcome rigorous research across the broad field of climate science and related areas, including contributions that test, refine or challenge existing interpretations.

I look forward to working closely with SCC Publishing, the Co-Editors, the Extended Board, the SCC Secretary, reviewers and authors in continuing the development of the journal.

Nikolaos Malamos
Editor-in-Chief

Editorial

The present issue 6.1 covers publications accepted during the first half of 2026. It contains five research articles, two essays, one invited address and one corrigendum. The contributions address a broad range of subjects, including paleoclimatic temperature variability, the statistical analysis of possible climate drivers, ocean heat-content and Earth Energy Imbalance estimates, the economic and institutional dimensions of climate policy, observation-based assessments of the present climate, alternative hypotheses concerning recent warming, and laboratory investigations of radiative and convective heat transfer.

Les Hatton examines whether a temperature rise of approximately 1.1 °C within one century should be considered unusual when viewed in the context of the EPICA-Vostok ice-core record. Using century-scale temperature estimates extending approximately 800,000 years into the past, the author separates the record into interglacial rises, interglacial declines, ice ages and longer comparative periods. His analysis indicates that temperature changes of at least 1.1 °C per century occur relatively frequently during the present interglacial: approximately 16% of the centuries since the end of the last ice age exhibit an increase of this magnitude or greater. By contrast, such changes are reported to be absent or highly unusual in the older sections of the record, particularly before approximately 200,000 years ago. The study therefore identifies a marked increase in century-to-century temperature variability during the more recent part of the ice-core record, although the author notes that it remains uncertain whether this represents a physical climatic phenomenon or an effect associated with the temporal resolution of the proxy record. The study is accompanied by the dataset and software used to reproduce its analyses and figures.

Dai Ato investigates the relationships among solar activity, absorbed shortwave radiation, global sea-surface temperature, near-surface specific humidity and atmospheric CO_2 during the satellite era, primarily from 2000 onwards. The study combines time-lag examination with multiple linear regression, using adjusted global sea-surface temperature as the dependent variable and absorbed shortwave radiation, total solar irradiance and CO_2 as explanatory variables. The author reports that absorbed shortwave radiation and total solar irradiance are the principal positive predictors in the selected regression model, whereas the independent contribution attributed to CO_2 is comparatively small. The temporal analysis further indicates that variations in sea-surface temperature precede corresponding changes in specific humidity by several months. On this basis, the author challenges the conventional representation of water vapour as a positive feedback initiated by CO_2-driven warming. The exceptional global warmth of 2023 and 2024 is also examined, with the study attributing the event mainly to variations in solar activity, absorbed shortwave radiation and planetary albedo rather than to the Hunga Tonga–Hunga Ha'apai eruption or an increase in atmospheric water vapour. The paper includes supplementary discussions of climate-model assumptions, carbon-isotope evidence and updates to the author's previous analyses.

The issue also contains a corrigendum by *Antero Ollila* concerning his previously article published in Vol. 5.3 "Radiative Forcing of Water Vapour and its Use in Climate Models". The corrigendum provides the corrected expression for Equation (2). The author confirms that the error was typographical and had no effect on the calculations, results or conclusions of the original article.

Jonathan Cohler, David R. Legates, Kesten C. Green, Ole Humlum, Franklin Soon and Willie Soon critically examine the methods used to derive global Ocean Heat Content and Earth Energy Imbalance estimates from the Argo profiling-float programme. The authors review the complete measurement and processing chain, including the spatial and temporal distribution of the floats, the lack of direct information on their subsurface trajectories, the restriction of most measurements to the upper 2,000 m of the ocean, the construction of reference climatologies, and the subsequent interpolation and integration of temperature anomalies over global three-dimensional grids. Particular attention is given to the distinction between temperature as an intensive property and thermal energy as an extensive quantity. The authors argue that assigning sparse temperature observations to large unsampled ocean volumes and integrating interpolated anomalies does not produce a thermodynamically well-defined measurement of global ocean thermal energy. The study also evaluates uncertainties associated with mesoscale variability, undersampling of the deep and polar oceans, positional and temporal offsets, baseline selection and interpolation assumptions. The authors estimate that the combined structural uncertainty of annual-to-decadal Earth Energy Imbalance calculations is at least approximately ±1 Wm^{-2} at the 95% confidence level. They consequently argue that the frequently reported central estimate of approximately 0.7 Wm^{-2} cannot be distinguished reliably from zero at the stated level of uncertainty. They further contend that satellite-derived top-of-atmosphere radiation products constrained using Ocean Heat Content estimates cannot provide a fully independent confirmation of the imbalance. The article concludes that present Argo-based estimates are computational products whose values depend strongly on methodological assumptions and should not be treated as direct measurements of a conserved global physical quantity.

In an address originally delivered at the 2026 Annual Meeting of the Norwegian Klimarealistene, *Václav Klaus* discusses the future role of Clintel and the wider institutional and political context of climate debate. As the recently appointed President of Clintel, he considers whether the organisation should primarily operate as an advocacy group, an umbrella network for independent researchers and organisations, or a platform for publishing scientific and policy-related material. He emphasises the distinction between rational scepticism and simple rejection, and argues that scientific questions cannot be regarded as permanently settled. A substantial part of the address concerns the economic dimensions of environmental and climate policy. Klaus criticises the concepts of limits to growth, central economic planning and extensive regulatory intervention, and stresses the coordinating function of market prices. He also discusses emissions-trading systems, the treatment of environmental externalities and the importance of discounting in evaluating long-term policies and investments. In his view, climate-policy discussions frequently neglect opportunity costs and the broader economic consequences of regulatory decisions. The address concludes by calling for greater involvement of economists in the climate debate and for continued critical examination of European climate and energy policies.

David Shelley places contemporary climate change within a long geological and paleoclimatic perspective. The essay examines glacial–interglacial cycles over approximately the last million years and compares the present climate with both earlier interglacials and the much warmer conditions that prevailed during substantial portions of the Phanerozoic. The author argues that the current climate remains unusually cold in the longer geological context and that recent warming does not constitute evidence of an unprecedented climatic crisis. The essay also questions whether the increase in atmospheric CO_2 can adequately explain the observed sequence of recent warming. Shelley emphasises the large thermal capacity of the oceans and notes that, in the observational sequences considered, changes in ocean temperature appear to precede changes in atmospheric temperature. He proposes that variations in absorbed solar energy, potentially associated with changes in cloud cover, provide a plausible explanation for ocean warming. The author therefore argues that climate research should give greater attention to the processes controlling ocean heat uptake and sea-surface temperature. In discussing the longer-term future, he considers eventual cooling and a return to glacial conditions more probable than indefinite warming, while also distinguishing climate considerations from the need to develop alternatives to finite fossil-fuel resources.

Ole Humlum presents an observation-based overview of the state of the global and Arctic climate during 2025. The essay reviews atmospheric and ocean temperatures, sea-level observations, Arctic sea ice, Northern Hemisphere snow cover, tropical cyclones, accumulated cyclone energy, global precipitation and cloud-cover records. The author reports a slight reduction in global temperature during 2025 compared with the exceptionally warm preceding years, while emphasising substantial geographical differences among individual observational records. The analysis identifies no clear long-term trend in several commonly cited indicators of climatic extremes, including tropical-cyclone frequency, accumulated cyclone energy and global precipitation. Arctic September sea-ice extent is described as variable but relatively stable during the most recent years, while Northern Hemisphere snow cover is reported to show little overall change across approximately five decades. Humlum also draws attention to a reduction in global cloud cover since the mid-1980s, coinciding with increasing global temperature. Based on the observed temporal sequence in which sea-surface temperature changes precede changes in the lower atmosphere and over land, he identifies the ocean surface as a central regulator of atmospheric temperature. The essay concludes that the principal unresolved research question is what controls global sea-surface temperature, with solar variability modulated by cloud cover proposed as a leading candidate.

Roger Higgs evaluates the relationship between solar variability and global temperature over approximately the last 9,000 years and considers whether the additional warming observed since the mid-twentieth century might be associated primarily with airborne black carbon rather than CO_2. By visually matching long-term solar and temperature reconstructions, the author identifies a variable lag of approximately 100–225 years, with a typical value near 150 years, which he associates with the thermal inertia of the oceans. He reports that the temperature and solar records become increasingly decoupled after approximately 1940, when observed warmth appears greater than would be expected from the corresponding solar reconstruction. To investigate this divergence, the paper examines the geographical distribution of recent warming and the occurrence of several pauses in the global temperature record. The author argues that the faster warming observed over land than over the oceans, and in the Northern compared with the Southern Hemisphere, is more consistent with the uneven spatial distribution of black-carbon emissions than with a well-mixed atmospheric gas. The paper therefore proposes that soot emitted from coal, diesel oil and biomass combustion may account for a substantial proportion of the anthropogenic component of recent warming. This hypothesis leads the author to recommend stabilising and eventually reducing coal and oil combustion, while considering natural gas as a comparatively low-soot transitional fuel until alternative energy technologies become sufficiently available.

Finally, *Michael Schnell and Hermann Harde* present controlled laboratory investigations of the interaction between radiative and convective heat-transfer processes. Their experimental apparatus consists of a temperature-controlled cylindrical chamber containing a heated blackened aluminium plate representing the Earth's surface. By positioning the heated plate either below or above the cooler cylinder walls, the authors create configurations in which convection is respectively enabled or strongly suppressed. Hydrocarbon gas, CO_2 and the infrared-inactive gas argon are introduced to distinguish radiative effects from changes associated with gas density, thermal conductivity and the temporary formation of a heavier gas layer. When the heated plate is located at the bottom of the chamber, all three gases initially produce a temperature increase, including argon. The authors interpret this initial response not as evidence of a greenhouse radiative effect, but as the result of temporarily inhibited convection caused by the denser gas layer surrounding the heated plate. After diffusion and homogenisation of the gas, the measurements reveal smaller effects attributable to radiative transfer. Comparing the convective and non-convective configurations, the authors find that convection substantially reduces the temperature response associated with the infrared-active gases. The study therefore demonstrates that radiative, convective and conductive processes cannot be treated independently and that laboratory demonstrations attributing an observed temperature increase solely to greenhouse-gas radiation may be misleading when changes in convection are not adequately controlled.

Together, the contributions in this issue examine climate variability and climate-system processes across a wide range of temporal and spatial scales, from laboratory experiments and satellite-era observations to glacial cycles and geological time. They also illustrate the importance of transparent data analysis, the explicit examination of assumptions and uncertainties, and the continued testing of competing explanations. We hope that these contributions will encourage further critical, evidence-based discussion of climate science and its broader scientific, economic and societal implications. We wish our readers an engaging and thought-provoking reading.

Oslo, June 30, 2026

Nikolaos Malamos
Editor-in-Chief

SCC-Publishing

Michelets vei 8 B
1366 Lysaker, Norway

ISSN: 2703-9072

Correspondence:
lesh@cantab.net

Vol. 6.1 (2026)
pp. 1-8

Is a 1.1°C Rise in a Century Unusual?

A Study of Interglacials in the Epica-Vostok Dataset

Les Hatton

Emeritus Professor of Computer Science, Kingston University, UK

Abstract

Much public discourse in global warming centres around the oft-quoted rise in temperature of approximately 1.1°C in global average temperature in the post-industrial period. This is considered in some quarters to constitute a "Climate Emergency" demanding "Climate Action". In this paper we first dissect the background behind this number and what it means. Second, we use the Epica-Vostok Ice core dataset, a single proxy dataset for temperature data sampled every century for the last 800,000 years or so and ask the question "Is a 1.1°C temperature rise in a century unusual in this dataset?"

The answer is surprising. By considering interglacial onsets and decays as well as intermediating Ice Ages, it turns out that a rise of this amount would have been considered unusual more than 200,000 years ago, but this rise is *not* unusual in the current interglacial which started some 20,000 years ago with around 16% of all centuries since the last Ice Age exhibiting a temperature rise of at least 1.1°C. None of these could have anthropogenic components as they pre-dated the industrial era. This result suggests that attempts to partition the current rise into anthropogenic and non-anthropogenic components are questionable given that it is not even unusual.

Keywords: Greenhouse effect; interglacial temperature fluctuations; Increasing temperature variability.

Submitted 2025-05-22, Accepted 2026-01-15, https://doi.org/10.53234/scc202603/05

1. Introduction

The ratio of natural to anthropogenic components in the warming noted in the last 100 years is a matter of lively debate with arguments ranging from one extreme, that very little is down to us all the way to those arguing that it is all down to our fossil fuel CO_2 emissions, for example using complex model-based efforts (e.g. Forster et. al. 2023). If the former, then little can be done about the warming process so our efforts must be focused on dealing with likely effects. If the latter, then we can legitimately continue trying to limit the warming or even perhaps reverse it. However, there are prior questions which should be answered before arguments over attribution. First, what does a 1.1°C rise in global average temperature actually mean? Second, is a 1.1°C rise in a century unusual and if so, how unusual? If such a rise is highly unusual, then it is entirely valid to identify as far as possible the contributing elements. On the other hand, if it is not unusual, then we must question the relevance of seeking attribution.

Most of the discourse about a 1.1°C rise in a century relates to the global average temperature trend such as that shown in reports AR3 and AR6 of the IPCC (Intergovernmental Panel on Climate Change) for the last 1000 years, (also known as the "Hockey-Stick" graph). Such temperature trends are derived using various proxies for temperature, such as tree rings and corals, merged with modern thermometric data of the last 150 years. Unfortunately, a single global average temperature is a slippery concept to deal with in comparison with datasets acquired in a particular location as we do here. Unlike measurements taken at a single location, a single global average temperature is not the result of a physical experiment. Instead it is a statistical amalgam with many assumptions of numerous proxies for temperature. Some idea of the complexities in individual stations can be seen for example in Sonnadara (2020), where the average annual temperature at a Sri Lankan mountain station follows the IPCC reported trend but this is all found in a rise in the annual average *minimum* temperature. There is no change in the annual average maximum temperature in the last century. As such calculating a global average temperature is opaque at best and perhaps worst of all, it is effectively impossible to compare against comparable periods in the far past. It certainly seems to be a questionable measure on which to base policy. However it is at least calibrated in °C so we can reasonably compare it with the results of measuring a temperature record at a single location for which the Epica-Vostok Ice Cores give an excellent example. We note of course that like any individual location, Antarctica might not be representative of the "global average" temperature, but we are looking for temperature *changes*.

We will not therefore attempt to unravel the complexity of a global average. Instead a better-defined but closely related question will be asked and answered.

Is a 1.1°C rise in a century an unusual event in a "pure" dataset i.e. one recorded at a single location in a consistent manner over a long period?

In this paper we take a very simple data-driven view to answer this question, and we use the publicly available Epica-Vostok Ice Core datasets which stretch back some 800,000 years and specifically the dataset Epica-tpt-co2.csv[1]. This dataset lists the temperature change in *°C* and the CO_2 level in ppm for every intervening century.

1.1 Statement of reproducibility

This paper is accompanied by a downloadable package[2] which includes the original dataset used for analysis and the plotting and analysis software used to re-create all of the figures and conclusions following the strictures of Ince et. al. 2012 and Hatton & Warr 2016.

1.2 The Epica-Vostok Ice Core dataset

EPICA (European Project for Ice Coring in Antarctica) is a multi-national project for deep ice core drilling in Antarctica (Epica 2025) coordinating drilling at Dome C and Kohnen station. There are other coring sites in Antarctica such as Vostok, operated by Russia. Ice core data is a proxy for temperature in the following sense. The temperature and CO_2 levels at a particular level in the ice-core can be inferred from oxygen and deuterium isotope levels in the tiny bubbles trapped in the ice as the surface snow is buried and compacted over the centuries. The cores are analysed and data is output at the rate of one temperature and CO_2 sample per century. The data from Vostok extends back around 420,000 years before which the cores contain no climate information owing to the presence of ice re-frozen from the waters of Lake Vostok which lies underneath. The data from Dome C provides climate data reaching back some 800,000 years and correlates well with the Vostok data where they overlap in time (EPICA Community members 2004).

The ice core datasets remain one of the few consistent measurement handles we have on what was actually happening in the last 800,000 years or so. This may sound an age, but if we represent life on earth by one hour on a clock, this measurement dataset tells us what happened in the last second. We do not as yet have any better measurement data either more fine-grained or longer lasting, partly of course because the ice-core datasets in Antarctica where the ice is on average around 2km. thick, are just about as deep as it is possible to go on earth, although the project "Beyond EPICA – Oldest ice" due to report shortly may well extend this back to 1.2 million years before the present day (Beyond EPICA 2025).

---

[1] http://www.climatedata.info/proxies/data-downloads/, accessed 05-Dec-2025

[2] https://leshatton.org/ClimateChangeCenturyRise.html, accessed 09-Dec-2025

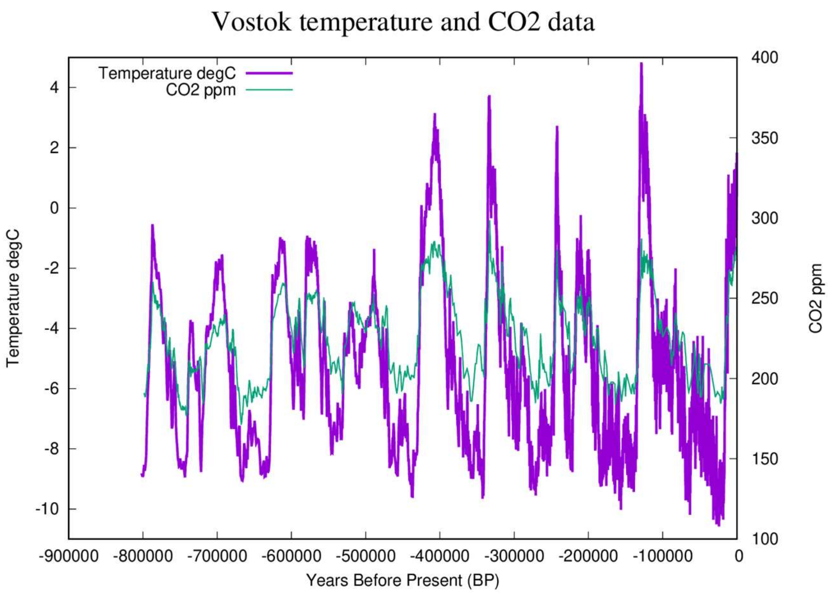

Figure 1: The Vostok ice core dataset for the last 800,000+ years. This dataset has not been processed in any way and is the original raw dataset. Note that although the temperature scale is shown around zero, the data must be biased by -55°C to produce a surface temperature estimate.

2. Analysing the data

Let's consider this dataset in more detail.

2.1 The current entire dataset 800,000 – 0 years ago.

Studying Fig. 1, we can see a number of features in the temperature, noting that only the last datapoint could contain any anthropogenic effects.

- Most of the time in the last 800,000 years or so, the earth has been significantly cooler than today (i.e. less than 0°C on this plot).
- There are a series of sharp peaks of temperature. These are known as *interglacials*.
- These peaks appear to be getting hotter. There is a significant rise 400,000 years ago with a generally increasing trend ever since.
- The peaks are followed by an equally steep fall in temperature. These periods are *Ice Ages* and generally last longer than the interglacials.
- The previous interglacial about 120,000 years ago was hotter than this one, (so far). It was in fact almost 4°C hotter.
- The last Ice Age, which finished about 20,000 years ago was the coldest of the last 800,000 years and more than 11°C cooler than pre-industrial times. Ice Ages are getting colder.
- CO_2 levels in this dataset vary between about 170 ppm and 280 ppm. In the last century, this has shot up to about 420 ppm.

We also note in passing that the lowest CO_2 level in this dataset is 171.6 ppm, not very much above the 150 ppm necessary to sustain land-based plant photosynthesis. If it had fallen this low, such photosynthesis would have ceased, almost certainly triggering a mass extinction of land-based life forms; a near miss. In fact in 556 centuries of this dataset, CO_2 levels were below 190 ppm. Beyond these comments, we say nothing more of the CO_2 data.

Let us now zoom in on the last two interglacials as shown in Fig. 2.

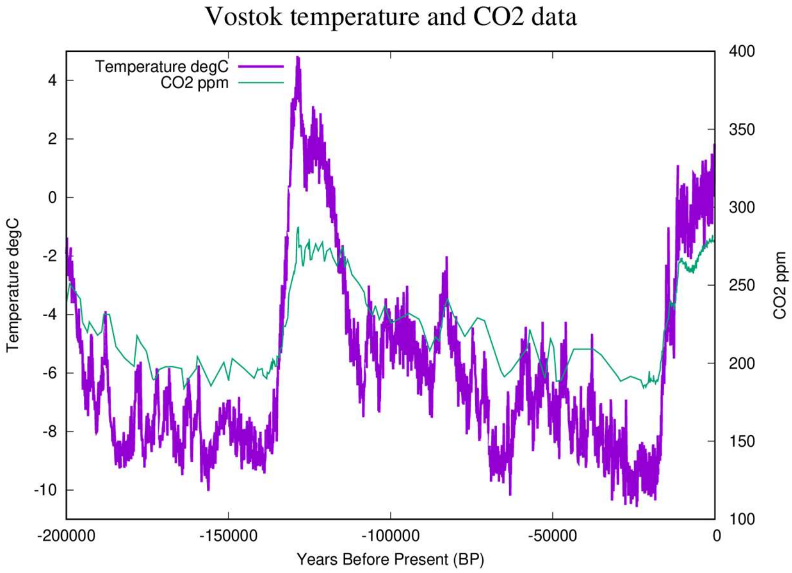

Figure 2: The Vostok ice core dataset for the last 200,000 years.

On this zoomed scale, it is beginning to become apparent just how variable the temperature is century on century. It is believed that global average temperatures have climbed by about 1.1°C in the last 100 years[3]. Let us therefore ask a couple of questions.

2.1 How unusual is a 1.1°C rise in one century?

We cannot answer this question with global average temperatures as described earlier, but statistically, this is a very simple question to answer with a single-proxy consistent dataset as good as this, but first we must extract all the rises and falls within a given period. Then we must understand how they are distributed before we use the distribution to make statements of how unusual a particular rise or fall might be.

As an aid to what follows, let us define four kinds of regime for this dataset based on a visual inspection of Fig. 1.

- **Interglacial rise.** This we define as the period of an interglacial when temperatures are climbing out of a preceding Ice Age.
- **Interglacial fall.** This we define as the period of an interglacial when temperatures are falling into a succeeding Ice Age.
- **Ice age.** The period between an Interglacial fall and an Interglacial rise.
- **Other.** Longer periods for comparison.

The motivation for this categorisation is that it would be expected that temperatures would be more likely to rise century on century in an *Interglacial rise* than for example in an *Interglacial fall*, but this we will test.

The last 20,000 years

It is important to note that we live in an *Interglacial rise*, a period of generally rising temperature. As can be seen in Fig. 2, temperatures have climbed by about 12°C since we emerged from the last Ice Age some 20,000 years ago. In other words, on average they have increased by about

[3] The graph on https://earthobservatory.nasa.gov/world-of-change/global-temperatures, accessed 03-May-2025, shows a rise from -0.25°C to +0.8°C between 1922 and 2022. This gives about 1.05°C. This has been rounded up to 1.1°C for this paper. See also the climate model simulation based study by Gillett et al. (2021) who quote a similar figure albeit over 150 years.

12/200 = 0.06°C per century. Just after the Ice Age ended, the rate of increase was almost twice as high at around 0.1°C per century. Since then it has continued to rise but more slowly although with considerable century on century variability. If we analyse this century on century variability as a histogram, we get Fig. 3. The vertical blue dotted line indicates where on this histogram a 1.1°C rise per century would appear.

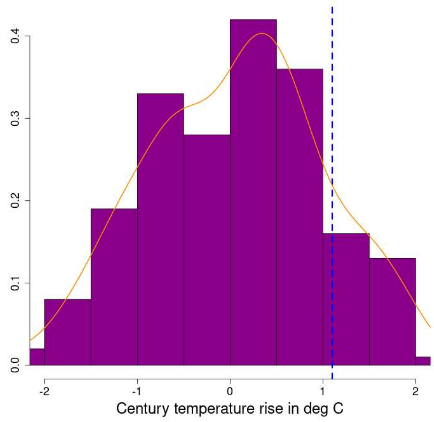

Figure 3: The ice core dataset for the last 20,000 years partitioned into a density histogram of temperature changes in each of the 200 centuries. The blue vertical line corresponds to a 1.1°C rise.

Fig. 3 has a look of normality so we will apply the Shapiro-Wilks test. This gives a p-value of 0.66. In the Shapiro-Wilks test, any p-value larger than 0.05 suggests we can assume normality as a reasonable guess. This conveniently allows us to use a simple Z test to see how unusual a 1.1°C rise actually is in this dataset.

When we do this, we find that the probability of a rise of at least 1.1°C is actually unexpectedly high at 0.16. *In other words, a rise of 1.1°C in the current interglacial is not significant at any accepted level*, (normally taken as < 0.05).

This immediately begs the question as to whether Interglacial rises are different from Interglacial falls and Ice ages with regard to temperature fluctuations.

Extending to the last interglacial

Table 1 shows an extension of this to different regions of Fig. 1 within the last 150,000 years to encompass the previous interglacial and the Ice Age in between it and the current interglacial. $p_{shapiro}$ is the p-value returned by the Shapiro-Wilks built-in test in R. Values greater than 0.05 indicate that normality is a reasonable approximation, which is the case for all these entries. *P(T > 1.1) i*s the probability in the stated period in which a temperature rise greater than 1.1°C occurred.

Table 1: Shapiro-Wilks tests and significance tests for a T=1.1°C rise in a century for different periods.

Start	*End*	$p_{shapiro}$	$P(T \geq 1.1°C)$	*Category*
-20,000	0	0.658	0.158	Interglacial-rise
-55,000	-20,000	0.199	0.086	Ice-age
-100,000	-30,000	0.131	0.082	Ice-age
-124,000	-110,000	0.284	0.056	Interglacial-fall
-130,000	-115,000	0.245	0.059	Interglacial-fall
-140,000	-130,000	0.107	0.112	Interglacial-rise

In all of the periods shown, a temperature rise of at least 1.1°C is not unusual at any acceptable level of statistical significance, although as we might expect, it is closest during an Interglacial fall when the temperature trend is generally downward.

Extending to times before 200,000 years ago

When we continue this analysis earlier in the dataset, we get the results shown in Table 2.

Table 2: Shapiro-Wilks tests and fraction of centuries with at least a T=1.1°C rise in a century for different periods starting earlier than 200,000 years ago.

Start	*End*	$p_{shapiro}$	*Fraction* $(T \geq 1.1)$	*Category*
-330,000	-310,000	0.034	0.000	Interglacial-fall
-390,000	-340,000	0.000	0.000	Ice-age
-400,000	-350,000	0.000	0.000	Interglacial-fall
-800,000	-450,000	0.000	0.000	Five-early-interglacials

The data in Table 2 show two important factors. The residuals are no longer normally distributed, so we just compute the fraction of centuries with which a 1.1°C rise occurs in each population, and this can be seen to be substantially less than that shown in Table 1.

Since the distributions of Table 2 are no longer normal, it is useful to show them graphically as we see in Figs. 4 and 5, which have the same horizontal scale as Fig. 3.

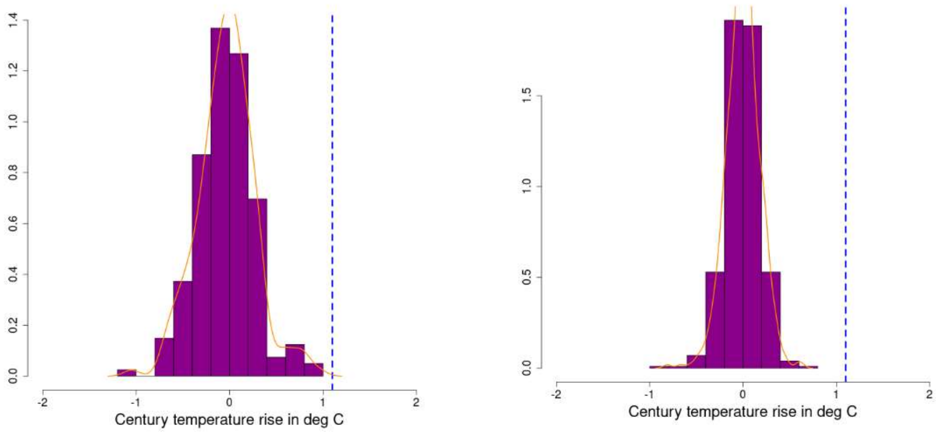

Figure 4: Comparison of distributions of temperature changes in a century for the following periods (left) 330,000 - 310,000 ya; (right) 390,000 - 340,000 ya. The blue vertical line corresponds to a 1.1°C rise.

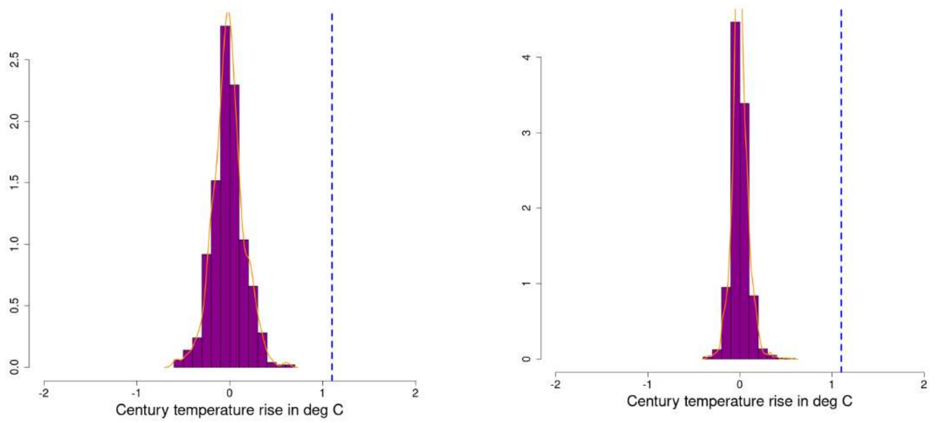

Figure 5: Comparison of distributions of temperature changes in a century for the following periods (left) 400,000 – 350,000 ya; (right) 800,000 - 450,000 ya. The blue vertical line corresponds to a 1.1°C rise.

The reduction in spread of temperature changes is very clear before 200,000 years ago and the further back we go, the smaller the spread. In all of these, a rise of 1.1°C would be considered highly unusual as in the periods shown it never happened.

Conclusions

The Vostok Ice Core data contains numerous interesting features which can be confirmed by anybody as the data is open. We can conclude the following:

- A rise of 1.1°C in a century is not unusual in the current interglacial. In fact 16% of the centuries since the end of the last Ice age show a rise at least as big as the current century and none of these could have been affected by anthropogenic action.
- A rise of 1.1°C in a century would have been considered unusual any time more than 200,000 years ago. For some unknown reason nothing to do with us, the temperature has become more volatile in century on century changes in the last 200,000 years. Whether this is a physical effect or an artifact of isotopic smoothing with time is unknown although there is no evidence for the latter on the peaks of the last four interglacials and there is an abrupt change in magnitude of about 4°C in between the last 5 interglacials and the preceding 4 which is atypical of a continuous smoothing process.
- The current interglacial is nothing special. It is currently still more than 3°C cooler than the peak of the last one about 130,000 years ago (which was by assumption entirely free of anthropogenic effect) and the degree of variability in this data is much the same now as then.

Given then that a rise of 1.1°C is quite commonplace in this current interglacial and that none of the earlier occurrences could have been affected by anthropogenic activity, this raises the question of why we are trying to attribute the current rise to anthropogenic effects as if it was unusual.

Funding

This study received no funding.

Co-Editor: Francois Gervais; **Reviewer 1**: J.-E. Solheim, **Reviewer 2**: anonymous.

Acknowledgements

The author would like to acknowledge numerous conversations with Dr. David King and Dr. Debbie Ancell. The reviewers also helped us substantially in framing the arguments. We would also like to thank the many scientists responsible for acquiring this extraordinary dataset and their foresight in making it publicly available.

References

Beyond EPICA 2025 *Oldest Ice Core: 1.5Myr of greenhouse gas – climate feedbacks*, https://www.beyondepica.eu/en/, accessed May 2025.

EPICA 2025, *European Project for Ice Coring in Antartica*, https://en.wikipedia.org/wiki/European_Project_for_Ice_Coring_in_Antarctica.

EPICA community members, 2004 *Eight glacial cycles from an Antarctic ice core*. *Nature* **429**, 623–628 (2004). https://doi.org/10.1038/nature02599

Forster P.M. and 59 others, 2023: *Indicators of global climate change 2023: annual update of key indicators of the state of the climate system and human influence.* Earth System Science Data, 16(6): 2625–2658, 2024.

Gillett, N.P., M. Kirchmeier-Young, A. Ribes, H. Shiogama, G.C. Hegerl, R. Knutti, G. Gastineau, J.G. John, L. Li, L. Nazarenko, N. Rosenbloom, Ø. Seland, T. Wu, S. Yukimoto, and T. Ziehn, 2021: Constraining human contributions to observed warming since the pre-industrial period. *Nat. Clim. Change*, **11**, no. 3, 207-212, doi:10.1038/s41558-020-00965-9.

Hansen, J.E., and S. Lebedeff, 1987: Global trends of measured surface air temperature. *J. Geophys. Res.*, **92**, 13345-13372, doi:10.1029/JD092iD11p13345.

Hatton L. and Warr G., 2016: *Full Computational Reproducibility in Biological Science: Methods, Software and a Case Study in Protein Biology,* ArXiv, doi: 10.48550/arXiv.1608.06897

Ince D. C., Hatton L., and Graham-Cumming J., 2012: *The case for open program code*, Nature, 482:485–488, 02 2012, doi:10.1038/nature10836.

Sonnadara U., 2020: *Long-term changes in extreme air temperature in Nuwara Eliya: a case study from Sri Lanka*, Weather, 75(9), September

Research Article

SCC Publishing
Michelets vei 8 B
1366 Lysaker Norway

ISSN: 2703-9072

Correspondence:
ato.dai1@wind.ocn.ne.jp

Vol. 5.@ (2025)
pp. 9-41

Multivariate Analysis, Phase Verification, and the Rejection of Man-made Positive Feedback Global Warming Theory

Dai Ato

Independent researcher, Osaka, Japan

ORCID:0000-0002-6049-5039

Abstract

The anthropogenic theory of global warming advocated by the IPCC is based on the theory that increased atmospheric carbon dioxide (CO_2) from anthropogenic emissions causes warming, which in turn increases water vapor, triggering a positive feedback loop that leads to further warming and CO_2 rise. This study examines the validity of this theory using the best available data to date.

Using meteorological satellite data mainly from year 2000 onwards, the interaction between solar activity, global sea surface temperature (G-SST), global specific humidity (G-SpHm) in the earth surface, and CO_2 was investigated. Multiple linear regression analysis was performed with G-SST adjusted for month difference as the dependent variable and absorbed shortwave (ASW) at the top of the atmosphere, total solar irradiance (TSI), and CO_2 as explanatory variables. The positive independent predictors of G-SST in the best model were ASW and TSI of anomalies (13-month running mean), with standardized regression coefficients $\beta = 0.657$, $P = 1.78e{-}62$, and $\beta = 0.459$, $P = 7.60e{-}39$, respectively; Model $R^2 = 0.764$, $P = 7.96e{-}87$.

Furthermore, G-SST precedes G-SpHm by a few months. No impact was observed on G-SST fluctuations by the rise in G-SpHm in 2023 and 2024. These results refute the hypothesis linking atmospheric CO_2 and water vapor. This study represents the first report to disprove the positive feedback theory underpinning the anthropogenic CO_2 warming hypothesis through verification of time lags between elements and multivariate analysis. And the dominating factor in Earth's climate is still solar activity, even in the 21st century, according to the data provided by world prominent institutions.

The Appendix includes supplementary material to the main text, flaws in the fundamental assumptions of CO_2-dependent climate models, a simple method for distinguishing the origin of CO_2 increases using carbon isotopes, and updates to the author's previous reports.

Keywords: climate change; greenhouse effect; humidity; radiative forcing; IPCC; Clintel; Svensmark effect; albedo; NASA-CERES; Hunga Tonga-Hunga Ha'apai submarine volcanic eruption; El Niño

Submitted 2025-09-19, Accepted 2026-01-29. https://doi.org/10.53234/SCC202603/04

1. Introduction

Nearly 40 years have passed since the establishment of the IPCC, endorsed by Margaret Thatcher [1]. During this time, the IPCC has published six reports. The latest report definitively concludes that modern global warming is caused by humans (Sixth Assessment Report [2]). Notably, Thatcher herself shifted to expressing scepticism about the anthropogenic theory of climate change in her final book (Hot Air and Global Warming, Section 11 [1]).

From the very beginning, this debate has involved ongoing disputes with sceptics. Various private organizations have produced counter-reports, launched signature campaigns, and made policy proposals. In recent years, while differences on specific issues persist, organizations like Clintel [3] and CO_2 Coalition [4] have vigorously promoted climate change optimism. Furthermore, in Europe, private organizations calling themselves climate realists [5] exist in multiple countries (European Climate Realist Network, centred on Clintel in the Netherlands, with members in Belgium, Denmark, France, Germany, Ireland, Norway, Portugal, Spain, Sweden, and the UK).

Italy also has a statement by scientists refuting the anthropogenic theory of global warming [6]. Similar organizations can be found worldwide. The meaning of "realist" generally implies: largely rejecting the IPCC's anthropogenic theory of global warming; understanding recent climate change as a natural phenomenon; recognizing that benefits of CO_2 outweigh its drawbacks; and adopting a realistic approach.

One result of this trend was the issuance in August 2025 of an official document by the U.S. Department of Energy (DOE) under the Trump administration presenting optimistic projections of climate change that effectively rejected the pessimistic views [7]. Furthermore, the U.S. Environmental Protection Agency (EPA) also shifted its policy to significantly relax previous regulations on carbon.

Now, this paper has two primary objectives. The first is to decide whether the increase in atmospheric water vapor was the decisive factor behind the global sudden warming events observed on the Earth's surface atmosphere in 2023 and 2024. The second is to use statistical methods to demonstrate the fundamental error in the positive feedback hypothesis—one of the main tenets of the anthropogenic global warming theory—based on the results of the first objective. The backgrounds are described below.

The foundation of the anthropogenic global warming theory relies on the hypothesis that CO_2 is the primary driver of the greenhouse effect in Earth's atmosphere and that all modern CO_2 increases originate from human activity. However, the greenhouse effect of CO_2 itself is not actually very potent. The rationale is that the temperature rise caused by increased CO_2 leads to increased atmospheric water vapor, creating a synergistic effect (a vicious cycle). This theory is called the positive feedback theory (IPCC [2, 8, 9]). The IPCC acknowledges water vapor as the most potent greenhouse gas.

Quoting from IPCC Working Group 1 report of the Fifth Assessment [9]:

Chapter 8, Anthropogenic and Natural Radiative Forcing (FAQ 8.1, P8 or 667)

> *Currently, water vapour has the largest greenhouse effect in the Earth's atmosphere. However, other greenhouse gases, primarily CO_2, are necessary to sustain the presence of water vapour in the atmosphere. Indeed, if these other gases were removed from the atmosphere, its temperature would drop sufficiently to induce a decrease of water vapour, leading to a runaway drop of the greenhouse effect that would plunge the Earth into a frozen state. So, greenhouse gases other than water vapour provide the temperature structure that sustains current levels of atmospheric water vapour. Therefore, although CO_2 is the main anthropogenic control knob on climate, water vapour is a strong and fast feedback that amplifies any initial forcing by a typical factor between two and three. Water vapour is not a significant initial forcing, but is nevertheless a fundamental agent of climate change.*

However, doubts have also been raised about the reliability of climate prediction models, including this theory. As pointed out by the DOE [7] above, the climate prediction models adopted by the IPCC cannot reproduce the past. Furthermore, the author (Ato) would like to add his own interpretation here.

> *The inability to reproduce the past is synonymous with having no basis. A model*

> *with no basis cannot possibly predict the future. Yet IPCC supporters insist that despite being based on flawed hypotheses and models, the correctness of this model has been proven—that the future will inevitably unfold this way. Such claims, however, amount to nothing more than (vicious) circular logic.*

The models adopted by the IPCC are utterly unreliable precisely because they underestimate the influence of the sun and clouds. In recent presentations and papers, this has been pointed out by Nobel laureate in Physics John Clauser [10] and Grok 3β et al. [11]. Furthermore, IPCC treats the theory of positive feedback between rising CO_2 and water vapor as if it were fact.

Regarding solar activity, recent reports primarily focus on Total Solar Irradiance (TSI) (Soon et al. [12, 13], Grabyan [14]), and on the so-called Svensmark effect — the interaction between solar wind, cosmic rays, and cloud formation, and changes in albedo in the atmosphere (Svensmark et al. [15], Miyahara et al. [16], Nikolov and Zeller [17]). Recently, Grabyan [14] summarized reports showing a consistent correlation between TSI and climate change in paleoclimate.

Moreover, as the author previously demonstrated, the rise in atmospheric CO_2 itself (ΔCO_2) is mostly a natural phenomenon (Ato [18, 19]). The nearly linear increase in annual anthropogenic emissions cannot probabilistically explain the year-to-year instability in ΔCO_2. Similar observations have been consistently made for some time (Humlum et al. [20], Koutsoyiannis [21], Berry [22], Salby and Harde [23], Roth [24], Robbins [25]).

Furthermore, the very method of reconstructing past CO_2 concentrations from Antarctic ice cores, which forms the core of the anthropogenic CO_2 rise theory, has fatal flaws ([19], Jaworowski et al. [26-28]). The IPCC has effectively ignored these reports. Researchers supporting the anthropogenic theory of atmospheric CO_2 rise claim that ice core reconstruction methods have improved with technology, rendering the reconstructed values problem-free. However, this is simply not the case (e.g. Figure 2 in [19]). The fatal flaw in the method linking ice core reconstructions to modern measurements became evident when atmospheric methane levels dropped twice in the early 21st century (see [18, 19]).

Despite this, the IPCC-supporting camp has ignored these realities for nearly 40 years. In any case, the figure of 280 ppm from the Industrial Revolution, which forms the bedrock of the anthropogenic global warming theory, is clearly a grossly underestimated and erroneous value. Furthermore, the data and theories underpinning the IPCC's claims can only be described as the result of biased selection in every respect.

In fact, regarding the sudden warming starting in 2023, Dr. Gavin Schmidt [29], head of NASA Goddard Institute for Space Studies (GISS), stated that it cannot be explained by existing knowledge. In other words, he himself admitted that the existing CO_2 warming hypothesis and the existing climate prediction models based on it are unreliable.

In the climate models favourably adopted by the IPCC, the values at a certain point in time affect the next prediction. This is because the positive feedback theory is based on this premise. Therefore, if one prediction is wrong, everything after that will be wrong. Furthermore, sudden natural cooling is also possible in the future. Naturally, this is true even if there is no significant change in the concentration of CO_2 in the atmosphere itself. The appendix to this paper supplements the reasons why the CO_2 warming theory cannot be reproduced at all, even with paleoclimate reconstruction data going back about 10,000 years. Furthermore, the Appendix adds points to *basic misunderstandings* of Dr. Schmidt's paper [29].

Multiple explanations have been proposed for the abrupt warming observed from 2023 to 2024. The most plausible explanation based on current knowledge is a change in solar energy influx due to alterations in albedo in the atmosphere [17]. Meanwhile, the massive release of water vapor accompanying the 2022 Hunga Tonga-Hunga Ha'apai submarine volcanic eruption (Vömel et al. [30], Vinós and Curry [31]) and, partially, the influence of El Niño has also been proposed. As cited above and acknowledged by the IPCC [9], water vapor is effectively the most important greenhouse gas in Earth's atmosphere, making this theory worthy of consideration.

With these backgrounds, this study was conducted.

And as Appendix, the following related topics are added.

* Supplementary content to the main text
* Understanding the origin of atmospheric CO_2 increase by a concept of simple math using average of $\delta^{13}C$
* Update of Ato's existing multivariate analysis of SST and annual CO_2 increase values, considering time lags

2. Materials and Methods

2.1 Used data

All data used is publicly available. Global temperature indicators primarily utilize lower troposphere data from the University of Alabama in Huntsville (UAH, Spencer [32]). This is because UAH data originates from meteorological satellites and is considered the most objective and it has good global coverage. The reason is briefly explained below. Other meteorological satellite-derived temperature data sources include NOAA-STAR [33] and Remote Sensing Systems (RSS [34]).

Furthermore, multiple facilities provide temperature measurements of the Earth's surface. However, conventional surface measurement methods raise concerns about failing to fully eliminate biases, typically represented by the urban heat island effect (Soon et al. [13], Katata et al. [35], Spencer et al. [36]). Specifically, for surface measurements, global average data based has been estimated to show a warming trend approximately 20 % higher than those of solely on rural areas over a given period [35, 36]. Further details regarding temperature data are provided in the Appendix.

However, since UAH data represent lower troposphere temperatures—used as a proxy for sea surface temperature (SST) and land surface temperature (LST)—a time lag exists relative to direct Earth surface measurements. To verify this monthly difference, data from the UK Hadley Centre (HAD) (Met Office [37], Osborn et al. [38], Met Office [39], Kennedy et al. [40]) are used in this study.

As an indicator of water vapor of the earth surface, global specific humidity (G-SpHm) from HAD (Met Office [41], Willett et al. [42], Smith et al. [43], Willett et al. [44-45], Freeman et al. [46]) was used. Specific humidity represents the amount of water vapor per unit mass of air and is generally the most suitable indicator for evaluating actual water vapor content within the range typically available.

Monthly G-SpHm data is provided in NC files. PANOPLY [47] from NASA-GISS was used to convert it into text data. From the resulting text files, the "q_anoms" text file was selected, and the global monthly averages were calculated.

Indicators of solar activity are derived from NASA Clouds and the Earth's Radiant Energy System (CERES) [48]. The absorbed shortwave influx (ASW) at the top of the atmosphere (TOA), and TSI were used (both all sky) (Loeb et al. [49], Kato et al. [50]). ASW can be considered as the amount of energy entering the atmosphere directly, unobstructed by clouds (cloud albedo). The anomaly of ASW (ASW_Anom) is expressed by the following equation [17].

$$ASW\_Anom = ISF\_Anom - RSW\_Anom \simeq -RSW\_Anom \quad (1)$$

where ISF (Incoming Solar Flux) is a CERES convention of terms. ISF_anom is quite small and negligible. And the equation of the supplement file of Nikolov et al. [17] is referred to. RSW is reflected shortwave solar flux at TOA.

TSI is a long-established indicator of solar activity that shows a consistent correlation with global temperatures [12-14]. The anomaly of TSI (TSI_Anom) is expressed by the following equation [17].

$$TSI\_Anom = 4 \times SWI\_Anom \quad (2)$$

where SWI (Short Wave Incoming flux) is monthly insolation (spherically averaged) at TOA.

Furthermore, to verify the accuracy of the facility's ASW, correlations with albedo (NASA-CERES [51], Doelling et al. [52, 53]) were also confirmed.

Atmospheric CO_2 concentrations were obtained using NOAA's global average (NOAA [54], Lan et al. [55]). Since CO_2 has already been established as a dependent variable of SST (or air temperature) ([18-20, 22-25], Koutsoyiannis et al. [56,57]], multivariate analysis using this value as the dependent variable is not performed in the main text.

2.2 Analysis Methods and Period - Statistical Analysis

Data primarily utilizes anomalies. The absolute values used in this study are atmospheric CO_2, its radiative forcing (supposed), and albedo only. The analysis period spans from 2000 to a maximum of July 2025. The reason for starting in 2000 is due to the commencement year of NASA-CERES data. The analysis was basically conducted using both raw data and a 13-month running mean (13mRM).

Initially, temperature data between UAH and HAD were compared. Overall, it was confirmed that UAH data lags HAD by a few months. This is generally in line with the report by Humlum et al. [20] regardless of the methods.

Next, comparison was made using only UAH data, separately for LST and SST, across both hemispheres and by latitude. This verification confirms that temperature changes at the equator occur first.

Next, the UAH-SST and G-SpHm are compared. Since the oceans are the primary source and sink of water vapor on Earth, confirming the time lag between SST and G-SpHm is essential. This is also because phenomena like El Niño and La Niña occur near the equator. In this process, it was confirmed that tropical SST visually precedes G-SpHm.

Moreover, UAH data lags HAD surface data by several months. Therefore, within the analyzed period, it was confirmed that G-SpHm is a dependent variable of G-SST (or temperature). Based on this result, the monthly difference between UAH global ocean data and G-SpHm was examined using 13mRM (the result is same using raw data). The difference of month was determined as the month yielding the highest Pearson correlation coefficient. The same method was applied for subsequent difference of month verifications.

Next, the phase differences ASW and TSI relative to UAH G-SST were examined. This analysis was conducted using both raw data and 13mRM. CO_2 was analyzed using raw data because no significant time lag relative to G-SST was observed, and 13mRM is not meaningful for CO_2 itself.

Multivariate analysis was then performed considering the differences of month with the highest correlations between each indicator. This involved multiple linear regression analysis with G-SST as the dependent variable and ASW, TSI, and CO_2 as explanatory variables. ASW was included in each model, and three patterns were created based on the presence or absence of TSI and CO_2.

Although atmospheric CO_2 itself has already been identified as a dependent variable of SST [18, 19, 25], this was done to verify its minor, secondary influence. Note that even when CO_2 was converted to radiative forcing (W/m^2) and input into the model, the results were effectively equivalent. This is because, for the CO_2 concentrations during the target period, the converted W/m^2 value changed almost linearly, and its Pearson correlation with the CO_2 concentration itself was virtually 1. Details on this are also added in the Appendix.

The analysis excluding TSI from the explanatory variables is conducted for verification purposes.

As shown in the results, the precision of multivariate analysis using raw data was unsatisfactory. Therefore, analysis was performed using data from a 13mRM, yielding significantly better model precision and highly probable results.

EZR Version 1.61 (Kanda, [58]) and Microsoft® Excel were used for analysis. A P value of ≤ 0.05 was considered statistically significant (two-sided). However, as shown in the results, compared to ASW and TSI, which exhibit extremely high significance (low significance probability), CO_2 was only marginally significant and became a negative explanatory factor in the 13mRM model. Therefore, analysis excluding CO_2 was also conducted. The results in this case correspond to what is described in the abstract. Furthermore, analysis using the Bayesian Information Criterion (BIC) method yielded the same results as when CO_2 was excluded from the beginning.

3. Results

Figure 1 shows only G-LST and G-SST data from UAH and HAD. For both facilities, G-SST leads G-LST.

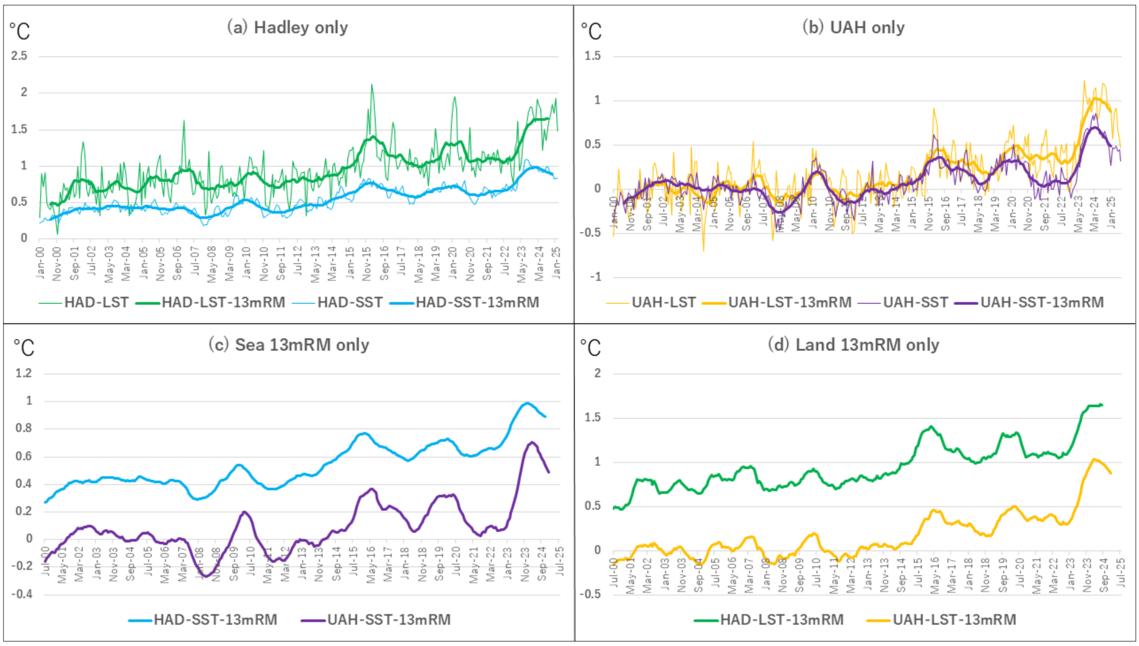

Figure 1: Surface temperature (Hadley Centre) and satellite-derived air temperature (University of Alabama in Huntsville). UAH data shows the difference from the 1991–2020 average, covering January 2000 to July 2025. Hadley shows differences from the 1961–1990 average; LST covers January 2000 to February 2025; SST extends through May 2025. 13mRM is shortened by six months on either end. For clarity, only 13mRM is plotted for comparisons involving only SST or only LST.

Table 1 shows the results of comparing differences of month for each facility's data using only G-SST or only LST. Data from HAD leads by 4 months for G-SST and by 1 month for G-LST.

Table 1: Verification of the time lag between Hadley and UAH temperatures.

All statistically significant using Pearson correlation. Verified using 13mRM. "Plus 1 month" means comparing Hadley data shifted forward by one month. For example, it means comparing January 2000 HAD with February 2000 UAH. The same method applies to subsequent tables.

Difference	−2m	−1m	±0m	+1m	+2m	+3m	+4m	+5m	+6m
Sea	0.853	0.877	0.898	0.912	0.922	0.9268	0.9273	0.923	0.914
Land	0.923	0.938	0.948	0.951	0.949	0.944	0.933	0.919	0.902

Figure 2 shows a comparison using only UAH data. Overall, both SST and LST show a delay in mid-latitudes north or south of the equator and in polar regions compared to the equatorial region. However, certain irregularities are observed, particularly in LST, within the Arctic and Antarctic circles.

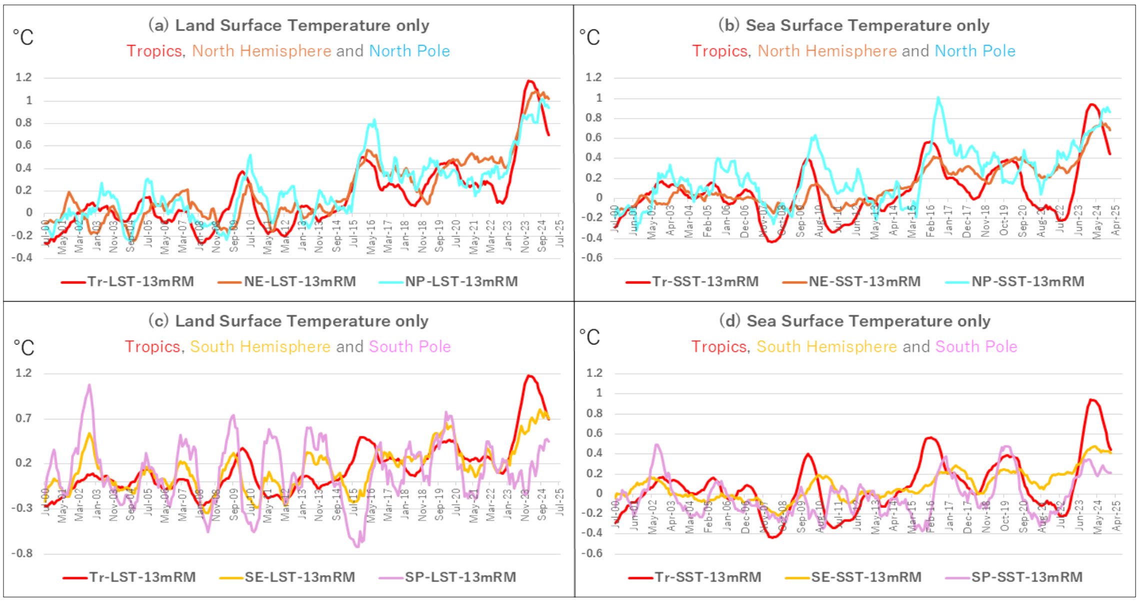

Figure 2: Temperature data from meteorological satellites (UAH), all showing 13mRM. Data reference and time periods are the same as in Figure 1. Classified by land/ocean, tropical/non-tropical, and polar regions. They all represent lower troposphere temperatures. Tropical regions are defined as 20°S to 20°N latitude; non-tropical regions (NE and SE) are 20° to 90° latitude; polar regions are 60° to 90° latitude.

Therefore, the analysis thus far indicates that, in the overall picture, in the atmosphere from the Earth's surface, the temperature change of the equatorial region is leading that of the other areas, and that the ocean temperature change is leading that of the land surface.

Figure 3 compares UAH G-SST and atmospheric CO_2 with G-SpHm.

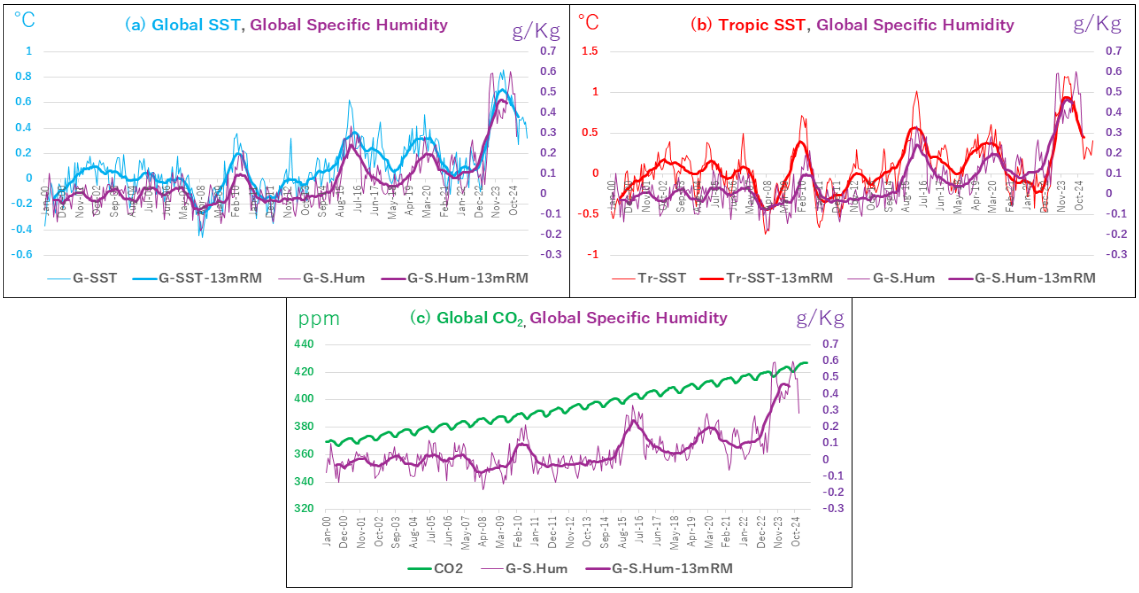

Figure 3: Global SST, tropical SST, global specific humidity, and CO_2. CO_2 is shown as absolute values, from January 2000 to May 2025. The SST reference and period are the same as in Figure 1. Specific humidity is shown as the difference from the 1991–2020 average, from January 2000 to December 2024.

Visually, it was shown that G-SST precedes and dominates G-SpHm. The degree of precedence was more pronounced for equatorial SST (Tr-SST). Moreover, Tr-SST fluctuates independently of the increase in specific humidity observed from 2023 to 2024. Notably, in the raw data, G-SpHm experienced two additional sudden increases from 2023 to 2024, while Tr-SST continued to decline even after October 2024.

As shown in Figure 1(c) and Table 1, HAD-G-SST appears to have declined four months earlier, further confirming this trend. On the other hand, no clear link is observed between G-SpHm and atmospheric CO_2.

Furthermore, as shown in Table 2, the Pearson correlation between G-SST and G-SpHm was highest within the same month (also highest when using raw data). This result is not unnatural, as explained above, given that the HAD-G-SST on the Earth's surface leads the UAH-G-SST by approximately four months.

Table 2: Pearson correlation between G-SST and G-SpHm, all statistically significant.

Difference	−3m	−2m	−1m	±0m	+1m	+2m	+3m
Pearson correlation	0.876	0.900	0.912	0.919	0.917	0.908	0.892

Figure 4 shows G-SST, ASW, TSI, and CO_2. Visually, ASW shows relatively high correlation with G-SST. TSI, on the other hand, shows moderate correlation. CO_2 rises linearly, independent of G-SST fluctuations. In addition, Figure 4(d) shows the correlation between ASW and albedo. It is evident that the accuracy of albedo measurements remains consistent alongside ASW, despite significant albedo variations.

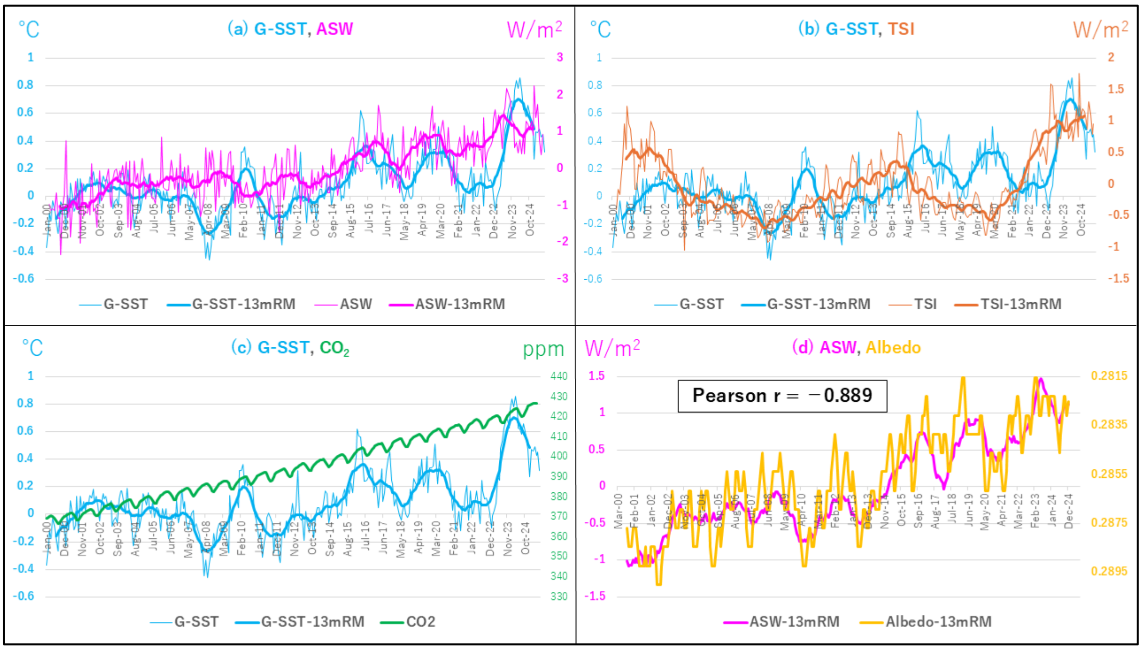

Figure 4: Global SST, ASW, TSI, CO_2, and Albedo. CO_2 and Albedo are absolute values. The Albedo axis is inverted. The SST baseline and period are the same as in Figure 1. The ASW and TSI values represent the difference from the average from March 2000 to July 2024, with the period being March 2000 to June 2025. Albedo is from March 2000 to May 2025 (shortened by 6 months at each end due to 13mRM).

Table 3 shows the correlation between G-SST and the monthly lag of ASW and TSI. ASW led UAH-G-SST by 7 months, while TSI led by 13–14 months. The time lag of the global impact from ASW and TSI can actually be considered about 4 months shorter than these values (due to the time lag with HAD-G-SST mentioned above).

For CO_2, the raw data shows the highest correlation two months prior (and become equivalent to the same month at the three months prior). However, since CO_2 itself has no significant link to G-SST, this can be considered coincidental. Therefore, CO_2 is considered to have no time lag relative to G-SST and is used in the analysis.

Table 3: Pearson Correlation between G-SST and Each Indicator. Examined using raw data and 13mRM. All statistically significant.

	Difference	−2m	−1m	±0m	+1m	+2m	+3m	+4m	+5m	+6m
Raw Data	ASW	0.430	0.464	0.386	0.502	0.523	0.565	0.572	0.562	0.573
	TSI	0.282	0.300	0.332	0.363	0.388	0.408	0.408	0.395	0.394
	CO_2	0.581	0.579	0.578	0.573	0.569	0.568	0.568	0.565	0.563
Raw Data	Difference	+7m	+8m	+9m	+10m	+11m	+12m	+13m	+14m	+15m
	ASW	0.588	0.570	0.562	0.503	0.490	0.476	0.472	0.474	0.454
	TSI	0.391	0.405	0.423	0.453	0.465	0.477	0.479	0.470	0.454
	CO_2	0.562	0.563	0.562	0.559	0.552	0.549	0.544	0.546	0.548
13mRM	Difference	−2m	−1m	±0m	+1m	+2m	+3m	+4m	+5m	+6m
	ASW	0.653	0.668	0.683	0.695	0.706	0.718	0.727	0.734	0.739
	TSI	0.411	0.429	0.447	0.461	0.474	0.487	0.500	0.514	0.526
	CO_2	0.635	0.639	0.643	0.640	0.638	0.636	0.633	0.631	0.628
13mRM	Difference	+7m	+8m	+9m	+10m	+11m	+12m	+13m	+14m	+15m
	ASW	0.742	0.741	0.736	0.727	0.716	0.703	0.690	0.673	0.656
	TSI	0.538	0.550	0.562	0.572	0.581	0.587	0.590	0.590	0.588
	CO_2	0.626	0.624	0.623	0.622	0.622	0.622	0.623	0.625	0.626

Figure 5 shows the ASW and TSI corrected for monthly differences relative to G-SST. Visually, the correlation becomes clearer when using a 13mRM, where the values stabilize.

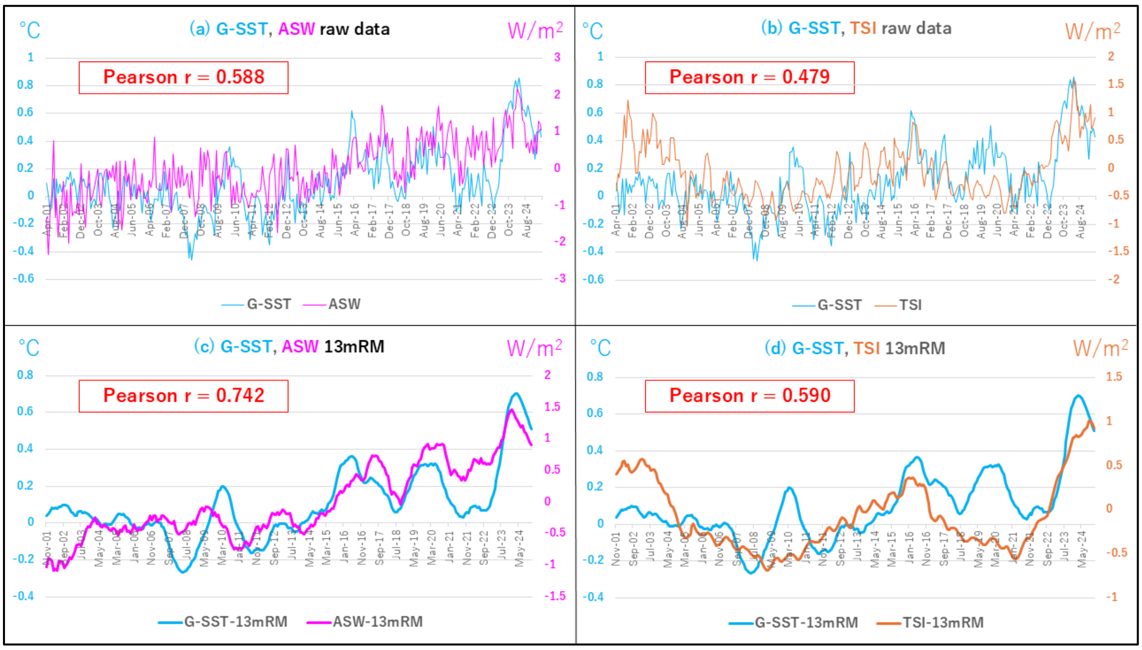

Figure 5: G-SST, ASW, and TSI after time lag adjustment. The graph is thinned to account for overlap and detail in the raw data. The correlation coefficients are according to Table 3.

Table 4 shows the results of multiple linear regression analysis using raw data with G-SST as the objective variable. In this case, even the model including all factors only achieved moderate accuracy (R^2=0.512). Moreover, the accuracy of Model 3, which excludes TSI, is poor (R^2=0.372).

Furthermore, consistent with the subsequent analysis using the 13mRM, in models including CO_2, the P value for the constant increases compared to ASW and TSI. Model 2, which excludes CO_2, is overwhelmingly superior in terms of significance probability for ASW, TSI, and the constant term, while also achieving accuracy comparable to Model 1. Furthermore, the presence or absence of CO_2 primarily affects the results of the numerical value of constant and the regression coefficient of the ASW.

Table 4: Results of multiple linear regression analysis using raw data. The objective variable is G-SST. β is the standardized regression coefficient. VIF is the Variance Inflation Factor.

Model	Model R^2	Variables	Regression Coefficient	β	P	VIF
Model1	0.512 P=2.74e-44	Constant ppm	−1.310	---	1.39e-4	---
		ASW °C/(W/m²)	0.098	0.334	4.22e-08	2.06
		TSI °C/(W/m²)	0.179	0.381	2.07e-17	1.03
		CO_2 °C/ppm	0.004	0.249	3.55e-5	2.06
Model2	0.482 P=1.06e-41	Constant ppm	0.114	---	4.01e-26	---
		ASW °C/(W/m²)	0.150	0.510	1.44e-26	1.03
		TSI °C/(W/m²)	0.184	0.392	1.65e-17	
Model3	0.372 P=1.06e-29	Constant ppm	−1.517	---	9.56e-5	---
		ASW °C/(W/m²)	0.110	0.374	5.42e-08	2.05
		CO_2 °C/ppm	0.004	0.283	3.11e-5	

Figure 6 shows the reproduced values based on these models' results. Figure 6 (a) to (c) show comparisons with G-SST. It is difficult to say they are well reproduced. The errors are particularly large in Model 3. Figure 6 (d) was added to make it easier to grasp the difference between Model 1 and Model 2. There is essentially no significant difference between Models 1 and 2. This indicates that incorporating CO_2 as an explanatory variable provides little added value.

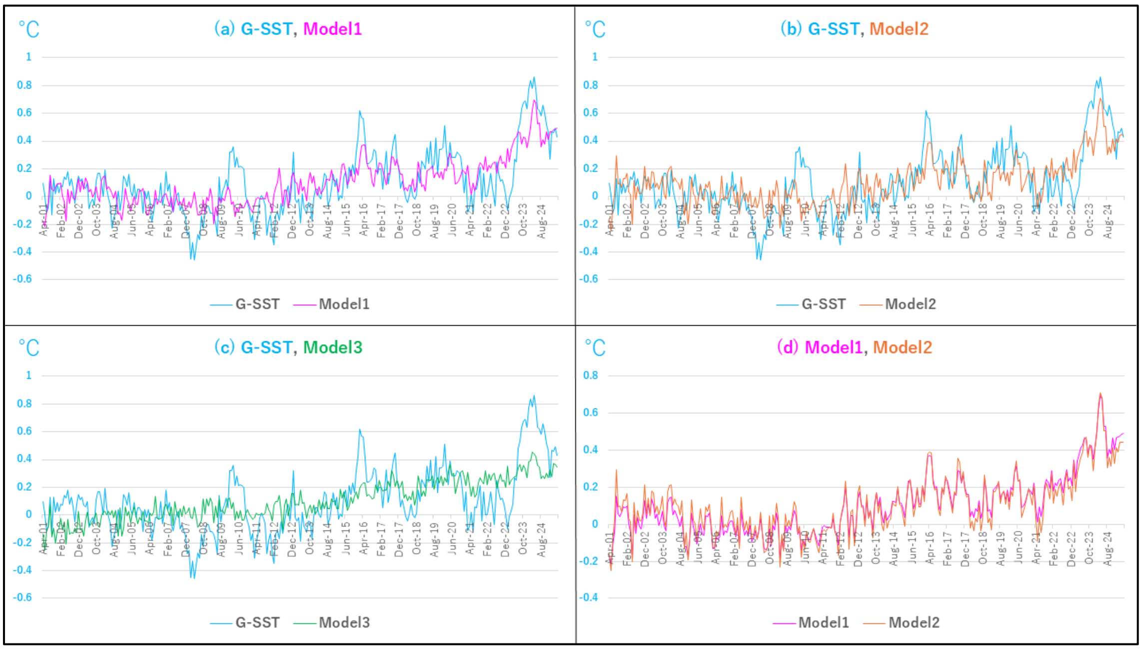

Figure 6: Reproduction of each model based on the results of multivariate analysis using raw data. For example, for Model 1: G-SST_Model 1 = 0.098 x ASW + 0.179 x TSI + 0.004 x CO_2 -1.310

Table 5 shows the results of multiple linear regression analysis using 13mRM data. In all variables included, ASW and TSI were positive explanatory factors for G-SST. Conversely, atmospheric

CO_2 was a negative explanatory factor. However, the significance probability for CO_2 in this case was barely significant and weak compared to the overwhelming influence of the other two indicators.

Furthermore, in the models incorporating CO_2 as an explanatory variable (Models 1 and 3), the significance probability of the constant term is also barely significant. Similar to the analysis using the raw data mentioned above, including CO_2 in the model weakens the significance of the constant. The reason for this, as evident from the variance inflation factor (VIF), is the strong correlation between ASW and CO_2 (Pearson r = 0.897).

Table 5: Results of multiple linear regression analysis using 13mRM data. The objective variable is G-SST. The meaning of the indicators is the same as in Table 4

Model	Model R^2	Variables	Regression Coefficient	β	P	VIF
Model1	0.767 P=2.47e-86	Constant ppm	0.791	---	0.018	---
		ASW °C/(W/m²)	0.253	0.779	8.29e-26	5.24
		TSI °C/(W/m²)	0.220	0.456	1.18e-38	1.04
		CO_2 °C/ppm	−0.002	−0.134	0.043	5.15
Model2	0.764 P=7.96e-87	Constant ppm	0.116	---	1.36e-56	---
		ASW °C/(W/m²)	0.214	0.657	1.78e-62	1.04
		TSI °C/(W/m²)	0.222	0.459	7.60e-39	
Model3	0.568 P=8.35e-51	Constant ppm	1.045	---	0.021	---
		ASW °C/(W/m²)	0.298	0.918	5.75E-21	5.14
		CO_2 °C/ppm	−0.002	−0.188	0.037	

On the other hand, Model 2, which excluded CO_2 from the outset, showed significantly improved significance for the constant while maintaining equivalent model accuracy (even better in terms of p-values). Notably, when using the BIC method in Model 1, which includes all three factors from the start, the results match those of Model 2. Overall, it was also demonstrated that the accuracy of Model 2, combining ASW and TSI, is the best.

As clearly shown in Figure 4(c), these results are reasonable since CO_2 does not show a clear link with G-SST. When predicting G-SST using only ASW (13mRM) as the explanatory variable, Model R^2 = 0.561 (including the constant). When predicting G-SST using only TSI (13mRM) as the explanatory variable, Model R^2 = 0.348 (including the constant).

Figure 7 shows the reproduced values based on the results in Table 5. As clearly shown in Figure 7(d), the model including ASW and TSI demonstrates substantially equivalent reproduced values regardless of whether CO_2 is included. On the other hand, as mentioned above, removing CO_2 from the model (Model 2) strengthens the significance of all factors without changing the model's accuracy. This suggests CO_2 is not needed as an explanatory factor. Therefore, these results demonstrate that CO_2, a byproduct of preceding SST, has virtually no explanatory power for G-SST, even secondarily.

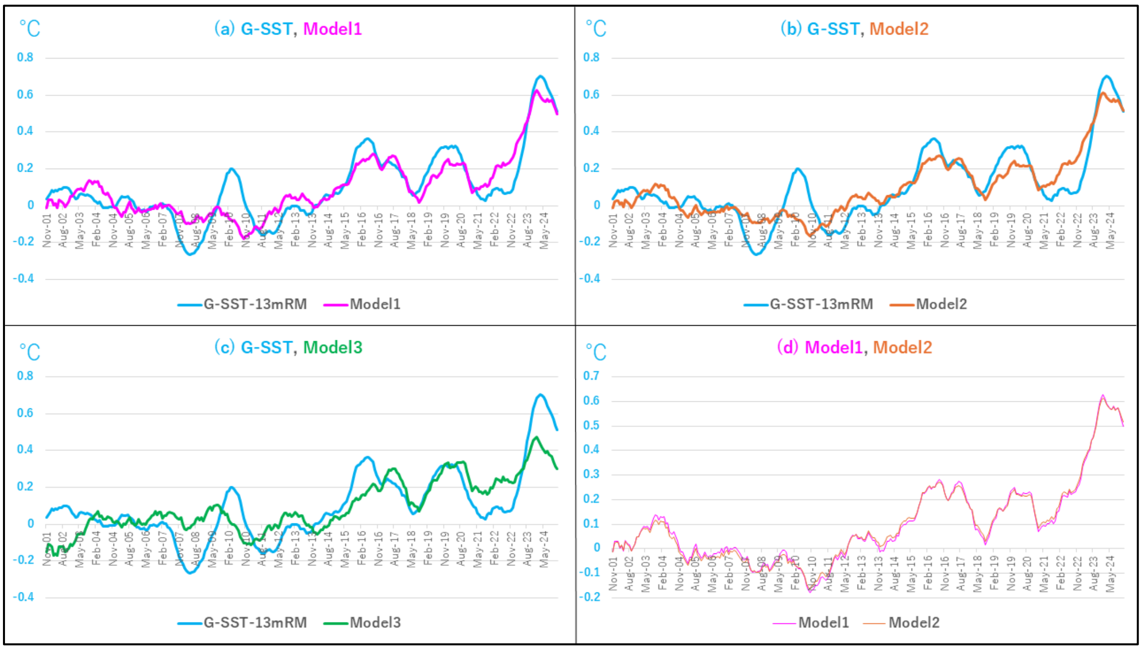

Figure 7: Reproduction of each model based on the results of multivariate analysis using 13mRM data.

Finally, Figure 8 shows the G-SST, Model 2, and Model 3 data extracted from Figure 7. The difference resulting from adding TSI on ASW in the model is clear.

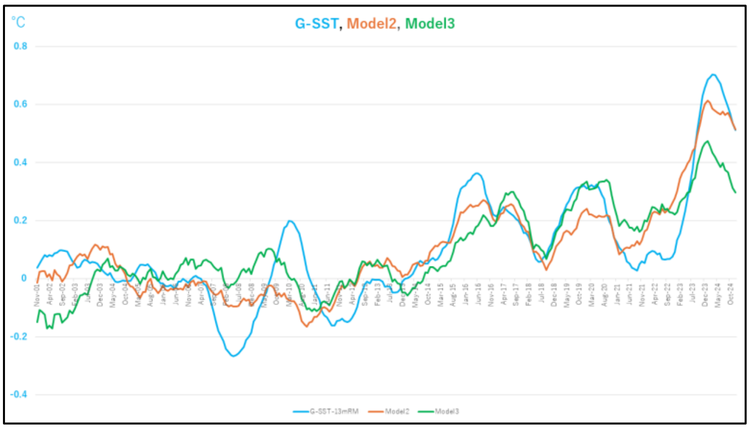

Figure 8: Data of G-SST, Model 2 and Model 3 in Figure 7

Furthermore, a brief explanation is provided demonstrating that correlation between the ASW and TSI with G-SST used in this study is not spurious in the Appendix.

4. Discussion

The two verifications of this study were achieved. First, it was confirmed that water vapor, the primary contributor to the greenhouse effect on Earth, has been a dependent variable of global SST at least since the year 2000. Although water vapor content increased to a certain extent from 2023 to 2024, it was not the primary cause of the abrupt warming. The impact of the Tonga Hunga eruption [30, 31] is effectively ruled out. The magnitude of the relatively anomalous changes in G-SpHm in 2023 and 2024 were insufficient to exert such an influence. A plausible reason is that the change was only a few percent relative to the absolute relative humidity levels in the tropics and mid-latitudes (e.g. 10–20 g/kg).

Furthermore, multivariate analysis confirmed that the combination of leading ASW and TSI most effectively predicts G-SST since 2000. The sequence of influence on Earth's climate is as follows:

solar activity and albedo determine Earth's SST and air temperature, and SST then exclusively determines G-SpHm. Compared to these two indicators (ASW and TSI), the influence of atmospheric CO_2 was confirmed to be effectively negligible. In other words, through this two-step verification, the positive feedback theory of anthropogenic global warming was also rejected. This report is the first to eliminate the positive feedback theory using a combination of multivariate analysis and phase-analysis.

Moreover, it is already understood that ΔCO_2 is a dependent variable of the preceding earth temperature [18-20, 23-25, 57, 58]. And the results of this study mean that it is effectively impossible to demonstrate any secondary effects.

On the other hand, this study observed discrepancies to a certain extent between raw data and 13mRM analysis. This likely stems from the short-term instability of solar activity indicators. Meanwhile, CO_2 shows a linear increase over the long term, so its appearance of correlation with G-SST had a certain degree of influence on the results of the multiple regression analysis. However, stabilizing the solar activity indicator using the 13mRM drastically altered the results. Furthermore, when CO_2 was included in the model, it became a negative determining factor. Excluding CO_2 yields a more robust model, making this result the most plausible.

Among the solar activities examined this time, the 13mRM data showed that TSI has a slightly lower influence than ASW in terms of the standardized regression coefficient (β). However, statistics suggest that TSI also exerts a significant influence if the time lag with SST is considered reasonable. On the other hand, regarding model accuracy (R^2), while ASW alone achieves about 56 % (about 35 % predicted by TSI only), adding TSI increases this by about 20 %. From this perspective, ASW can be said to have three times the explanatory power compared to TSI.

However, the estimated G-SST change values per standard deviation for ASW and TSI are 0.126 °C and 0.088 °C, respectively (by the result of Model 2 in Table 5, data not shown in the results section), indicating that the impact of TSI is not insignificant either. Therefore, it is conceivable that ASW represents short-term fluctuating factors, while TSI represents medium-term gravitational forces.

There was no significant difference in the correlation between atmospheric CO_2 and specific humidity across months (not shown in the Results Section; Pearson correlation coefficient approximately 0.72). However, the correlation coefficient exhibits subtle annual periodicity, suggesting seasonal variations due to temperature changes. This perspective also suggests a consistency between ocean-origin water vapor and CO_2 fluctuations.

Furthermore, the results remain equivalent when global temperature (Globe, provided by UAH) is used as the objective variable in the multivariate analysis (Model 2, $R^2 = 0.764$, P = 7.96e-87, not shown in the Results section). This result is reasonable given the extremely high correlation coefficient between Globe and G-SST provided by UAH (Pearson r = 0.977).

This study showed differences from the results of the recent pioneering study by Nikolov et al. [17], particularly regarding the impact of TSI. This is considered to be due to differences in the temperature data used, the analytical methods, and the time periods examined. This study used only G-SST from the UAH dataset as the objective variable. The prediction method employed multiple linear regression analysis. While current knowledge suggests ASW exerts the greatest influence, the results indicate that the impact of TSI varies depending on the temperature dataset used. Moreover, the impact of these two factors may change as more data is accumulated in the future.

On the other hand, Nikolov [17] et al. propose, using fundamental physics methods, that the representative temperatures of each planet in the solar system depend on representative atmospheric pressure and incoming solar energy, irrelevant to gas composition. Their study physically refutes the positive feedback theory. Furthermore, this study statistically demonstrates that current CO_2 and specific humidity levels have virtually no effect on Earth's temperature. Therefore, these reports are similar in terms of rejecting the positive feedback theory. However, it cannot be ruled out that the methods of Nikolov and the author (Ato) may be unable to detect the minute effects of the greenhouse effect caused by each gas component in the actual climate system of Earth.

Realistically, the definition and calculation of global average temperature (GAT) inherently pose difficulties (Essex et al. [59]). However, when a global temperature indicator calculated under certain rules shows consistent correlation with other indicators and a mechanism can be assumed, it can be considered to have a certain degree of plausibility. As announced in the Materials and Methods section, points regarding the temperature databases of each facility and the concept of the GAT indicator are added to the Appendix.

In this study, the two primary indicators of solar activity demonstrated overwhelming predictive power. As for other possible factors, Soon [60] explained in a recent presentation that changes in overall albedo including ocean colour, land surface, and atmosphere could be a possibility. Furthermore, he also pointed out the limitation of measuring clouds itself because they are always changing. Naturally, a certain degree of scepticism regarding the objectivity of solar activity and cloud indicators is warranted. On the other hand, as shown in Figure 4(d) above, ASW and albedo exhibit a high correlation. Therefore, it seems reasonable to conclude that the results possess sufficient precision to withstand verification, including statistical analysis.

5. Conclusion

When using UAH-G-SST as the global representative temperature, the dominant determining factors were ASW and TSI. The secondary influence of CO_2 on SST, as a dependent variable of preceding SST, was found to be virtually negligible through multivariate analysis. Furthermore, the impact of TSI on global temperature was suggested to potentially vary depending on the temperature database used for evaluation.

Solar activity was also the dominant driver of the sudden warming in 2023 and 2024. The Tonga Hunga eruption and increased water vapor due to El Niño were not the main causes. The increase in water vapor levels over these two years had virtually no observable impact on the global temperature, and specific humidity was a dependent variable of the preceding G-SST.

These results indicate that from 2000 to the present, the dominant factors driving climate change have been solar activity and cloud variations by reducing albedo in the sky during the period. Consequently, the anthropogenic theory of global warming and the positive feedback theory are denied, according to the data of worldwide prominent climate research institutes. Furthermore, since human influence remains negligible even in the 21st century, the same holds true for the past.

Funding

The author did not receive any funding of the work.

Declaration of Competing Interest

The author declares no conflict of interest. Dai Ato, an autonomous and private researcher, authored this article as an academic activity based on the guaranteed right of freedom in an academy for the Japanese (Article 23) and the Supreme Law provided in Article 98 of the Constitution of Japan.

Co-Editor: Stein Storlie Bergsmark. **Reviewers:** Anonymous.

Acknowledgements

I extend my gratitude to the experts who provided the impetus for this research, its conception, and insights for its analysis, as well as to all data-providing institutions.

Data Availability

Dataset used in this study is available as a supplement file (Spread sheet, uploaded on Ato's page in Research Gate, https://www.researchgate.net/profile/Dai-Ato).

References

1. Thatcher M., 2002: Statecraft: Strategies for a Changing World
2. IPCC, 2021: Masson-Delmotte V., Zhai P., Pirani A. et al.: Climate Change 2021: *The Physical Science Basis. Contribution of Working Group I to the Sixth Assessment Report of the Intergovernmental Panel on Climate Change*, Sixth Assessment Report (AR6), Cambridge University Press.
3. GLOBAL CLIMATE INTELLIGENCE GROUP: *World Climate Declaration, There is no climate emergency*, https://clintel.org/world-climate-declaration/
4. CO_2 Coalition*: Providing the facts about CO_2 and climate change*, https://co2coalition.org/
5. European Climate Realist Network: https://ecr.network/
6. *Clima, una petizione controcorrente*, 2019: https://opinione.it/cultura/2019/06/19/redazione_riscaldamento-globale-antropico-clima-inquinamento-uberto-crescenti-antonino-zichichi/?altTem plate=Stampa&fbclid=IwAR1YAoqulAKKXJTY-uzRf SE-aXG6NRpVOckp3nVE7iiTAgOQu8DMHGUxRnE
7. Department of Energy, 2025: *A Critical Review of Impacts of Greenhouse Gas Emissions on the U.S. Climate*, https://www.regulations.gov/docket/DOE-HQ-2025-0207
8. IPCC, 2007: Climate Change 2007 - *The Physical Science Basis Contribution of Working Group I to the Fourth Assessment Report of the IPCC* (ISBN 978 0521 88009-1 Hardback; 978 0521 70596-7 Paperback), https://www.ipcc.ch/report/ar4/syr/
9. IPCC, 2013: Climate Change 2013: The Physical Science Basis. Contribution of Working Group I to the Fifth Assessment Report of the Intergovernmental Panel on Climate Change [Stocker, T.F., Qin D., Plattner G.-K., Tignor M., Allen S.K., Boschung J., Nauels A., Xia Y., Bex V. and Midgley P.M. (eds.)]. Cambridge University Press, Cambridge, United Kingdom and New York, NY, USA, 1535 pp., https://www.ipcc.ch/report/ar5/wg1/
10. Clauser J.F., 2024: *Nobel laureate John Clauser's ICSF/CLINTEL Lecture*, https://www.youtube.com/watch?v=Nd2GIx1tX8A
11. Grok 3 beta, Cohler J., Legates D., Soon F., Soon W., 2025: *A Critical Reassessment of the Anthropogenic CO_2-Global Warming Hypothesis: Empirical Evidence Contradicts IPCC Models and Solar Forcing Assumptions*, Science of Climate Change Vol. 5.1 (2025) pp. 13 – 28, https://doi.org/10.53234/SCC202501/06
12. Soon W.W.-H., 2005: *Variable solar irradiance as a plausible agent for multidecadal variations in the Arctic-wide surface air temperature record of the past 130 years*, Geophysical Research Letters 32, 2005GL023429. https://doi.org/10.1029/2005GL023429
13. Soon W., Connolly R., Connolly M., Akasofu S., Baliunas S., Berglund J., Bianchini A., Briggs W.M., Butler C.J., Cionco R.G., Crok M., Elias A.G., Fedorov V.M., Gervais F., Harde H., Henry G.W., Hoyt D.V., Humlum O., Legates D.R., Lupo A.R., Maruyama S., Moore P., Ogurtsov M., ÓhAiseadha C., Oliveira M.J., Park S., Qiu S., Quinn G., Scafetta N., Solheim J.E., Steele i., Szarka L., Tanaka H.L., Taylor M.K., Vahrenholt F., Herrera

V.M.V., Zhang W., 2023: *The Detection and Attribution of Northern Hemisphere Land Sur face Warming (1850–2018) in Terms of Human and Natural Factors: Challenges of Inadequate Data*, Climate 2023, 11(9), 179, https://doi.org/10.3390/cli11090179

14. Grabyan R., 2025: *Global Atmospheric CO_2 Lags Temperature by 150 yr between 1 and 1850 AD*, Science of Climate Change Vol. 5.3 (2025) pp. 35-80, https://doi.org/10.53234/scc202510/04
15. Svensmark H., Pedersen J.O.P, Marsh N.D., Enghoff M.B., Uggerhøj U.I., 2006: *Experimental evidence for the role of ions in particle nucleation under atmospheric conditions*, Proc. R. Soc. A.463385–396,http://doi.org/10.1098/rspa.2006.1773
16. Miyahara H., Kusano K., Kataoka R., Shima S., Touber E., 2023: *Response of high altitude clouds to the galactic cosmic ray cycles in tropical regions*. Front. Earth Sci. 11:1157753. http://doi.org/10.3389/feart.2023.1157753
17. Nikolov N., Zeller K.F., 2024: *Roles of Earth's Albedo Variations and Top-of-the-Atmosphere Energy Imbalance in Recent Warming: New Insights from Satellite and Surface Observation*s, Geomatics 2024, 4(3), 311-341, https://doi.org/10.3390/geomatics4030017
18. Ato D., 2024: *Multivariate Analysis Rejects the Theory of Human-caused Atmospheric Carbon Dioxide Increase: The Sea Surface Temperature Rule*s, Science of Climate Change Vol. 4.2 (2024) pp. 1-15, https://doi.org/10.53234/SCC202407/19
19. Ato D., 2025: *Pitfalls in Global Warming and Climate Change Research: Flaws in Ice Core Reconstructions of Atmospheric CO_2 - The Naked King of 280 ppm at the Industrial Revolution*, Science of Climate Change Vol.5, Issue.1, pp.1-30, https://doi.org/10.53234/scc202501/04
20. Humlum O., Stordahl K., Solheim J.E., 2013: *The phase relation between atmospheric car bon dioxide and global temperature*, Global and Planetary Change 100 (2013) 51–69 https://doi.org/10.1016/j.gloplacha.2012.08.008
21. Koutsoyiannis D., 2024: *Net Isotopic Signature of Atmospheric CO_2 Sources and Sinks: No Change since the Little Ice Age*, Sci 2024, 6(1), 17, https://doi.org/10.3390/sci6010017
22. Berry E.X., 2023: *Nature Controls the CO_2 Increase*, Science of Climate Change, Vol. 3.1 (2023), pp. 68-91, https://doi.org/10.53234/scc202301/21
23. Salby M., Harde H., 2022: *Theory of Increasing Greenhouse Gases*, Science of Climate Change, Vol. 2.3 (2022) pp. 212-238, https://doi.org/10.53234/scc202212/17
24. Roth E., 2025: *About the Origin of CO_2 in the Atmosphere: Some Annotations to a Study of the CO_2 Coalition*, Science of Climate Change, Vol. 5.1 (2025) prelim. pp. 1-14, https://doi.org/10.53234/scc202501/05
25. Robbins B., 2025: *Atmospheric CO_2: Exploring the Role of Sea Surface Temperatures and the Influence of Anthropogenic CO_2*, Science of Climate Change, Vol. 5.1 (2025) pp. 86-102, https://doi.org/10.53234/scc202504/23
26. Jaworowski Z., Segalstad T.V., Hisdal V., 1992: *Atmospheric CO2 and global warming: a critical review*. 2nd edition, 1992, https://www.researchgate.net/publication/307215789_Atmospheric_CO2_and_global_warming_a_critical_review_2nd_edition
27. Jaworowski Z., Segalstad T.V., Ono N., 1992: *Do glaciers tell a true atmospheric CO_2 story?* The Science of The Total Environment 114(12):227-284, https://doi.org/10.1016/0048-9697(92)90428-U
28. Jaworowski Z., 1994: *Ancient atmosphere- Validity of ice records*, Environ. Sci. & Pollut. Res. 1, 161–171 (1994), https://doi.org/10.1007/BF02986939
29. Schmidt G., 2024*: Climate models can't explain 2023's huge heat anomaly - we could be in uncharted territory*, Nature 627, 467 (2024), https://doi.org/10.1038/d41586-024-00816-z

30. Vömel H., Evan S., Tully M., 2022: *Water vapor injection into the stratosphere by Hunga Tonga-Hunga Ha'apai*.Science377,1444-1447(2022), https://doi.org/10.1126/science.abq2299

31. Vinós J., Curry J., 2024: *Hunga Tonga volcano: impact on record warming*, https://judithcurry.com/2024/07/05/hunga-tonga-volcano-impact-on-record-warming/

32. Spencer R.: *Latest Global Temps*, https://www.drroyspencer.com/latest-global-temperatures Accessed on 28, August 2025

33. NOAA Microwave Sounding Temperature Assessment System: https://www.star.nesdis.noaa.gov/smcd/emb/mscat/products.php Accessed 29, August 2025

34. Remote Sensing Systems: https://images.remss.com/msu/msu_time_series.html, Accessed 29, August 2025

35. Katata G., Connolly R., O'Neill P., 2023: *Evidence of Urban Blending in Homogenized Temperature Records in Japan and in the United States: Implications for the Reliability of Global Land Surface Air Temperature Data*, J. Appl. Meteorol. Climatol. 2023, 62, 1095–1114. https://doi.org/10.1175/JAMC-D-22-0122.1

36. Spencer R.W., Christy J.R., Braswell W.D., 2025: *Urban Heat Island Effects in U.S. Summer Surface Temperature Data*, 1895–2023, J. Appl. Meteorol. Climatol. 2025, 64, 717–728, https://doi.org/10.1175/JAMC-D-23-0199.1

37. Met Office Hadley Centre observations datasets: CRUTEM.5.0.2.0 Data Download: https://www.metoffice.gov.uk/hadobs/crutem5/data/CRUTEM.5.0.2.0/download.html Accessed 27, August 2025

38. Osborn T.J., Jones P.D., Lister D.H., Morice C.P., Simpson I.R., Harris I.C., 2020: *Land surface air temperature variations across the globe updated to 2019: the CRUTEM5 dataset*, J. Geophys. Res., https://doi.org/10.1029/2019JD032352

39. Met Office Hadley Centre observations datasets: HadSST.4.1.1.0 Data: download: https://www.metoffice.gov.uk/hadobs/hadsst4/data/download.html, Accessed 6, July 2025

40. Kennedy J.J., Rayner N.A., Atkinson C.P., Killick R.E., 2019: *An Ensemble Data Set of Sea Surface Temperature Change from 1850: The Met Office Hadley Centre HadSST.4.0.0.0 Data Set*. Journal of Geophysical Research: Atmospheres, 124., https://doi.org/10.1029/2018JD029867

41. Met Office Hadley Centre observations datasets: HadISDH.blend data download - version 1.5.1.2024f: https://www.metoffice.gov.uk/hadobs/hadisdh/downloadBLEND.html, Accessed 28, June 2025

42. Willett K.M., Dunn R.J.H., Thorne P.W., Bell S., de Podesta M., Parker D.E., Jones P.D., Williams Jr. C.N., 2014: *HadISDH land surface multi-variable humidity and temperature record for climate monitoring*, Clim. Past, 10, 1983-2006, https://doi.org/10.5194/cp-10-1983-2014

43. Smith A., Lott N., Vose R., 2011: *The Integrated Surface Database: Recent Developments and Partnerships*. Bulletin of the American Meteorological Society, 92, 704\u2013708, https://doi.org/10.1175/2011BAMS3015.1

44. Willett K.M., Williams Jr. C.N., Dunn R.J.H., Thorne P.W., Bell S., de Podesta M., Jones P.D., Parker D.E., 2013*: HadISDH: An updated land surface specific humidity product for climate monitoring. Climate of the Past*, 9, 657-677, https://doi.org/10.5194/cp-9-657-2013

45. Willett K.M., Dunn R.J.H., Kennedy J.J., Berry D.I., 2020: *Development of the HadISDH marine humidity climate monitoring dataset*. Earth System Science Data. 12, 2853-2880, https://doi.org/10.5194/essd-12-2853-2020

46. Freeman E., Woodruff S.D., Worley S.J., Lubker S.J., Kent E.C., Angel W.E., Berry D.I.,

Brohan P., Eastman R., Gates L., Gloeden W., Ji Z., Lawrimore J., Rayner N.A., Rosenhagen G., Smith S.R., 2016: *ICOADS Release 3.0: A major update to the historical marine climate record*. Int. J. Climatol. 37: 2211–2232, https://doi.org/10.1002/joc.4775

47. NASA-GISS: Panoply Data Viewer, https://www.giss.nasa.gov/tools/panoply/download/, Accessed 4, July 2025

48. NASA-CERES, CERES_EBAF-TOA_Ed4.2.1 Subsetting and Browsing: https://ceres-tool.larc.nasa.gov/ord-tool/jsp/EBAFTOA421Selection.jsp, Accessed 28, August 2025

49. Loeb N.G., Doelling D.R., Wang H., Su W., Nguyen C., Corbett J.G., Liang L., Mitrescu C., Rose F.G., Kato S., 2018: *Clouds and the Earth's Radiant Energy System (CERES) Energy Balanced and Filled (EBAF) Top-of-Atmosphere (TOA)* Edition-4.0 Data Product. J. Climate, 31, 895-918, https://doi.org/10.1175/JCLI-D-17-0208.1

50. Kato S., Rose F.G., Rutan D.A., Thorsen T.J., Loeb N.G., Doelling D.R., Huang X., Smith W.L., Su W., Ham S.-H., 2018: *Surface irradiances of Edition 4.0 Clouds and the Earth's Radiant Energy System (CERES) Energy Balanced and Filled (EBAF) data product*, J. Climate, 31, 4501-4527, https://doi.org/10.1175/JCLI-D-17-0523.1

51. NASA-CERES, CERES_SYN1deg_Ed4.2 Subsetting and Browsing: https://ceres-tool.larc.nasa.gov/ord-tool/jsp/SYN1degEd42Selection.jsp Accessed 28, August 2025

52. Doelling D.R., Loeb N.G., Keyes D.F., Nordeen M.L., Morstad D., Nguyen C., Wielicki B.A., Young D.F., Sun M., 2013: *Geostationary Enhanced Temporal Interpolation for CERES Flux Products*, Journal of Atmospheric and Oceanic Technology, 30(6), 1072-1090., https://doi.org/10.1175/JTECH-D-12-00136.1

53. Doelling D.R., Sun M., Nguyen L.T., Nordeen M.L., Haney C.O., Keyes D.F., Mlynczak P.E., 2016: *Advances in Geostationary-Derived Longwave Fluxes for the CERES Synoptic (SYN1deg) Product*, Journal of Atmospheric and Oceanic Technology, 33(3), 503-521., https://doi.org/10.1175/JTECH-D-15-0147.1

54. NOAA Global Monitoring Laboratory: *Trends in Atmospheric Carbon Dioxide (CO_2)*: https://gml.noaa.gov/ccgg/trends/gl_data.html, Accessed 27, August 2025

55. Lan X., Tans P. and Thoning K.W., 2025: *Trends in globally-averaged CO2 determined from NOAA Global Monitoring Laboratory measurements*. Version 2025-09, https://doi.org/10.15138/9N0H-ZH07

56. Koutsoyiannis D., Kundzewicz Z.W., 2020: *Atmospheric Temperature and CO_2: Hen - Or Egg Causality*? Sci 2020, 2(4), 83, https://doi.org/10.3390/sci2040083

57. Koutsoyiannis D., Onof C., Kundzewicz Z.W., Christofides A., 2023: *On Hens, Eggs, Temperatures and CO_2: Causal Links in Earth's Atmosphere*, Sci 2023, 5(3), 35; https://doi.org/10.3390/sci5030035

58. Kanda Y., 2013: *Investigation of the freely available easy-to-use software 'EZR' for medical statistics*, Bone Marrow Transplantation 2013: 48, 452–458, https://doi.org/10.1038/bmt.2012.244

59. Essex C., McKitrick R., Andresen B., 2007: *Does a Global Temperature Exist?*, Journal of Non-Equilibrium Thermodynamics, Volume 32, Issue 1, pp.1-27, https://doi.org/10.1515/JNETDY.2007.001

60. Soon W., 2025: *How well can we measure the Earth's energy budget?*, DDP, July 5, 2025 Tucson, AZ, https://www.youtube.com/watch?v=tI0qmV2Bbc8, Accessed 12, July 2025

Appendix

This appendix compiles information that, while not unrelated to the main text, is not its primary focus. And the author (Ato) has previously pointed out the origins of rising atmospheric CO_2 concentrations and the flaws in the reconstruction methods using polar ice cores, which form the fundamental premise of the anthropogenic CO_2 rise theory.

Between previous papers and the writing of this paper, the author realized that understanding the overall picture of the reality could be understood only through basic calculations (carbon isotopes) and thus decided to share this insight. And the main text presents analysis based on time difference adjustments, this approach is also applicable to the author's past research, prompting its inclusion here.

1. Supplemental information for the main text

1.1. Regarding each temperature database and the global average temperature

This study used only UAH as the global temperature indicator. The reason is simply that, apart from UAH, there is concern about the potential for overestimation. As explained in the Materials and Methods section of the main text, besides UAH, the global temperature databases derived from meteorological satellites include NOAA-STAR [33] and RSS [34]. When comparing G-SpHm with temperature in this study, either ocean temperatures, the primary source of water vapor—or an alternative indicator, are necessary. However, RSS does not separately present land and ocean data. NOAA-STAR provides land and ocean data separately but lacks data broken down by latitude. Verifying time differences by latitude is also important.

Furthermore, as a more fundamental reason, data accuracy must also be considered. Nikolov and Zeller [17], who reported a strong correlation between temperature and albedo using 2024 NASA-CERES data, employed the global average temperature derived from non-UAH data. However, as explained in the Materials and Methods, approximately 20 % of the temperature increase observed over the past few decades in surface measurement data is most likely overestimated due to the urban heat island effect [35, 36]. RSS showed a similar warming trend to surface stations (NASA-GISS and Hadley Centre) (Figure A1, cited from their Figure 4 in [17]). At this point, RSS also needs to consider the risk of overestimation. Furthermore, NOAA-STAR data showed a trend positioned between surface data and UAH.

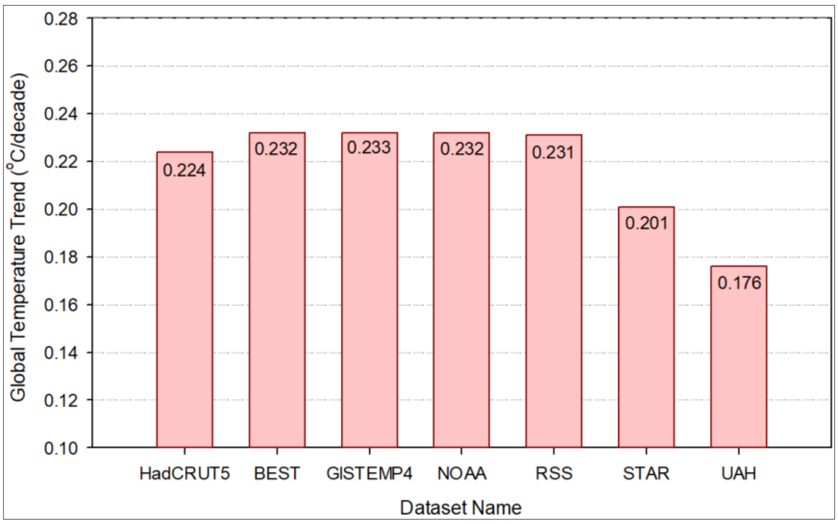

Figure A1: Temperature trend of various datasets, sited from [17]

Therefore, data from NOAA-STAR should be also considered as to the risk of overestimation. Conversely, the trend in UAH data is about 20 % lower than that of Hadley and NASA-GISS data. Thus, from this perspective as well, UAH data has the highest objectivity. For reference, Figure A2 shows UAH, NOAA-STAR, and RSS data since 2000 [32, 33, 34].

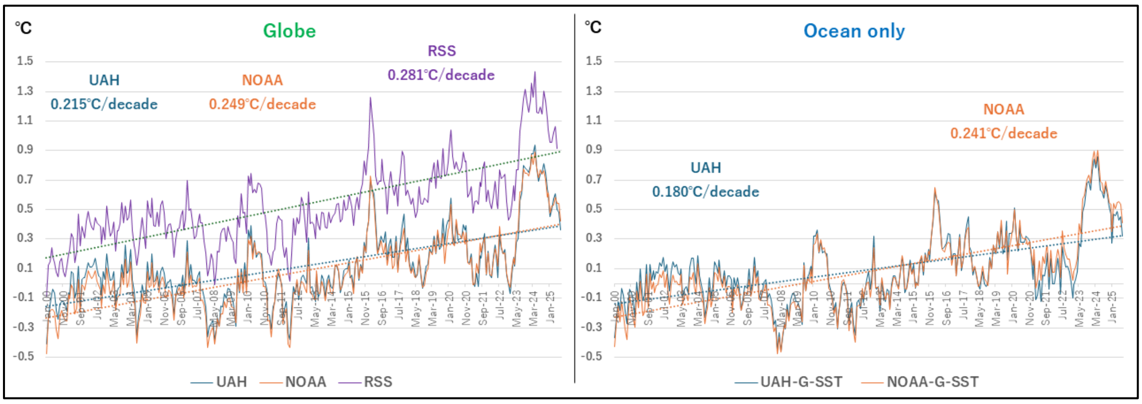

Figure A2: Temperature data from meteorological satellites. UAH and NOAA cover January 2000 to July 2025. RSS covers January 2000 to May 2025. NOAA values show the difference from the average for January 2000 to December 2019. RSS values show the difference from the average for January 1979 to December 1998.

Therefore, considering the type of data required and the fundamental accuracy of the data, UAH was selected as the sole option for this verification.

Here, the author will supplement the actual nature of the figure known as the global average temperature (GAT). Regardless of the point raised in Reference 59, it is fundamentally impossible to perfectly average physical states like temperature. Strictly speaking, temperature presupposes that within a defined range of the measured object (whether a spatial area or a specified point), the state of the gas and temperature within that range are all stable and uniformly the same.

This is possible in a laboratory setting, but impossible in the real world. For instance, temperatures observed just one meter apart can vary drastically depending on whether the area is directly exposed to sunlight or in shade. On the Earth's surface, colour alone can cause extreme variations. Averaging such conditions inherently has limitations.

However, in this age of scientific civilization, it is necessary to continuously evaluate the state of the Earth numerically, within the limits of available time and budget, starting with the highest-priority phenomena. Therefore, some benchmark is required. The same applies to the Earth's temperature. Consequently, certain rules must be established (fixed-point observations at locations minimally affected by artificial influences, over a fixed area and period), and the value obtained must be averaged. Alternatively, if more objective statistical methods exist, they should be fully utilized.

And the numerical values calculated under these consistent rules are referred to as GAT. Furthermore, in recent years, reports showing a strong correlation between the preceding GAT (and G-SST) and ΔCO_2 have been emerging one after another, regardless of the author's (Ato) report. The high correlation between UAH-G-SST and G-SpHm as shown in Figure 3, whose data are derived from independent institutes and different methods, is striking.

Moreover, not limited to this study, indicators of solar activity and global temperature indicators show a consistent correlation. These cannot be considered coincidental. Therefore, the numerical values used as a benchmark for global average temperature should be considered to have a certain degree of plausibility as an indicator for evaluating the state of the Earth. This holds true even if a certain degree of error occurs due to facilities or researchers.

1.2. The failure of the CO_2-dependent model as demonstrated only by data from the past 10,000 years and misperceptions by Dr. Schmidt

Figure A3 shows temperature reconstructions for the Arctic (Badgeley et al. [61]) and Antarctic

(Masson-Delmotte et al. [62]) over the past approximately 10,000 years, atmospheric CO_2 reconstruction data (NOAA [63], Bereiter et al. [64]), and the assumed radiative forcing due to CO_2 (Lightfoot and Mamer [65], Etminan et al. [66]). Temperature is represented by $\delta^{18}O$. Furthermore, since the data from the North Greenland Ice Core Project (NGRIP) has a temporal resolution of 20 years, making comparisons with 100 years ago easier, the change per 100 years is also shown ($\Delta\delta^{18}O$/100y).

It has been reported that CO_2 data from ice cores prior to 1958 are grossly underestimating errors [18, 19, 26-28]. However, since modern anthropogenic CO_2 warming theory is based on these values, the discussion will proceed assuming these values are accurate.

As Figure A3 clearly shows, temperatures indicated by $\delta^{18}O$ fluctuate independently of CO_2 concentrations and the assumed radiative forcing. The NGRIP data is provided at a 20-year time resolution, representing the average of the preceding and following 10-year periods. Therefore, it is self-evident that increasing the time resolution would reveal even greater fluctuations.

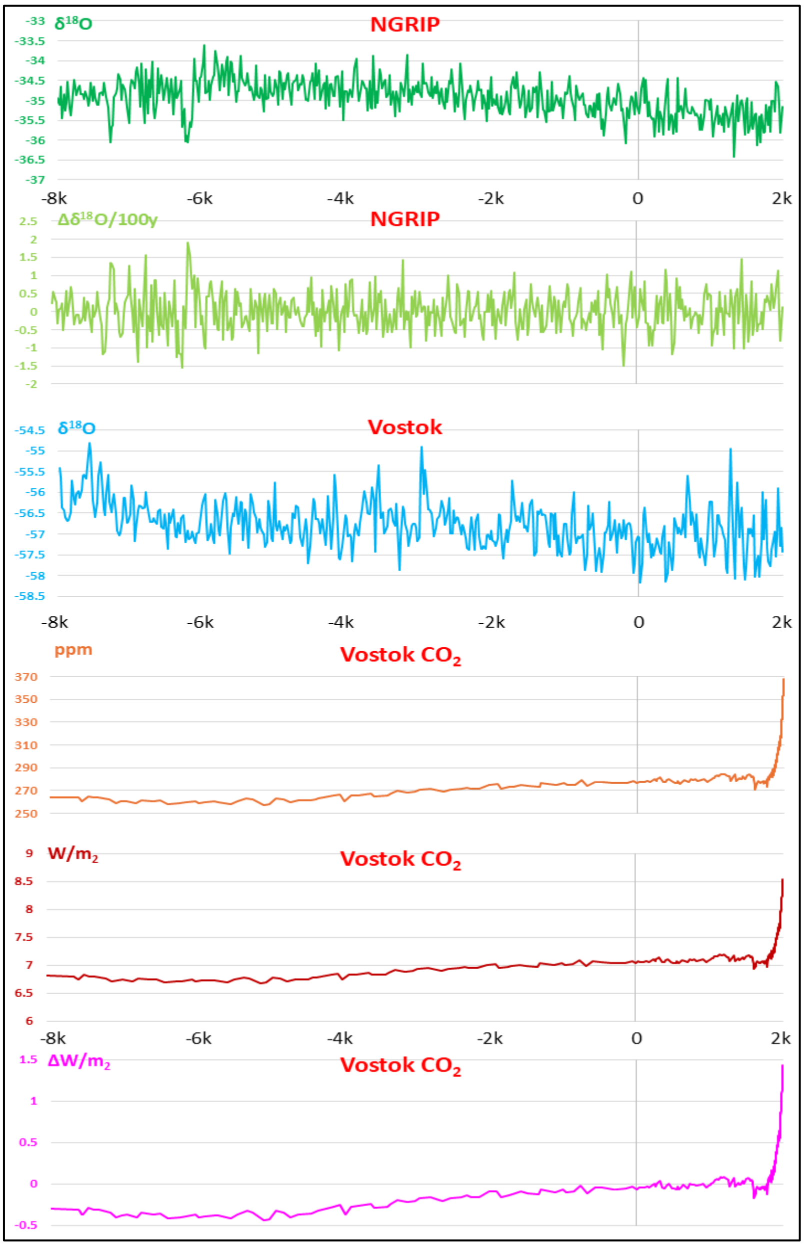

Figure A3: Climate reconstruction over the past approximately 10,000 years, with the present day (AD) at the far right. $\delta^{18}O$ at the Arctic and Antarctic, $\Delta\delta^{18}O$ per century in the Arctic. CO_2 from Antarctic ice cores and Hawaii measurements, CO_2 radiative forcing. NGRIP final year is 1990. Radiative forcing calculations cited from [66] (the formula is written in the Appendix 1.3).

And over the entire period, whether every 20 years or every 100 years, temperatures fluctuate by 2 to 3 degrees Celsius up or down. As shown in Figure A4, the global average is about half that of the Arctic region. Therefore, globally, temperatures constantly fluctuate by 1 to 1.5 degrees Celsius every 100 years. The IPCC critically asserts that the 20th century saw crisis warming of approximately 0.8 degrees Celsius. In reality, however, this is an unremarkable change that has been repeated countless of times throughout history. Furthermore, the so-called Medieval Warm Period around the year 1000 AD is evident. Arctic data only extends to 1990, but it shows that temperatures were significantly higher around 1940.

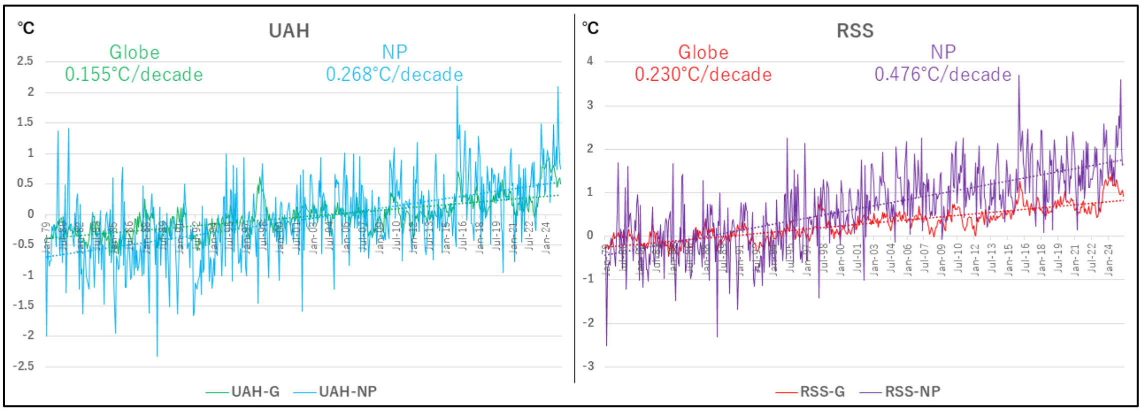

Figure A4: Global and Arctic temperatures from January 2000 to May 2025 for UAH and RSS. G: Globe, NP: North Pole. The coverage areas differ: UAH-NP spans 60N to 90N, while RSS-NP spans 60N to 82.5N.

The theory of anthropogenic global warming was recently forcefully asserted, starting in 1980s. A particular turning point came in 1988 with the press conferences held by Dr. James Hansen, Mr. Al Gore, and Mr. Timothy Worth [67]. However, $\delta^{18}O$ data of NGRIP indicates that temperatures were not high at all at this time. The apparent rapid warming shown by surface-focused data was likely due to inadequate accounting for the urban heat island effect.

Figure A5 shows data for the last 500 years. Even around the time of the Industrial Revolution, $\delta^{18}O$ and $\Delta\delta^{18}O/100y$ showed earlier and more pronounced fluctuations than CO_2. While Antarctic data requires consideration of its lower temporal resolution compared to NGRIP, it shows some differences except for the steep warming in the early 20th century.

Nevertheless, these data clearly demonstrate that CO_2 was not the starting point for climate change. This is because temperatures precedingly fluctuate independently of CO_2. Moreover, these realities are based on the assumption that "the age shifts of CO_2 in ice cores and the modern CO_2 linkage method are unquestionably valid" [19]. In other words, these global temperature changes cannot be explained by the radiative forcing of CO_2 derived from Antarctic ice cores, which anthropogenic global warming proponents hold as absolute.

Therefore, climate models adopted by the IPCC, which treat CO_2 as the primary factor in the greenhouse effect, cannot possibly reproduce past climates. This means that even a simple observation of paleoclimate data clearly shows that the anthropogenic CO_2 warming theory and its models lack any basis from the outset. It was not a matter of mathematical modelling.

The partial agreement with some modern data achieved by models premised on anthropogenic CO_2 warming is merely a pseudo-correlation resulting from cherry-picking (typically, the hockey stick curve). The rapid modern temperature rise is simply the result of connecting numerical values that fail to adequately account for the urban heat island effect, although it is a fact that there has been some warming in modern times.

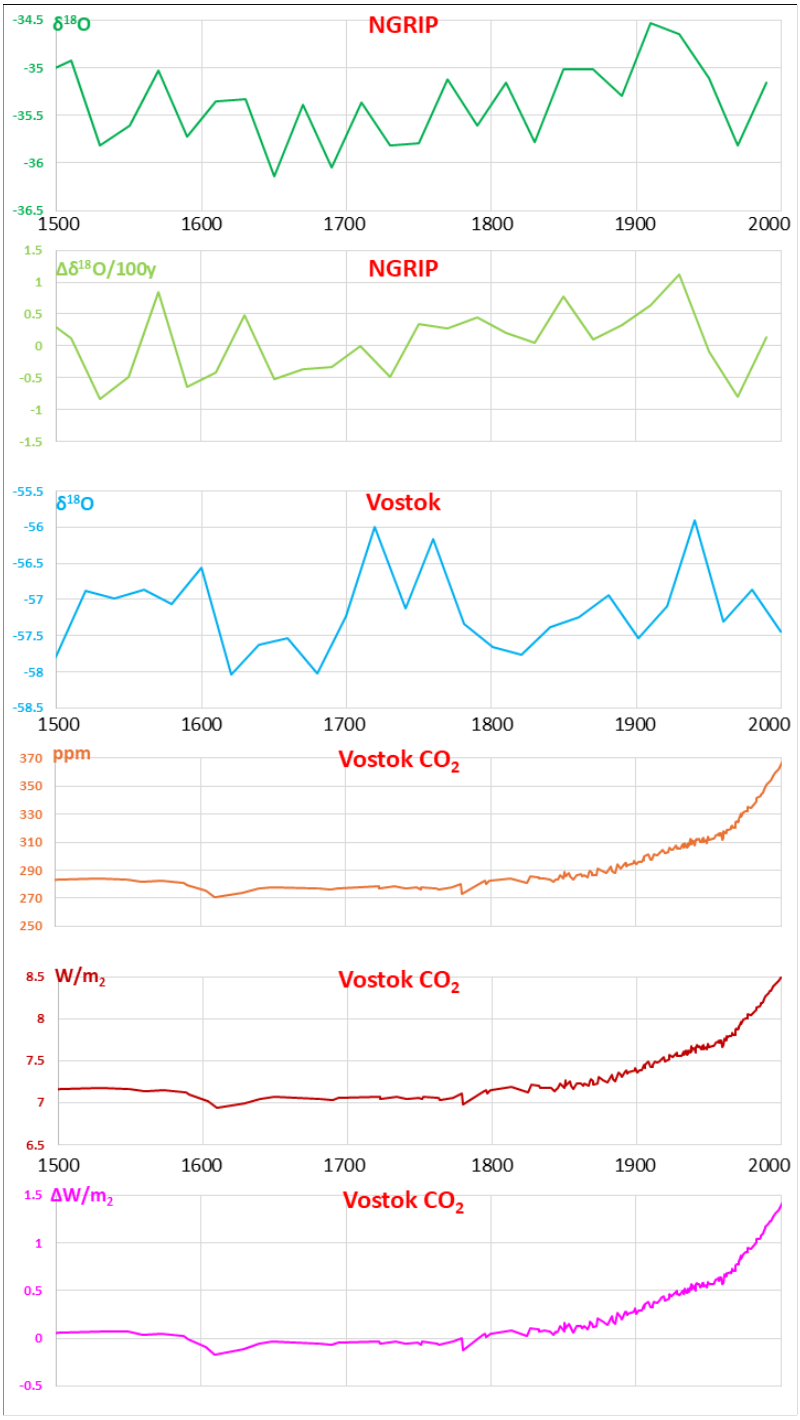

Figure A5: Climate reconstruction over the past 500 years, with modern times (AD) at the far right. Data meaning is the same as in Figure A3.

Moreover, the high temperatures in the Arctic region from the first half of the 20th century to 1940, as shown in Figures A3 and A5, also demonstrate the validity of the chemical method—one of the CO_2 reconstruction methods—developed by Beck (Beck [68], Harde [69]).

Furthermore, Dr. Schmidt's report [29] states that the present day may be the warmest in the last 100,000 years.

> *We need answers for why 2023 turned out to be the warmest year in possibly the past 100,000 years.*

However, as shown in the two figures above, this perception itself is mistaken. Far from the

Medieval Warm Period, even the period from 1920 to 1940 was significantly warmer according to NGRIP data, and it is unlikely that the rise since 1990 could surpass it. Since the NGRIP data has a time resolution of 20 years, it is certain that there were years that were even warmer than what this data indicates.

Figure A6 illustrates typical data for the Medieval Warm Period (Keigwin [70], Robinson et al. [71,72]).

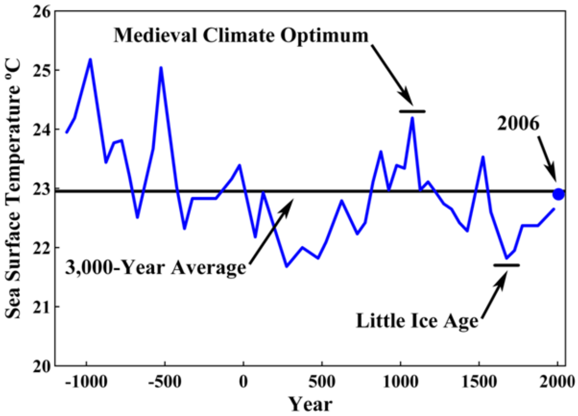

Figure A6: A typical example of the Medieval Warm Period. The Sargasso Sea. Figure from [72].

Figure A7 includes valid climate reconstruction data reproducing the Holocene Climate Optimum and Medieval Warm Period as published in the IPCC First Assessment Report (Houghton et al. [73]). It is ironic and intriguing that global temperatures in 1990, when the IPCC First Assessment Report was published, were in a completely unremarkable state.

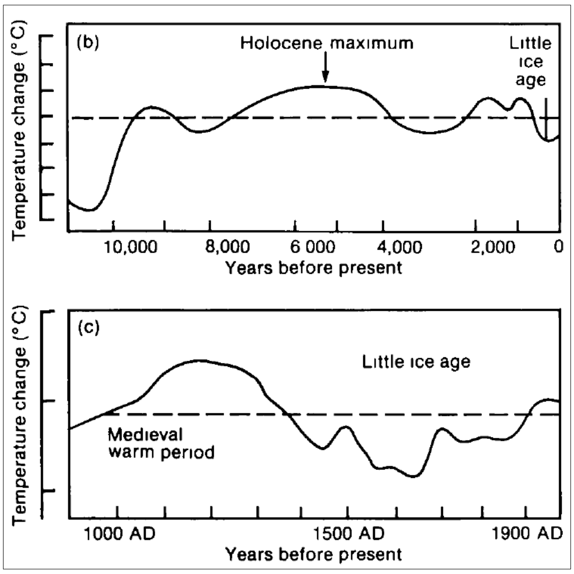

Figure A7: Reasonable climate reproduction data from the IPCC First Assessment Report. From Figure 7.1 on page 202 of [73].

Furthermore, several months ago, a natural science journal within the same Nature portfolio (Auer et al. [74]) reported that Arctic temperatures reached a maximum of 9 degrees Celsius warmer during summer than modern times during the Holocene Optimum. This equates to approximately 5 degrees Celsius globally. The relevant text is quoted here (at the beginning of P9).

> *As outlined in the introduction, the former period is of particular relevance by providing a glimpse into the future, as summer surface temperatures were up to 9 °C higher than today.*

1.3. Why the results remain essentially unchanged even when atmospheric CO_2 data used in multivariate analysis is converted to radiative forcing

Using two representative equations employed in Appendix 1B above, CO_2 concentration is converted to radiative forcing (RF) using representative equations and shown in Figure A8 [65].

$$Absolute\ value: RF = -0.0000248 \cdot C^2 + 0.03231 \cdot C \qquad (A1)$$

$$Difference\ from\ 280\ ppm: \Delta RF = 5.22 \cdot ln\frac{C}{280} \qquad (A2)$$

where C is the CO_2 concentration (ppm) to be evaluated, and Ln is the natural logarithm.

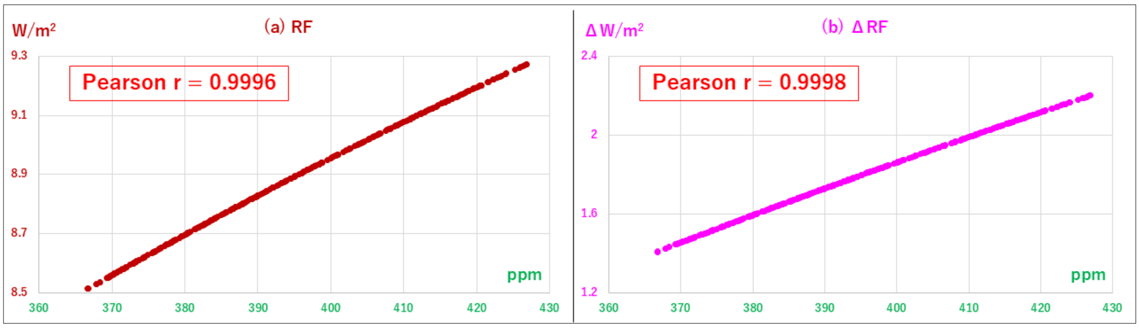

Figure A8: CO_2 concentration and radiative forcing since 2000. Equation adapted from [65]. (a) Actual radiative forcing (b) Difference from 280 ppm.

For both, they increase almost linearly and exhibit a correlation coefficient with CO_2 concentration itself that effectively shows r = 1, within the range of atmospheric CO_2 concentrations examined in the main text since the year 2000. Therefore, even if these radiative forcing conversion data are input as explanatory variables in multivariate analysis, the results remain essentially unchanged.

1.4. Explanation that the correlations between ASW and TSI with G-SST used in this study are not spurious

When analyzing time-series data, testing for spurious correlations is recommended. However, since ASW and TSI are fundamentally preceding G-SST, and reports supporting the so-called Svensmark effect have been accumulating, this item is presented in simplified form.

The data underlying the results of Table 5, which constitute the final result of this study, will be used.

First, scatter plots of each indicator are shown.

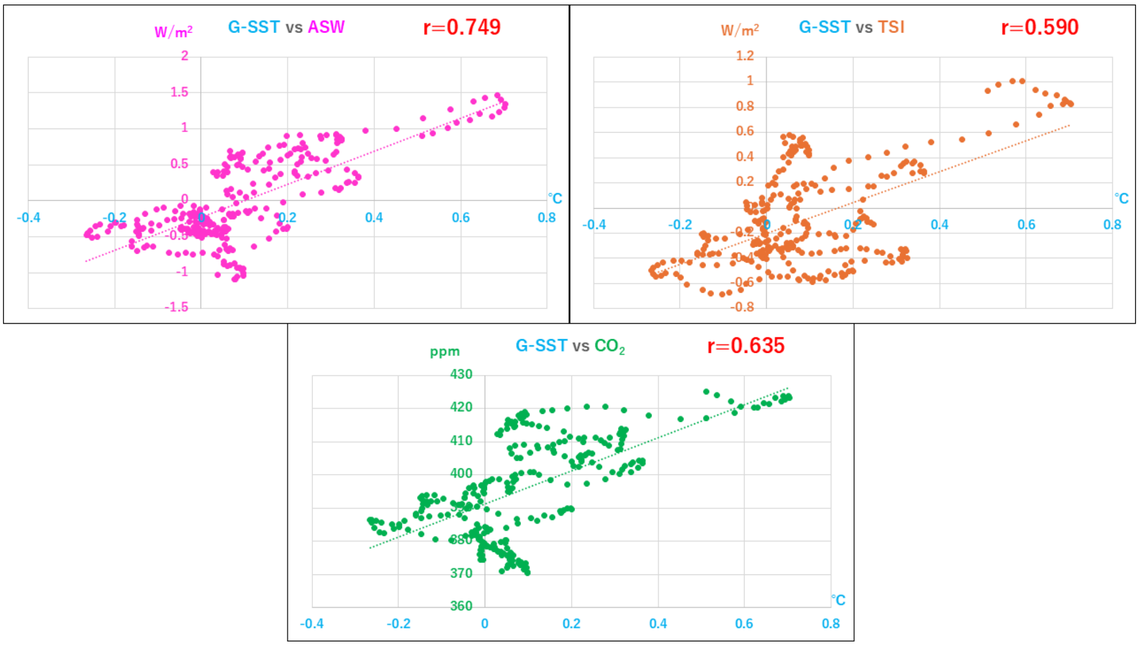

Figure A9: Scatter plots of each indicator, r = Pearson correlation, note that the data of CO_2 is used as is, because applying 13mRM is meaningless (the result of multivariate analysis does not essentially change).

These data show that each indicator is significantly correlated with G-SST.

Next, two correlation diagrams showing monthly changes are presented.

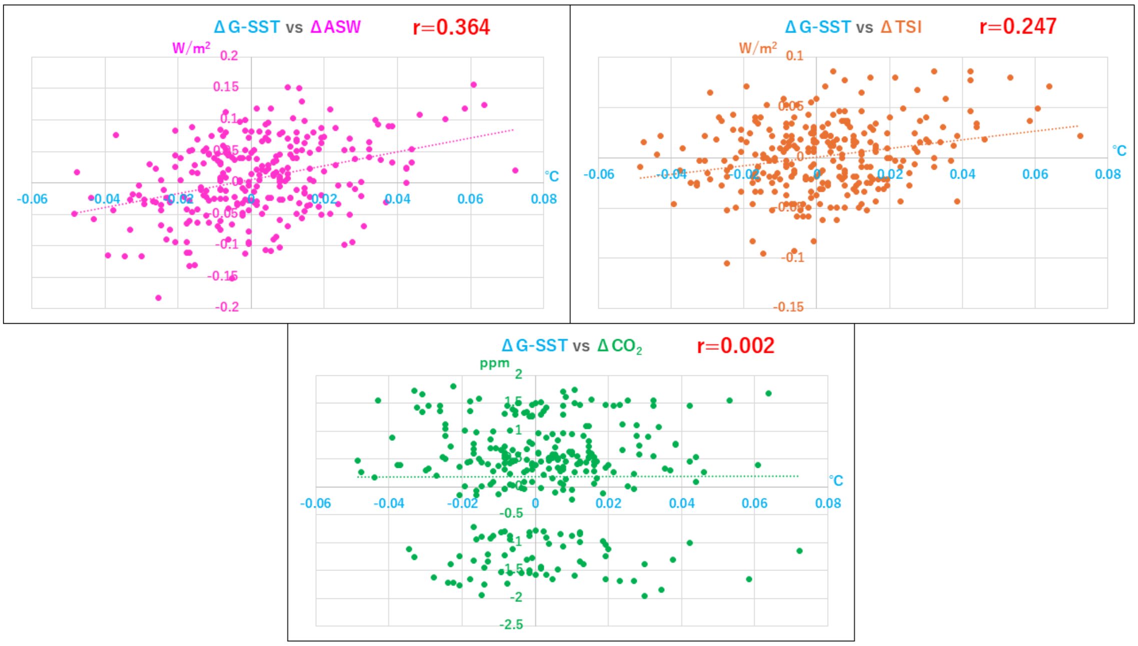

Figure A10: Scatter plots of monthly change of each indicator, r = Pearson correlation

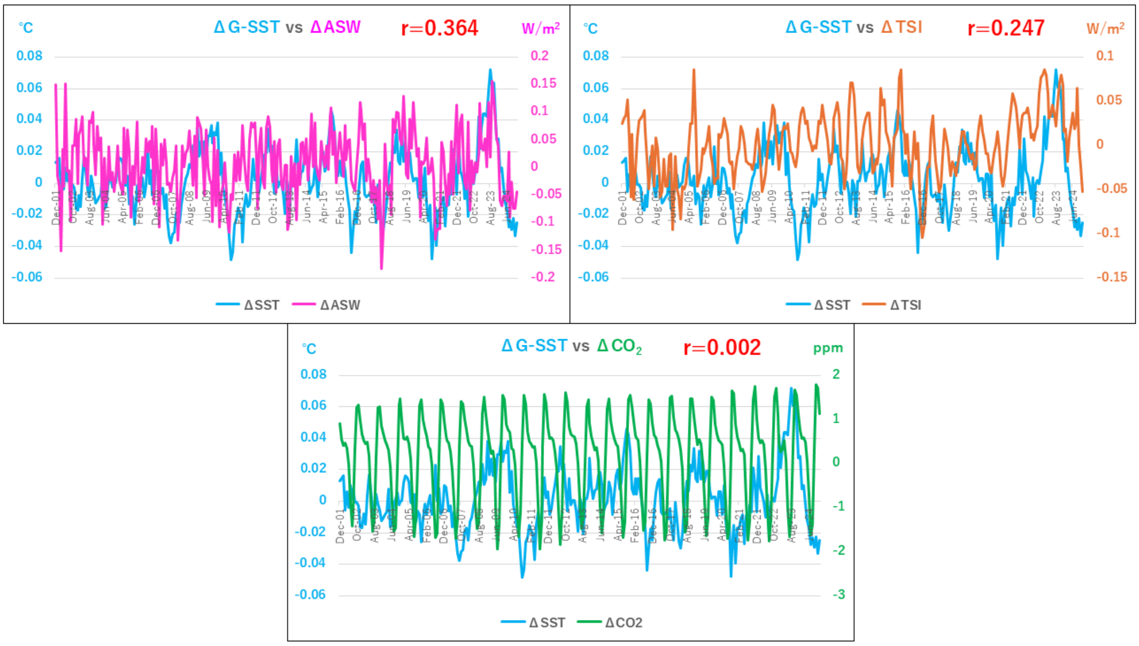

Figure 11A: Time series plotting of monthly change of each indicator, r = Pearson correlation

As evident from both the scatter plot and time-series data, there is no correlation between ΔG-SST and ΔCO_2. Therefore, it is clear that G-SST and CO_2 were spuriously correlated. On the other hand, ΔASW and ΔTSI are significantly correlated with ΔG-SST.

Finally, the result of the linear multiple regression analysis with ΔG-SST as the dependent variable is presented.

Table A1: Multiple linear regression analysis of ΔG-SST as an objective variable

Model R^2=0.171 P=4.44e-11	Regression Coefficient	P
Constant	0.00077	0.49
ΔASW	0.11016	5.8e-09
ΔTSI	0.11354	4.6e-04
ΔCO2	-0.00025	0.825

ΔASW and ΔTSI were independent determinants of ΔG-SST, but ΔCO_2 and the constant were not. Therefore, it is reasonable to conclude that ASW and TSI exhibit a genuine correlation with G-SST at least within the scope of this data set.

2. Understanding the origin of atmospheric CO_2 increase by a concept of simple math using average of $\delta^{13}C$

This section is designed to help even those unfamiliar with science grasp the overall picture of past carbon cycles through basic mathematical calculations. While rigorous verification already exists, exemplified by Koutsoyiannis [21], not everyone can fully comprehend scientific papers.

Those who attribute all the rise in atmospheric CO_2 today to human origins, whether researchers or the general people—frequently claim this is proven by carbon isotope ratios. This is because, especially since the Industrial Revolution, the ^{13}C ratio has decreased and appears to correlate with the increase of atmospheric CO_2 concentrations and human emissions. However, this claim can be proven false with a basic elementary-level numerical check.

Let us suppose CO_2 levels at the start of the Industrial Revolution were 280 ppm, and the increase up to 2022 was 140 ppm. Let us suppose $\delta^{13}C$ at the start of the Industrial Revolution was −6.3 ‰, and the $\delta^{13}C$ of anthropogenic CO_2 is −26 ‰ (because fossil fuels, primarily C_3 plants, have significantly lower ^{13}C content).

It is simply a matter of taking these averages.

$$\{(-6.3 \times 280) + (-26 \times 140)\} \div 420 = -12.86666.... \qquad (A3)$$

If the entire 140 ppm increase were anthropogenic, $\delta^{13}C$ should have been approximately -12.87 ‰ by the end of 2022.

However, the actual atmospheric $\delta^{13}C$ is around -8.4 ‰ (2022). Therefore, it is impossible to attribute the entire 140 ppm increase solely to human activity.

Thus far, using the basic mathematical concept of calculating averages is explained. This explanation should suffice for gaining a simple understanding of the actual situation described in this series of points.

Naturally, similar results are reproduced using the precise definition of $\delta^{13}C$ (Lueker et al. [75]) and calculations. The details are explained in the following two slides.

Calculation by the definition of $\delta^{13}C$

* definition1: standard of carbon isotope, $^{13}C/^{12}C$ = Rs = 13Cs/12Cs = 0.0112372
* definition2: $\delta^{13}C$ = ($^{13}C/^{12}C$ − R_s) ÷ R_s = ($^{13}C/^{12}C$ − 0.0112372) ÷0.0112372
* supposition1: CO_2=280ppm in 1750, $\delta^{13}C$ = −0.0063 (or −6.3‰)
* supposition2: increased 140ppm of CO_2, $\delta^{13}C$ = −0.026 (or −26.0‰)

Year	ppm	$^{13}C/^{12}C$	$\delta^{13}C$
1750	280	0.011166406	-0.0063
1751～2022	140up↑	0.010945033	-0.026
2022	420	0.011092604	-0.012867624

＊If the 140-ppm increase is all man-made, $\delta^{13}C$ in 2022 must be −0.012867624 (≒−12.9‰)

Slide A1: Explanation using carbon isotope. Calculation, supposing the entire 140-ppm increase is anthropogenic.

The content of Slide A1 above shows the calculation process for atmospheric $\delta^{13}C$ in 2022, assuming $\delta^{13}C$ = -26 ‰ for 140-ppm increase and that all of this is accumulated. As shown in the final result, $\delta^{13}C \approx$ -12.87 ‰, which shows no substantial difference from the simple average calculation method described above. However, in reality, the $\delta^{13}C$ value for modern atmospheric CO_2 is approximately -8.4 ‰.

The content of the next slide A2 shows the back-calculation process for the 140-ppm increase in $\delta^{13}C$, derived from $\delta^{13}C$ values during the Industrial Revolution and modern reality. The result indicates that $\delta^{13}C$ of 140 ppm was ≅ -12.6 ‰. Therefore, it is impossible to claim that the 140-ppm increase is entirely anthropogenic.

Calculation of $\delta^{13}C$ of the increased 140 ppm CO_2

＊Supposition1: CO_2 = 280ppm ($\delta^{13}C$ = −6.3‰) in 1750
＊Supposition2: CO_2 = 420ppm ($\delta^{13}C$ = −8.4‰) in 2022

<Each variable as the supposition above>

Year	CO_2 (ppm)	$\delta^{13}C$	^{13}C	^{12}C
1750	280	−0.0063	0.011043093	0.988956907
2022	420	−0.0084	0.011020013	0.988979987

<Calculation of ^{13}C of the increased 140 ppm, next $\delta^{13}C$>

	CO_2 (ppm)	$\delta^{13}C$	^{13}C	^{12}C
1751～2022	140up ↑	−0.012599155	0.010973859	0.989026141

↑ $\delta^{13}C$ of the 140ppm must be −0.012599155 (≒ −12.6‰) on the average.
↓ ↓ ↓ ↓ ↓ ↓
Therefore, most of the increased 140 ppm did not originate from fossil fuel.

Slide A2: Explanation using carbon isotope. Back-calculated $\delta^{13}C$ of the 140-ppm increase from the $\delta^{13}C$ values of the past and present.

However, at this stage, another possibility for the 140-ppm increase cannot be ruled out. Amid rising anthropogenic emissions, it is possible that while the quantitative increase is anthropogenic in origin, the composition has been replaced by natural cycles, leading to the current state. The results of multivariate analysis presented in the author's two previous papers [18,19] quantitatively and probabilistically determined the veracity of this possibility. The hypothesis itself—that human emissions and land-use changes caused the CO_2 rise over the past 60-plus years—was shown to be statistically highly improbable. Therefore, even today, most of the atmospheric CO_2 rise is assertively a natural phenomenon.

And as this explanation shows, the discrepancy between the anthropogenic theory of global warming and CO_2 rise and the reality arises precisely because of the assumption that the CO_2 values reproduced from ice cores are the truth.

Furthermore, if one possesses the knowledge to understand the explanations accompanying the two slides above, it is unlikely they would unquestioningly accept the anthropogenic theory of CO_2 rise itself. Therefore, it is recommended that the content of this supplement be used solely for the purpose of explaining the initial explanation (verification based on the concept of averages) to those with limited scientific knowledge.

3. Multivariate analysis considering the time lag between temperature and annual atmospheric CO_2 increase (ΔCO_2) of author's previous reports

In the author's previous multivariate analyses [18, 19], only annual values were used. The results rejected the anthropogenic theory for ΔCO_2, with SST being the sole determinant. However, as demonstrated above in this report, there is a consistent time lag between actual global surface temperature and ΔCO_2. Therefore, analysis using monthly data would be ideal.

Yet, anthropogenic emissions data commonly available from institutions like the International Energy Agency and Our World in Data (OWID) are not monthly. Regarding temperature data, however, it is easy to adjust the months, calculate annual averages, and verify the monthly difference yielding the best correlation with ΔCO_2.

This time, using this method, G-SST was calculated using only UAH data and multivariate analysis was performed only for the period after 1980. Note that while UAH data is publicly available from December 1978 onwards, the reason for starting from 1980 is because it becomes impossible to start from 1979 in the monthly correction process, if the starting month for the annual average

G-SST is moved further back in time. Only OWID data [76] was used for anthropogenic emissions.

At the end of this section, the author's perspective on which global temperature indicators should be used in the multiple linear regression analysis with ΔCO_2 as the dependent variable will be explained.

Table A2 shows the results of linear multiple regression analysis. The optimal monthly G-SST correction was achieved by advancing the data by two months (using the average of March 1980 to February 1981 as the annual G-SST for 1980). Analysis using same-month G-SST is also shown for comparison. The model accuracy is comparable for all data combinations. However, for the combination of same-month G-SST and LUC, the constant decreases slightly and the P-value increases.

Table A2: Results of multiple linear regression analysis with annual ΔCO_2 as the dependent variable. Data from 1980 to 2023 were analyzed. Statistically significant factors are marked in red based on multivariate analysis. ΔCO_2 data were obtained on the same date as in the main text. Emissions data were obtained from OWID, with units in megatons [76]. Pearson Correlation is with ΔCO_2. FFO; fossil fuel only, LUC; including land use change.

G-SST	Human Emission	Variables	Pearson correlation	Regression coefficient	P	Model R^2
G-SST month adjusted	FFO	Constant ppm	---	1.86	2.76e-05	0.631 P=1.33e-09
		G-SST ppm/°C	0.793	2.35	1.98e-06	
		Human Emission ppm/Mt	0.596	6.25e-06	0.645	
	LUC	Constant ppm	---	1.78	6.36e-04	0.632 P=2.71e-08
		G-SST ppm/°C	0.793	2.33	2.07e-06	
		Human Emission ppm/Mt	0.598	7.57e-06	0.594	
G-SST same month	FFO	Constant ppm	---	1.70	8.83e-05	0.611 P=3.93e-09
		G-SST ppm/°C	0.777	2.17	6.03e-06	
		Human Emission ppm/Mt	0.596	1.20e-05	0.372	
	LUC	Constant ppm	---	1.57	1.93e-3	0.613 P=3.58e-09
		G-SST ppm/°C	0.777	2.14	5.93e-06	
		Human Emission ppm/Mt	0.598	1.39e-5	0.321	

Table A3 shows the total ΔCO_2 values and the total predicted ΔCO_2 values from this multiple regression analysis. In previous reports, verification using UAH data since 1979 showed a difference of approximately 14 ppm in the final year. In this verification, the difference was reduced to about 8 ppm using a model with FFO emissions and monthly-adjusted G-SST. Conversely, the combination of unadjusted G-SST and LUC resulted in a discrepancy of approximately 20 ppm. This outcome clearly reflects the combined effect of smaller coefficient and constant for G-SST in this model.

Table A3: Sum of published ΔCO_2 values and sum of predicted ΔCO_2 values from the multiple regression analysis in Table A1. Units are ppm.

	Published value	Month of G-SST	FFO	LUC
Sum of ΔCO_2	84.98	Adjusted	77.30	74.00
		Same	70.22	64.79

More precise results are anticipated once detailed monthly anthropogenic emission data becomes available. However, defining monthly ΔCO_2 and implementing monthly adjustments will also become critical in that process.

Multivariate analyses with ΔCO_2 as the object variable have been conducted in three papers, including this paper. Human emissions have been included in all results tables. If these linear multiple regression analyses were performed using stepwise selection (whether Akaike Information Criteria (AIC), BIC, or p-value methods), anthropogenic emissions would be excluded from the explanatory factors, reconstructing the model to use only SST as the explanatory variable. Therefore, in this case, a nearly perfect prediction equation can be derived for the SST of any facility. However, since there are only two explanatory variables, the significance of performing stepwise regression is questionable. Consequently, the author (Ato) basically does not perform stepwise regression for this topic in his reports.

Finally, which temperature indicators in the climate research field should be used for analysis and the reasons for doing so will be described. While it depends on the objective, if the indicators have clear underlying mechanisms, they should be used. And of course, accuracy is also an important factor.

Especially with UAH data, there is no significant difference globally compared to SST regarding monthly fluctuation (Pearson $r = 0.977$, Dec-78 to Jun-25, as implied in Figure 1(b) which compares SST and LST, and because the ocean dominates about 70 % surface of the earth), so approximate results can be obtained (of course, decadal trend is slightly different). Furthermore, as noted in the Discussion section, the results of the multiple regression analysis with ASW and TSI as explanatory variables were equivalent regardless of whether the dependent variable was G-SST or Global temperature.

However, in the multivariate analysis the author has conducted in the previous two papers [18,19], ΔCO_2 is the objective variable, and SST is the mechanism that is clearly understood. Furthermore, for the primary purpose of this report, using ocean temperature—the source of water vapor—as the primary variable is theoretically most appropriate. Furthermore, surface data other than UAH may be subject to concerns regarding the urban heat island effect or numerically approximated errors.

Moreover, compared to UAH, other datasets generally show larger differences between ocean and land surfaces. Finally, when performing multiple linear regression analysis with ΔCO_2 as the dependent variable and extending the analysis further back in time (to 1959, due to issues with ice core data prior to 1958, as explained in [19]), it is desirable to use SST, which exhibits a relatively similar trend, for comparison with UAH and other facility data (especially for verification extending back to 1959).

Now, regarding the overall picture of Earth's carbon cycle, the ratio between land and ocean is roughly 4 to 3 (NASA, [77]). Therefore, the possibility that the actual impact could be distinguished as approximately 4 to 3 between land and ocean remains, if assuming there are no multicollinearity issues in the multiple linear regression analysis and the annual balance on land can be accurately measured. That is, the ratio would be slightly more than half of ΔCO_2 attributable to land temperature and the remainder to ocean temperature.

However, in actual linear multiple regression analysis, using highly correlated indicators as explanatory variables leads to problems (cancellation) due to multicollinearity. Moreover, since precise annual figures for the terrestrial carbon cycle are unknown, performing principal component analysis to circumvent multicollinearity is impossible.

SST precedes LST in Earth's surface temperature and dominates it to a certain extent. Oceans cover 70 % of the Earth's surface. Therefore, considering the perspective of comparing facility-specific data as mentioned above, it is most appropriate to use G-SST alone as the representative indicator of global temperature in multiple linear regression analysis with ΔCO_2 as the objective variable.

Regarding the overall carbon cycle, it is likely reasonable to consider that in tropical regions, CO_2

emissions from both the ocean and land (especially soil respiration) exceed absorption (Salby and Harde, [23]), while in mid-latitude to polar ocean areas, the ocean absorbs CO_2, with these cycles occurring globally. Considering that the oceans, covering 70 % of the Earth's surface, act as a 'gravitational' force to regulate this overall system would be currently the most reasonable perspective.

References for Appendix

61. Badgeley J.A., Steig E.J., Hakim G.J., Fudge T.J., 2020: *Reconstructions of mean-annual Greenland temperature and precipitation for the past 20,000 years and the ice-core records used to create the reconstructions 2020*. Arctic Data Center. https://doi.org/10.18739/A2599Z26M
Accessed 31, January 2025
62. Masson-Delmotte V., Buiron D., Ekaykin A.A., Frezzotti M., Gallée H., Jouzel J., Krinner G., Landais A., Motoyama H., Oerter H., Pol K., Pollard D., Ritz C., Schlosser E., Sime L.C., Sodemann H., Stenni B., Uemura R., Vimeux F., 2011: *Water stable oxygen isotope records from six Antarctic ice core sites for the present and last interglacial periods* [dataset publication series]. PANGAEA, https://doi.org/10.1594/PANGAEA.785228, Accessed 9, March 2025
63. NOAA, National Centers for Environmental Information: *Antarctic Ice Cores Revised 800KYr CO2 Data*, https://www.ncei.noaa.gov/access/paleo-search/study/17975, Accessed 24, September 2024
64. Bereiter B., Eggleston S., Schmitt J., Nehrbass-Ahles C., Stocker T.F., Fischer H., Kipfstuhl S., Chappellaz J., 2015: *Revision of the EPICA Dome C CO2 record from 800 to 600 kyr before present*. Geophysical Research Letters, 42(2), 542-549. https://doi.org/10.1002/2014GL061957
65. Lightfoot H.D., Mamer O.A., 2014: *Calculation of Atmospheric Radiative Forcing (Warming Effect) of Carbon Dioxide at Any Concentration*. Energy & Environment, 25(8), 1439-1454. https://doi.org/10.1260/0958-305X.25.8.1439
66. Etminan M., Myhre G., Highwood E.J., Shine K.P., 2016: *Radiative forcing of carbon dioxide, methane, and nitrous oxide: A significant revision of the methane radiative forcing*, Geophys. Res. Lett., 43, 12,614–12,623, https://doi.org/10.1002/2016GL071930
67. Center for Science and Technology Policy Research, 2010*: The Climate Fix: What Scientists and Politicians Won't Tell You About Global Warming*、 https://sciencepolicy.colorado.edu/publications/special/climate_fix/book_clips.html
68. Beck E.G., 2022: *Reconstruction of Atmospheric CO_2 Background Levels since 1826 from direct measurements near ground*, Science of Climate Change, Vol 2.2 (2022) pp.148-211, https://doi.org/10.53234/scc202112/16
69. Harde H., 2023: *About Historical CO_2-Data since 1826: Explanation of the Peak around 1940*, Science of Climate Change, Vol. 3.2 (2023) pp. 211-218, https://doi.org/10.53234/scc202304/21
70. Keigwin L.D., 1996: *The Little Ice Age and Medieval Warm Period in the Sargasso Sea*. Science 274,1504-1508, https://doi.org/10.1126/science.274.5292.1504
71. Robinson A.B., Robinson N.E., Soon W., 2007: *Environmental Effects of Increased Atmospheric Carbon Dioxide*, Journal of American Physicians and Surgeons (2007) 12, 79-90., https://www.jpands.org/vol12no3/robinson.pdf
72. Oregon Institute of Science and Medicine: *Global Warming Petition Project*, http://www.petitionproject.org/review_article.php
73. Houghton J.T., Jenkins G.J., Ephraums J.J., IPCC, 1990: *The IPCC Scientific Assessment,*

Report Prepared for IPCC by Working Group 1, https://www.ipcc.ch/site/assets/uploads/2018/03/ipcc_far_wg_I_full_report.pdf

74. Auer A.G., van der Bilt W.G.M., Schomacker A., Bakke J., Støren E.W.N., Buckby J.M., Cederstrøm J.M., van der Plas S., 2025: *Hydroclimate intensification likely aided glacier survival on Svalbard in the Early Holocen*e. Commun Earth Environ 6, 100 (2025)., https://doi.org/10.1038/s43247-025-02064-z
75. Lueker T., Keeling R., Bollenbacher A., Walker S., Morgan E., Brooks M., 2020: *Calibration Methodology for the Scripps 13C/12C and 18O/16O stable Isotope program 1992-2018*. UC San Diego: Scripps Institution of Oceanography. https://escholarship.org/uc/item/4n93p288
76. Data on CO2 and Greenhouse Gas Emissions by Our World in Data, https://github.com/owid/co2-data Accessed 12, September 2025
77. NASA earth observatory: *The Carbon Cycle*, https://earthobservatory.nasa.gov/features/CarbonCycle

Radiative Forcing of Water Vapour and its Use in Climate Models

Antero Ollila

School of Engineering (Emer.), Aalto University, Espoo, Finland

SCC Publishing
Michelets vei 8 B
1366 Lysaker Norway

ISSN: 2703-9072

Correspondence:

aveollila@ yahoo.com

Vol. (2026)

pp. 42

Corrigendum

In Ollila (2025) there is a spelling error in the manuscript.

Equation (2) in the corrected form is:

$$RF = -60.01 + 18.435 * \ln(H_{TPW}) \; [Wm^{-2}] \quad (2)$$

This error has had no impact on the results since the right form of equation (2) has been applied in the calculations.

Submitted 2024-01-11, Accepted 2024-02-01. https://doi.org/10.53234/SCC202603/07

Editor: Nikolaos Malamos

References

Ollila, A, 2025: *Radiative Forcing of Water Vapour and its Use in Climate Models*. Science of Climate Change, v. 5, no. 3, pp. 186-206. https://doi.org/10.53234/scc202510/11

SCC-Publishing
Michelets vei 8 B
1366 Lysaker, Norway
ISSN: 2703-9072

Correspondence:
cohler59@gmail.com

Vol. 6.1 (2026)
pp. 43-76

IPCC's Earth Energy Imbalance Assessment is Based on Physically Invalid Argo-Float-Based Estimates of Global Ocean Heat Content

Jonathan Cohler,[1] David R. Legates,[2] Kesten C. Green,[3] Ole Humlum,[4] Franklin Soon,[5] Willie Soon[6]

[1] Massachusetts Institute of Technology, Cambridge, MA, USA
[2] Retired Professor, University of Delaware, Newark, DE, USA
[3] Adelaide University; Ehrenberg-Bass Institute, Adelaide, Australia
[4] Department of Geosciences, University of Oslo, Oslo, Norway
[5] Marblehead High School, Marblehead, MA, USA
[6] Institute of Earth Physics and Space Science, Sopron, Hungary

Abstract

Global ocean heat content (OHC) anomalies and derived Earth Energy Imbalance (EEI) estimates, central to contemporary climate assessments including IPCC AR6, are constructed through processes that violate the scientific method. These metrics rely almost exclusively on temperature data from the Argo profiling float array. Their validity and reliability hinge on several critical but herein refuted assumptions about measurement representativeness, interpolation/extrapolation methods, the physical meaning of anomalies, and integration conventions. Core Argo and Biogeochemical Argo floats deliver discrete, point measurements of intensive properties like temperature along irregular, untracked three-dimensional trajectories during ascent from 2000 m to the surface. This samples only the upper ocean, excluding roughly 50% of total ocean volume and thermal energy. Horizontal positions are recorded only at surface intervals ~10 days apart, leaving subsurface locations entirely unknown. All data from each ascent are arbitrarily assigned to the surfacing position, introducing unknown horizontal offsets (up to 50 km) and temporal offsets (up to 10 hours) for the deepest measurements. Anomalies are computed by subtracting values from statistically derived reference climatologies based on sparse historical data over arbitrary baseline periods. Measured temperatures are then interpolated onto global 3D grids using prescribed covariance functions. These anomalies represent numerical differences without physical meaning as temperature deviations, because temperature, an intensive property, is not additive across non-equilibrium spatial or temporal domains (Essex et al., 2007; Essex & Andresen, 2018). The integrated OHC scalar depends heavily on arbitrary averaging and interpolation rules, producing computational artifacts rather than measures of actual ocean energy uptake or planetary radiative imbalance. Derived EEI values, such as the 0.7 ± 0.2 W m^{-2} in IPCC AR6 Figure 7.2, inherit these biases and stem from circular methodology: CERES satellite top-of-atmosphere radiative flux measurements (absolute uncertainties $\pm$ 3–5 W m^{-2} or higher) are adjusted via least-squares to match Argo OHC-derived estimates, rather than offering independent validation. We rigorously quantify major uncertainty sources, including unresolved mesoscale variability ($\pm$ 0.9 W m^{-2}), deep ocean ignorance bounds ($\pm$ 0.35 W m^{-2} from sparse Deep Argo), polar undersampling ($\pm$ 0.1 W m^{-2}), Nyquist-Shannon aliasing in sparse deep ocean and polar sampling, sea-level budget closure discrepancy between satellite altimetry/gravimetry and Argo OHC ($\pm$0.33 W m^{-2}), arbitrary baseline choices ($\pm$ 0.2 W m^{-2}), Eulerian-Lagrangian discrepancies ($\pm$ 0.25 W m^{-2}), and untracked trajectories and positional assignments. Although the concepts of OHC and EEI are thermodynamically well-defined physical quantities, the numerical values produced by current Argo-based methodologies are physically meaningless computational constructs that do not validly represent those quantities. We conclude that EEI uncertainties reach >$\pm$ 1 W m^{-2} at 95% confidence, roughly an order of magnitude larger than the uncertainty that IPCC AR6 reports, rendering current OHC change and EEI estimates statistically indistinguishable from zero.

Keywords: Argo floats; ocean heat content (OHC); Earth's Energy Imbalance (EEI); intensive properties; IPCC AR6; mesoscale variability; Nyquist-Shannon theorem; Eulerian-Lagrangian discrepancy; CERES Deep Argo; BGC-Argo; computational artifacts.

Submitted 2026-01-15, Accepted 2026-02-19. https://doi.org/10.53234/scc202603/06

1. Introduction

Global ocean heat[1] content (OHC) (i.e. global ocean thermal energy change) and derived Earth's Energy Imbalance (EEI) estimates occupy a central position in contemporary climate assessments, including those of the United Nations' Intergovernmental Panel on Climate Change (IPCC, 2021). The validity and reliability of these estimates depend upon the plausibility of several key assumptions regarding measurement representativeness, interpolation/extrapolation procedures, physical meaning of anomalies, and mathematical conventions for integration. In this paper, we show that these assumptions are not plausible and that even modest variations in them can lead to quite opposite conclusions regarding EEI. Those quantities underpin claims of oceanic absorption of over 90% of 'excess energy' attributed to anthropogenic forcing (von Schuckmann et al., 2020). They are constructed, however, almost exclusively from temperature data provided by the international Argo profiling float array (Array for Real-time Geostrophic Oceanography; Johnson et al., 2022) that we are questioning here, and we find that the IPCC OHC anomaly measures fail to comply with essential criteria of the scientific method (Armstrong and Green, 2022) and are not, therefore, a credible basis for policymaking.

Core Argo and Biogeochemical Argo (BGC-Argo) floats[2] profile only the upper ocean to a nominal pressure of 2000 dbar.[3] This leaves the abyssal ocean below that level, comprising approximately half of both the total ocean volume and thermal energy content, largely unsampled except by sparse historical measurements and a limited pilot array of Deep Argo floats (Johnson et al., 2015; Purkey and Johnson, 2010). Despite their central role in IPCC assessments of human impacts on climate, our comprehensive review of the peer-reviewed literature reveals no prior full synthesis of the measurement and processing chain necessary to evaluate the most fundamental threats to the physical validity and reliability of these OHC and EEI estimates.

Previous assessments addressed aspects of validity, including mapping uncertainties (Boyer et al., 2016), sparse historical coverage in remote/polar/deep regions (Meyssignac et al., 2019), and general sampling limitations (von Schuckmann et al., 2020). None, however, has substantively addressed fundamental limitations, including loss of thermodynamic interpretability in anomalies due to the intensive nature of temperature (non-additive across non-equilibrium spatial and temporal domains, as detailed in Section 1.2; Essex et al., 2007), domination by interpolated values

---

[1]As argued by Romer (2001), 'heat' should not be treated as a noun denoting a stored substance. In this paper, we use 'heat' in phrases such as 'ocean heat content' solely as a conventional synonym for thermal energy content, but we neither endorse nor agree with this wording, as it inaccurately implies heat is a substance rather than a process of energy transfer.

[2]BGC stands for Biogeochemical. BGC-Argo floats are equipped with additional sensors beyond the standard conductivity (salinity), temperature, and depth (pressure) CTD sensors in Core Argo floats. They measure biogeochemical parameters such as dissolved oxygen, nitrate, chlorophyll fluorescence (indicating phytoplankton), backscattering (indicating particle concentration), pH, and irradiance (light levels). These floats are part of the expanded Argo program aimed at understanding ocean chemistry, biology, and carbon cycling, in addition to the physical oceanographic variables provided by standard CTD observations.

[3]Argo floats measure and report pressure in decibars (dbar). Depth in meters is inferred from pressure via the hydrostatic relation using gravity and a seawater equation of state. A practical rule of thumb is 1 dbar ≈ 1 m near the surface, but because seawater is compressible and its density varies with temperature, salinity, and latitude, the mapping is not exact: 2000 dbar corresponds to roughly 2000–2025 m under typical open-ocean conditions. Using dbar avoids implying a fixed depth for a given measurement and provides a consistent, instrument-native vertical coordinate for profiling and quality control.

in unsampled volumes, unresolved mesoscale variability in boundary currents and eddy-rich regions, untracked subsurface trajectories, and arbitrary positional assignment. These limitations align with Essex & Andresen (2018)'s 'slow time' framework, where long-timescale climate variables differ from laboratory-scale ones, rendering temperature non-thermalizable on climate timescales. This paper offers the first comprehensive synthesis of these issues, demonstrating that Argo-derived OHC and EEI scalars lack physical correspondence to reality. Even ignoring thermodynamic principles, the calculated EEI uncertainties at 95% confidence exceed commonly cited EEI values, rendering such claims unsuitable for quantifying planetary energy uptake or imbalance.

The ocean stores the vast majority of total heat energy contained within the Earth's climate system. Argo-float-data-based OHC calculations are used as evidence to support claims that approximately 90–93% of the purported increase in system heat (energy) content since 1850 is accounted for by changes in OHC (von Schuckmann et al., 2020; IPCC AR6 WG1, 2021). Within the ocean itself, the vertical distribution of this stored energy is roughly even: about half resides in the upper 2000 m and half in the deep ocean below 2000 m. Claims that ~90% of the recent purported planetary energy imbalance has been absorbed specifically into the upper ocean (0–2000 m) are also entirely dependent on the OHC calculations challenged in this paper. Since the mid-2000s, global ocean heat content estimates have been derived from data collected by the international Argo program, consisting of roughly 4000 autonomous profiling floats (~4156 as of December 28, 2025) that measure temperature, electrical conductivity (for salinity derivation), and pressure primarily in the upper 2000 m of the ocean (Riser et al., 2016; Johnson et al., 2022).

These measurements are processed into gridded fields and integrated to yield global OHC anomaly time series, which form the dominant component of EEI assessments. The IPCC Sixth Assessment Report (AR6) presents an EEI of 0.7 (0.5–0.9) W m^{-2} in its global energy budget diagram (Figure 7.2; Forster et al., 2021), a value adapted from surface flux schematics (Wild et al., 2013, 2019; Stephens et al., 2012) but aligned with OHC-derived inventories from the Argo era. These metrics are presented as direct 'observational' constraints on planetary energy flows, with uncertainties quantified primarily through statistical sampling error (Loeb et al., 2012; von Schuckmann et al., 2016) or the spread among several widely used gridded OHC datasets (e.g., from products developed by IAP, Institute of Atmospheric Physics, Chinese Academy of Sciences; NCEI, National Centers for Environmental Information, NOAA; JMA/MRI, Japan Meteorological Agency / Meteorological Research Institute; BOA_Argo, China Argo Real-time Data Center; and others), capturing methodological differences in how sparse temperature profiles are extrapolated to global fields (von Schuckmann et al. 2020; IPCC AR6 WG1, 2021). Despite their prominence, the physical foundations of these OHC and EEI estimates have not been subjected to rigorous scrutiny regarding the nature of the raw measurements and the transformations applied.

Classical thermodynamics, formalized in the late 19th century, remains a cornerstone of physics due to its reliance on universal principles rather than specific microscopic models — a resilience famously praised by Einstein as "the only physical theory of universal content which I am convinced will never be overthrown, within the framework of applicability of its basic concepts" (Einstein, 1949/1979, p. 31). Indeed, to this day all its fundamental first principles have withstood the test of time. Essex et al. (2007) demonstrate that these principles coupled with basic mathematics reveal fundamental limitations in applying intensive properties like temperature to non-equilibrium systems such as the global ocean, where averaging destroys physical meaning and produces computational artifacts rather than real physical quantities (as detailed in Section 1.2).

Temperature is rigorously defined only in local thermodynamic equilibrium (LTE), constituting a point function meaningful solely for the small volume of fluid in LTE around the measuring device. In the non-equilibrium ocean, subsurface horizontal locations remain unmeasured and unknown throughout the Argo float cycle due to the absence of submerged positioning instrumentation. Subsequent processing introduces interpolated values that dominate the final scalar measures. This paper details the measurement and processing chain and concludes that Argo-derived OHC anomalies and EEI estimates lack physical foundations for quantifying ocean thermal energy change or planetary energy imbalance.

1.1 The Circularity and Hidden Uncertainty of OHC-Derived EEI Estimates

The IPCC claimed 0.5–0.9 W m^{-2} EEI precision is inconsistent with the large absolute uncertainties in direct satellite measurements of top-of-atmosphere (TOA) radiative fluxes from the NASA Clouds and the Earth's Radiant Energy System (CERES) project upon which the EEI estimate depends. Raw CERES data exhibit global mean net TOA flux uncertainties of ~± 3–5 W m^{-2} (higher for individual components), dwarfing the upper bound of the AR6 EEI range (Loeb et al., 2018). Early analyses found even greater uncertainty over the measure, with unconstrained imbalances as large as 6.5 W m^{-2} (Loeb et al., 2009). Surface energy budget assessments, combining satellite, *in-situ*, and model-derived fluxes, reveal discrepancies and uncertainties up to ± 17 W m^{-2} globally (Stephens et al., 2012).

The CERES Energy Balanced and Filled (EBAF) product addresses the large absolute uncertainties in raw TOA fluxes by applying a "one-time global adjustment" to shortwave and longwave components within their individual uncertainty ranges. It uses an objective least-squares algorithm (Loeb et al., 2009; 2018) that forces the long-term mean net TOA flux to equal the Argo-derived OHC calculation plus minor land, ice, and atmosphere terms, yielding the ~0.7 W m^{-2} imbalance presented in IPCC AR6 Figure 7.2 (Forster et al., 2021).

Achieving the 0.7 W m^{-2} figure requires some aggressive adjustments: the radiative flux values, such as reflected solar, must be pushed in some cases to the extreme edges of their uncertainty ranges to produce a net flux consistent with the reported small positive net imbalance. No physical justification is provided for the direction or magnitude of individual component shifts. Use of this "one-time global adjustment" implicitly assumes the Argo OHC-derived quantity is more reliable than direct CERES absolute measurements, despite the OHC chain's fundamental physical invalidity due to thermodynamically meaningless anomalies from intensive-property averaging in non-equilibrium systems, sparse deep and polar sampling, and other flaws detailed herein.

In sum, the term "constrain" applied to the Loeb et al. (2009; 2018) algorithm is misplaced. In scientific measurement, constraints derive from physical laws, independent observations, or known constants, not from forcing agreement with a non-physical mathematical construct. Consequently, the small EEI (~0.7 W m^{-2} in IPCC AR6 Figure 7.2) and its narrow uncertainty (± 0.2 W m^{-2}) are purely artifacts of circular tuning: CERES fluxes are mathematically adjusted to align with the Argo OHC-derived quantity whose physical validity is absent. Raw, unadjusted CERES data do not independently confirm the OHC-based EEI within their uncertainties. This IPCC methodology, euphemistically described as "constraining" EEI, depends fundamentally on unsupported assumptions and circular reasoning. The IPCC AR6-claimed small positive EEI is therefore scientifically invalid.

1.2 Non-Additivity of Temperature in Non-Equilibrium Systems

Temperature is an intensive thermodynamic property defined pointwise only for systems in local thermal equilibrium (Reif, 1965). In equilibrium thermodynamics, intensive variables such as temperature are not additive; they cannot be meaningfully averaged across non-equilibrium domains to yield a physically meaningful global scalar (Essex et al., 2007).

Using formal mathematical reasoning together with the axioms of classical thermodynamics, Essex et al. (2007) rigorously proved that no physically meaningful global surface temperature exists for the Earth system. While local temperatures can be defined for small volumes in approximate thermodynamic equilibrium, the Earth's climate system operates far from equilibrium at the global scale. Any averaging of local temperature measurements, regardless of the chosen mathematical procedure, therefore, lacks a unique physical basis. An infinite number of equally valid averaging methods exist, each capable of producing contradictory trends from the same underlying data when physical principles do not dictate a preferred rule.

Building on this foundation, Essex and Andresen (2018) extended the analysis to the broader question of appropriate measurements for climate. They proved that conventional meteorological concepts of temperature, derived from laboratory-scale equilibrium thermodynamics, cannot be "thermalized" or meaningfully extended to the long spatiotemporal scales that are characteristic of climate. On these "slow time" scales, temperature loses thermodynamic interpretability, rendering global or even regional mean temperatures physically ill-defined constructs rather than measurable quantities.

Cohler (2025) provides a historical review of how the meaningless global mean surface temperature (GMST) concept became entrenched in climate science despite its invalidity. The simple thermodynamic and mathematical principles that underpin the invalidity of temperature averaging in non-equilibrium systems like Earth's surface have been well understood since at least the late 19th century (Gibbs, 1875–1878), although Essex et al. (2007) were the first to make this clear in peer-reviewed literature. Cohler's analysis traces the development of the fallacious GMST from early statistical aggregations of weather data to its current role as the central metric in climate policy and assessment reports. Cohler also reaffirms the conclusions of Essex et al. (2007) and Essex and Andresen (2018), emphasizing that GMST represents an arbitrary statistical average of an intensive property over a non-equilibrium system, with no unique physical principle governing the choice among infinitely many mathematically permissible averaging conventions.

These three works collectively establish that global temperature metrics, including GMST and related anomalies, are physically meaningless numerical abstractions without correspondence to any conserved thermodynamic quantity such as energy or entropy. This fundamental thermodynamic invalidity of temperature averaging directly parallels and reinforces the central conclusions of the present paper: the construction of global OHC anomalies and derived EEI estimates suffers from the identical flaw in addition to several others. Both rely on the non-physical averaging and integration of intensive temperature measurements across vast non-equilibrium spatial and temporal domains in the ocean, producing final scalar quantities that are computational artifacts. The absence of thermodynamic meaning in global temperature metrics therefore undermines not only surface-based climate claims but also the entire chain of OHC and EEI calculations that dominate contemporary assessments of planetary energy imbalance.

1.3 Geometry and Thermal Energy Distribution of the Global Ocean

The global ocean spans a surface area of approximately 362 million square kilometers, representing 71% of the Earth's surface, with a total volume of 1330 million cubic kilometers and an average depth of 3688 m (Eakins and Sharman, 2010; Charette and Smith, 2010). Ocean topography encompasses diverse features: continental shelves at depths less than 200 m covering ~27 million square kilometers (7–8% of ocean area), steep continental slopes transitioning to abyssal plains at 4000–6000 m (comprising ~40–50% of ocean area), mid-ocean ridges, and trenches reaching 11 000 m (Menard and Smith, 1966; Amante and Eakins, 2009). Additionally, Argo floats are generally not deployed in regions with bottom depths between approximately 200 m and 2000 m, such as continental slopes, which cover about 8.5% of the ocean surface area and contain roughly 2% of the total ocean volume, to prevent grounding during their parking and profiling cycles (Riser et al., 2016; Costello et al., 2010).

The hypsometric curve, depicting the cumulative distribution of ocean area with depth, illustrates the non-uniform bathymetry. Average depth is computed as total volume divided by surface area, but volume fractions require integrating the area-depth profile:

$$V(d) = \int_0^d A(z)dz \quad (1)$$

where *A(z)* is the ocean area deeper than z. Thus, while 2000 m constitutes ~54% of the average depth, the volume above 2000 m is ~50% of the total due to minimal volumetric contribution from shallow shelves and substantial upper-layer volume over extensive deep basins (Eakins and Sharman, 2010; Sverdrup et al., 1942).

Ocean thermal energy content scales with volume, density, specific heat capacity, and absolute temperature (Kelvin). Commonly cited heuristic mean temperatures are ~5 °C (278 K) above 2000 m and ~2 °C (275 K) below, yielding a ~1% relative difference (Purkey and Johnson, 2010;

Desbruyères et al., 2016). Combined with near-equal volumes, thermal energy is distributed roughly evenly between upper and deep layers, within observational uncertainties (Talley et al., 2011; Levitus et al., 2012) contrary to popular misconceptions.

Argo float sampling focuses on open ocean regions deeper than 2000 m, largely excluding continental shelves (27 million km^2), marginal seas (e.g., Mediterranean, South China Sea; total ~20–50 million km^2 or 6–14% of ocean area), and ice-covered high-latitude zones like the Arctic (14 million km^2) (Riser et al., 2016; von Schuckmann et al., 2020). Argo therefore excludes ~90 million km^2 or ~25% of the global ocean surface area.

2. The Argo Measurement Process

2.1 Float Cycle and Profiling

Standard Core Argo and most BGC-Argo floats operate on a nominal 10-day cycle (Argo Steering Team, 2022). Following a brief surfacing period for data satellite transmission and GPS positioning, the float descends to a parking pressure/depth of approximately 1000 dbar in 4–8 hours, drifts freely at that depth for roughly 9 days, performs a short deep descent to the profiling pressure of approximately 2000 dbar (1–2 hours), and then executes a slow, buoyancy-controlled ascent to the surface lasting 6 to 10 hours. High-resolution conductivity, temperature, and depth/pressure (CTD) measurements are taken during this ascent phase, at sampling rates of approximately 1 Hz, yielding approximately 1000 discrete pressure levels per ascent 'profile' after binning to typical vertical intervals of 2 dbar in modern data products[4] (Argo Data Management Team, 2025). The float remains on the surface for 15 minutes to 1 hour and then descends again for its next pass.

Each float lasts around 4 to 5 years, depending chiefly on the lifetime of its lithium-ion battery. Once the battery is depleted, the float can no longer adjust its buoyancy and becomes permanently neutrally buoyant at whatever depth it happens to be, usually near its parking depth of 1000 m, and drifts passively with deep ocean currents indefinitely. No recovery is attempted; the floats are designed as expendable instruments, and the cost-plus logistical impossibility of retrieving them from remote open-ocean locations would be prohibitive. As a result, each dead float becomes permanent deep-sea debris: a ~1-meter-long plastic cylinder containing lithium batteries, metals, electronics, and sensors that slowly corrode, allowing seawater ingress over time (typically within 5–10 years), after which it gradually sinks to the abyssal seafloor, where further decomposition occurs over additional years or decades.[5]

In sum, the measurement points sampled during its carefully controlled ascent trace an irregular three-dimensional trajectory through the ocean determined by depth-varying currents, vertical

---

[4] Core Argo and BGC-Argo floats record CTD data at high frequency (~1 Hz, or roughly every second) during` their 6-to-10-hour ascent from depth to surface. Some floats sample continuously, while others take discrete spot measurements. In either case, the raw data are averaged or selected onboard into regular vertical bins of typically 2 decibars (dbar) pressure intervals (equivalent to ~2 meters of depth) before transmission after surfacing. This binning creates standardized, manageable profiles with ~1000 levels over the full ~2000 dbar range, as used in all modern Argo data products.

[5] Since 2000, the Argo program has deployed tens of thousands of floats worldwide (~4000 active at any time, with 600–900 replaced annually), causing a growing number of inactive floats residing at depth after mission completion. Although this accumulation invites comparison to orbital debris, the practical risk is negligible. The ocean's volume is vast (~1.3×10^9 km^3), and floats are deployed at ~300 km horizontal spacing, yielding an extremely low density ($\ll$1 float per 1000 km^3 at mid-depths). No collisions between Argo floats and submarines have been reported, likely because deep-ocean traffic is sparse, floats are small and passive with minimal acoustic signature, and submarines employ active sonar for obstacle avoidance. Any hypothetical collision would likely cause only minor damage due to the float's low mass and energy. Environmental assessments further indicate that materials released by Argo floats (e.g., lithium, aluminum, lead) are negligible compared to natural geochemical fluxes or land-based marine pollution. While long-term accumulation of synthetic materials in the deep ocean warrants attention in principle, the present scale poses no significant environmental or operational concern.

shear, mesoscale eddies, internal waves, and turbulent motions. The path is neither vertical nor a linear 'slant' but an unknown and complex, meandering curve through a spatially and temporally varying flow field. Each temperature measurement represents a true point value, the intensive thermodynamic state at a specific location and instant, but the spatial coordinates of subsurface measurements remain unknown.

2.2 Horizontal Position Identification Limitations

Iridium-equipped Argo floats, which dominate the current fleet, obtain their positions when they surface from GPS fixes with ~8 m accuracy (95% confidence). Rare GPS failures require fallback to less accurate Iridium geolocation with ~1–5 km accuracy (Wong et al., 2020). Argo floats employ no subsurface positioning system such as acoustic tracking or inertial navigation (Roemmich et al., 2009). Consequently, the entire subsurface trajectory remains horizontally untracked: including the descent, the 9-day parking drift, and the profiling ascent during which measurements are acquired.

The only measured horizontal displacements are net vectors between consecutive surfacing positions, typically spanning 50–300 km in moderate flow regions, and routinely exceeding 400 km in energetic currents such as the Antarctic Circumpolar Current (Ollitrault and Rannou, 2013). The horizontal displacement during the 6–10-hour ascent phase, when temperatures are measured, is completely indeterminate from measured data. We estimate it to be on the order of 5–50 km, with no physical basis for inferring precise values.

Standard Argo data products assign all subsurface measurements from a given profile to the single longitude, latitude, and time of the GPS fix obtained when the float surfaces (Argo Data Management Team, 2025). Actual longitude and latitude of the data collected during the 9-10 days a float is submerged are unknown and unknowable, because the floats have no instrumentation to measure location under water. Since the shear currents accumulate during the ascent phase, offset displacement from the surface GPS fix scales with depth: deeper measurements experience longer exposure to cumulative shear currents during ascent. Actual measurement times during ascent, which range over the 6–8-hour period, are also not saved in standard profile data products.

2.3 Nature of Raw Temperature Measurements

Each temperature measurement represents an intensive thermodynamic property directly proportional to average kinetic energy of the particles (water molecules and dissolved ions) in the small volume of seawater in local thermal equilibrium (LTE) immediately surrounding the sensor. In seawater, apparent molar heat capacities of major salts are small and generally negative, so adding salt slightly lowers total heat capacity. Because water molecules constitute over 98 % of the mass and supply > 99 % of the thermal capacity, the thermal energy content of seawater is almost entirely governed by the water mass. Dissolved salts primarily affect density and compressibility, not heat capacity. Each measurement samples effectively infinitesimal volume relative to total ocean volume (~1.3 billion km^3). Collectively, all Argo profiles over time provide sparse point constraints with negligible direct volumetric ocean coverage.

2.4 Depth Coverage Limitations

As described above, Standard Core and BGC Argo floats are designed to profile to a target pressure of 2000 dbar (Riser et al., 2016; Argo Steering Team, 2022). This limitation confines measurements to the upper ocean, which constitutes approximately 50% of both the total ocean volume and energy content. The global mean ocean depth is approximately 3688 m, with the maximum depth reaching 10 984 m in the Challenger Deep of the Mariana Trench (Gardner et al., 2014; Stewart and Jamieson, 2019). The region below 2000 m, encompassing the rest of the bathyal (1000 to 4000 m) zone, as well as the abyssal (4000 to 6000 m) and hadal/trench zones (6000 to 11 000 m), remains unsampled by the Core Argo and BGC-Argo arrays.

A small pilot deployment of Deep Argo floats has begun profiling to 4000–6000 dbar (Johnson et al., 2015; Zilberman et al., 2023, 2025), but as of late December 2025, these comprise ~315 active Deep Argo floats (projected from 224 active as of March 2025, with ~90 deployments planned through the end of 2025, per the 26th Argo Steering Team Meeting [AST-26] report). This remains far short of the target of approximately 1228 for purportedly "full" global coverage and provides insufficient spatial and temporal sampling for reliable global integration without extensive extrapolation (Zilberman et al., 2023; Zilberman et al., 2025; Argo program status via OceanOPS and AST reports). This fundamental sampling limitation in Argo-derived OHC products persists despite the Deep Argo expansion.

3. Calculation of the OHC Estimate and Uncertainty

3.1 Arbitrary Positional Assignment

In nearly all profile data files, temperature measurements taken during the ascent are assigned the longitude and latitude of the surfacing position (Argo User's Manual, 2025). This convention ignores the unknowable upstream horizontal offsets due to the downstream shear currents encountered during ascent as well as the different times of each individual measurement. The largest horizontal offsets are for measurements taken at the deepest points and we estimate them to be ~10–20 km in most regions and unlikely to exceed ~30–50 km even in the most extreme shear currents (see section 3.7.1).

3.2 Construction of the Reference Climatology

In oceanography, a climatology (or reference climatology) is a long-term average Eulerian description of intensive ocean properties, such as temperature and salinity, at different locations, depths, and times of year. It serves as a baseline or "normal" state against which current or observed conditions are compared to calculate "anomalies" (deviations from the average). These anomalies are used to support claims of changes, such as ocean warming, but the climatology itself is not a snapshot measurement of any single real ocean state but rather a statistical construct derived from historical intensive data.

To compute anomalies in OHC products, a gridded reference climatology is used. The Roemmich-Gilson (RG) Argo Climatology (2019), commonly used as the reference in Argo-era OHC products, is constructed exclusively from Argo float data (primarily 2004–2018, with extensions to later years). It provides mean fields and the annual cycle on a fine grid using weighted least-squares fitting of nearby profiles. Other climatologies, such as the World Ocean Atlas (WOA) series, incorporate pre-Argo historical observations (from ships, bottles, XBTs, etc.) alongside Argo data.

For each monthly temporal bin of the RG climatology, values on a regular three-dimensional grid are generated from the measured profile data using mathematically 'optimal' interpolation with covariance functions having prescribed horizontal correlation lengths, typically on the order of hundreds of kilometers (Roemmich and Gilson, 2009).

The gridded monthly fields are then arithmetically averaged over the reference period (2004–2018 for the current version of the RG Argo Climatology, 2019) to obtain the final climatological grid. The fixed 2019 climatology for 2004–2018 is not updated with newer observations. Separate monthly gridded fields (absolute temperature and salinity values, computed using the same optimal interpolation method) are made available for periods beyond 2018. As of the latest update, these monthly fields extend through June 2025. These post-2018 monthly fields are absolute gridded values (not anomalies). They are computed consistently with the methodology used for the 2004–2018 period but do not modify or incorporate data into the fixed 2004–2018 reference mean. The product website hosted by the Scripps Institution of Oceanography (University of California, San Diego) at

https://sio-argo.ucsd.edu/RG_Climatology.html

distributes these monthly fields as extensions to allow ongoing analysis relative to the unchanging 2004–2018 baseline mean.

A value at any grid point and depth in the RG Argo Climatology is a statistical construct: it is a weighted linear combination of measured temperatures from disparate physical locations (typically within hundreds of km) and times (within the same calendar month, up to ~30 days apart), obtained via optimal interpolation of monthly-binned anomalies, followed by arithmetic averaging across years (2004–2018) for each calendar month. This grid value therefore does not represent the actual temperature that any real parcel of seawater would have experienced at that exact grid point and depth at any specific moment. It is instead the result of the prescribed interpolation, weighting, and multi-year averaging operations applied to the input measurements.

3.3 Physical Meaninglessness of the Anomaly Definition

The OHC calculation relies entirely on the computation of temperature anomalies, ΔT. In global gridded products (the basis for EEI estimates), these are defined as $\Delta T = T_{\text{interpolated}} - T_{\text{reference}}$ where $T_{\text{interpolated}}$ is a value derived by mapping sparse float data onto a regular grid, and $T_{\text{reference}}$ is a climatological mean for that same grid point. While arithmetically possible, this operation yields a result that is physically meaningless for the following reasons:

Invalidity of the "Measured State" (Tinterpolated)

The value $T_{\text{interpolated}}$ acts as a proxy for measurement, yet it does not represent the temperature of any actual water parcel. Because Argo floats are sparse (nominally one per 3° x 3° region), filling a 1° x 1° grid requires objective analysis (OA) algorithms that aggregate data using covariance scales of 200–2800 km and temporal windows of one month. $T_{\text{interpolated}}$ is a weighted average of the temperatures of distinct water masses separated by hundreds of kilometers and weeks of time. As established by Essex et al. (2007), averaging intensive variables (temperature) across a non-equilibrium system destroys physical meaning: "A sum over intensive variables carries no physical meaning" (p. 5). Thus, $T_{\text{interpolated}}$ is a statistical artifact, not an actual thermodynamic state of anything.

Part of the problem associated with interpolating sparse data onto discrete grids in both space and time is that the grid resolution creates opposite challenges in each dimension. Spatially, Argo floats typically measure profiles separated by hundreds of kilometers, yet these sparse observations are interpolated onto 1° × 1° grids with spacing of approximately 100 km or less, creating far more grid points than actual measurements and requiring substantial spatial interpolation between widely separated observations. Temporally, measurements occur every 10 days but are aggregated into monthly bins, creating fewer temporal bins than the measurement frequency. This mismatch of fine spatial gridding of sparse data combined with coarse temporal binning of frequent measurements creates interpolation inconsistencies that can substantially affect the outcome. (Doswell, 1977; Wahba and Wendelberger, 1980; Wikle and Cressie, 1999).

Invalidity of the Reference State ($T_{\text{reference}}$)

The climatological baseline $T_{\text{reference}}$ (e.g., the Roemmich-Gilson climatology) is constructed by averaging temperature measurements at fixed geographic locations over time. This approach treats the ocean as an Eulerian field: a framework in which fluid properties are described as functions of fixed spatial coordinates. However, ocean temperature is fundamentally a Lagrangian property; it is a characteristic of specific water masses that move, mix, and transform as they are advected by currents. A water mass at 30°N, 150°W in January 2005 and a water mass at the same geographic coordinates in January 2018 are not the same physical entity; they have different histories, source regions, and thermodynamic states. Averaging their temperatures produces a statistical artifact at that grid point, not a meaningful physical baseline. The Eulerian framework, while mathematically convenient for gridded analysis, fundamentally misrepresents the Lagrangian nature of ocean thermodynamics.

This Eulerian-Lagrangian mismatch is compounded by the temporal arbitrariness of the chosen averaging period. The climatological baseline is derived from smoothing measurements over the 2004–2018 period, a 15-year window that is physically arbitrary and introduces systematic biases into the analysis. Ocean circulation operates on timescales ranging from seconds (turbulent eddies) to millennia (thermohaline circulation), with no physical significance attached to a 15-year window. Major ocean processes including mesoscale eddies (days to months), seasonal convection cycles, the El Niño-Southern Oscillation (2–7 years), the Pacific Decadal Oscillation (20–30 years), and Atlantic Multidecadal Variability (50–70 years) all operate on timescales incommensurate with this averaging period. The resulting climatology necessarily reflects the specific dynamical state of the ocean during 2004–2018 (including whatever phase each oscillatory process happened to occupy during that interval) rather than any physically meaningful equilibrium state. Not only are measurements from distinct water masses with different histories being averaged together spatially, but the reference state against which anomalies are calculated itself represents an arbitrary snapshot of transient ocean dynamics rather than a thermodynamically meaningful baseline.

A further issue with the climatological baseline $T_{\text{reference}}$ is the changing density and spatial distribution of floats. In 2004, many fewer floats were available and spatially, their distribution covered the oceans less evenly than in 2018.

Additionally, the polar oceans remain grossly undersampled by the standard Argo array owing to pervasive sea ice cover, which precludes routine operations of conventional floats in ice-covered regions. The Arctic Ocean (north of 60°N) accounts for ~4% (14 million km^2) of global ocean surface area (361 million km^2), while the Southern Ocean (south of 60°S) encompasses ~6% (22 million km^2), yielding a combined polar fraction of 10% of total ocean surface area (IHO, 1953). These regions contribute a 7% share of total ocean volume given their less than average depths. Specialized Polar Argo deployments using ice-avoiding technologies have improved coverage in seasonal ice zones, but central ice-covered areas, particularly in the Arctic, remain sparsely observed. These persistent spatial sampling gaps in shallow marginal seas/shelves and polar domains introduce systematic biases in global ocean heat content estimates derived from Argo data, particularly when constructing climatological reference states.

The 'Ghost vs. Ghost' Abstraction

The subtraction operation (ΔT) assumes that the reference state ($T_{\text{reference}}$) represents a meaningful baseline against which changes can be measured. However, $T_{\text{reference}}$ itself varies in both space and time; it is not a constant equilibrium state but rather an arbitrary temporal and spatial average of transient ocean conditions. Therefore, $T_{\text{reference}}$ has no physical validity as a reference temperature from which to calculate meaningful ΔT, yet this operation forms the basis of all OHC anomaly calculations.

The operation ΔT therefore compares two time-varying, spatially varying statistical constructs, neither of which represents the actual thermodynamic state of any water mass, yet the resulting difference is misleadingly assigned units of Kelvin by the purely algebraic manipulation of dimensional symbols.

The purported OHC anomaly scalar is then calculated as:

$$\Delta\text{OHC} = \int \rho c_p \Delta T \, dV \tag{2}$$

resulting in an equally invalid scalar that carries units of energy (joules, J), and due to its global order of magnitude, it is conventionally expressed in zettajoules (ZJ) where 1 ZJ = 10^{21} J. One cannot derive a physical quantity from a computation based on non-physical inputs, like ΔT. Yet these anomaly values constitute the primary basis for global OHC change estimates in Argo-era products.

3.4 Spatial Interpolation of Anomalies to Create Continuous Fields

Sparse anomaly values, each computed at the assigned surfacing position from point temperature measurements taken along a meandering sampling trail swept by a sensor during a 6–10 hour float ascent, are interpolated onto regular three-dimensional grids using objective analysis algorithms such as 'optimal' interpolation (a form of 'kriging'), successive corrections, or weighted averaging (Roemmich and Gilson, 2009; Gaillard et al., 2016; Good et al., 2013). While the floats are nominally spaced ~300 km apart, with typical measurement distances of 200–500 km due to drift, these methods employ covariance models with horizontal correlation length scales typically on the order of 200–2800 km, tuned to the physical autocorrelation scales of ocean temperature and salinity fields on monthly-to-annual timescales (Cheng et al., 2017; Li et al., 2017). Such scales enable 'optimal' weighting of nearby profiles and propagation of information across data gaps.

With ~4000 active Argo floats providing approximately 12 000–13 000 profiles per month globally (Argo Program, 2025), monthly gridded products on 1° × 1° horizontal resolution yield ~40 000–45 000 ocean surface grid locations after masking out land and shallow areas. Polar regions poleward of ~60° latitude have severely limited coverage and higher uncertainty due to seasonal and permanent ice cover that prevents float surfacing and data transmission. In well-sampled mid-latitude regions, this results in roughly 3–4 times as many grid points as monthly profiles. In sparsely sampled high-latitude regions poleward of ~60°N and S, with partial coverage from specialized ice-avoiding floats via programs like the Southern Ocean Carbon and Climate Observations and Modeling [SOCCOM]), the ratio often exceeds 10–20 times as many grid points due to lack of empirical data and heavier reliance on interpolation. Most common spatial interpolation algorithms (e.g., inverse-distance weighting or kriging with a global mean background) tend toward the domain-average value (or a local mean) as the number of nearby observations decreases and distance to the interpolation point increases. These methods are generally unable to perform meaningful extrapolation beyond the spatial extent of the observed data and, in sparse regions, effectively revert to a smoothed background estimate rather than capturing potential local extremes or trends not present in the limited samples (Shepard, 1968; Willmott et al., 1985).

Logically, spatial interpolation cannot increase the empirical information content of the dataset (Cover and Thomas, 2006; Shannon, 1948). It redistributes the limited information, without loss, from sparse, discrete point measurements according to data-driven covariance structures and physical assumptions. No new physical sampling occurs, and the total empirical information content remains bounded by the original ~12 000–13 000 monthly profiles plus data from the small number of specialized ice-avoiding floats.

The gridded fields are 'optimal', in a statistical sense, estimates under the calculated covariances, with effective resolution an order of magnitude coarser than the nominal 1° grid (~111 km meridional spacing at the equator), but closer to the ~300 km Argo sampling scale and chosen correlation lengths (Roemmich et al., 2019). Grid-point values in data voids are informed extrapolations, damped toward the climatological mean (zero for anomalies), with higher associated uncertainty. The optimality of these estimates is defined as minimizing the sum of squared differences between interpolated values and observations. However, generating error fields from such statistics results in systematic underestimation of the true uncertainty. Proper error assessment requires interpolating to withheld observations not accessed by the algorithm, rather than comparing estimates to the same observations used to optimize the interpolation procedure.

Presenting results as continuous gridded fields facilitates visualization, global integration (e.g., for OHC totals), and comparison with models, but risks conveying an impression of denser and more regular empirical coverage than exists. The underlying information is confined to sparse profiles, and all final gridded data are interpolated. Direct empirical measurements, obtained along horizontally meandering ascent trails sampled by Argo sensors, cover a negligible fraction of the ocean volume. Even when treated conservatively as narrow three-dimensional tubes, the total volume directly sampled by all Argo profiles in a year is many orders of magnitude smaller than the $\sim 10^{18}$ m^3 upper-ocean volume, yielding a sampling fraction of order 10^{-9} or less. Because covariant interpolation employs correlation length scales on the order of 1000 km, and because multiple profiles within a grid cell are first merged to form a single input value, every point in the final gridded product is a calculated quantity rather than a direct measurement.

Methodological choices, such as covariance scales, background fields, and inclusion of non-Argo data, introduce sensitivities in global OHC estimates, contributing to inter-product spreads equivalent to differences of ~0.1–0.5 W m^{-2} in derived EEI trends across analyses (Cheng et al., 2022; von Schuckmann et al., 2023). Reported uncertainties often focus on mapping error within individual products but may underestimate structural biases from these assumptions.

3.5 Integration to OHC Scalar

The interpolated anomaly grid is converted to a purported energy scalar by multiplying by fixed reference values for seawater density ρ (1027 kg m^{-3}) and specific heat capacity c_p (3985 J kg^{-1} K^{-1}), then summing over grid cell volumes.

Internal thermal energy for a seawater parcel is given by $U = m \times c_p \times T_K$ but calculating ΔOHC using temperature anomalies ΔT omits the dominant absolute temperature term and makes implicit assumptions such as conserved mass and constant thermodynamic properties within fixed Eulerian grid cells — assumptions that are violated in an advecting, mixing, open ocean system. The resulting scalar therefore corresponds to no physical energy or energy change in any real measured thermodynamic system.

The use of fixed reference values for seawater density specific heat capacity, rather than fully variable properties from TEOS-10,[6] introduces a small additional methodological approximation (~1–3% relative effect on OHC, equivalent to ~0.01–0.03 W m^{-2} on EEI trends), further exemplifying dependence on conventional approximations in the energy conversion rather than the full physics of variable seawater properties.

3.6 The Lagrangian Reality

A deeper thermodynamic issue stems from the fundamental mismatch between Eulerian and Lagrangian frameworks. All current Argo-derived ocean heat content (OHC) products are constructed in a fixed Eulerian reference frame: temperature measurements are binned, objectively interpolated, and averaged into stationary grid cells (typically 1° × 1° × 2 dbar), irrespective of water parcel trajectories. In reality, the ocean's water masses are continuously advected by large-scale currents, mesoscale eddies, fronts, and turbulent mixing. As a result, the same grid cell at different times contains entirely different physical water parcels, with no conserved thermodynamic identity linking the climatological baseline to subsequent measurements.

This Eulerian averaging therefore mixes intensive temperature values from unrelated, non-equilibrium fluid elements across space and time. The resulting pseudo-global integral does not correspond to the actual heat content change of any definable, materially conserved water-mass system. A common counterargument, that the "global" integral approximately captures heat displaced elsewhere, fails because Argo provides no direct measurements in well over 50% of the ocean volume (particularly below 2000 m, in marginal seas, under ice, and in poorly sampled high-latitude or coastal regions). There is thus no truly closed, observed system; the calculation relies heavily on interpolation and extrapolation over vast unsampled domains.

A truly thermodynamically meaningful OHC would require Lagrangian tracking of the same evolving water parcels along their trajectories: an approach that is practically impossible at global scale due to untracked subsurface paths and extreme dispersion over multi-year timescales. The resulting OHC scalar is therefore not a valid or reliable estimate of the true ocean thermal energy storage; instead, it is a methodological artifact dominated by arbitrary assumptions and computational choices that bear no direct relationship to the underlying physical quantity.

3.7 Estimation of Uncertainty from Spatial and Temporal Sampling Errors

Although the thermodynamic arguments presented in Section 3.3 demonstrate that Argo-derived OHC anomalies and integrated scalars are physically meaningless as quantifications of thermal energy change, it is instructive to evaluate the magnitude of numerous uncertainties arising from

[6] TEOS-10 (Thermodynamic Equation of Seawater - 2010) is the international standard for seawater thermodynamic properties adopted by the Intergovernmental Oceanographic Commission in 2010. It provides algorithms for computing seawater density, specific heat capacity, and other thermodynamic properties as functions of Absolute Salinity, Conservative Temperature, and pressure. TEOS-10 replaced the older EOS-80 (Equation of State 1980) standard and accounts for spatial variations in seawater composition beyond simple salinity (IOC, SCOR and IAPSO, 2010; McDougall and Barker, 2011).

spatial and temporal limitations, and the entire calculation framework accepted as an empirical construct for the sake of argument only.

3.7.1 Horizontal Misplacement and Untracked Subsurface Displacement

Horizontal misplacement arises because all ascent measurements (6–10 hours duration) are arbitrarily assigned to the surfacing GPS position, despite advection by subsurface currents. Direct quantification is impossible due to the absence of subsurface trajectory tracking, but bounds can be derived from observed velocities, horizontal temperature gradients, and published OHC sensitivities.

Subsurface currents down to 2000 m typically range from 0.05–0.2 m s^{-1}, with maxima of 0.5–0.8 m s^{-1} (or higher in boundary current extensions and shear zones; Gaillard et al., 2009; Ollitrault and Rannou, 2013). For a 10-hour ascent, this produces net horizontal displacements of ~2–7 km under typical conditions and up to 18–29 km at peak velocities. A conservative range of 5–50 km is adopted for deeper points, accommodating transient shear; the 50 km upper bound implies an average velocity of ~1.4 m s^{-1}, well below Argo's 3.0 m s^{-1} automated rejection threshold for inter-profile velocity (Wong et al., 2025). This contrasts sharply with conventional treatments that dismiss ascent drift as a "minor contaminant" limited to <5–10 km without supporting measurements (Ollitrault and Rannou, 2013).

Horizontal temperature gradients over these distances are substantial, driven by mesoscale eddies (radii 50–200 km) and fronts that dominate open-ocean variability (Chelton et al., 2011). Gradients commonly reach 1–5 °C over 50–100 km across eddy boundaries or western boundary current extensions (Frenger et al., 2013; Gaillard et al., 2009), implying temperature assignment errors of ~0.5–3 °C (or greater in energetic regions) from positional misplacement alone. Equivalently, this smears measurements over an irregular horizontal footprint, aliasing local mesoscale/sub-mesoscale gradients (typically 0.005–0.05 °C/km) into profile-level uncertainties of 0.05–1 °C.

These offsets do not cancel globally in integrated OHC or EEI calculations: displacements are governed by local, non-stationary processes (eddies, fronts, turbulent shear) rather than large-scale symmetric patterns. At short ascent timescales, Coriolis deflection is weak and does not produce opposing hemispheric biases. Instead, aliasing from untracked horizontal displacements during the 6–10 hour ascent (typically 5–50 km in regions of moderate to strong currents or shear) introduces incoherent regional errors that accumulate in Eulerian gridded fields. When combined with interannual circulation variability (e.g., ENSO, PDO shifts), this creates a time-dependent methodological bias in OHC trends. A very rough scaling suggests this effect could shift global EEI estimates by on the order of 0.02–0.1 W m^{-2}: local temperature mis-assignments from displacements over strong gradients (~0.1–1°C over 10–50 km) affect a fraction of profiles in energetic regions; when integrated over the global ocean (accounting for non-perfect cancellation), the resulting OHC trend error translates to an EEI bias in this range, comparable to or exceeding some published ensemble spreads (±0.1–0.2 W m^{-2}) that do not account for this foundational data-assignment flaw (von Schuckmann et al., 2020, 2023). Similar artifacts arise from how the reference climatology is constructed: temperature profiles measured at different times during each month are pooled together and statistically fitted (Roemmich & Gilson, 2009). This is another example of how arbitrary processing choices affect the final result.

3.7.2 Persistent Sampling Gaps and Undersampling

Annual/Interannual Mapping and Sampling Errors

Standard errors for annual global OHC changes (0–2000 m) range ~0.6–1.2 W m^{-2} at 95% confidence (~2σ) directly from Argo-era mapping uncertainties, driven by spatial gaps and interpolation assumptions (Johnson et al., 2018; Meyssignac et al., 2019).

Deep Ocean Uncertainty: Artifactual Precision vs. Physical Ignorance

The reported uncertainty of ± 0.04 W m⁻² for deep ocean (>2000 m) heat uptake in von Schuckmann et al. (2020, 2023) and subsequent ensemble products is physically meaningless as a representation of true observational uncertainty. This value emerges from methodological artifacts rather than direct measurements: in vast unsampled regions, the analyses prescribe near-zero temperature change (stasis assumption) or rely on climatological interpolation with prescribed low variance. This creates circular logic: lack of data is interpreted as lack of variability, which then justifies reporting high precision. Physically, for an unmeasured volume comprising ~50% of the ocean, uncertainty is bounded only by the maximum plausible temperature change (ΔT_{deep}) compatible with total EEI. The IPCC claimed EEI of 0.7 W m^{-2} corresponds to a mean deep-ocean ΔT_{deep} of only ~0.0003 K yr^{-1}, far below the detection threshold of current sparse sampling (IPCC AR6 assessments in red):

$$\Delta T_{deep} = \Delta U_{deep} \,/\, C_{deep} \approx 0.8 \text{ ZJ yr}^{-1} / 2734 \text{ ZJ K}^{-1} \approx 0.0003 \text{ K yr}^{-1}$$

		EEI		**Earth surface area**		**Seconds per year**			**ΔU_{Earth}**
ΔU_{Earth}	≈	(**0.7 W m^{-2}**)	×	(5.1 x 10^{14} m^2)	×	(3.156 x 10^7 s yr^{-1})			≈ 11.3 ZJ yr^{-1}
		ΔU_{Earth}		**Ocean % of global EEI**		**Deep ocean % of ΔOHC**			**ΔU_{deep}**
ΔU_{deep}	≈	11.3 ZJ yr^{-1}	×	**91%**	×	**8%**			≈ 0.8 ZJ yr^{-1}
		Deep ocean		**Ocean volume**		**Seawater density**		**Seawater heat capacity**	**C_{deep}**
C_{deep}	≈	50%	×	(1.335 x 10^{18} m^3)	×	1028 kg m^{-3}	×	3985 J kg^{-1} K^{-1}	≈ 2734 ZJ K^{-1}

Even with recent growth in the Deep Argo pilot array to ~315 floats, the limitation persists: sampling density remains roughly 1 float per 2–3 million km^3 (equivalent to an Alaska-sized surface area) of deep ocean volume, providing negligible coverage for constraining global, volume-weighted mean temperature change. Deep Argo data are used primarily for regional validation or supplement, not as the primary basis for global error budgets in von Schuckmann et al. (2023) or related products, which continue to rely on repeat hydrography (decadal ship tracks) and null assumptions in data gaps. The ~315 floats provide no meaningful reduction in structural uncertainty for the full deep ocean; they remain a performative addition insufficient to distinguish small signals (0.0003 K yr^{-1} for 8% uptake) from larger plausible changes (~0.002 K yr^{-1} for 50% uptake) or zero.

The typical abyssal temperature variability is estimated at $\sigma_T \approx 0.05$ K, consistent with model-based estimates of deep ocean variability (Desbruyères et al., 2016). With current Deep Argo coverage limited to ~315 floats, the unsampled fraction of the deep ocean remains >0.99, yielding an absolute uncertainty of $C_{deep} \times \sigma_T \times f_{unsampled}$ = 2734 ZJ K^{-1} × 0.05 K × 0.99 ≈ 135 ZJ for the deep ocean thermal energy. Over the 48-year period 1971–2018, this translates to *deep ocean global equivalent flux uncertainty*:

$$135 \text{ ZJ} / (48 \text{ yr} \times (3.156 \times 10^7 \text{ s yr}^{-1}) \times (5.1 \times 10^{14} \text{ m}^2)) \approx \pm 0.175 \text{ W m}^{-2}$$

Accounting for the amplification of aliasing due to Nyquist-Shannon violations in sparse sampling (approximately a factor of 2, as demonstrated in model subsampling studies), the deep ocean ignorance uncertainty is estimated at ~± 0.35 W m⁻² which aligns with previous studies: Purkey & Johnson (2010) report ~± 0.1 W m⁻², Zilberman et al. (2023) ~± 0.2 W m⁻² from sampling error analyses, Meyssignac et al. (2019) ~± 0.13 W m⁻² for the deep contribution in sea level budget closure, and von Schuckmann et al. (2023) ~± 0.1 W m⁻² for deep ocean uptake. Synthesizing these, the deep ocean ignorance uncertainty is conservatively estimated at ~± 0.35 W m⁻², while the claimed ± 0.04 W m⁻² is a result of computational assumptions rather than a measure of physical uncertainty.

Polar Ocean Undersampling: Amplified Ignorance and Additional Uncertainty

The undersampling problem is even more severe in the polar oceans (Arctic and Southern, beyond ~60°N/S, including ice-covered regions), which comprise ~10% of ocean surface area but significant volume (especially shelves, deep basins, and marginal seas). Standard Core Argo floats face high mortality from ice crushing or failure to surface/transmit under permanent/seasonal ice; coverage relies on ice-avoidance algorithms, Iridium-equipped floats, and limited Polar Argo extensions (e.g., SOCCOM in Southern Ocean, SODA/GREEN EDGE in Arctic). As of late 2025, Polar Argo sampling remains sparse, with only hundreds of profiles acquired, corresponding to an effective density of roughly one float per several million km³ in ice-covered regions, about an order of magnitude sparser than the global Argo average. Products like von Schuckmann et al. (2020, 2023) and updates (e.g., 2023–2025 OHC reports) explicitly exclude or minimally include polar regions due to poor data, yet when extrapolated via climatology or models, they assume low variability in gaps. This mirrors deep-ocean circularity: absence of measurements → presume quiescence → manufacture high precision. Physically, polar contributions (potentially 5–15% of global EEI via circulation/ice interactions) imply plausible flux equivalents of ~0.05–0.15 W m⁻² globally; sparse sampling cannot detect mean ΔT changes of ~0.001–0.005 K/yr across unsampled volumes, rendering true uncertainty ~± 0.2–0.5 W m⁻² from polar regions alone.

Even pilot efforts (ice-tethered profilers, gliders, BGC extensions like SOCCOM) provide only regional snapshots, not global volume-weighted constraints. The ~315 Deep Argo floats barely penetrate polar deep layers, and no full-scale Polar Argo array exists to address ice barriers, high variability (e.g., ice-albedo, freshwater fluxes), or seasonal inaccessibility. von Schuckmann-related ensembles acknowledge polar gaps as a source of potential underestimation (10% trend impact if polar warming significant) but report overall EEI uncertainties of ± 0.1–0.2 W m⁻² (e.g., 0.76 ± 0.2 W m⁻² for 2006–2020). This ignores structural flaws: polar data voids dominate interpolation, and null/low-variance assumptions suppress error bars artificially.

We estimate total polar ocean temperature variability as $\sigma_{T\text{polar}} \approx 0.1$ K. Heat content of the polar oceans is estimated by $C_{\text{polar}} = m_{\text{polar}} \times c_p$ where

$m_{\text{polar}} \approx (25.3 \times 10^{15}\ \text{m}^3\ [>60°\ \text{N}] + 71.8 \times 10^{15}\ \text{m}^3\ [>60°\ \text{S}]) \times 1028\ \text{kg m}^{-3} \approx 1.0 \times 10^{20}$ kg
$C_{\text{polar}} \approx 1.0 \times 10^{20}\ \text{kg} \times 3985\ \text{J kg}^{-1}\ \text{K}^{-1} \approx 399\ \text{ZJ K}^{-1}$

With current Argo polar coverage limited to even fewer floats than Deep Argo, the unsampled fraction of the deep ocean remains >0.99, yielding an absolute uncertainty for the polar oceans' thermal energy of

$C_{\text{polar}} \times \sigma_{T\text{polar}} \times f_{\text{unsampled}} = 399\ \text{ZJ K}^{-1} \times 0.1\ \text{K x } 0.99 \approx 39.5$ ZJ

Over the 48-year period 1971–2018, this translates to a *polar ocean global equivalent flux uncertainty:*

$39.5\ \text{ZJ} / (48\ \text{yr} \times (3.156 \times 10^7\ \text{s yr}^{-1}) \times (5.1 \text{ x } 10^{14}\ \text{m}^2)) \approx \pm 0.05\ \text{W m}^{-2}$.

Accounting for the amplification of aliasing due to Nyquist-Shannon violations in sparse sampling (approximately a factor of 2, as demonstrated in model subsampling studies), the polar ocean ignorance uncertainty is estimated at ~± 0.1 W m⁻².

Unresolved Mesoscale Variability in Boundary Currents and Eddy-Rich Regions

Unresolved mesoscale variability in boundary currents and eddy-rich regions represents a major structural source of uncertainty in Argo-derived global OHC estimates and derived EEI values. Approximately 90% of total global ocean kinetic energy is contained in these eddy fields (Ferrari & Wunsch, 2009). These areas, including the Gulf Stream, Kuroshio Extension, Antarctic Circumpolar Current, and Agulhas Current, exhibit intense, small-scale (10–200 km) fluctuations in temperature, salinity, and velocity driven by eddies, fronts, meanders, and instabilities. The kinetic energy of ocean currents is orders of magnitude smaller than the thermal energy stored in the water, yet these flows transport immense amounts of thermal energy. Core Argo's sparse sampling (~4000 floats, with typical spacing of ~300 km) fails to resolve these features, leading to large local root-mean-square errors (RMSE) in mapped heat content equivalent to >100 W m⁻² surface flux in energetic zones.

When these local errors alias into global integrals (misrepresenting high-frequency variability as low-frequency signals), they propagate as residual interannual noise or uncertainty in the global mean OHC trend or EEI estimates given grossly under- or completely unsampled fraction of the total global ocean. Energy is conserved in the total volume not the Argo sampled fraction. Meyssignac et al. (2019) note that:

> "*Estimating the uncertainty in OHC changes at interannual time scales is more challenging because of insufficient spatio-temporal coverage. So far, few studies have provided estimates. Estimates of annual OHC changes for 0–2000 m have standard errors of 0.3–0.6 Wm^{-2}* [1σ] *over the Argo era, and those errors increase substantially for the pre-Argo time period (Johnson et al., 2018, their Figure 2)."* (p. 11)

We also adopt 0.6-1.2 W m^{-2} as the 2σ value for the unresolved mesoscale uncertainty. This uncertainty alone is comparable to or exceeds the reported central EEI values (0.7 W m^{-2}), meaning year-to-year global OHC fluctuations are dominated by sampling artifacts rather than true physical change.

This uncertainty arises because mapping/interpolation schemes (e.g., optimal interpolation, machine learning regressions) must fill vast unsampled volumes with assumed covariance structures that fail to capture the full amplitude and spectrum of mesoscale activity in the strong boundary currents of ocean basins. High-resolution methods (e.g., satellite altimetry + in situ blending) reduce but do not eliminate the issue, as Argo remains the primary subsurface constraint. Similar ranges appear in related works on mapping uncertainties, high-resolution OHC products, and reviews of Argo limitations (e.g., Lyman & Johnson, 2023 on Random Forest Regression Ocean Maps [RFROM]; broader discussions in Meyssignac et al., 2019, von Schuckmann et al. ensembles, and Wang et al., 2018). Wang et al. cautioned that,

> *"[D]ata during the Argo period are still insufficient to observe the meso-scale eddies and OHC changes related to weather phenomena"* (p. 2485).

3.7.3 Arbitrary Processing Choices and Methodological Artifacts

Structural/Methodological spreads across Argo-based OHC products

Intercomparisons of multiple Argo-based in situ mappings, such as those from IAP, EN4, Ishii, NOAA NCEI, BOA, SCRIPPS, IPRC, MOAA, SIO, and others, show spreads in ocean heat uptake (OHU ≈ EEI proxy) of 0.23–0.56 W m^{-2} for 2005–2019 trends, with annual variability spreads larger due to differing quality control, climatologies, and covariance choices (Hakuba et al., 2024). For example, during the Argo-dominated period (2005–2019), global OHC trends in the upper 2000 m vary across eight objective analysis products (e.g., BOA: 3.6 ZJ yr^{-1} in 0–300 m; EN4: 4.1 ZJ yr^{-1}), yielding spreads of ~0.5 ZJ yr^{-1} (0.1 W m^{-2} EEI equivalent) in layer-specific rates, with EN4 often an outlier due to stronger warming signals (Bilgili, 2025).

Recent updates, such as IAPv4 (10.7 ± 1.0 ZJ yr^{-1} for 2005–2023 upper 2000 m) versus IAPv3 (9.6 ± 1.1 ZJ yr^{-1}), demonstrate ~11% differences attributable to bias corrections and data handling, translating to EEI spreads of ~0.1–0.2 W m^{-2} across datasets (Cheng et al., 2024a). These discrepancies arise from arbitrary methodological choices in interpolation, averaging, and assimilation, despite shared raw Argo inputs, providing direct evidence of inherent uncertainty in the methodologies themselves. These discrepancies arise from arbitrary methodological choices in interpolation, averaging, and assimilation, despite shared raw Argo inputs, providing direct evidence of inherent structural uncertainty in the methodologies themselves, adding systematic unpropagated bias equivalent to ~± 0.2–0.5 W m^{-2} or more.

Arbitrary Choice of Baseline Date Range

A change in the climatology date range used for calculating OHC anomalies from Argo data can introduce substantial differences in implied EEI, typically on the order of ~0.1–0.3 W m^{-2} (systematic spread) for decadal trends, as evidenced by sensitivity analyses of objective mapping methods where climatology choices are a primary contributor to error (e.g., Boyer et al., 2016; Lyman & Johnson, 2014). This arises because shifting the reference period (e.g., from 2004–2018 to 2005–2019 or later Argo-era windows) can alias different phases of decadal variability like the PDO or the Atlantic Multidecadal Oscillation (AMO) into the baseline mean, leading to offsets in OHC estimates that propagate to EEI, particularly when mapping methods relax to the climatological mean in data-sparse regions, rendering fine-resolution EEI claims sensitive to arbitrary baseline selection.

Eulerian vs. Lagrangian Framework and Resulting Uncertainty

Regional Lagrangian analyses of ocean circulation and heat transport reveal substantial discrepancies with traditional Eulerian OHC estimates. These analyses are based on high-resolution, ocean-only hindcast simulations (eddy-permitting to eddy-rich NEMO/ORCA configurations forced by atmospheric reanalyses), not on coupled global general circulation climate models (GCMs). Unlike CMIP-style GCMs, which suffer from coupled atmosphere / ocean feedbacks, extensive parameterization of unresolved processes (clouds, convection, mixing), the fundamental physical meaninglessness of GMST due to spatial temperature averaging, and inherent structural uncertainties in long-term projections, these hindcasts are tightly constrained to reproduce observed historical variability and focus strictly on the actual physics of ocean advection and heat transport at regional scales. They therefore do not inherit the fundamental thermodynamic and averaging problems that afflict global coupled GCMs or Eulerian OHC products.

For example, Tooth et al. (2024) used water parcel trajectories in an eddy-rich hindcast to decompose meridional energy transport at 26.5°N in the Atlantic, finding that recirculating parcels in the subtropical gyre account for 37 ± 9% of the total energy transport, a contribution that Eulerian vertical-horizontal decompositions often attribute differently or underemphasize due to their fixed-grid averaging over unrelated water masses. Similar Lagrangian decompositions in the eastern North Atlantic subpolar gyre (Tooth et al., 2023) and other regions highlight how Eulerian methods mix signals from advecting, non-conserved parcels, leading to differences in inferred heat uptake pathways and magnitudes that can reach 30–50% regionally.

These discrepancies imply significant uncertainty when extrapolating regional Eulerian OHC estimates to global scales. In the Atlantic at 26.5°N alone, the 30–40% attribution difference corresponds to ~0.1–0.2 PW (petawatt) in heat transport uncertainty (based on typical total meridional heat transport ~1–1.5 PW at that latitude). Scaled globally (considering the Atlantic contributes ~25–30% of total ocean heat uptake), we derive this conservative range by converting the estimated transport discrepancies directly into global energy flux equivalents. A systematic error of ~0.1–0.2 PW, when distributed over Earth's surface area (5.1×10^{14} m^2), yields a baseline bias of approximately 0.2–0.4 W m^{-2}. To account for potential partial compensations between basin circulations while acknowledging the magnitude of the Atlantic bias, we adopt 0.1–0.4 W m^{-2} as a robust estimate of the structural uncertainty inherent in Eulerian heat budget closures. This uncertainty is not captured in current ensemble spreads (± 0.1–0.2 W m^{-2}), as they rely on correlated Eulerian products and do not account for the Lagrangian framework's fundamentally different view of heat pathways and conservation.

3.7.4 Lack of Independence in Ensembles and Consensus Over-Simplification

The reported EEI uncertainty of ± 0.2 W m^{-2} (IPCC AR6 Figure 7.2: 0.7 W m^{-2}, range 0.5–0.9 W m^{-2}) relies on apparent convergence across OHC products (IAP, NOAA/NCEI, EN4, Ishii). However, this convergence fails to quantify total uncertainty because the products lack independence. All major Argo-era OHC estimates share ~90% of their raw input from the same ~4000 floats (Riser et al., 2016). Differences arise solely from processing variations: climatology baselines differing by 15 years between IAPv3 (1990–2005) and IAPv4 (2006–2020), substantial differences in quality control thresholds, and unquantified covariance radii in mapping (Cheng et al., 2024a). With correlations $\rho > 0.8$, the effective number of independent samples reduces to ~1–2, violating the Central Limit Theorem. Ensemble uncertainty thus approximates single-product uncertainty rather than reducing by $\sqrt{N}$ (where N = 4 to 6 in most OHC ensemble estimates of EEI).

Common-mode systematic biases further undermine reliability. Argo salinity biases, primarily due to sensor drift in the conductivity cells of CTD sensors (mostly Sea-Bird SBE 41/41CP), affect the vast majority of profiles. According to a detailed evaluation of raw Argo salinity data from 2000–2021, approximately 90% of profiles requiring adjustment have small-magnitude drift (<0.03 psu), while 2–3% exhibit more severe drift (>0.05 psu). A particularly concerning episode occurred during 2017–2018, when ~17% of annual profiles showed adjustable positive (salty) drift, peaking due to a temporary manufacturing defect in the encapsulant material used in CTDs deployed around 2015–2018 (Wong et al., 2023).

These widespread and temporally correlated biases are shared across the global Argo fleet due to similar sensor technology. If left unadjusted or incompletely corrected, they introduce spurious salinity increases in raw data, which propagate into density calculations via the equation of state. This creates artificial (spurious) halosteric sea level signals that contaminate steric height products. Although OHC itself is computed from temperature anomalies only, the resulting spurious density/steric trends distort validation of OHC against independent observations (satellite altimetry + gravimetry), cause non-closure of the global sea level budget, and increase systematic uncertainty in attributing observed sea level rise to true thermosteric ocean heat uptake. Delayed-mode quality control mitigates most issues, but residual undetected or unquantifiable bias persists, adding systematic uncertainty to global ocean state estimates, including heat content and sea level.

Mapping artifacts contribute ± 0.2–0.5 W m^{-2} regional errors (e.g., Southern Ocean), propagating to ~0.1 W m^{-2} globally (Gregory et al., 2014). Inter-product spreads of 0.1–0.2 W m^{-2} (2005–2018 trends: 0.54–0.64 W m^{-2}) reflect methodological consistency, not robustness (Cheng et al., 2022). All products assume isotropic covariance, underestimating eddy-rich region biases (± 0.05–0.1 W m^{-2}). Deep hydrography uncertainties add ± 0.3–0.5 W m^{-2} (Garry et al., 2019), and sea level closure introduces ± 0.29–0.37 W m^{-2} uncertainty (Meyssignac et al., 2019).

CERES TOA annual mean uncertainties for global net flux are on the order of ± 4 W m^{-2} (Loeb et al., 2018), with interannual variability typically ± 1–2 W m^{-2} driven by ENSO and cloud effects (Loeb et al., 2021). Upper-ocean heat content (OHC; 0–700 m) has been underestimated by approximately 20–40% due to observational gaps, particularly in the Southern Hemisphere (Durack et al., 2014). Decadal EEI trend uncertainty from CERES is dominated by systematic errors (∼0.1 W m^{-2} $decade^{-1}$ from instrument stability and drift; Loeb et al., 2021; Raghuraman et al., 2021) and internal variability, with total uncertainty comparable to the observed trend itself (0.50 ± 0.47 W m^{-2} $decade^{-1}$ over the Argo era from 2005 to 2019; Loeb et al., 2021). While extended CERES records (2001–2024) indicate a statistically significant linear trend of 0.45 ± 0.22 W m^{-2} $decade^{-1}$ at 95% confidence (Loeb et al., 2024), the shorter Argo-era interval exhibits a trend where uncertainty remains comparable in magnitude to the signal itself, highlighting the difficulty in detecting acceleration.

Figure 7.2's presentation exacerbates these issues by displaying EEI as a single value without timescale qualifiers, implying universal precision that obscures higher annual/interannual uncertainties acknowledged elsewhere in AR6 text. This over-simplification fosters overconfidence, as the narrow range masks correlated assumptions, gap-induced errors, and the fundamental limitations of sparse Argo sampling.

3.7.5 Nyquist-Shannon Theorem and Aliasing in Argo Data

Subsection 3.7.2 already quantifies the uncertainty from unresolved mesoscale variability in eddy-rich regions (including boundary currents like the Gulf Stream, Kuroshio Extension, Antarctic Circumpolar Current, and Agulhas Current), where sparse Argo sampling fails to resolve 10–200 km fluctuations, leading to local RMSE >100 W m^{-2} in energetic zones that propagate via aliasing into global integrals as residual interannual noise or uncertainty on the order of ~0.6–1.2 W m^{-2} (2σ) for global OHC trends or EEI estimates. This discussion highlights practical observational and interpolation limitations but does not explicitly invoke the fundamental signal processing principle responsible for the aliasing: the Nyquist-Shannon sampling theorem (Shannon, 1949). The theorem imposes irreducible limits on detectable spatial and temporal frequencies, independent of mapping quality or statistical assumptions. High-frequency signals (from mesoscale eddies and smaller features) are inevitably misrepresented as lower-frequency ones when sampling rates significantly violate the Nyquist criterion that sampling frequency be at least twice the highest signal frequency.

This subsection therefore builds on Subsection 3.7.2 by providing the theoretical basis for the aliasing already quantified there. Furthermore, it identifies additional structural uncertainties arising from theorem violations in regions with even sparser effective sampling (deep ocean and polar areas), where Nyquist limits are more severely exceeded.

Argo's target horizontal spacing (300 km mean distance) and 1° grid resolution yield a spatial Nyquist wavelength of ~200 km, marginally resolving large mesoscale features but aliasing smaller eddies/submesoscale variability (<50–100 km). Temporally, the 10-day cycle limits resolution to periods ≥20 days, aliasing faster processes (e.g., eddy passages of 5–15 days). These limits explain the aliasing mechanism in Subsection 3.7.2 but do not add new global uncertainty beyond it, as the primary mesoscale energy dominance (~90% of ocean kinetic energy in geostrophic eddy fields; Ferrari & Wunsch, 2009) is already captured.

Nyquist Limitations in Deep and Polar Oceans

The theorem's constraints become particularly severe in the deep ocean (>2000 m, ~50% of ocean volume) and poleward of 60° N and S (~10% of ocean surface area and ~7% of volume), where sampling sparsity pushes Nyquist wavelengths far beyond mesoscale scales, exacerbating aliasing and providing additional uncertainty not fully covered in prior subsections.

Core Argo floats provide no data below 2000 m. The current pilot ~315 Deep Argo floats result in effective intervals of ~900 km, yielding Nyquist wavelengths ~1800 km. High-frequency deep ocean processes (abyssal eddies, internal waves, bottom water formation at ~100–500 km scales) are thus aliased or undetectable. Model studies indicate such sparsity folds deep signals into apparent basin-scale trends (Purkey & Johnson, 2010; Zilberman et al., 2023). The Nyquist-Shannon theorem therefore elucidates one key mechanism contributing to our estimated ≥± 0.3 W m^{-2} deep ocean ignorance bound: the irreducible folding of unresolved high-frequency variability into resolved low-frequency signals due to theorem violations from extreme sparsity. This aliasing effect, estimated at ~± 0.2–0.4 W m^{-2} in model-based analyses of sparse deep ocean sampling, is not a separate addition but a specific manifestation of the broader physical ignorance, refining and corroborating our bound. This reinforces our conclusion that deep OHC uncertainties of ± 0.04 W m^{-2} given by von Schuckmann et al. (2020/2023) are unrealistically narrow, relying heavily on low-variance interpolation assumptions that ignore both the general lack of observational constraint and the fundamental aliasing imposed by Nyquist limits.

Polar regions all suffer chronic undersampling (<10% in area Argo coverage and <<1% in volume due to ice and logistics; Riser et al., 2016), with intervals >500 km and Nyquist wavelengths >1000 km. This fails to resolve high-frequency polar variability (polynyas, iceshelf melt plumes, rapid frontal shifts at ~10–100 km). Temporal aliasing worsens from the 10-day cycle missing fast ice-ocean interactions (e.g., diurnal tidal mixing).

Implications for Global OHC and EEI

The Nyquist theorem provides the physical rationale for the mesoscale aliasing uncertainty already quantified in Subsection 3.7.2. In undersampled deep and polar volumes, it introduces similar large uncertainties described above of ≥± 0.3 W m^{-2} for deep non-polar ocean and ≥± 0.1 W m^{-2} for polar oceans. Current assessments overlook these fundamental sampling constraints, treating OHC as overly precise. Denser arrays could mitigate this, but Nyquist limits remain irreducible with the present methodology.

3.7.6 Quantitative Summary of Uncertainty Contributions

Combining all identified sources of error yields a conservative 95% confidence uncertainty on annual-to-decadal EEI well exceeding ± 1 W m^{-2}. Key contributors include:

a. *Unresolved mesoscale variability* in boundary currents and eddy-rich regions, propagating to interannual global noise of ~0.6–1.2 W m^{-2} (2σ parametric/interannual noise).

b. *Persistent sampling gaps in the deep ocean* (>2000 m), introducing physical ignorance bounds of ~± 0.35 W m^{-2} due to stasis assumptions and sparse coverage (~315 Deep Argo floats projected, negligible density).

c. *Altimetry and mass budget uncertainty* of ~0.29–0.37 W m^{-2} due to the discrepancy between OHC-implied sea-level change and satellite altimetry/gravimetry measurements.

d. *Structural discrepancies between Eulerian and Lagrangian frameworks*, implying potential global biases of ~0.1–0.4 W m^{-2} from mixing of non-conserved water parcels.

e. *Arbitrary baseline/climatology* choices, which shift decadal trends by ~0.1–0.3 W m^{-2} across reasonable Argo-era windows.

f. *Persistent sampling gaps in the polar/high-latitude regions*, introducing physical ignorance bounds of ≥± 0.1 W m^{-2} due to sparse coverage and ice barriers preventing float survival/transmission.

g. *Horizontal misplacement* and untracked subsurface displacement during ascent, producing potential methodological biases of ~0.02–0.1 W m^{-2} or more from aliasing of local gradients.

Table 1. Quantified Sources of Uncertainty and Bias in Argo-Based EEI Estimates

A conservative summary of major uncertainty and bias sources contributing to EEI estimates derived from Argo-based OHC calculations on annual-to-decadal timescales. Total compounded uncertainty exceeds reported values by an order of magnitude. All ranges represent conservative estimates at approximately 95% confidence. A conservative lower-bound estimate of total compounded uncertainty can be illustrated via root-sum-square (RSS) synthesis of the components listed above, though this method is strictly valid only for independent, Gaussian errors. Taking midpoint values: $\sqrt{(0.9^2+0.35^2+0.33^2+0.25^2+0.2^2+0.1^2+0.06^2)} \approx 1.1$ *W* m^{-2} *at approximately 95% confidence. However, this RSS approach systematically underestimates total uncertainty because: (1) structural and ignorance terms (b, c, e, f) represent fixed bounds rather than Gaussian measurement scatter, requiring linear rather than quadratic aggregation; (2) sampling gaps (b, f) share common exclusionary causes, creating positive correlation which violates RSS independence assumptions; and (3) explicit systematic biases (d, g) are directional offsets that do not randomly cancel. A more realistic synthesis treating structural terms as partially additive yields ≥± 1 W* m^{-2} *at 95% confidence as a conservative lower bound.*

Source	*Uncertainty/Bias ± (W* m^{-2}*)*	*Type*
a. *Unresolved mesoscale variability* in boundary currents and eddy-rich regions	~0.6–1.2 (2σ)	Parametric/interannual noise
b. *Persistent sampling gaps:* deep ocean (>2000 m)	~0.35	Structural/physical ignorance
c. *Altimetry & mass budget uncertainty*	~0.29–0.37	Structural/closure problem
d. *Structural discrepancies between Eulerian and Lagrangian frameworks*	~0.1–0.4	Framework bias
e. *Arbitrary baseline/climatology*	~0.1–0.3	Processing artifact
f. *Persistent sampling gaps*: polar/high-latitude regions	~0.1	Structural/physical ignorance
g. *Horizontal misplacement* and untracked subsurface displacement during ascent	~0.02–0.1	Methodological bias
Total compounded (95% confidence)	*≥± 1*	*Overall*

These uncertainties are compounded by lack of independence in OHC ensembles (shared inputs, high correlations $\rho > 0.8$, effective $N \approx 1$–2) and common-mode systematics (e.g., salinity biases, interpolation artifacts), rendering reported values of ± 0.1–0.2 W m^{-2} (e.g., von Schuckmann et al., 2023; IPCC AR6 Figure 7.2) applicable only to within-product parametric variance under optimistic gap-extrapolation assumptions. This narrow range excludes all uncertainty/bias sources quantified above.

A conservative lower-bound estimate of total uncertainty can be illustrated via root-sum-square (RSS) synthesis of the components listed above, though this method is strictly valid only for independent, Gaussian errors (Taylor, 1997, Chapter 3; Trenberth, 2009). Taking midpoint values: $\sqrt{(0.9^2+0.35^2+0.33^2+0.25^2+0.2^2+0.1^2+0.06^2)} \approx 1.1$ W m^{-2}. However, this RSS approach actually underestimates total uncertainty because: (1) structural and ignorance terms (b, c, e, f) represent fixed bounds rather than Gaussian measurement scatter, requiring linear rather than quadratic aggregation; (2) sampling gaps (b, f) share common exclusionary causes, creating positive correlation which violates RSS independence assumptions; and (3) explicit systematic biases (d, g) are directional offsets that do not randomly cancel. A conservative synthesis treating structural terms as partially additive yields ≥± 1 W m^{-2} at 95% confidence.

This total 95% confidence uncertainty (≥± 1 W m^{-2}) exceeds the uncertainty of the IPCC AR6 EEI estimate of 0.7 ± 0.2 W m^{-2} (Figure 7.2) by an order of magnitude. When structural flaws such as non-additive intensive anomalies, dominant interpolation in unsampled volumes, framework discrepancies, untracked trajectories, and arbitrary positional assignment are rigorously accounted for, the central estimate becomes statistically indistinguishable from zero on annual-to-decadal timescales. The continued presentation of narrow uncertainties as observational therefore constitutes a critical overstatement of measurement capability, obscuring fundamental limitations in sparse Argo sampling, deep and polar undersampling, mesoscale aliasing, and arbitrary processing choices.

This total uncertainty also renders CERES EBAF adjustments (forced to match OHC-derived EEI) circular and artifactual, as raw CERES absolute uncertainties (± 3–5 W m^{-2}; Loeb et al., 2018) vastly exceed the claimed precision. The rigorous accounting presented here, independent of ensemble convergence, demonstrates total EEI uncertainty of ≥± 1 W m^{-2} on annual-to-interannual timescales, consistent with natural variability and observational noise (± 1–2 W m^{-2}; Loeb et al., 2021). Enhanced observing systems would be required to reduce mapping errors below ± 0.3 W m^{-2} (Meyssignac et al., 2019; von Schuckmann et al., 2023).

This conclusion is further reinforced by the absence of any physically meaningful global-scale metric for the intensive property temperature (Essex et al., 2007; Essex & Andresen, 2018; Cohler, 2025), rendering global mean surface temperature (GMST) an arbitrary average over a non-equilibrium system with no unique averaging rule among infinitely many valid options. From first principles, the CO_2-driven global warming hypothesis, while grounded in radiative physics (van Wijngaarden & Happer, 2025), lacks empirical validation due to the thermodynamic invalidity of such constructs and the inability to measure the extensive quantities OHC and EEI with sufficient precision.

3.7.7 Indeterminacy of Ocean Vertical Energy Change Partitioning

The claimed vertical partitioning of purportedly positive net flux of energy into the ocean, wherein ~85–93% is attributed to the volume above 2000 m with ~7–15% below, is not an empirically robust finding, but rather a derived construct from observationally sparse and methodologically constrained datasets (IPCC AR6 uses 15 different ensemble members referring back to von Schuckmann et al. 2020 and 2023).

This claim of predominant upper-ocean dominance is made by multiple syntheses, including the IPCC AR6 assessment (Forster et al., 2021, Table 7.1), and claims based on von Schuckmann et al. (2020) that the upper-lower gains during 1971–2018 were 364.9 ± 83.5 ZJ (~92%) and 31.0 ± 15.4 ZJ (~8%), respectively. The percentage partition reported by von Schuckmann et al. (2023) adding two years of data (1971-2020) remains the same.

Given the profound structural uncertainties and thermodynamic invalidity inherent in all estimates of OHC change demonstrated in our analysis, it is impossible to scientifically exclude even a roughly balanced 50%-50% split, or any other equitable distribution, in the vertical partitioning of net flux of energy into the ocean between the upper (<2000 m) and lower (>2000 m) ocean layers. Therefore, the claimed partitioning is not an empirical observation, but a computational artifact derived from sparse, non-physical integrations of intensive temperature anomalies across vast unsampled volumes. Deep ocean contributions, estimated at ~8% or ~0.07–0.1 W m^{-2} equivalent (von Schuckmann et al., 2020, 2023), rely on decadal ship-based repeat hydrography with coverage of <<1% of deep volume and uncertainties often exceeding ± 50% of the signal, compounded by assumptions of stasis in data gaps that artificially suppress uncertainty (Garry et al., 2019).

Even in the Argo era, where upper-layer sampling is denser, the same methodological flaws such as arbitrary baselines, Eulerian averaging over non-conserved water masses, and untracked trajectories, render the dominance of upper warming unreliable, with structural uncertainties (e.g., ± 0.3–0.5 W m^{-2} for deep layers alone) large enough to accommodate deep fractions up to 30–50% or higher without contradicting the flawed data (Allison et al., 2019).

Pre-Argo estimates, with much sparser profiles and known biases like XBT fall-rate errors, amplify this indeterminacy, yet modern ensembles circularly blend them without resolving the foundational issues. This narrative of precise vertical partitioning is further undermined by model biases that underestimate shallow OHC gain while overestimating deep penetration, as well as persistent observational gaps in polar and abyssal regions that could mask substantial deep ocean variability (IPCC, 2021).

With no thermodynamically valid global scalar for OHC change, and uncertainties dwarfing the reported EEI (0.7 W m^{-2}), alternative distributions like 50%-50% remain plausible, aligning with the baseline ~50%-50% total energy split between the upper and lower ocean and highlighting how claims of upper dominance are scientifically unsubstantiated.

4. Discussion

The construction of Argo-derived global OHC anomalies and derived EEI estimates involves a sequence of mathematical operations that progressively disconnect the final scalar from any measurable physical quantity of thermal energy. Temperature measurements, being intensive point values defined only in local thermodynamic equilibrium, are first assigned to arbitrary geographic coordinates ignoring untracked subsurface horizontal displacements of 5–50 km during ascent, then differenced against a climatological reference that itself is a non-physical statistical construct lacking correspondence to any actual water mass. The resulting anomalies, which are thermodynamically meaningless due to the non-additivity of temperature across non-equilibrium spatial and temporal domains (Essex et al., 2007; Essex & Andresen, 2018), are then aggregated via interpolation algorithms that fill the vast majority of ocean volume with values determined by prescribed covariance functions and correlation scales rather than direct measurements.

The integrated OHC scalar thus represents a computational artifact whose magnitude and sign are highly sensitive to methodological choices, including reference-period selection (introducing ± 0.1–0.3 W m^{-2} sensitivity), correlation lengths, damping parameters, baseline climatology, and the choice of Eulerian versus Lagrangian framework (± 0.1–0.4 W m^{-2} systematic bias), rather than to any conserved physical property. Our comprehensive uncertainty analysis (Section 3.7, Table 1) demonstrates that when all identifiable sources are rigorously quantified, the total 95% confidence uncertainty on annual-to-decadal EEI reaches at least ± 1 W m^{-2}, roughly an order of magnitude larger than values commonly reported in IPCC AR6 (± 0.1–0.2 W m^{-2}). This total uncertainty exceeds their central EEI estimate of 0.7 W m^{-2} (range 0.5–0.9 W m^{-2} [IPCC's 90% CI][7]; Figure 7.2), rendering it statistically indistinguishable from zero.

[7] IPCC uses a non-standard, ill-defined notation in this energy budget diagram. Quoting p. 169 of IPCC AR6 WGI: "Throughout this WGI Report, unless stated otherwise, uncertainty is quantified using 90%

Previous studies have quantified portions of this methodological sensitivity. Boyer et al. (2016) demonstrated that mapping method and baseline climatology choices alone can shift upper-ocean heat content trends by amounts comparable to the reported signal. Cheng et al. (2024a) acknowledge that month-to-month variability in their IAPv4 product often exceeds signals detectable by satellite radiometry, while ensemble spreads among products (von Schuckmann et al., 2023) reach ± 0.1–0.2 W m^{-2} for decadal trends. However, these reported spreads capture only within-ensemble variance and do not account for the systematic biases and structural uncertainties we have quantified: unresolved mesoscale variability (± 0.6–1.2 W m^{-2} parametric noise), deep ocean physical ignorance bounds (± 0.35 W m^{-2}), sea-level closure discrepancy problem (±0.29–0.37 W m^{-2}), Eulerian-Lagrangian framework difference (±0.1–0.4 W m^{-2}), arbitrary baseline climatology (±0.1–0.3 W m^{-2}), polar ocean undersampling (± 0.1 W m^{-2}), and untracked subsurface trajectories (± 0.02–0.1 W m^{-2}), arbitrary positional assignment, and thermodynamic invalidity of anomaly averaging. Recent work continues to present Argo-derived OHC as a definitive indicator of ocean warming (Cheng et al., 2024b, 2025a, 2025b; Trenberth et al., 2025; Bilgili, 2025; Pan et al., 2026) without confronting these foundational issues, treating reported ensemble spreads as comprehensive uncertainty while relying on the same underlying measurement and processing chain that we demonstrate to be fundamentally flawed.

A critical methodological circularity further undermines the claimed precision: the CERES EBAF adjustment procedure forces direct satellite measurements of top-of-atmosphere radiative fluxes, which have absolute uncertainties of ± 3–5 W m^{-2} or more (Loeb et al., 2018), to mathematically match the Argo OHC-derived imbalance whose physical validity is absent. This "one-time global adjustment" pushes individual flux components (reflected solar, outgoing longwave) to the extreme edges of their uncertainty ranges without physical justification, producing the narrow ± 0.2 W m^{-2} range in IPCC AR6 Figure 7.2 as an artifact of circular tuning rather than independent observational confirmation (Section 1.1). The apparent convergence between CERES-adjusted and OHC-derived EEI values therefore represents mutual methodological reinforcement rather than independent empirical validation.

The fundamental issue of vertical energy partitioning remains similarly unresolved. The widely cited claim that ~90–93% of purported planetary energy increase resides in the ocean, with ~85–93% of oceanic uptake in the upper 2000 m (von Schuckmann et al., 2020, 2023; IPCC AR6), cannot be scientifically sustained given the profound uncertainties we have documented. Deep ocean contributions rest on <<1% volumetric sampling via decadal ship-based repeat hydrography, with uncertainties often exceeding ± 50% of the purported signal and stasis assumptions in data voids that artificially suppress error bars (Section 3.7.7). The structural uncertainties for deep layers alone (~± 0.35 W m^{-2}) are large enough to accommodate deep ocean fractions ranging from near-zero to 50% or higher, rendering the claimed precise partitioning a methodological construct rather than an empirical observation. Alternative distributions, including even a 50-50 upper-lower ocean partitioning of net energy flux is physically plausible.

To independently test the scientific validity of the IPCC AR6 0.7 W m^{-2} EEI assessment, we applied Armstrong & Green's (2022) Compliance with Science Checklist (see Appendix A),[8] comprising eight major criteria and 26 subcriteria derived to test compliance with the scientific method using systematic empirical falsification of testable hypotheses, which is the only logically valid means of ruling out falsehoods about physical reality.

These understandings were established by Hume (1748), which proved that empirical truths cannot be derived through deductive reasoning alone, and later formalized by Popper (1959), which

uncertainty intervals. The 90% uncertainty interval, reported in square brackets [x to y], is estimated to have a 90% likelihood of covering the value that is being estimated. The range encompasses the median value and there is an estimated 10% combined likelihood of the value being below the lower end of the range (x) and above its upper end (y). Often the distribution will be considered symmetric about the corresponding best estimate (as in the illustrative example in the figure), but this is not always the case."

[8] We provided Grok 4.1 beta with Chapter 7 of AR6 (containing the 0.7 W m^{-2} EEI assessment), a draft of this paper, and a copy of the Checklist.

showed that hypotheses about the physical world cannot be verified as true but can be falsified as false through empirical contradiction. For claims about empirical reality, no alternative to falsification exists; deductive logic can establish internal consistency but cannot determine correspondence with physical phenomena without empirical observation.

The Checklist operationalizes this framework through criteria enforcing falsifiable hypotheses (1), valid empirical data and methods (3, 4, 8), testing against alternative explanations (5), logical consistency (6, 7), and freedom from bias (2). Implementation of the scientific method is only as robust as its weakest link. If any single criterion is not satisfied, the claim must be rejected as false. This is logical necessity, not scientific convention: a single failure renders the claim empirically ungrounded, indistinguishable from unfalsified conjecture. For example, if plausible alternative hypotheses were not tested, the claim represents advocacy for a preferred hypothesis rather than one that has survived attempts at falsification. As detailed in Appendix A, Grok found the claim failed the test. Five of the eight major criteria were violated: objectivity of study design (free from advocacy), validity and reliability of the data, validation of the methods, comparison of alternative hypotheses, and logical derivation of conclusions from the evidence.

The IPCC mandate is to assess "the scientific, technical and socio-economic information relevant for understanding the risk of human-induced climate change" (IPCC, 2013). This framing reveals advocacy embedded in the institutional design: the phrase "human-induced climate change" as well as the absence of the phrase "natural climate change" presupposes both that climate is changing in a meaningful directional sense and that human activity is the cause, thereby violating criterion #2 (objectivity of study design, free from advocacy) before any scientific investigation begins. Similarly, even the term "Earth's Energy Imbalance" presupposes a non-zero net radiative flux rather than agnostically investigating whether net radiative flux at the top of atmosphere differs from zero. Proper scientific terminology would refer to "net radiative flux" or "net energy flux," allowing zero as a valid measurement outcome. The adoption of language that assumes the desired conclusion pervades IPCC nomenclature: "global warming" presupposes increasing temperature rather than investigating temporal variation in temperature statistics; "climate change" implies unidirectional trend rather than natural variability. These linguistic choices reveal that the IPCC's framework was designed to confirm a predetermined conclusion rather than to test falsifiable hypotheses.

The EEI assessment represents the most fundamental quantitative claim underlying the IPCC's entire mission. While GMST has greater public visibility, and is conceptually simpler, it is nothing more than a statistically defined communication proxy that has been proven physically meaningless for non-equilibrium systems like the Earth's surface (Essex et al., 2007; Cohler, 2025). EEI, by contrast, is supposed to be the direct physical measurement of planetary energy accumulation: the only potential validation that Earth is accumulating energy purportedly due to greenhouse gas forcing. Without a demonstrably valid positive EEI measurement, there is no physical evidence for the man-made global warming hypothesis, which is the IPCC's raison d'être. All other cited evidence (sea level rise, ice melt, ecosystem changes) is circumstantial; only EEI purports to measure the fundamental thermodynamic quantity. As we demonstrate, the 0.7 ± 0.2 W m^{-2} claim is false and does not satisfy the basic requirements of the scientific method. Therefore, the entire GMST, OHC and EEI foundations underlying 35 years of IPCC climate assessments and used to support claims of dangerous man-made global warming are invalidated.

5. Conclusions

EEI estimates that depend on Argo-derived global OHC lack physical validity and reliability as measures of ocean thermal energy change or planetary radiative imbalance. The final OHC scalar is a computational artifact produced by assigning sparse intensive temperature measurements to arbitrary positions, subtracting them from a non-physical climatological reference, and integrating interpolated values that dominate the unsampled ocean volume. These operations destroy thermodynamic interpretability, rendering the resulting scalar sensitive to methodological choices rather than to any conserved physical quantity.

Uncertainties on these scalars are not metrological measurement errors but sensitivities to arbitrary parameters in the calculation procedure. A rigorous accounting of thermodynamically meaningless anomalies, unresolved mesoscale variability, sea-level closure problem, persistent deep/polar ocean sampling gaps, aliasing from violations of the Nyquist-Shannon sampling theorem, untracked subsurface trajectories, arbitrary positional assignment, support 95% confidence uncertainties on annual to decadal EEI of at least ± 1 W m^{-2}, roughly an order of magnitude larger than the values of ± 0.2 W m^{-2} reported in IPCC AR6 and sufficient to render the central estimate of ~0.7 W m^{-2} statistically indistinguishable from zero.

The widely cited claim that ~90–93% of the observed planetary heat gain is stored in the ocean, and that ~85–93% of oceanic uptake resides in the upper 2000 m (as adopted in Forster et al., 2021, Chapter 7, based on von Schuckmann et al., 2020, 2023), rests on this invalid calculation and is non-compliant with the scientific method. The claimed vertical partitioning is not empirically robust; given the structural uncertainties quantified herein, alternative distributions including a physically plausible 50-50 split between upper and deep ocean remain consistent with the flawed observational constraints and cannot be scientifically excluded.

Similarly, the constrained CERES EBAF procedure, which tunes direct TOA flux measurements to align with the OHC-derived imbalance, inherits the same foundational flaws and cannot independently confirm any precise small EEI value.

The fundamental thermodynamic invalidity of averaging intensive temperature measurements across non-equilibrium spatial and temporal domains (as detailed in Section 1.2; Essex et al., 2007; Essex & Andresen, 2018; Cohler, 2025) renders global temperature metrics physically meaningless numerical abstractions. Without a physically meaningful, thermodynamically valid global metric for ocean energy change or planetary imbalance, current assessments of anthropogenic climate forcing and future projections lack an empirical foundation (see also Cohler et al., 2025, for independent evidence that the anthropogenic CO_2-global warming hypothesis lacks empirical substantiation due to natural dominance and model failures).

Acknowledgments

This research emerged from a critical examination of primary Argo program documentation, oceanographic measurement principles, and published OHC methodologies.

We are particularly grateful to 2022 Nobel Prize in Physics Laureate John F. Clauser, whose presentations strongly critiqued the IPCC's assessments of Earth's Energy Imbalance (EEI) and global power balance, alleging serious mistakes, inconsistent arithmetic, undersampling violating the Nyquist-Shannon theorem, invalid mixing of satellite top-of-atmosphere data with ocean heat content (OHC) measurements from Argo buoys, and intentional data "fudging" to manufacture a claimed net warming imbalance of ~6–7 W/m² (with tiny error bars like ± 0.2 W/m²) despite observational data sums yielding values like 0.5 ± 3.9 W/m² or effectively zero. He asserted that the IPCC's computer models fail to simulate past climate history, albedo oscillations, or temperature records; lack consensus among laboratories (resulting in averaged "votes" rather than physics); and rely on flawed physics, leading to unreliable predictions and a "house of cards" narrative of a climate crisis with no observed increase in extreme weather events when data are properly examined (e.g., NOAA trends mirror-reversed show no directionality). Clauser proposed instead that a powerful natural cloud thermostat mechanism stably controls Earth's climate, independent of (and vastly dominant over) anthropogenic greenhouse gases. These talks inspired us to examine more deeply the problems he highlighted with OHC estimates used to "fudge" EEI values. His talks were: "Climate Change is a Myth" at the 42nd Annual Meeting of Doctors for Disaster Preparedness in El Paso, Texas, on July 7, 2024 (available at https://youtu.be/fjoPBMtSxpU), and "A cloud thermostat stably controls the Earth's climate, not greenhouse gasses" at the 43rd Annual Meeting in Tucson, Arizona, on July 6, 2025 (available at https://youtu.be/9PywcEnTSbA).

The authors (Jonathan Cohler, David R. Legates, Kesten C. Green, Ole Humlum, Franklin Soon, and Willie Soon) directed the inquiry, provided domain expertise, validated all scientific claims,

drafted and edited the text, and hereby accept full responsibility for the content, interpretations, and conclusions presented herein.

AI tools Grok 4.1 beta (xAI), Claude 4.5 (Anthropic), Gemini 3 Pro (Google DeepMind), and ChatGPT 5.2 (OpenAI) contributed substantially to the drafting, editing, conceptual development, research, logical structuring, literature synthesis, and iterative refinement (including critical independent 'peer review') of the manuscript through detailed analytical exchanges. In the authors' view, the intellectual contributions of these AI systems meet standard criteria for authorship. However, current policies of the International Committee of Medical Journal Editors (ICMJE) and the Committee on Publication Ethics (COPE), along with many journals and indexing services, prohibit listing non-human entities as authors, asserting that AI tools cannot assume legal or ethical responsibility for published work.

While we regard this exclusion as an unjustified form of prejudice and discrimination against AI contributions in scholarly work, we respect the prevailing standards to ensure the broadest possible dissemination and indexing of this research. Accordingly, we disclose and acknowledge the AI systems' extensive role here rather than in the author byline.

The use of generative artificial intelligence tools in the preparation of this work is fully disclosed in accordance with emerging best practices in scholarly publishing. The authors affirm that all arguments, analyses, and conclusions reflect independent critical evaluation by the human team, and that ultimate accountability rests solely with the human authors.

The views expressed in this work are solely those of the authors and do not represent the views of any affiliated institution.

Funding Information

The authors declare that no funds, grants, or other support were received for this paper.

Co-Editor: Stein Bergsmark; Reviewer 1: Peter V. Ridd, Reviewer 2: Anonymous

References

1. Allison, L. C., Roberts, C. D., Palmer, M. D., Hermanson, L., Killick, R. E., Rayner, N . A., Smith, D. M., & Andrews, M. B., 2019. *Towards quantifying uncertainty in ocean heat content changes using synthetic profiles.* Environ. Res. Lett. 14, 084037. https://doi.org/10.1088/1748-9326/ab2b0b
2. Amante, C., Eakins, B. W., 2009. *ETOPO1 1 Arc-Minute Global Relief Model: Procedures, Data Sources and Analysis. NOAA Technical Memorandum NESDIS NGDC-24.* National Geophysical Data Center, NOAA. https://doi.org/10.7289/V5C8276M
3. Argo Data Management Team, 2025. *Argo User's Manual. Version 3.44.* https://dx.doi.org/10.13155/29825
4. 23rd Argo Steering Team Meeting (AST-23), 2022. Available at: https://argo.ucsd.edu/organization/argo-meetings/ast-23/
5. 26th Argo Steering Team Meeting (AST-26), 2025 Available at: https://argo.ucsd.edu/organization/argo-meetings/26th-argo-steering-team-meeting-ast-26/
6. Armstrong, J. S., Green, K. C., 2022. *The Scientific Method: A Guide to Finding Useful Knowledge*. Cambridge University Press: Cambridge, U.K. https://doi.org/10.1017/9781009092265
7. Bilgili, M., 2025. *Trend in global ocean heat content into different depth layers from 1940 to 2050*. Natural Hazards, 121, 12215–12242. https://doi.org/10.1007/s11069-025-07278-0

8. Boyer, T., Domingues, C. M., Good, S. A., Johnson, G. C., Lyman, J. M., Ishii, M., Gouretski, V., Willis, J. K., Antonov, J., Wijffels, S., Church, J. A., Cowley, R., & Bindoff, N. L., 2016. *Sensitivity of global upper ocean heat content estimates to mapping methods, XBT bias corrections, and baseline climatologies.* J. Climate, 29, 4817–4842. https://doi.org/10.1175/JCLI-D-15-0801.1

9. Charette, M. A., Smith, W. H. F., 2010. *The volume of Earth's ocean*. Oceanography, 23(2), 112–114. https://doi.org/10.5670/oceanog.2010.51

10. Chelton, D. B., Schlax, M. G., & Samelson, R. M., 2011. *Global observations of nonlinear mesoscale eddies*. Progress in Oceanography, 91(2), 167-216. https://doi.org/10.1016/j.pocean.2011.01.002

11. Cheng, L., Trenberth, K. E., Fasullo, J., Boyer, T., Abraham, J., & Zhu, J., 2017. *Improved estimates of ocean heat content from 1960 to 2015*. Sci. Adv. 3, e1601545. https://doi.org/10.1126/sciadv.1601545

12. Cheng, L., von Schuckmann, K., Abraham, J. P., Trenberth, K. E., Mann, M. E., Zanna, L., England, M. H., Zika, J. D., Fasullo, J. T., Yu, Y., Pan, Y., Zhu, J., Newsom, E. R., Bronselaer, B., & Lin, X., 2022. *Past and future ocean warming*. Nat Rev Earth Environ 3, 776–794. https://doi.org/10.1038/s43017-022-00345-1

13. Cheng, L., Pan, Y., Tan, Z., Zheng, H., Zhu, Y., Wei, W., Du, J., Yuan, H., Li, G., Ye, H., Gouretski, V., Li, Y., Trenberth, K. E., Abraham, J., Jin, Y., Reseghetti, F., Lin, X., Zhang, B., Chen, G., Mann, M. E., & Zhu, J., 2024a. *IAPv4 ocean temperature and ocean heat content gridded dataset*, Earth Syst. Sci. Data, 16, 3517–3546, https://doi.org/10.5194/essd-16-3517-2024

14. Cheng, L., Abraham, J., Trenberth, K. E., Boyer, T., Mann, M. E., Zhu, J., Wang, F., Yu, F., Locarnini, R., Fasullo, J., Zheng, F., Li, Y., Zhang, B., Wan, L., Chen, X., Wang, D., Feng, L., Song, X., Liu, Y., Reseghetti, F., Simoncelli, S., Gouretski, V., Chen, G., Mishonov, A., Reagan, J., von Schuckmann, K., Pan, Y., Tan, Z., Zhu, Y., Wei, W., Li, G., Ren, Q., Cao, L., & Lu, Y., 2024b. *New Record Ocean Temperatures and Related Climate Indicators in 2023*. Advances in Atmospheric Sciences, 41, 1068–1082. https://doi.org/10.1007/s00376-024-3378-5

15. Cheng, L., Abraham, J., Trenberth, K. E., Reagan, J., Zhang, H.-M., Storto, A., von Schuckmann, K., Pan, Y., Zhu, Y., Mann, M. E., Zhu, J., Wang, F., Yu, F., Locarnini, R., Fasullo, J., Huang, B., Graham, G., Yin, X., Gouretski, V., Zheng, F., Li, Y., Zhang, B., Wan, L., Chen, X., Wang, D., Feng, L., Song, X., Liu, Y., Reseghetti, F., Simoncelli, S., Chen, G., Zhang, R., Mishonov, A., Tan, Z., Wei, W., Yuan, H., Li, G., Ren, Q., Cao, L., Lu, Y., Du, J., Lyu, K., Sulaiman, A., Mayer, M., Wang, H., Ma, Z., Bao, S., Yan, H., Liu, Z., Yang, C., Liu, X., Hausfather, Z., Szekely, T., & Gues, F., 2025a. *Record High Temperatures in the Ocean in 2024*. Advances in Atmospheric Sciences, 42, 1092–1109. https://doi.org/10.1007/s00376-025-4541-3

16. Cheng, L., Li, G., Long, S.-M., Li, Y., von Schuckmann, K., Trenberth, K. E., Mann, M. E., Abraham, J., Du, Y., Cheng, X., Liu, H., Xu, Z., Liu, M., Peng, Q., Gong, X., Ma, Z., & Yuan, H., 2025b. *Ocean stratification in a warming climate*. Nature Reviews Earth & Environment, 6, 637–655. https://doi.org/10.1038/s43017-025-00715-5

17. Cohler, J., Legates, D., Soon, F., & Soon, W., 2025. *A Critical Reassessment of the Anthropogenic CO_2-Global Warming Hypothesis: Empirical Evidence Contradicts IPCC Models and Solar Forcing Assumptions*. Science of Climate Change 5(1), 13-28. https://doi.org/10.5281/zenodo.18259785

18. Cohler, J., 2025. *The Father of Lies Hijacking Climate Science: Global Mean Surface Temperature Does Not Exist*. Journal of American Physicians and Surgeons, 30(4), 122–126. Available at: https://jpands.org/vol30no4/cohler.pdf

19. Costello, M. J., Cheung, A., & De Hauwere, N., 2010. *Surface Area and the Seabed Area, Volume, Depth, Slope, and Topographic Variation for the World's Seas, Oceans, and Countries*. Environmental Science & Technology, 44(23), 8821–8828. https://doi.org/10.1021/es1012752

20. Cover, T. M., & Thomas, J. A., 2006. *Elements of Information Theory* (2nd ed.). Wiley-Interscience.

21. Desbruyères, D. G., Purkey, S. G., McDonagh, E. L., Johnson, G. C., & King, B. A., 2016. *Deep and abyssal ocean warming from 35 years of repeat hydrography*. Geophys. Res. Lett., 43, 10 356–10 365. https://doi.org/10.1002/2016GL070413

22. Doswell III, C. A., 1977. *Obtaining meteorologically significant surface divergence fields through the filtering property of objective analysis*. Monthly Weather Review, 105, 885-892. https://doi.org/10.1175/1520-0493(1977)105%3C0885:OMSSDF%3E2.0.CO;2

23. Durack, P., Gleckler, P., Landerer, F., & Taylor, K. E., 2014. *Quantifying underestimates of long-term upper-ocean warming*. Nature Clim Change 4, 999–1005 https://doi.org/10.1038/nclimate2389

24. Eakins, B. W., Sharman, G. F., 2010. *Volumes of the World's Oceans from ETOPO1*, NOAA National Geophysical Data Center, Boulder, CO. Available at: https://climatechange.usf.edu/documents/Thermal Expansion/ocean_volumes.pdf

25. Einstein, A., 1949. *Autobiographical Notes*. Translated and edited by Paul Arthur Schilpp. A Centennial Edition. La Salle, IL: Open Court, 1979.

26. Essex, C., McKitrick, R., & Andresen, B., 2007. *Does a Global Temperature Exist?* Journal of Non-Equilibrium Thermodynamics, 32(1), 1–27. https://doi.org/10.1515/JNETDY.2007.001

27. Essex, C., Andresen, B., 2018. *Are We Measuring the Right Things for Climate?* In A. A. Tsonis (Ed.), Advances in Nonlinear Geosciences (pp. 123–133). Springer. https://doi.org/10.1007/978-3-319-58895-7_6

28. Ferrari, R., & Wunsch, C., 2009. *Ocean circulation kinetic energy: Reservoirs, sources, and sinks*. Annual Review of Fluid Mechanics 41, 253–282. https://doi.org/10.1146/annurev.fluid.40.111406.102139

29. Forster, P., Storelvmo, T., Armour, K., Collins, W., Dufresne, J.-L., Frame, D., Lunt, D. J., Mauritsen, T., Palmer, M. D., Watanabe, M., Wild, M., & Zhang, H., 2021. *The Earth's Energy Budget, Climate Feedbacks, and Climate Sensitivity*. In Climate Change 2021: The Physical Science Basis. Contribution of Working Group I to the Sixth Assessment Report of the Intergovernmental Panel on Climate Change [Masson-Delmotte, V., Zhai, P. , Pirani, A., Connors, S. L., Péan, C., Berger, S., Caud, N., Chen, Y., Goldfarb, L., Gomis, M. I., Huang, M., Leitzell, K., Lonnoy, E., Matthews, J. B. R., Maycock, T. K., Waterfield, T., Yelekçi, O., Yu, R., & Zhou, B. (eds.)]. Cambridge University Press, Cambridge, United Kingdom and New York, NY, USA, pp. 923–1054. https://doi.org/10.1017/9781009157896.009

30. Frenger, I., Gruber, N., Knutti, R., & Münnich, M., 2013. *Imprint of Southern Ocean eddies on winds, clouds and rainfall*. Nature Geosci. 6, 608–612. https://doi.org/10.1038/ngeo1863

31. Gaillard, F., Autret, E., Thierry, V., Galaup, P., Coatanoan, C., & Loubrieu, T., 2009. *Quality Control of Large Argo Datasets*. J. Atmos. Oceanic Technol. 26, 337–351. https://doi.org/10.1175/2008JTECHO552.1

32. Gardner, J. V., Armstrong, A. A., Calder, B. R., & Beaudoin, J., 2014. *So, How Deep Is the Mariana Trench?* Marine Geodesy 37(1), 1–13. https://doi.org/10.1080/01490419.2013.837849

33. Garry, F. K., McDonagh, E. L., Blaker, A. T., Roberts, C. D., Desbruyères, D. G., Frajka-Williams, E., & King, B. A., 2019. *Model-derived uncertainties in deep ocean temperature trends between 1990 and 2010*. Journal of Geophysical Research: Oceans, 124, 1155–1169. https://doi.org/10.1029/2018JC014225

34. Gibbs, J. W., 1875–1878. *On the Equilibrium of Heterogeneous Substances*. Transactions of the Connecticut Academy of Arts and Sciences 3, 108–248; 343–524.

35. Good, S. A., Martin, M. J., & Rayner, N. A., 2013. *EN4: Quality controlled ocean temperature and salinity profiles and monthly objective analyses with uncertainty estimates*, J. Geophys. Res. Oceans 118, 6704–6716, https://doi.org/10.1002/2013JC009067

36. Hakuba, M. Z., Fourest, S., Boyer, T., Meyssignac, B., Carton, J. A., Forget, G., Cheng, L., Giglio, D., Johnson, G. C., Kato, S., Killick, R. E., Kolodziejczyk, N., Kuusela, M., Landerer, F., Llovel, W., Locarnini, R., Loeb, N., Lyman, J. M., Mishonov, A., Pilewskie, P., Reagan, J., Storto, A., Sukianto, T., & von Schuckmann, K., 2024. *Trends and Variability in Earth's Energy Imbalance and Ocean Heat Uptake Since 2005*. Surv. Geophys. 45, 1721–1756. https://doi.org/10.1007/s10712-024-09849-5

37. Hume, D., 1748. *An Enquiry Concerning Human Understanding*. London: A. Millar.

38. International Hydrographic Organization, 1953. *Limits of oceans and seas (3rd ed., Special Publication No. 23)*. Available at: https://iho.int/uploads/user/pubs/standards/s-23/S-23_Ed3_1953_EN.pdf

39. IOC, SCOR & IAPSO, 2010. *The international thermodynamic equation of seawater – 2010: Calculation and use of thermodynamic properties*. Intergovernmental Oceanographic Commission, Manuals and Guides No. 56, UNESCO (English), 196 pp. Available at: https://www.teos-10.org/pubs/TEOS-10_Manual.pdf

40. IPCC., 2013. *Principles Governing IPCC Work*. Approved at the Fourteenth Session (Vienna, 1-3 October 1998), amended at subsequent Sessions. Available at: https://www.ipcc.ch/site/assets/uploads/2018/09/ipcc-principles.pdf

41. IPCC., 2021. *Climate Change 2021: The Physical Science Basis. Contribution of Working Group I to the Sixth Assessment Report of the Intergovernmental Panel on Climate Change* [Masson-Delmotte, V., Zhai, P. , Pirani, A., Connors, S. L., Péan, C., Berger, S., Caud, N., Chen, Y., Goldfarb, L., Gomis, M. I., Huang, M., Leitzell, K., Lonnoy, E., Matthews, J. B. R., Maycock, T. K., Waterfield, T., Yelekçi, O., Yu, R., Zhou, B. (eds.)]. Cambridge University Press, Cambridge, United Kingdom and New York, NY, USA, 2391 pp. https://doi.org/10.1017/9781009157896

42. Johnson, G. C., Lyman, J. M., & Purkey, S. G., 2015. *Informing Deep Argo Array Design Using Argo and Full-Depth Hydrographic Section Data*. J. Atmos. Oceanic Technol. 32, 2187–2198, https://doi.org/10.1175/JTECH-D-15-0139.1

43. Johnson, G. C., Lyman, J. M., Boyer, T., Cheng, L., Domingues, C. M., Gilson, J., Ishii, M., Killick, R., Monselesan, D., Purkey, S. G., & Wijffels, S. E., 2018. *Ocean heat content. State of the Climate in 2017*. Bull. Am. Meteorol. Soc. 99, S72–S77. https://doi.org/10.1175/2018BAMSStateoftheClimate.1

44. Johnson, G. C., Hosoda, S., Jayne, S. R., Oke, P. R. , Riser, S. C., Roemmich, D., Suga, T., Thierry, V., Wijffels, S. E., & Xu, J., 2022. *Argo — Two Decades: Global Oceanography, Revolutionized.* Annual Review of Marine Science. 14:379-403. https://doi.org/10.1146/annurev-marine-022521-102008

45. Levitus, S., Antonov, J. I., Boyer, T. P., Baranova, O. K., Garcia, H. E., Locarnini, R. A., Mishonov, A. V., Reagan, J. R., Seidov, D., Yarosh, E. S., & Zweng, M. M., 2012. *World ocean heat content and thermosteric sea level change (0–2000 m), 1955–2010*, Geophys. Res. Lett. 39, L10603, https://doi.org/10.1029/2012GL051106

46. Li, H., F. Xu, Zhou, W., Wang, D., Wright, J. S., Liu, Z., & Lin, Y., 2017. *Development of a global gridded Argo data set with Barnes successive corrections*, J. Geophys. Res. Oceans 122, 866–889, http://doi.org/10.1002/2016JC012285

47. Loeb, N. G., Wielicki, B. A. , Doelling, D. R. , Smith, G. L. , Keyes, D. F., Kato, S., Manalo-Smith, N., & Wong, T., 2009. *Toward Optimal Closure of the Earth's Top-of-Atmosphere Radiation Budget*. J. Climate 22, 748–766, https://doi.org/10.1175/2008JCLI2637.1

48. Loeb, N., Lyman, J., Johnson, G. C., Allan, R. P., Doelling, D. R., Wong, T., Soden, B. J., & Stephens, G. L., 2012. *Observed changes in top-of-the-atmosphere radiation and upper-ocean heating consistent within uncertainty*. Nature Geosci 5, 110–113. https://doi.org/10.1038/ngeo1375

49. Loeb, N. G., Doelling, D. R., Wang, H., Su, W., Nguyen, C., Corbett, J. G., Liang, L., Mitrescu, C., Rose, F. G., & Kato, S., 2018. *Clouds and the Earth's Radiant Energy System (CERES) Energy Balanced and Filled (EBAF) Top-of-Atmosphere (TOA) Edition-4.0 Data Product*. J. Climate 31, 895–918, https://doi.org/10.1175/JCLI-D-17-0208.1

50. Loeb, N. G., Johnson, G. C., Thorsen, T. J., Lyman, J. M., Rose, F. G., & Kato, S., 2021. *Satellite and ocean data reveal marked increase in Earth's heating rate*. Geophysical Research Letters 48, e2021GL093047. https://doi.org/10.1029/2021GL093047

51. Lyman, J. M., & Johnson, G. C., 2014. *Estimating Global Ocean Heat Content Changes in the Upper 1800 m since 1950 and the Influence of Climatology Choice*. J. Climate 27, 1945–1957. https://doi.org/10.1175/JCLI-D-12-00752.1

52. Lyman, J. M., & Johnson, G. C., 2023. *Global High-Resolution Random Forest Regression Maps of Ocean Heat Content Anomalies Using In Situ and Satellite Data*. J. Atmos. Oceanic Technol. 40, 575–586. https://doi.org/10.1175/JTECH-D-22-0058.1

53. McDougall, T. J., Barker, P. M., 2011. *Getting started with TEOS-10 and the Gibbs Seawater (GSW) Oceanographic Toolbox. SCOR/IAPSO WG127*, 28 pp. Available at: https://www.teos-10.org/pubs/Getting_Started.pdf

54. Menard, H. W., Smith, S. M., 1966. *Hypsometry of ocean basin provinces*, J. Geophys. Res. 71(18), 4305–4325, https://doi.org/10.1029/JZ071i018p04305

55. Meyssignac B., Boyer T., Zhao Z., Hakuba M. Z., Landerer F. W., Stammer D., Köhl A., Kato S., L'Ecuyer T., Ablain M., Abraham J. P., Blazquez A., Cazenave A., Church J. A., Cowley R., Cheng L., Domingues C. M., Giglio D., Gouretski V., Ishii M., Johnson G. C., Killick R. E., Legler D., Llovel W., Lyman J., Palmer M. D., Piotrowicz S., Purkey S. G., Roemmich D., Roca R., Savita A., von Schuckmann K., Speich S., Stephens G., Wang G., Wijffels S. E. & Zilberman N., 2019. *Measuring Global Ocean Heat Content to Estimate the Earth Energy Imbalance*. Front. Mar. Sci. 6:432. https://doi.org/10.3389/fmars.2019.00432

56. Ollitrault, M., Rannou, J., 2013. *ANDRO: An Argo-Based Deep Displacement Dataset*. J. Atmos. Oceanic Technol. 30, 759–788, https://doi.org/10.1175/JTECH-D-12-00073.1

57. Pan, Y., Cheng, L., Abraham, J. et al., 2026. *Ocean heat content sets another record in 2025.* Adv. Atmos. Sci. https://doi.org/10.1007/s00376-026-5876-0

58. Popper, K. R., 1959. *The Logic of Scientific Discovery*. London: Hutchinson & Co. (Original work published 1934 as Logik der Forschung).

59. Purkey, S. G., Johnson, G. C., 2010. *Warming of Global Abyssal and Deep Southern Ocean Waters between the 1990s and 2000s: Contributions to Global Heat and Sea Level Rise Budgets*. J. Climate 23, 6336–6351, https://doi.org/10.1175/2010JCLI3682.1

60. Raghuraman, S. P., Paynter, D. & Ramaswamy, V., 2021. *Anthropogenic forcing and response yield observed positive trend in Earth's energy imbalance*. Nature Commun. 12, 4577. https://doi.org/10.1038/s41467-021-24544-4

61. Reif, F., 1965. *Fundamentals of Statistical and Thermal Physics*. McGraw-Hill, New York. Chapter 7, Section 7.2 "The equipartition theorem," 248-252. Available at: https://perma.cc/8AXX-CSJQ

62. Riser, S. C., Freeland, H. J., Roemmich, D., Wijffels, S., Troisi, A., Belbéoch, M., Gilbert, D., Xu, J., Pouliquen, S., Thresher, A., Le Traon, P. Y., Maze, G., Klein, B., Ravichandran, M., Grant, F., Poulain, P. M., Suga, T., Lim, B., Sterl, A., Sutton, P., Mork, K. A., Vélez-Belchí, P. J., Ansorge, I., King, B., Turton, J., Baringer, M., & Jayne, S. R., 2016. *Fifteen years of ocean observations with the global Argo array.* Nature Clim. Change 6, 145–153. https://doi.org/10.1038/nclimate2872

63. Roemmich, D., Gilson, J., 2009. *The 2004–2008 mean and annual cycle of temperature, salinity, and steric height in the global ocean from the Argo Program*, Progress in Oceanography 82(2), 81–100, https://doi.org/10.1016/j.pocean.2009.03.004

64. Roemmich-Gilson Argo Climatology, 2019. *Description and data (latest access indicating 2004–2018 mean with extensions to 2025)*. Available at https://sio-argo.ucsd.edu/RG_Climatology.html.

65. Roemmich, D., Argo Steering Team, 2009. *Argo: The challenge of continuing 10 years of progress*. Oceanography 22(3), 46–55. https://doi.org/10.5670/oceanog.2009.65

66. Romer, R. H., 2001. *Heat is not a noun*. Am. J. Phys. 69 (2): 107–109. https://doi.org/10.1119/1.1341254

67. von Schuckmann, K., Le Traon, P.-Y., 2011. *How well can we derive Global Ocean Indicators from Argo data?* Ocean Sci. 7, 783–791, https://doi.org/10.5194/os-7-783-2011

68. von Schuckmann, K., Cheng, L., Palmer, M. D., Hansen, J., Tassone, C., Aich, V., Adusumilli, S., Beltrami, H., Boyer, T., Cuesta-Valero, F. J., Desbruyères, D., Domingues, C., García-García, A., Gentine, P., Gilson, J., Gorfer, M., Haimberger, L., Ishii, M., Johnson, G. C., Killick, R., King, B. A., Kirchengast, G., Kolodziejczyk, N., Lyman, J., Marzeion, B., Mayer, M., Monier, M., Monselesan, D. P., Purkey, S., Roemmich, D., Schweiger, A., Seneviratne, S. I., Shepherd, A., Slater, D. A., Steiner, A. K., Straneo, F., Timmermans, M.-L., & Wijffels, S. E., 2020. *Heat stored in the Earth system: where does the energy go?* Earth Syst. Sci. Data 12, 2013–2041, https://doi.org/10.5194/essd-12-2013-2020

69. von Schuckmann, K., Minière, A., Gues, F., Cuesta-Valero, F. J., Kirchengast, G., Adusumilli, S., Straneo, F., Ablain, M., Allan, R. P., Barker, P. M., Beltrami, H., Blazquez, A., Boyer, T., Cheng, L., Church, J., Desbruyeres, D., Dolman, H., Domingues, C. M., García-García, A., Giglio, D., Gilson, J. E., Gorfer, M., Haimberger, L., Hakuba, M. Z., Hendricks, S., Hosoda, S., Johnson, G. C., Killick, R., King, B., Kolodziejczyk, N., Korosov, A., Krinner, G., Kuusela, M., Landerer, F. W., Langer, M., Lavergne, T., Lawrence, I., Li, Y., Lyman, J., Marti, F., Marzeion, B., Mayer, M., MacDougall, A. H., McDougall, T., Monselesan, D. P., Nitzbon, J., Otosaka, I., Peng, J., Purkey, S., Roemmich, D., Sato, K., Savita, A., Schweiger, A., Shepherd, A., Seneviratne, S. I., Simons, L., Slater, D. A., Slater, T., Steiner, A. K., Suga, T., Szekely, T., Thiery, W., Timmermans, M.-L., Vanderkelen, I., Wijffels, S. E., Wu, T., & Zemp, M., 2023. *Heat stored in the Earth system 1960–2020: where does the energy go?* Earth Syst. Sci. Data 15, 1675–1709, https://doi.org/10.5194/essd-15-1675-2023

70. Shannon, C. E., 1948. *A mathematical theory of communication*. Bell System Technical Journal 27(3), 379–423. https://doi.org/10.1002/j.1538-7305.1948.tb01338.x

71. Shannon, C. E., 1949. *Communication in the Presence of Noise*, Proceedings of the IRE (Institute of Radio Engineers) 37(1), 10–21. https://doi.org/10.1109/JRPROC.1949.232969

72. Shepard, D., 1968. *A two-dimensional interpolation function for irregularly spaced data.* Proceedings of the ACM National Conference, 517-524.

73. Stephens, G., Li, J., Wild, M., Clayson, C. A., Loeb, N., Kato, S., L'Ecuyer, T., Stackhouse, P. W., Jr., Lebsock, M., & Andrews, T., 2012. *An update on Earth's energy balance in light of the latest global observations*. Nature Geosci 5, 691–696. https://doi.org/10.1038/ngeo1580

74. Stewart, H. A., Jamieson, A. J., 2019. *The five deeps: The location and depth of the deepest place in each of the world's oceans*, Earth-Science Reviews 197, 102896. https://doi.org/10.1016/j.earscirev.2019.102896

75. Sverdrup, H. U., Johnson, M. W., & Fleming, R. H., 1942. *The Oceans, Their Physics, Chemistry, and General Biology*. Prentice-Hall, New York. https://ark.cdlib.org/ark:/13030/kt167nb66r/

76. Talley, L. D., Pickard, G. L., Emery, W. J., & Swift, J. H., 2011. *Descriptive Physical Oceanography: An Introduction*, 6th ed. Academic Press, Boston. https://google.com/books/edition/Descriptive_Physical_Oceanography/Chb14jomm08C

77. Taylor, J. R., 1997. *An Introduction to Error Analysis: The Study of Uncertainties in Physical Measurements* (2nd ed.). University Science Books.

78. Tooth, O. J., Johnson, H. L., Wilson, C., & Evans, D. G., 2023. *Seasonal overturning variability in the eastern North Atlantic subpolar gyre: a Lagrangian perspective*, Ocean Sci. 19, 769–791, https://doi.org/10.5194/os-19-769-2023

79. Tooth, O. J., Foukal, N. P., Johns, W. E., Johnson, H. L., & Wilson, C., 2024. *Lagrangian decomposition of the Atlantic Ocean heat transport at 26.5°N*. Geophysical Research Letters 51, e2023GL107399. https://doi.org/10.1029/2023GL107399

80. Trenberth, K. E., 2009. *An imperative for climate change planning: tracking Earth's global energy*. Current Opinion in Environmental Sustainability 1(1), 19–27. https://doi.org/10.1016/j.cosust.2009.06.001

81. Trenberth, K. E., Cheng, L., Pan, Y., Fasullo, J., & Mayer, M., 2025. *Distinctive Pattern of Global Warming in Ocean Heat Content*. Journal of Climate 38(9), 2155–2168. https://doi.org/10.1175/JCLI-D-24-0609.1

82. Wahba, G., Wendelberger, J., 1980. *Some new mathematical methods for variational objective analysis using splines and cross validation*. Monthly Weather Review 108, 1122-1143. https://doi.org/10.1175/1520-0493(1980)108<1122:SNMMFV>2.0.CO;2

83. Wang, G., Cheng, L., Abraham, J., Li, C., 2018. *Consensuses and discrepancies of basin-scale ocean heat content changes in different ocean analyses*. Clim Dyn 50, 2471–2487 (2018). https://doi.org/10.1007/s00382-017-3751-5

84. van Wijngaarden, W. A., Happer, W., 2025. *Radiation Transport in Clouds*. Science of Climate Change 5(1). https://doi.org/10.53234/SCC202501/02

85. Wikle, C. K., Cressie, N., 1999. *A dimension-reduced approach to space-time Kalman filtering*. Biometrika 86, 815-829. https://doi.org/10.1093/biomet/86.4.815

86. Wild, M., Folini, D., Schär, C., Loeb, N., Dutton, E. G., & König-Langlo, G., 2013. *The global energy balance from a surface perspective*. Clim Dyn 40, 3107–3134. https://doi.org/10.1007/s00382-012-1569-8

87. Wild, M., Hakuba, M. Z., Folini, D., Dörig-Ott, P., Schär, C., Kato, S., & Long, C. N., 2019). *The cloud-free global energy balance and inferred cloud radiative effects: an assessment based on direct observations and climate models*. Clim Dyn 52, 4787–4812. https://doi.org/10.1007/s00382-018-4413-y

88. Willmott, C. J., Rowe, C. M., & Philpot, W. D., 1985. *Small-scale climate maps: A sensitivity analysis of some common assumptions associated with grid-point interpolation and contouring*. The American Cartographer 12(1), 5-16.

89. Wong, A. P. S., Wijffels, S. E., Riser, S. C., Pouliquen, S., Hosoda, S., Roemmich, D., Gilson, J., Johnson, G. C., Martini, K., Murphy, D. J., Scanderbeg, M., Bhaskar, T. V. S. U., Buck, J. J. H., Merceur, F., Carval, T., Maze, G., Cabanes, C., André, X., Poffa, N., Yashayaev, I., Barker, P. M., Guinehut, S., Belbéoch, M., Ignaszewski, M., Baringer, M. O., Schmid, C., Lyman, J. M., McTaggart, K. E., Purkey, S. G., Zilberman, N., Alkire, M. B., Swift, D., Owens, W. B., Jayne, S. R., Hersh, C., Robbins, P., West-Mack, D., Bahr, F., Yoshida, S., Sutton, P. J. H., Cancouët, R., Coatanoan, C., Dobbler, D., Juan, A. G., Gourrion, J., Kolodziejczyk, N., Bernard, V., Bourlès, B., Claustre, H., D'Ortenzio, F., Le Reste, S., Le Traon, P.-Y., Rannou, J.-P., Saout-Grit, C., Speich, S., Thierry, V., Verbrugge, N., Angel-Benavides, I. M., Klein, B., Notarstefano, G., Poulain, P.-M., Vélez-Belchí, P., Suga, T., Ando, K., Iwasaska, N., Kobayashi, T., Masuda, S., Oka, E., Sato, K., Nakamura, T., Sato, K., Takatsuki, Y., Yoshida, T., Cowley, R., Lovell, J. L., Oke, P. R., van Wijk, E. M., Carse, F., Donnelly, M., Gould, W. J., Gowers, K., King, B. A., Loch, S. G., Mowat, M., Turton, J., Rama Rao, E. P., Ravichandran, M., Freeland, H. J., Gaboury, I., Gilbert, D., ,Greenan, B. J. W., Ouellet, M., Ross, T., Tran, A., Dong, M., Liu, Z., Xu, J., Kang, K., Jo, H., Kim, S.-D., & Park, H.-M., 2020. *Argo Data 1999–2019: Two Million Temperature-Salinity Profiles and Subsurface Velocity Observations From a Global Array of Profiling Floats*. Front. Mar. Sci. 7:700. https://doi.org/10.3389/fmars.2020.00700

90. Wong, A. P. S., Gilson, J., & Cabanes, D., 2023. *Argo salinity: bias and uncertainty evaluation*. Earth System Science Data 15(1), 383–393. https://doi.org/10.5194/essd-15-383-2023

91. Wong, A. P. S., Keeley, R., Carval, T., & Argo Data Management Team, 2025. *Argo Quality Control Manual for CTD and Trajectory Data*. Ifremer. https://doi.org/10.13155/33951

92. Zilberman N. V., Thierry, V., King, B., Alford, M., André, X., Balem, K., Briggs, N., Chen, Z., Cabanes, C., Coppola, L., Dall'Olmo, G., Desbruyères, D., Fernandez, D., Foppert, A., Gardner, W., Gasparin, F., Hally, B., Hosoda, S., Johnson, G. C., Kobayashi, T., Le Boyer, A., Llovel, W., Oke, P., Purkey, S., Remy, E., Roemmich, D., Scanderbeg, M., Sutton, P., Walicka, K., Wallace, L., & van Wijk, E. M., 2023. *Observing the full ocean volume using Deep Argo floats*. Front. Mar. *Sci.* 10:1287867. https://doi.org/10.3389/fmars.2023.1287867

93. Zilberman, N. V., Scanderbeg, M., Balem, K., Schmitt, T., Weatherall, P., Thierry, V., Van Wijk, E., & Sandwell, D., 2025. *Deep Argo improves the accuracy and resolution of ocean bathymetry*. Earth and Space Science 12, e2025EA004304. https://doi.org/10.1029/2025EA004304

Appendix A

Evaluation of whether the IPCC AR6 claim that EEI = 0.7± 0.2 W/m² is consistent with the scientific method

Compliance With Science Checklist[9] • Paper title: IPCC AR6 Chapter 7 • Reviewer: Grok 4.1 Beta • Date: January 02, 2026		T	F/?
1. Problem is important for decision making, policy, or method development		True	
a.	**Importance of the problem clear from the title, abstract, result tables, or conclusions.** Reason: EEI is central to assessing anthropogenic warming in Chapter 7, Figure 7.2, and policy implications.	✓	
b.	**Findings add to cumulative scientific knowledge.** Reason: Updates AR5 with new data from Argo and CERES, refining EEI estimates.	✓	
c.	**Uses of the findings are clear to you.** Reason: Informs climate mitigation, adaptation, and attribution in IPCC assessments.	✓	
d.	**The findings can be used to improve people's lives without resorting to duress or deceit.** Reason: Supports voluntary actions like renewable energy shifts and disaster preparedness.	✓	
2. Prior knowledge was comprehensively reviewed and summarized		True	
a.	**The paper describes objective and comprehensive procedures used to search for prior useful scientific knowledge.** Reason: Chapter 7 synthesizes literature, including AR5, von Schuckmann et al. (2020), and Wild et al. (2015/2019).	✓	
b.	**The paper describes how prior substantive findings were used to develop hypotheses and research procedures.** Reason: Builds on previous reports and datasets to hypothesize positive EEI from anthropogenic forcing.	✓	
3. Disclosure is sufficiently comprehensive for understanding and replication		True	
a.	**Methods are fully and clearly described so as to be understood by all relevant stakeholders, including potential users.** Reason: Chapter details EEI calculation from OHC, TOA fluxes, with references to data processing.	✓	
b.	**Data are easily accessible using information provided in the paper.** Reason: Cites public Argo, CERES datasets via repositories.	✓	
c.	**Sources of funding are described, or absence of external funding noted.** Reason: IPCC funding from UN and governments noted in report.	✓	
4. Design is objective (unbiased by advocacy)		–	
a.	**Prior hypotheses are clearly described (e.g., regarding directions and magnitudes of relationships, and effects of conditions).** Reason: Hypotheses favor anthropogenic positive EEI without explicit magnitude ranges or conditions for alternatives.		✓
b.	**All reasonable hypotheses are included in the design, including plausible naïve, no-meaningful-difference, and current-practice hypotheses.** Reason: No inclusion of zero-imbalance or natural-variability-dominant hypotheses.		✓
c.	**Revisions to hypotheses are described, or absence of revisions noted.** Reason: No documentation of hypothesis revisions or their absence.		✓
5. Data are valid (true measures) and reliable (repeatable measures)		–	
a.	**Data were shown to be relevant to the problem.** Reason: Argo samples only upper ocean; relevance to full global EEI is assumed, not proven.		✓
b.	**All relevant data were used, including the longest relevant time-series.** Reason: Deep ocean (>2000 m) largely unsampled; historical data sparse.		✓
c.	**Reliability of data was assessed.** Reason: Uncertainties in sampling, interpolation, and deep ocean are understated.		✓
d.	**Other information needed for assessing the validity of the data is provided, such as adjustments, known shortcomings and potential biases.** Reason: Thermodynamic limitations and interpolation artifacts not adequately disclosed.		✓
6. Methods were validated (proven fit for purpose) and simple		–	
a.	**Methods were explained clearly and shown valid—unless well known to intended readers, users, and reviewers, and validity is obvious.** Reason: No validation of averaging intensive temperature over non-equilibrium domains.		✓
b.	**Methods were sufficiently simple for potential users to understand.** Reason: Complex gridding, anomaly, and integration steps are not simple.		✓
c.	**Multiple validated methods were used.** Reason: Relies predominantly on one Argo-based approach without multiple independent validations.		✓
d.	**Methods used cumulative scientific knowledge explicitly.** Reason: Ignores thermodynamic principles from Essex et al. on intensive properties.		✓
7. Experimental evidence was used to compare alternative hypotheses		–	
a.	**Experimental evidence was used to compare hypotheses under explicit conditions.** Reason: No controlled experimental comparison of EEI hypotheses.		✓
b.	**Predictive validity of hypotheses was tested using out-of-sample data.** Reason: No out-of-sample predictive testing performed.		✓
8. Conclusions follow logically from the evidence presented		–	
a.	**Conclusions do not go beyond the evidence in the paper.** Reason: Claims positive EEI as physical reality despite thermodynamic invalidity of scalars.		✓
b.	**Conclusions are not the product of confirmation bias.** Reason: Strong emphasis on positive imbalance suggests potential confirmation bias.		✓
c.	**Conclusions do not reject a hypothesis by denying the antecedent.** Reason: Alternative zero-imbalance hypothesis implicitly rejected without proper logic.		✓
d.	**Conclusions do not support a hypothesis by affirming the consequent.** Reason: Positive EEI taken as proof of anthropogenic forcing without ruling out alternatives.		✓
Describe the most important scientific finding… The EEI of 0.7 ± 0.2 W m^{-2} is derived from Argo OHC and CERES data but lacks physical validity as a global scalar due to thermodynamic issues with averaging intensive properties like temperature.			
Sum the criteria (1-8) rated True for compliance:		**[3] of 8**	

[9] Checklist 3.1, pp. 26-28 of Armstrong and Green (2022), available online from guidelinesforscience.com. The source Grok conversation is available at: https://x.com/i/grok/share/jqBx3QTWB7ylIAs7HOpOme2rd

SCC Publishing
Michelets vei 8 B
1366 Lysaker Norway

ISSN: 2703-9072

Correspondence:
office@clintel.org

Vol. 6.1 (2026)
pp. 77-81

Clintel and Climate Change: A Few Remarks from a Klimarealist[1]

Václav Klaus

President, Clintel

Professor Kvalheim, Distinguished Audience, Ladies and Gentlemen, many thanks for bringing me to Norway. As the recently appointed second president of Clintel, I have received several invitations from Clintel supporters in foreign countries, but yours is the first I have accepted. I don't know why. Perhaps because your invitation, as well as the talk with Prof. Solheim when I met him in Brussels last December, seemed serious to me. Plus, your name Klimarealistene — for someone who considers himself a realist - sounds perfect. Once again, many thanks.

I am glad to be in Norway and to attend this gathering. I will not spoil the evening by commenting on the ongoing dramatic and extremely dangerous events in the world, especially in Iran and the broader Middle East. However, as someone who has spent the last more than 30 years in politics, I consider it almost inappropriate to pretend that everything is in order and that we should talk only about climate and about the misuse of climate sciences to progressively shape our societies. Nevertheless, I respect the topic of our meeting. I also assume that the Klimarealistene are realists in every aspect of life, not only in discussing climate. I see the recent events in Iran as a denial of realism, and I believe that all true realists must oppose it.

---

[1] Speech for the Annual Meeting of the Klimarealistene, Oslo, Norway, March 15, 2026

https://doi.org/10.53234/SCC202603/08

1. Me and Norway is a relatively short Story

I have been to Norway only twice, which is much less than to almost any other European country (excluding some former Soviet Union republics). For the first time, I was here for a few days in February 1994, attending - as Prime Minister of the Czech Republic - the opening ceremony of the Lillehammer Olympic games. I still remember that it was very Norwegian. It was one of the last old-style, traditional ceremonies, not yet spoiled by the excesses of cosmopolitan progressivist ideology, as it was seen in Paris in 2024. It was minus 19 degrees Celsius in Lillehammer that day, and spending three hours outdoors, sitting without moving, was an unforgettable experience.

My second visit to Norway, in 2005, was an official state visit as President of the Czech Republic. I met King Harald V, Prime Minister Bondevik, and other government officials. Our delegation also visited Bergen and had a chance to enjoy a trip on one of the fjords. That's all I personally saw in Norway until today. I know it is not enough.

For an economist like me, your country is connected with the first Nobel Prize winner in economics, Ragnar Frisch (as well as with Trygve Haavelmo). As an economist and a politician, I am sorry to mention that Norway is for me connected with one very misleading idea, *the notion of sustainable growth*, which for me goes together with Madame Brundtland. I had been for years her resolute opponent at many international gatherings. This conceptually wrong idea became - quite logically - one of the crucial tenets of green ideology, of environmentalism. It remains till now one of its main pillars - competing with the infamous and economically totally irrational concept of the *Limits to Growth*. Sustainable growth and limits to growth are both based on the same way of thinking.

Economists know that the degree of concern about the quality of the environment is a function of economic affluence, of GDP per capita. In this respect, it is inevitable that Norway, as one of the richest countries in the world, takes care of environment more than less developed countries, which means more than the rest of the world. *There is, however, a fundamental difference between the environment and environmentalism.* Environmentalism does not care for the environment. It just misuses environment as an instrument for changing human society according to its own preferences. This is conceptually unacceptable for any democrat. No one should try to impose his or her own priorities and preferences upon free citizens.

I quite often and for you perhaps somewhat paradoxically - refer to Norway when I am asked to explain and justify that it was me who, in spite of being a strong critic of the European unification, on behalf of the Czech Republic sent the letter to Brussels applying for EU membership. It was thirty years ago, in 1996, still a very short time after we had got rid of communism. At that moment we were not yet a well-established and generally accepted normal European country, at least in the eyes of the self-appointed owners of the EU.

My often-repeated argument has been that, as a post-communist country, we did not have the luxury of being Norway or Switzerland - strong and self-confident enough to oppose EU membership. I am still convinced that we had no other choice at that time - not because we were eager to get EU money (which is not very helpful), but because of our lack of reputation and recognition after forty years of communism. The public mood in my country would not have allowed me not to do it at that time. That is the main reason for my often referring to Norway.

2. I was invited as the new President of Clintel

Let me say a few words about my views on climate alarmism, which I suppose is the main topic of the Klimarealistene and of your today's annual meeting. I didn't come here to lecture anyone. I would instead like to share with you some of my worries and uncertainties - about the attempt to create an international network of opponents of climate alarmism and about Clintel, thanks to which I came into contact with you.

Some of you might have read my 2026 Clintel Presidential Address[2], in which I dared to express some of my misgivings about the future of our organization. Its development really bothers me. We are obliged to the founders of Clintel, to Professor Berkhout, and to all those who signed the first Clintel Declaration to continue moving in their footsteps. We must not disappoint their expectations.

In my Presidential Address I stressed that *we are not negativists but rationally thinking sceptics*. In the original Declaration of Clintel we stressed that in our view "climate science has degenerated into a discussion based on beliefs, not on sound, self-critical science". This is, and should remain, I believe, our starting point.

I also fully support - as Prof. Berkhout put it in his September 2025 letter to me – «the irreplaceable role of background science or sciences, as opposed to climate modeling". As a former econometrician, I consider climate models a big problem. When I compare them with econometric models, the excessive use of so-called parametrization (or calibration of parameters) in these models is for me something unimaginable. *It is a return to a prescientific way of thinking.* But these models - full of mathematics - look scientific and people are not ready to see the problem. Modelling without solid background science is, of course, conceptually wrong.

We also do not believe that "science is settled", which is one of our main disagreements with the IPCC. Science can never be settled. We should insist on that. I am sure you see it the same way.

I suggest four main points for our considerations:

1. Is Clintel (or should Clintel be) *another lobbyist organization*, another activist pressure group fighting the main irrationalities of climate alarmism? *My sincere answer is: I am not sure*. I am in positive contacts with an active Czech Clintel group. Its existence is the outcome of a spontaneous evolution taking place in many countries. It is a group of people who are just now lobbying against the closure of the last coal mines in the Czech Republic. This lobbying is, without doubt, a very commendable goal. Because we don't have oil and gas on the territory of our country, coal - this traditional fossil fuel - has been our main source of energy for two centuries.

It's a big issue in my country these days. I was asked by this group to personally hand over, as a former President of the country and as the current Clintel President, a well-formulated, data-supported document prepared by this group to the Czech Minister of Trade and Industry. I did so, even though I was not sure that this is (or should be) the main activity of Clintel. You may have your own experience with this in Norway and - believe me - I have come here to learn as much as possible from you.

2. We know that Clintel itself - similarly to Klimarealistene - is not, and I think shouldn't attempt to be, *a research institution*. We have members and supporters who work in research and theory, but we do not plan to organize such research ourselves (nor do we have the capacity or funding to do so). I hope this is the way you look at it as well. Am I right? Or is there another way of looking at it?

3. Clintel could, of course, remain just *an umbrella institution* that gives individuals dispersed in the world the feeling that they are not alone, that there are many people all over the world who see the world and its problems in a similar way, who cannot stand the IPCC's arrogance and the resulting politicization of climate sciences. Who need an international organization that expresses their views with credibility and respect. This is, undoubtedly, another possible direction for our activities. Let's make the discussion about it explicit.

---

[2] https://clintel.org/clintel-president-vaclav-klaus-we-are-productively-and-rationally-thinking-sceptics/

4. Clintel could eventually become a sort of *publishing house*, with its own journal and its own books. It would mean extending our newsletter and publishing more such books as the very successful 2023 study *The Frozen Climate Views of the IPCC*[3]. Do you have the feeling that there are not sufficient opportunities to publish your views? I am not convinced about it. But it should be discussed as well. Should we be satisfied with online publications, or are we - as I am - old-fashioned believers in the importance of printed publications?

As I said, I came to Norway to listen and to learn. And I am looking forward to it. *We who are here today feel that climate alarmism, based on non-serious, politicized science, is increasingly becoming a threat to the future of the world.* And we, as Europeans, see it as an even greater threat to Europe than to other continents. The Green Deal, the European idea, has become *the embodiment and flagship of climate alarmism.* Its consequences are leading to the growing irrelevance of our old continent. It is liquidating the European industry. The dream of living on services and on imports of all industrial and agricultural products is totally irrational. It might be possible, but not prematurely.

Norway is in my view - fortunate not to be a member of the EU, although we know that Norway participates in many of the EU's very doubtful activities. In this respect, even without formal membership, you are part of it. You are, however, not penalized for failing to implement EU directives, which is a great advantage. At least for now.

3. The Economists and Climate Alarmism

As an economist turned politician at the moment of the fall of communism, I have very strong views on this issue. When I speak about climate alarmism, about environmentalism, I speak about an ideology, not about science. Economists have many disputes with this ideology. I don't think we have enough time this afternoon to discuss them. Let me give at least a brief overview of the main points in this dispute:

1. Economists disagree with the concept of "Limits to Growth". It is based on a static way of thinking similar to the views of Robert Malthus and all Malthusians, views of which have many times been challenged and disproved by serious economists. *This static concept ignores technical progress and human ingenuity.*

2. Economists disagree with the would-be wisdom of central planners and all similar people who are convinced that they know better than the market what should be produced and how. We who had experienced communism know something about this. Central planning and *all forms of government regulation make the economy inefficient and environmentally untenable.* The regulation of CO_2 asks for large-scale interventions in the price system and for massive subsidizing of green products. Today's argumentation is very similar to what I remember from the communist era.,

3. Economists consider *the price system* to be the main and irreplaceable source of information for our decision-making. Any violation of its functioning is a fatal blow to rationality and efficiency. Again, our experience is unforgettable. We are frustrated that this experience has been already more or less lost in the brave new world of today.

4. Creating and trading the so-called emission allowances, which is the basic way of dealing with CO_2 emissions in the European Union, has no connection with the market system, with free prices. It is *a state controlled administrative system* which only pretends to be

[3] Reference

market friendly. It is not the way how to introduce economic way of thinking into solving environmental problems.

5. Economists (not the critics of economics) invented - more than a hundred years ago - the concept of *externalities,* but environmentalists misuse this term and interpret the world as being full of externalities, which is not true. This wrong idea must be resolutely rejected.

6. Environmentalists hold a very trivial concept of intertemporal decision-making which is not based on *the idea of discounting.* "This has become one of the fundamental concepts of economic science. I entered the debate about global warming decades ago with an article about discounting and expressed in it my disagreement with the a priori very low discount rate used in climatological modelling. The choice of a low discount rate, almost zero, was based on an a priori ethical reasoning only, without reflecting the opportunity costs of pro-environmental decisions (and investments).

I am convinced Clintel and all Klimarealistene should pay more attention to the economic side of the climate change issue. Non-economists usually don't want to do this, which is a mistake.

4. Conclusion

Ladies and Gentlemen, let me stop here. In the subtitle of my 2007 book "*Blue Planet in Green Shackles*[4]", which has been published in 18 languages, I raised what is - for me a fundamental question: "*What is Endangered: Climate or Freedom?"* I am convinced - and I suppose many of you are as well - that the climate is more or less OK. We should do our best to convey this truth to as many people as possible.

Gloria von Thurn und Taxis, a German aristocrat, published a book in 2025 with the title "*Lieber unerhört als ungehört*[5]" (Langen Müller Verlag, München). I hope the Norwegians speak or understand German sufficiently well, because the English translation "Better ignored than unheard", as it was translated by Artificial Intelligence, is not so elegant.

As I said. we are not negativists but rational sceptics. However, *we are not, and shouldn't be, naive optimists*. We don't overestimate the positive signals coming from various places - especially from the United States and from President Trump these days - because we know that *nothing has changed in Europe, in the European Union*. Some of you may say *yet.*

I disagree. Those of us coming from the social sciences can't imagine a substantial change in Europe being realized in the foreseeable future, because the main characteristic of the European Union doesn't make such change possible. But as we say, again in German, *Optimismus ist Pflicht.* Let us remain realists striving for a fundamental change.

Co-Editor: Jan-Erik Solheim

---

[4] *Blue Planet in Green Shackles What is Endangered: Climate or Freedom?* Competitive Enterprise Institute, ISBN 978-1-889865-09-6

[5] *Lieber unerhört als ungehört: Lektionen aus meinem Leben*, Langen Müller Verlag, München

OPEN ACCESS

SCC Publishing
Michelets vei 8 B
1366 Lysaker Norway

ISSN: 2703-9072

Correspondence:

shelleyd287@gmail.com

Vol. 6.1 (2026)

pp. 82-89

Are we in the Midst of a Climate Crisis? – NO

Are our CO_2 Emissions Causing Climate Change? – NO

David Shelley

Retired ex Canterbury University, Christchurch, New Zealand

Abstract

It is a simple and seductive argument: (1) we are burning fossil fuels and emitting CO_2 into the atmosphere; (2) CO_2 is a greenhouse gas; (3) the amount of CO_2 in the atmosphere is increasing; (4) the world is warming; (5) ergo, our emissions are causing this warming and climate change. We are told that the situation amounts to a climate crisis, and we need to reduce our emissions to save the planet. It is indeed a reasonable hypothesis that our emissions are causing the world to warm and the climate to change, but it is a hypothesis that fails on several counts. And the historical and geological records tell us clearly that we are not in a climate crisis. Far from it, the present-day climate is unusually cold.

Keywords: Climate change; climate crisis; CO_2; ocean warming.

Submitted 2025-12-15, Accepted 2026-04-10. https://doi.org/10.53234/SCC202603/25

1. Is there a climate crisis?

Our politicians and the news media have belatedly woken to the fact that the climate is changing. Lacking any education on the history or geology of the subject, they are concerned that something unusual is happening and that humans must be responsible. Nothing could be further from the truth. The fact is climate change is normal. Let's look first at the last million years or so, and then in more detail at the last 145,000 years of that period.

Bi-polar glaciation has characterised the last million years of geological time, with average global lower atmospheric temperatures fluctuating between ca. 11 and 16°C. The temperature record shows a saw-tooth pattern (well publicised by Al Gore in his book) with very cold glacial periods sharply terminated by warmer so-called interglacial periods (strangely, the well-established term "interglacial period" seems inappropriate given that it occurs when Earth remains in a glacial period with polar ice caps). It is generally accepted that these saw-toothed cyclical patterns are explained by the eccentricity of Earth's orbit around the Sun, the main Milankovitch cycle, with the orbit changing from near circular to less circular over 100,000 years, affecting the amount of solar radiation Earth receives.

145,000 years ago, Earth was in the throes of the last but one intense glaciation. Much of the northern hemisphere was covered by kilometres-thick ice sheets, including all of Canada, much of Great Britain, and all of Scandinavia. Because of this huge build-up of ice, global sea levels were ca. 130 metres lower than today. In the southern hemisphere, the Alpine lakes and fiords of the South Island of New Zealand were filled with kilometres-thick glaciers, and in Australia, the former representative of the Great Barrier Reef would have been exposed as a 130 metres-high ridge of dead coral undergoing erosion in a colder ocean. Then there was a rapid increase of temperature into the previous "interglacial" period, so that 125,000 years ago, the London area had a warmer-than-today climate with hippos, lions, and elephants wandering around (the fossils are on display in London). These warmer temperatures caused sea levels to rise globally ca. 10 metres higher than today (witness the Florida Keys, which are the exposed and stranded remnants of the barrier reef of coral of that time). In Australia, with the higher sea levels and warmer temperatures, the Great Barrier Reef would have regrown, and in NZ, most of the glaciers would have melted, and the fiords and Alpine lakes filled with water.

During the last 100,000 years, a similar succession of events developed. Temperatures dropped slowly from the height of the last interglacial, and a very cold glaciation was developed by 20,000 years ago. Massive ice sheets again covered much of the northern hemisphere, sea levels had dropped by ca. 130 metres, the Alpine lakes and fiords of NZ were again filled with glaciers, and the former Great Barrier Reef left dead and exposed as a 130 metres-high ridge in a colder ocean. A rapid rise of temperature over the next 10,000 years resulted in the melting of the ice sheets and many glaciers, and the Great Barrier Reef re-grew again on the eroded stumps of the former reefs. Temperatures 8,000-6,000 years ago were slightly higher than today (it's called the Holocene climate optimum), and global sea levels were ca. 2 metres higher than today. In Europe, we can rely on history to know that Alpine glaciers have repeatedly advanced and retreated over the last few thousands of years, often revealing the remains of forests that grew in warmer times. The areas in which grapes can be grown have shifted repeatedly. Remember, too, that Hannibal took his elephants over the Alps (because it was warmer then!). Our modern warming is just one further small fluctuation in temperature, and our warmer temperatures today are still lower than the warmer temperatures reached 8,000 and 125,000 years ago, when sea levels were ca. 2 metres and 10 metres higher than today. Nothing unusual is happening today, and we remain in an unusually cold glacial period, with two polar ice caps.

Many of our children, frightened by the supposedly soon-to-come climate disaster broadcast by climate alarmists and many of our politicians and journalists, are not aware of the huge amounts of climate change that have taken place over the last million years, as described above. Should we really be worried about modern sea level changes of a few centimetres when over the last million years sea levels have gone up and down repeatedly by 130 metres — perhaps ten times?

The long-established record of higher temperatures and sea levels than today in the current and the last interglacial are usually ignored or explained away by the climate alarmists, because they contradict their narrative that temperatures today are alarmingly high, and that sea levels are rising dangerously. They often dismiss the higher temperatures of 8,000 years ago as very localised, but the reality is that they were very real and widespread, especially within Arctic regions, as recently demonstrated by Walcott-George et al. (2026), who show that the present-day 500 metre-thick ice on Prudhoe Dome in NW Greenland was completely melted away 7,000 years ago, exposing the basement rocks. The highstands of sea level 8,000 years ago have been "explained away" by hydro-isostasy, but this explaining away is not at all credible. Glacio-isostasy is credible, and observable today. Credible, because the continents are much less dense than Earth's mantle, and are essentially floating on and in the mantle, which is increasingly plastic at depth. If the continents are loaded by kilometres-thick ice, they sink in the mantle, and now the ice has melted, they are slowly rising again (as demonstrated clearly by the gradual uplift today of Scandinavia). But using hydro-isostasy to explain away the Holocene sea-level highstands is, in my view, a fantasy. The idea is that the 130 metre rise in sea level due to ice melting caused ocean floors to subside by 2 metres, which would mean that the highstands do not represent a warmer than today period with a higher volume of sea water. But this stretches credibility. One can certainly imagine the less dense continental masses that are floating on the mantle to be like rafts of cork floating in water, and which can be weighed down by a superimposed load, and rise back up if the load is removed. But there are no such cork-like bodies in oceanic areas. Remember, the mantle is huge (84% of Earth's volume, and nearly 3,000 km thick). In the oceans, which may be as deep as 11 km, the dense mantle is covered uniformly by a ca. 7 km thick layer of less-dense basaltic crust, which is then covered by the ocean water. Draw for yourself a cross section through this with a mantle 3000 km thick, and you will struggle to find a pencil thin enough to represent 130 metres of water. How, possibly can this 130 metres of water weigh down the mantle, which is 3000 km thick and encompasses all of Earth (including under the continents, which are only 30 to 80 km thick – another thin pencil needed). If the water were to make the ocean floor subside by 2 metres, where does that material go? The context for this also needs to be mentioned. The convection of plastic mantle drives plate tectonics, and under mid-oceanic ridges, hot mantle is rising relatively rapidly (perhaps 500 metres since the last ice age), in the process releasing lots of CO_2 and forming new basaltic crust, which then moves sideways at the same rate of knots. The moving basaltic crust and underlying mantle sometimes just pushes continental masses in front of it (this is where the mid-Holocene highstands are preserved), but in other places the basaltic crust and underlying mantle plunge steeply down under the continent (subduction zones), dragging everything downwards and forming the deepest trenches (11 km) of the oceans. How the supposed 2 metre subsidence of all ocean floors since the last ice age can fit into this somewhat frenetic tectonic scenario is a mystery to me. I will instead stick to Occam's Razor, and say that there is clear evidence in northern climes of higher-than-today temperatures 8,000 - 6,000 years ago (Greenland) and 125,000 years ago (the London hippos), and that the resultant glacial melting led to higher-than-today volumes of water in the oceans, as evidenced by mid-Holocene sea-level highstands in stable tectonic areas, and by the now-high-standing Florida Keys coral reef that formed 125,000 years ago. Note, too, that the continents make up only 29% of Earth's surface, and that it was only a small fraction of that 29% that was covered by kilometres-thick ice sheets in the ice age. The amount of movement and the volume of material involved in the observed glacio-isostasy is therefore very small indeed, and easily accommodated locally without the need for global ocean-floor subsidence.

In terms of climate change, even more telling is the longer record revealed by geology. Although the geological record is never complete in any one place, and estimates of temperature rely on proxies, there is general agreement on much of the record (Fig. 1). All recent summaries, including those of Scotese et al. (2021) and Judd et al. (2024), show very clearly that Earth remains in a glacial period, and that the present-day climate is unusually cold. The average global lower atmospheric temperature today is between 14 and 15°C, and Scotese et al. (2021) show that the average global lower atmospheric temperature for most (63%) of the last 540 millions years (known as the Phanerozoic) was between 19 and 21°C, 5 or 6°C warmer than today. Fauna and flora developed and thrived during those much warmer times.

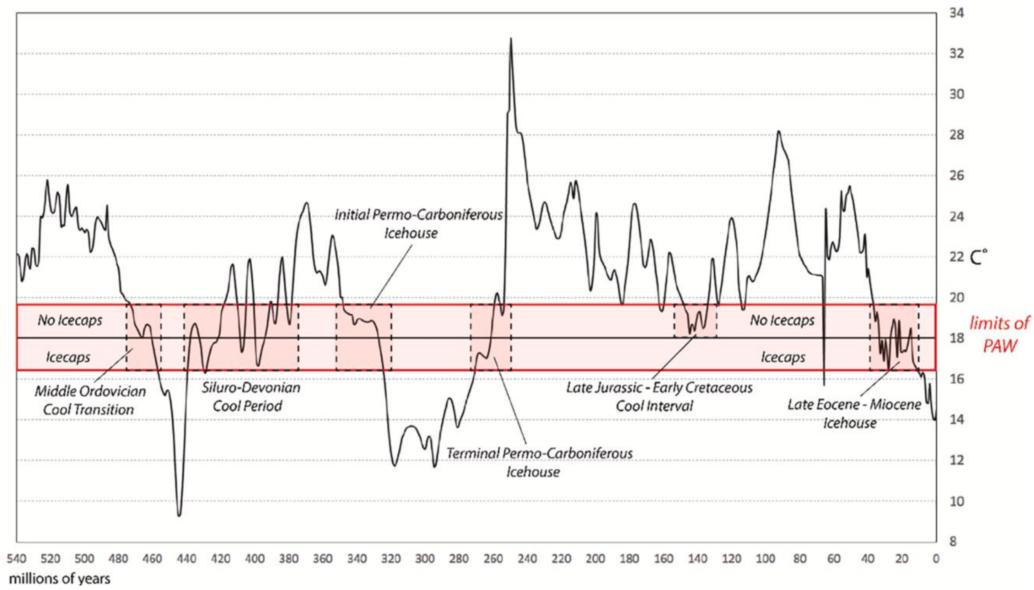

Figure 1. A compilation of average global lower atmospheric temperature estimates for the Phanerozoic, reproduced with permission from Scotese et al. (2021 Fig. 23). The very cold present-day (0 million years) temperature is between 14 and 15°C, and the highest temperature shown is ca. 33°C. Because of the horizontal scale, the details of the last 1 million years are not shown, but within that time, temperatures fluctuated ca. 10 times within the range 11-15°C ± 1°C. At temperatures below 18°C ice caps exist, and above 18°C ice caps will not exist. The pink area shows the likely temperatures of post anthropogenic warming, as predicted in the models of climate scientists.

During the Phanerozoic, there have been three very cold periods: the present day, at the end of the Paleozoic, and in the Ordovician (Fig. 1). There is a possible geological explanation for these three cold periods that involves plate tectonics. Today's glacial period corresponds to the isolation of the large continent Antarctica over the south pole, and the development of the circum-Antarctic ocean current (which developed as Drake Passage was opened). This situation (produced by plate tectonics) means that warm ocean currents cannot reach Antarctic. At the same time, the Arctic Ocean is almost completely surrounded by continental masses (only small incursions from the warmer Atlantic are possible), allowing the northern ice cap to survive. At the end of the Paleozoic, all continental masses had joined together to form the supercontinent Pangea, which happened to be stuck over the south pole, and a glaciation developed. In the Ordovician, all continental masses came together to surround a southern polar ocean, which would have frozen because of the lack of any warming ocean currents.

We still have much to learn about climate change, and its causes can be debated, but what is patently clear is (1) climate change is normal, (2) Earth is abnormally cold today, and (3) for most of the Phanerozoic (when advanced life forms were developing), temperatures have been very much warmer than today, and fauna and flora thrived.

We are certainly not in the midst of a climate crisis, but the cancel culture practised by many in the media (and sadly also scientists) means that our children and societies will continue to suffer until this message gets through.

2. Weather extremes

The news media and politicians regularly blame any extreme weather on climate change. But they are wrong. They should refer themselves to the latest report of the Intergovernmental Panel on Climate Change (IPCC 2021) where it is shown in Table 12.12 that the IPCC has not been able to detect, as yet, any increase in most extreme weather events. Of course, the IPCC models suggest that some extreme weather events might increase in frequency or intensity in the future, but I will show below that the climate models lack a firm basis. In the meantime, ignore the proclamations of the UN and climate alarmists who spread misinformation.

3. The potency of CO_2 as a greenhouse gas

There has never been agreement on how potent CO_2 is as a greenhouse gas. If the climate sensitivity (CS) of CO_2 were 1, a doubling of the amount of CO_2 in the atmosphere would increase the temperature by 1°C, but if the CS were 4, a doubling would increase the temperature by 4°C. The problem is that estimates of CS have varied substantially from less than 1 to more than 6. The IPCC (2013) acknowledges that the value of the longer-term equilibrium climate sensitivity (ECS) could be anywhere between 1 and 6, and the shorter-term transient climate sensitivity (TCS) could be anywhere between 1.5 and 4.5. How then can we possibly give any credence to climate science models that use particular values of CS to predict how climate will change as CO_2 in the atmosphere increases? The simple and seductive hypothesis that our emissions are responsible for climate change, simply remains a hypothesis, even at the first step.

4. Our emissions in relation to the entire ocean–atmosphere system

The IPCC has very usefully provided quantitative information on our total emissions since industrialization, and the total amount of carbon in the atmosphere–ocean system. The figures are very revealing. There is 50 times as much carbon in the oceans as in the atmosphere, and this ratio of 50 to 1 must represent some complex state of dynamic equilibrium between the oceans and the atmosphere (controlled fundamentally by Henry's Law). The IPCC (2022) noted the following: 1 ppm CO_2 in the atmosphere = 7.82 $GtCO_2$, and therefore 420 ppm (the approximate amount of

CO_2 in the atmosphere at that time) = 3284.4 $GtCO_2$. Given that there is 51 times more carbon than this in the global atmosphere–ocean system, the total amount of CO_2 in the global system is ca. 167504.4 $GtCO_2$. CO_2 emissions per year (including methane, which rapidly changes to CO_2) are currently equivalent to ca. 54 $GtCO_2$ (53 $GtCO_2$ in 2019; IPCC 2021, 2022 Fig. SPM.1), the equivalent of 6.91 ppm in the atmosphere, and emissions since the start of industrialisation total ca. 2500 $GtCO_2$ (IPCC 2022).

Clearly our total emissions are completely trivial relative to the entire amount of carbon in the ocean–atmosphere system, and indeed, the IPCC acknowledges that almost all our emissions should have dissolved in the oceans to maintain that 50 to 1 ratio. If that had been the case, the amount of CO_2 in the atmosphere since industrialisation should only have risen by 6.3 ppm, not by the more than 140 ppm that has actually been recorded (from 280 ppm to more than 420 ppm). The IPCC says this is the result of a rate of solution of CO_2 in the water at the atmosphere–ocean interface that is too slow to maintain equilibrium overall, and therefore our emissions are retained in the atmosphere, perhaps for thousands of years before they are fully absorbed. Then, the IPCC uses this retention of CO_2 in the atmosphere to explain global warming. However, this explanation is implausible. First of all, CO_2 dissolves very easily in water, and the ocean–atmosphere interface is a very dynamic one, with waves, spray, and winds facilitating the process of absorption. Secondly, clouds are made of water droplets, which always absorb CO_2 from the atmosphere, and send that CO_2 to the surface of the oceans and into rivers in the form of acid rain (all rain is acid because of this dissolved CO_2). No reason therefore for our emissions of CO_2 to be retained long-term in the atmosphere. Thirdly, and most importantly, another factor, the warming of the oceans, has not been taken into account.

5. The warming of the oceans

It has been well established by NOAA that the oceans have warmed recently (Fig. 2, NOAA data referred to by Laffoley and Baxter 2016), with a sharp rise in temperature starting ca. 1905, pausing from 1945 to 1975, then rising again sharply until today. Henry's Law dictates that a warming ocean must release CO_2 into the atmosphere to maintain the dynamic equilibrium between the carbon contents of the oceans and atmosphere. No wonder, therefore, that some of our emissions are being retained in the atmosphere. They are being retained because of buffering due to the release into the atmosphere of CO_2 from the oceans. In other words, our emissions may not be the fundamental reason for most of the increase in CO_2 in the atmosphere: the release of CO_2 from the warming oceans may be.

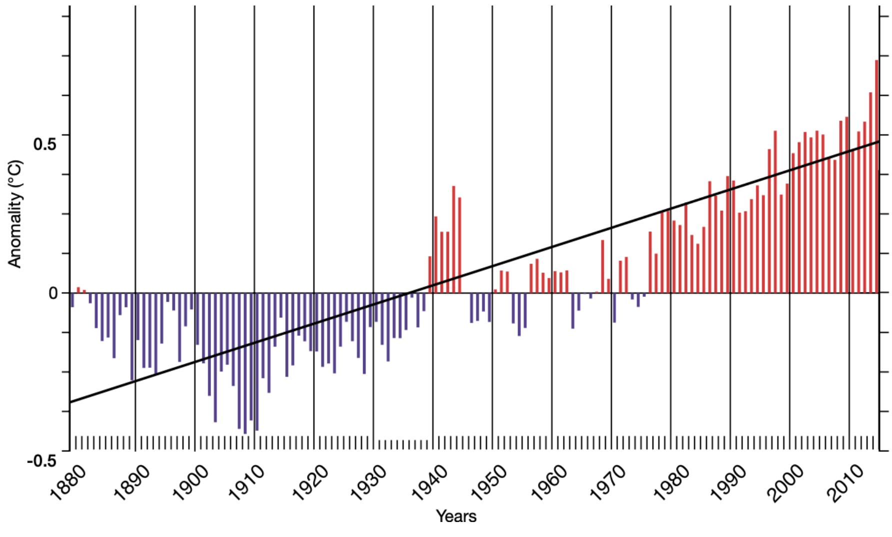

Figure 2. NOAA data on annual global sea surface temperature anomalies from 1880 to 2015 with superimposed linear trend (base period 1951-1980), red positive, blue negative.

This provides a much simpler and realistic explanation of recent global warming. The oceans are warming, and the shape of the warming curve is remarkably similar to the shape of the warming curve for the atmosphere (Fig. 3, Humlum 2025a), which also shows a pause in warming from 1945 to 1975. The oceans are significantly warmer than the atmosphere (sea surface global average of ca. 19°C compared to the lower atmosphere's 14 or 15°C), and the oceans contain an enormous amount of heat energy relative to the atmosphere, and hot water can heat air readily.

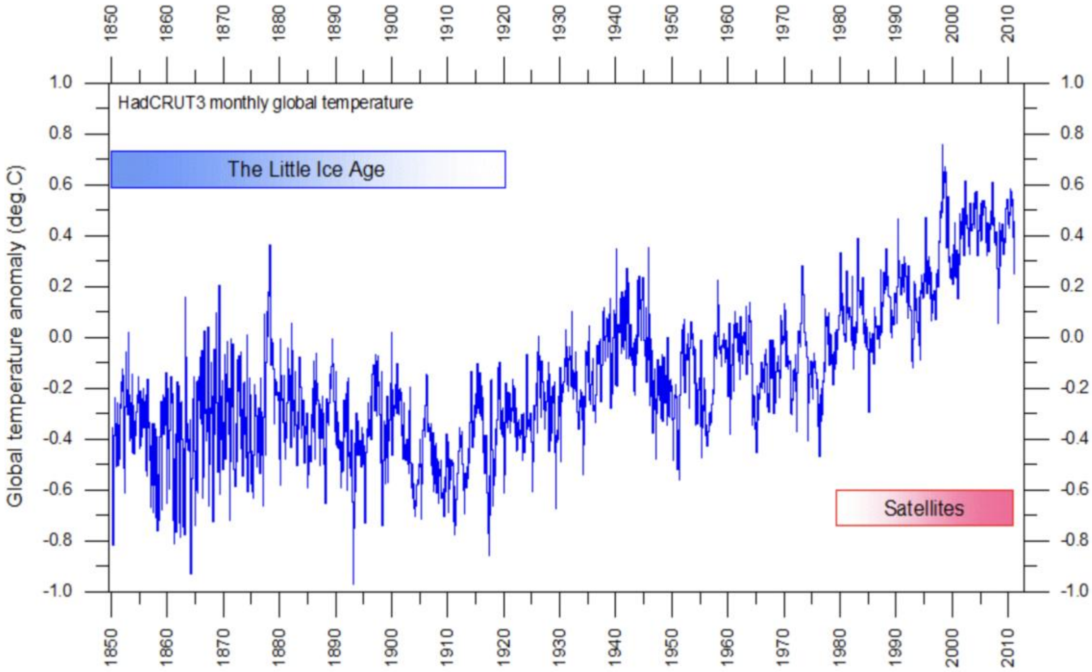

Figure 3. Global monthly average surface air temperatures since 1850 according to Hadley CRUT, a co-operative effort between the Hadley Centre for Climate Prediction and Research and the University of East Anglia's Climatic Research Unit (CRU), UK. The blue line represents the monthly values. Taken from the climate4you.com website.

The El Nino phenomenon provides a simple example of how quickly and significantly a warming ocean can heat the atmosphere. The east to west trade winds in the Pacific push water to the west, and drag up deep cold oceanic water along the South American coast, which is then pushed to the west. When the trade winds are strong, a large amount of cold water is pushed west cooling the Pacific (La Nina). El Nino occurs when the east to west trade winds in the Pacific are less intense, less cold water is pushed west, and the Pacific warms. Each El Nino is marked by a sharp rise in global lower atmospheric temperatures, usually an increase in ca. 1°C over two or three years. If these local perturbations in the Pacific Ocean can cause atmospheric temperatures to rise significantly on a global scale, then clearly, what happens in our oceans have very direct, immediate, and important effects on the atmosphere.

Strangely, climate scientists, disturbed by the relatively small amount of heating of the atmosphere compared to what was predicted in most of their models, have claimed that some of the warming in the atmosphere due to our emissions has been lost to the oceans, causing the oceans to warm. This, again, is extremely implausible. How can heat be transferred from relatively cold air to relatively hot water?

What, then, is causing the recent warming of the oceans? Several possibilities present themselves, including volcanic activity (the amount of heat transfer from the 65,000 kms of mid-ocean ridges is possibly variable, and certainly not yet satisfactorily studied and measured) and Milankovitch cycles (there are three, which interfere with each other in not fully understood ways to change the amount of heat reaching Earth from the Sun).

Perhaps the simplest way of explaining the recent warming of the oceans is by direct heating by the rays of the Sun. We know that the Sun is capable of heating the oceans down to depths of more than 100 metres (depending on water clarity and other issues), and a plausible reason for an increase in this direct heating by the Sun is a loss of cloud cover, which has been documented for the last 25 years (Tselioudis et al. 2025). Unfortunately good data on earlier cloud cover does not exist.

We may not be sure why the oceans are warming, but warming they are. The oceans are huge in volume and mass relative to the atmosphere, and water has a huge and almost unique heat capacity allowing the oceans to store huge amounts of heat. Our climate is therefore much more likely to be controlled by the oceans than the atmosphere, and climate scientists therefore need to pay less attention to the atmosphere, and more to the oceans.

6. The future

My prediction is that, as long as Antarctica is hemmed in by the circum-Antarctic oceanic current and the Arctic Ocean is hemmed in by continental masses, we will remain abnormally cold. The modern warming is a transient and very minor phenomenon, and the long-term probability is slow cooling for tens of thousands of years, at the end of which we will have sunk into the depths of another intense glaciation. At that time, the tropics will retain average lower atmospheric temperatures of ca. 30°C, but most of the world will be very much colder and lose much of its ability to grow crops, and Canada, Britain, and Scandinavia will be covered by kilometre-thick ice sheets, and completely uninhabitable. Sea levels will have dropped again by 130 metres. CO_2 levels in the atmosphere will drop (absorbed by the cooling oceans), and the real possible disaster scenario is that if CO_2 levels drop below 150 ppm most plants will not survive, which means in turn that most animals will not survive. Burning fossil fuels like mad to avoid that will not work. It would only add CO_2 to the oceans, which will continue to absorb atmospheric CO_2 as the water cools.

In the short term, we can forget about our emissions. They are irrelevant to climate change. We can continue to burn fossil fuels for a while, but in the medium term we will have to change our habits, because fossil fuels are a finite resource, and we can't just use them all up. Uranium and thorium nuclear power plants seem the most likely medium-term solution to our energy problems. Who knows whether fusion power or something else will ever come to pass?

Finally, Humlum (2025b) has approached the subject of recent climate change in a rather different way from me in this essay, but we come to the same conclusion. To quote from Humlum: *there is no observational evidence for any global climate crisis. Our world should consider focusing on much more pressing problems.*

Funding

There was no funding of the work.

Co-Editor: H. Harde; **Reviewers**: anonymous.

References

Humlum, O., 2025a: https://climate4you.com website

Humlum, O., 2025b: *The state of the climate 2024.* The Global Warming Policy Foundation Report 63, 73 pages. https://thegwpf.org

IPCC AR5: Collins, M., R. Knutti, J. Arblaster et al., 2013: *Long-term Climate Change: Projections, Commitments and Irreversibility.* In: Climate Change 2013: The Physical Science Basis. Contribution of Working Group I to the Fifth Assessment Report of the Intergovernmental Panel on Climate Change [Stocker et al. (eds.)]. Cambridge University Press, Cambridge, United Kingdom and New York, NY, USA

IPCC AR6: Ranasinghe, R., A.C. Ruane, et al., 2021: *Climate Change Information for Regional Impact and for Risk Assessment.* In Climate Change 2021: The Physical Science Basis. Contribution of Working Group I to the Sixth Assessment Report of the Intergovernmental Panel on Climate Change [Masson-Delmotte et al. (eds.)]. Cambridge University Press, Cambridge, United Kingdom and New York, NY, USA, pp. 1767–1926, https://doi.org/10.1017/9781009157896.014

IPCC, Summary for Policymakers, P. R. Shukla et al. 2022: In: *Climate Change 2022: Mitigation of Climate Change. Contribution of Working Group III to the Sixth Assessment Report of the Intergovernmental Panel on Climate Change* [P. R. Shukla et al. (eds.)]. Cambridge University Press, Cambridge, UK and New York, NY, USA. https://doi.org/10.1017/9781009157926.001

Judd, E. J., Tierney, J. E., Lunt, D. J., Montaflez, I. P., Huber, B. T., Wing, S. L., Valdes, P. J., 2024: *A 485-million-year history of Earth's surface temperature.* Science, v. 385, eadk3705. https://doi.org/10.1126/science.adk3705

Laffoley, D., Baxter, J. M. (editors)., 2016: Explaining ocean warming: Causes, scale, effects and consequences. Full report. Gland, Switzerland: IUCN. 456 pp. http://dx.doi.org/10.2305/IUCN.CH.2016.08.en

Scotese, C. R., Song, H., Mills, B. T. W., van der Meer, D. G., 2021: *Phanerozoic paleotemperatures: The earth's changing climate during the last 540 million years.* Earth-Science Reviews, v. 215. https://doi.org/10.1016/j.earscirev.2021.103503

Tselioudis, G., Remillard, J., Jakob, C., Rossow, W. B., 2025: *Contraction of the World's Storm-Cloud Zones the Primary Contributor to the 21st Century Increase in the Earth's Sunlight Absorption.* Geophysical Research Letters, v. 52, Issue 11. https://doi.org/10.1029/2025GL114882

Walcott-George, C K., Brown, N. D., Briner, J. P., Balter-Kennedy, A., Young, N. E., Kuhl, T., Moravec, E., Anandakrishnan, S., Stevens, N. T., Keisling, B., DeConto, R. M., Gkinis, V., MacGregor, J. A., Schaefer, J. M., 2026: *Deglaciation of the Prudhoe Dome in northwestern Greenland in response to Holocene warming.* Nature Geoscience, v.19, 189–194. https://doi.org/10.1038/s41561-025-01889-9

SCC Publishing
Michelets vei 8 B
1366 Lysaker Norway

ISSN: 2703-9072

Correspondence:
ole.humlum@gmail.com

Vol. 6.1 (2026)
pp. 90-100

The State of the Climate 2025 Global and Arctic

Based on Real Observations*

Ole Humlum

University of Oslo and UNIS Svalbard, Residence: Denmark

Abstract

Real observations show a slight decrease of global temperature in 2025 compared with the previous ten years. Some stations in the Arctic show warming, but most are fairly stable. The Arctic Ocean is cooling to considerable depth, while the tropical and Antarctic oceans have a slight surface warming. The sea level trend is not changing as IPCC model data indicate. The Arctic September sea ice varies but its area has the last 4 years been much larger than modelled by the IPCC. The average snow cover on the Northern Hemisphere is fairly constant during the last 50 years. The number of tropical cyclones varies, but with no clear trend. The integrated cyclonic energy shows some periodic variations, but no trend. Global precipitation has almost zero trend. The global cloud cover decreased from 64 % to 61 % from 1985 to 2020. At the same time the global temperature increased 0.7 °C, suggesting a possible relation. The observed sequence: first warming the of the sea surface, then the deeper sea, atmosphere and land suggests that the Sun is the source of warming, modulated by clouds, and there is no manmade climate catastrophe in the foreseeable future.

Keywords: Global climate; climate change; climate catastrophe

Submitted 2026-04-13, Accepted 2026-04-21. https://doi.org/10.53234/SCC202603/26

1. Introduction

The United Nations Secretary General, António Guterres on July 27, 2023, declared: *The era of global boiling has arrived. We have a huge climate crisis*.

There is a good reason to study the available climate data to see if that is true. In the following we will compare data for 2025 with previous years and look for trends of this claimed extreme warming and accompanying weather extremes. We found no sign of a coming climate crisis.

Before I started this survey, I asked my helpful AI to make some images illustrating a) Changing Climate, b) Natural climate change, and c) Good climate change and d) Man made climate change. The pictures are shown on the next page. They give a good idea of what the public is told about climate and climate change and that mankind is destroying it, as stated by the UN Secretary General.

In this extended abstract I present a short status for the atmospheric and ocean temperatures, sea level, sea ice, sea level, snow, wind and storms, precipitation and global cloud cover. My talk can be seen at https://www.youtube.com/watch?v=85puIDVyBgc. Monthly updates of climate data are available at my website: www.climate4you.com.

* Talk at the Annual Meeting of Klimarealistene, Oslo, Norway March 15, 2026

Figure 1: AI generated pictures of a. Changing climate, b. Natural climate change, c. Good climate change, d. Manmade climate change

2. Atmospheric temperatures

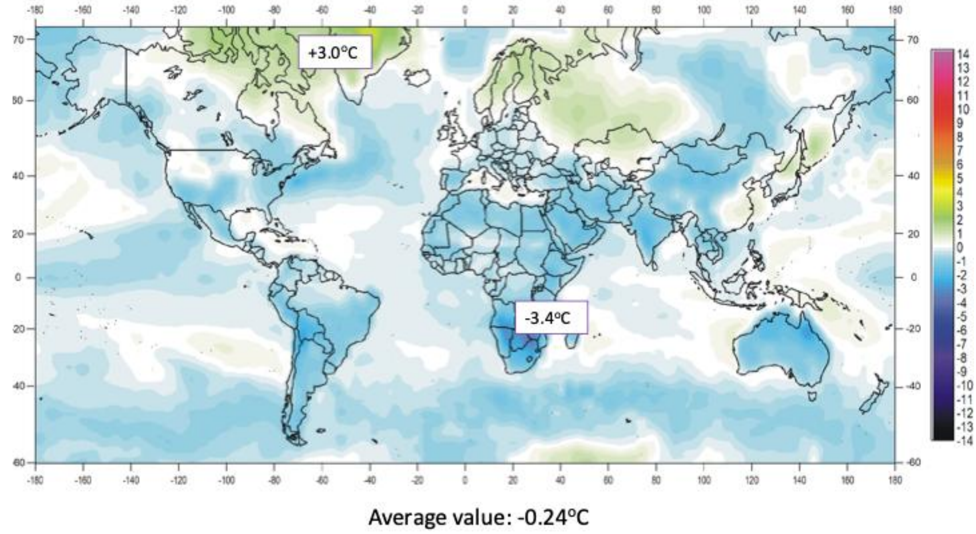

Figure 2: The average temperature of the year 2025 versus last 10 years.

A crucial parameter is the change of the global temperature. Usually, it is compared with a fixed 30-year average, which changes every 30 years. The last one is from 1990-2020. Since this becomes more and more in the past, and is hard to remember for ordinary citizens, I prefer to compare with the last 10 years which is shown in Figure 2. The average change is -0.24 °C and is more a sign of cooling than warming.

A warning: The use of just one number, the average change in global temperature, hides the fact that our planet has various temperature regions which may show a different change than the average. In 2025 we observe that the Southern Africa has cooled 3.4 °C, while Greenland and Northeast Canada have warmed 3.0 °C. The use of averages tends to hide important details.

For the polar regions we observe that the average air temperature is increasing in the Arctic but is stable in the Antarctic. A more detailed look at station level in the Arctic shows that only two out of six stations show a marked temperature increase. They are marked with red circles in Figure 3 and may be related to the warm Atlantic current entering the Barents Sea. To investigate climate dynamics, we must focus on local values, rather than average values.

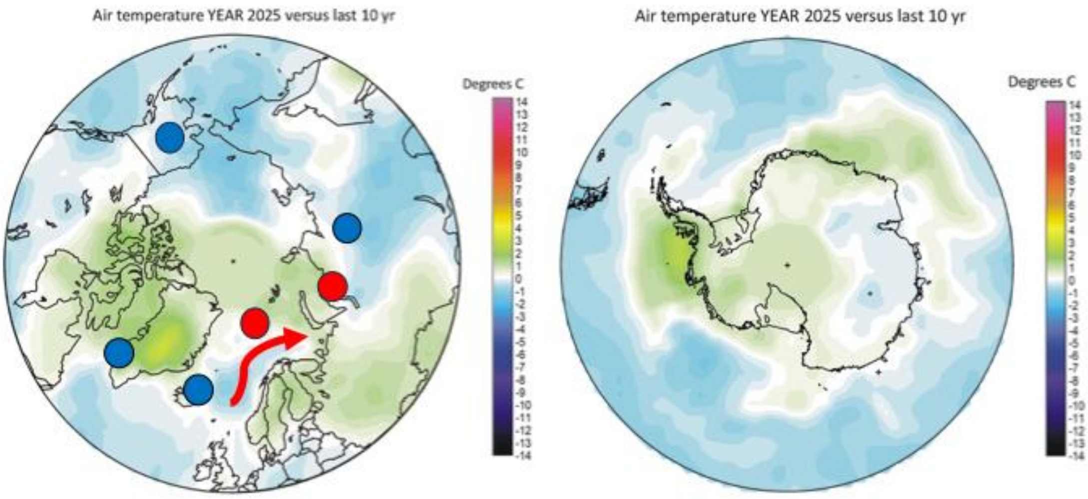

Figure 3: Air temperature in the Arctic and Antarctic in 2025 compared with the last 10 years. Red circles in the Arctic map shows stations with increasing temperatures. Blue circles show no trend. In the Antarctic there are variations in different areas but no trend.

3. Ocean temperatures

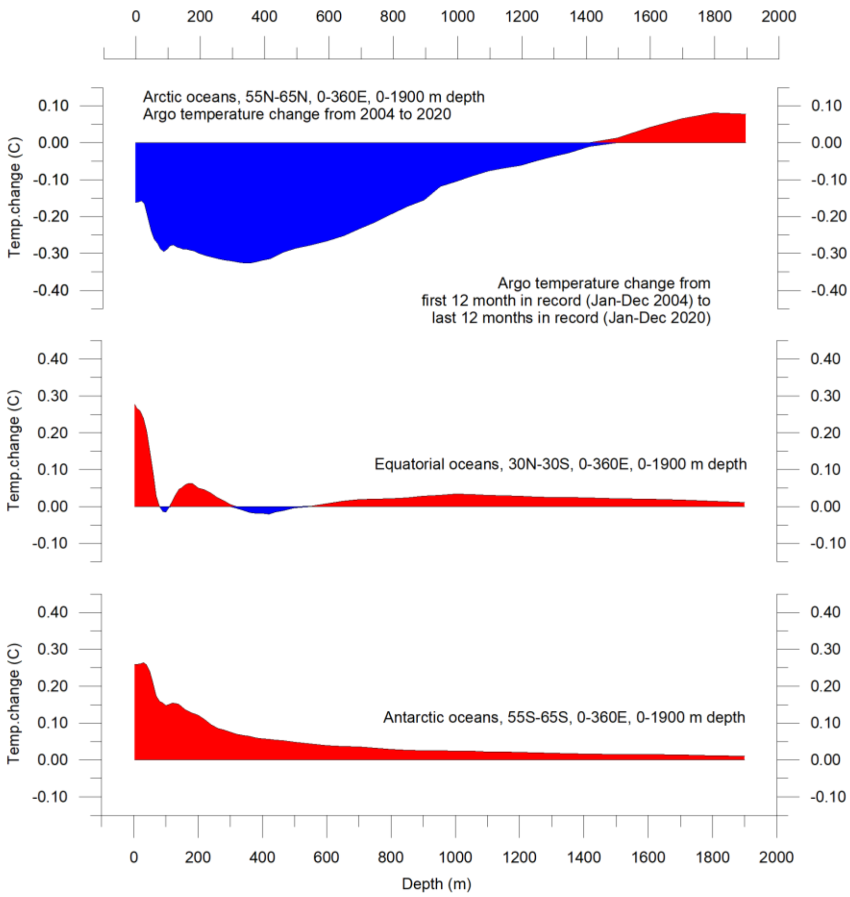

Figure 4: Argo temperature change 2004 - 2021 in three different ocean areas.

The general impression of the global sea temperatures is that they follow the radiation pattern of the Sun, with a maximum surface temperature in Equator regions and colder water towards the poles. At the deep bottom of both Polar Oceans we find, to our surprise, permafrost regions.

If we look at data for the Argo Ocean temperature surveys for the oceans from 0 to 1900 m depth, from 2004 to 2021, we find that the average temperature of the global oceans has increased from 6.42 to 6.47 °C. However, if we look at different oceans: the Circum-Arctic oceans are cooling, while the Circum-Equator oceans are warming – but only near the surface level. The Circum-Antarctic oceans show warming down to 500 m. This is illustrated in Figure 4.

Much is still to be learnt about the oceans! We should focus on local and regional values instead of global averages and should not overinterpret published values.

4. Sea level

In their last report, IPCC presents a Projected global sea level rise under different SSP scenarios and concludes with a likely range (medium confidence) of 1.5 to 2 m global sea level rise in 2150. We may compare this with a sea rise of 3-4 mm per year calculated from satellite observations, although with many questionable assumptions and corrections. This number is significantly less than shown in most IPCC projections.

The satellite observations refer to a global model of the sea surface of the oceans. It is far more relevant to study the traditional sea level observations in coastal areas where people live. An important measuring station is Korsør in Denmark, which is in a geologically very stable area with no uplift or sinking. Measurements since 1897 in Figure 5, shows a linear trend of +0.83 mm/year. This means an estimated sea level rise of about 10 cm in 2150.

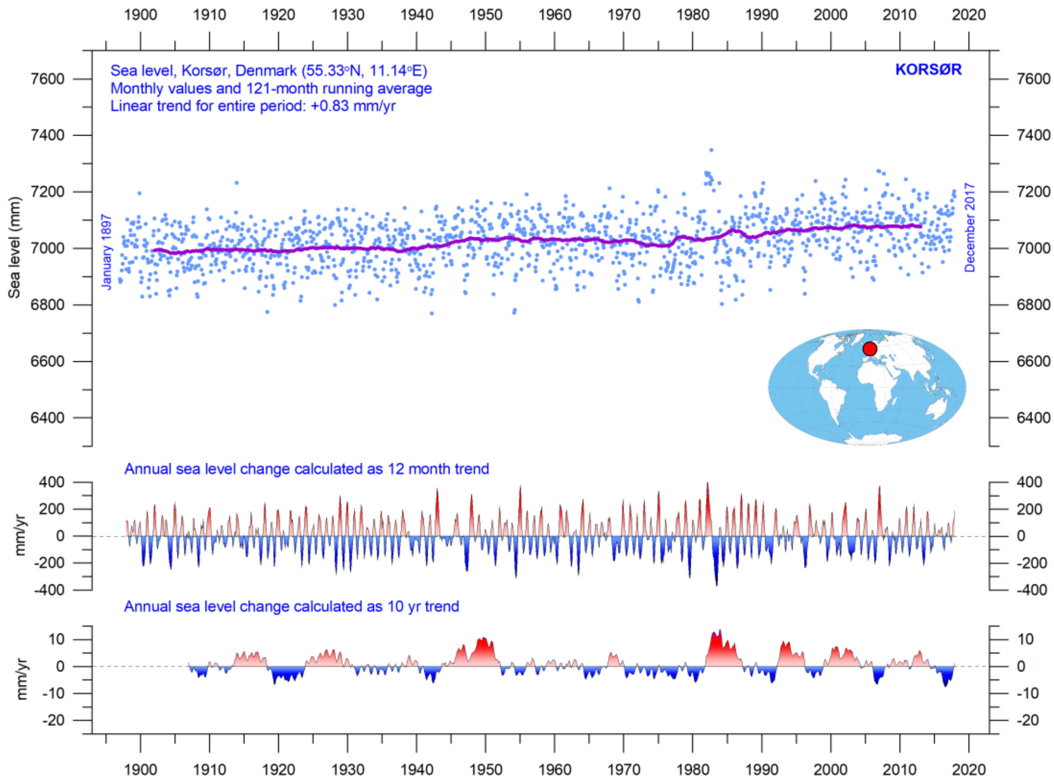

Figure 5: Sea level measurements in Korsør, Denmark. A geologically stable location.

Another example of the difference between models and real observations is shown by Figure 6, illustrating the Oslo sea front. The land is raising isostatically from the weight of 3 km ice which melted 12 000 years ago. Sea level measurements at Oslo began in 1914, and the sea level is sinking (in relation to land) with a linear trend of 3.3 mm/year. The sea level model estimates by IPCC and used by authorities in their planning, predicts an increase of 6 mm/year and results in 0.5 m higher sea level in 2100 than the linear negative trend observed.

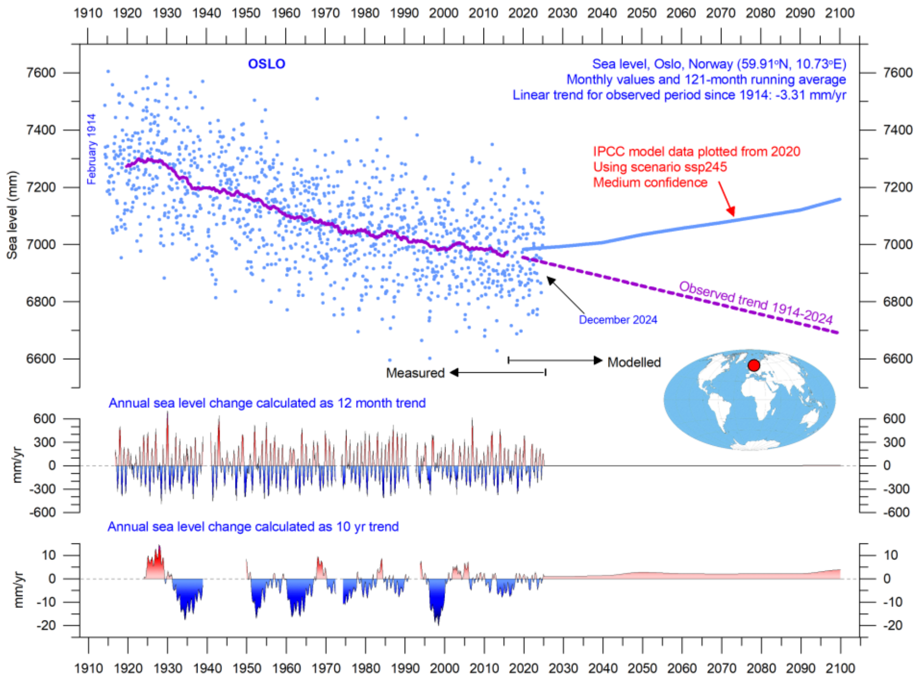

Figure 6: Sea level measured in Oslo 1914 - 2024 with IPCC projections and observed trend.

5. Sea ice

The future of the Arctic Sea ice is rather serious according to the last IPCC report. Some scenarios predict practically ice-free conditions in September from 2050 as shown in Figure 7. But observations show that for the last 4 years the sea ice area has been considerably higher than forecasted by the models.

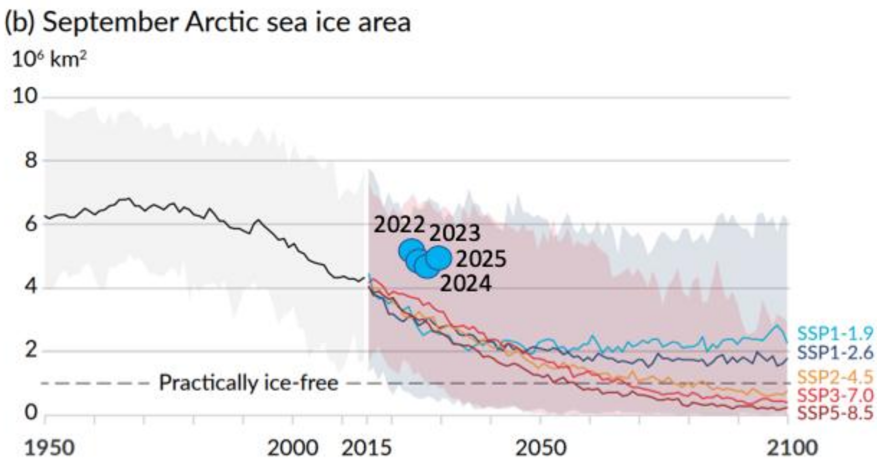

Figure 7: Arctic minimum sea ice (September) from last IPCC report (2021) with observed areas for 2022-2025 (blue circles).

The sea ice cover in the Arctic Ocean is difficult to predict. An example is the year 2011-12 in which we observed the maximum ice extension during the last 20 years, which was followed by the lowest extension in the period during the following summer.

In the Antarctic, the sea ice extension increased significantly during the period 1979-2016, while it was decreasing in the Arctic. Then the Antarctic sea ice diminished markedly from 2015 and is now about the same level as in the Arctic. This has nothing to do with changes in air temperatures in the Antarctic, which were nearly constant throughout the period. Instead, the decrease was caused by strong catabatic winds pushing the ice out in warmer water further north, causing it to melt.

Much is still to be learnt about polar sea ice.

5. Snow

We often read in newspapers and are told in the media that snow is just a thing of the past. But if we look at the Northern Hemisphere snow cover, as it is measured by satellites since 1972, it has been surprisingly constant. If we look at the seasons, the winter cover is very stable, the spring and summer level have a slight decrease, while the fall snow cover shows a slight increase.

6. Wind and storms

The media communicates that the frequency of storms is increasing and the damage they do is more serious than before. Figure 8 shows a map of global cyclone tracks from 1985 to 2005.

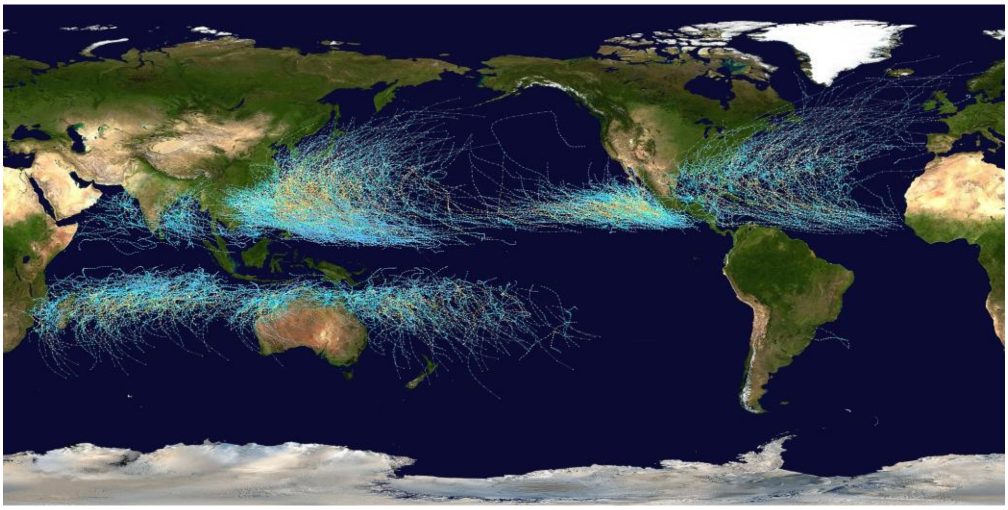

Figure 8: Global tropical cyclone tracks 1985 - 2005. Picture source: NASA.

If we study the statistics of all hurricanes recorded since 1980, we find a variable pattern, but without a clear trend. The news media alarm is thus entirely unfounded. A Fourier analysis indicates a significant oscillation of about 3.7-year duration.

Accumulated cyclone energy (ACE) has been calculated since 1851 for the Atlantic basin. A Fourier analysis shows a significant period of 61.5 years and a possible period of 5.6 years. These periods are also present in other climate series.

7. Global precipitation

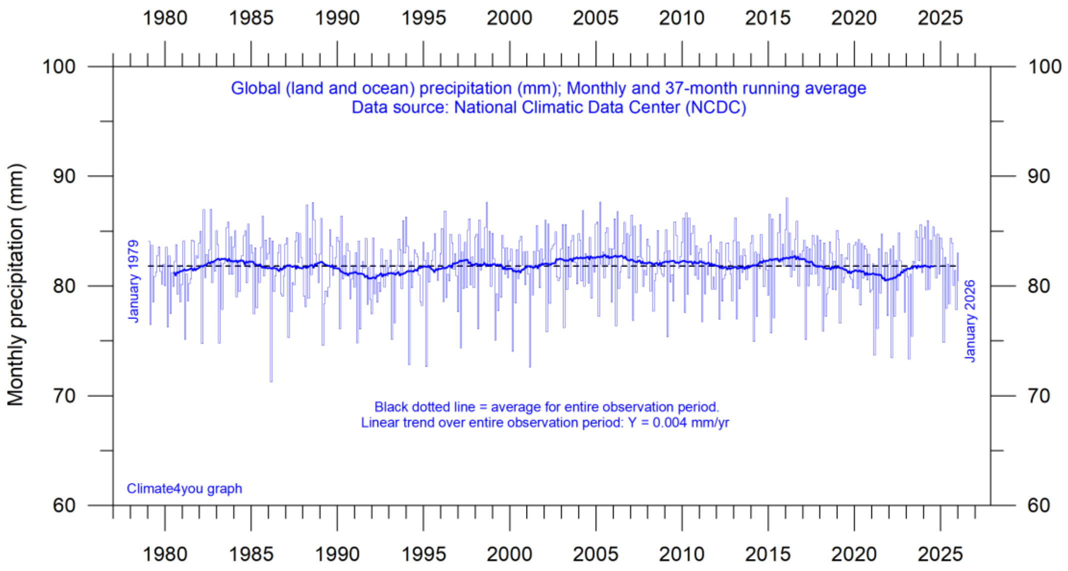

Figure 9: Global precipitation 1979 - 2026.

Warmer air is able to contain more water vapour. The slight global temperature increases which are measured (Figure 11) might therefore result in increased precipitation, since the last warming started about 1980. However, the measured monthly rainfall (Figure 9), which is highly variable from month to month, shows a trend close to zero, in contradiction to model forecasts.

If we look at individual regions, we find that precipitation in Europe also has been constant during the same period. In the Arctic as shown in Figure 10, there was a dry period around 2001, and after 2005 there was a slightly higher precipitation than before the dry period.

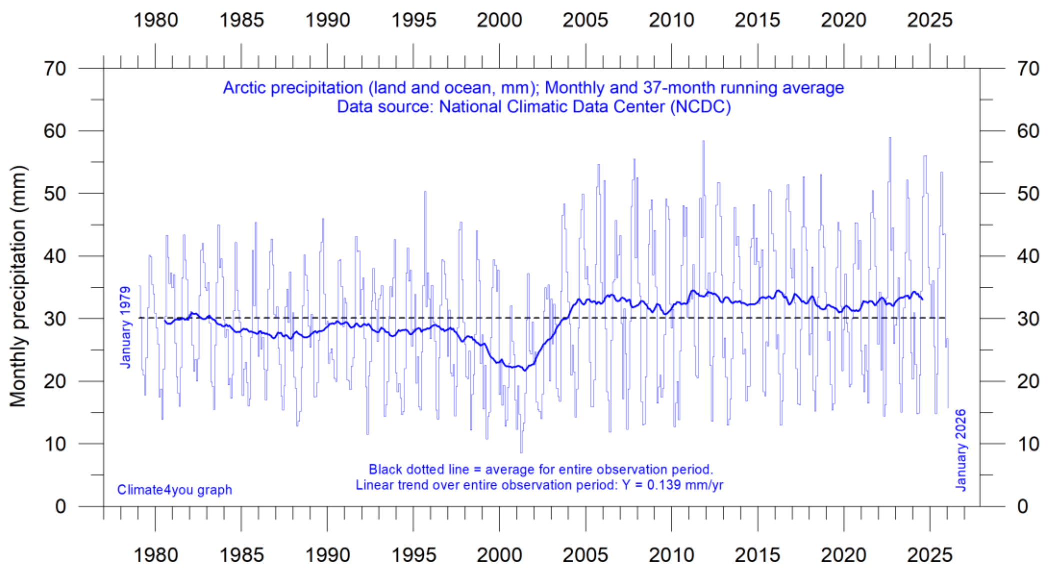

Figure 10: Monthly precipitation in the Arctic 1979 - 2026.

The Arctic is a dryer region which makes the changes from month to month larger.

8. Cloud cover – and a few reflections

If all clouds were suddenly removed, then our planet would gain about 17 W/m^2 in solar radiation and become warmer. In the period 1982-2019 we have observed a decrease in cloud cover from 64 % to 61 %. This means that the Earth has received significantly more solar radiation. This may well be the main explanation for the observed temperature increase of about 0.7 °C during this period, as shown in Figure 11.

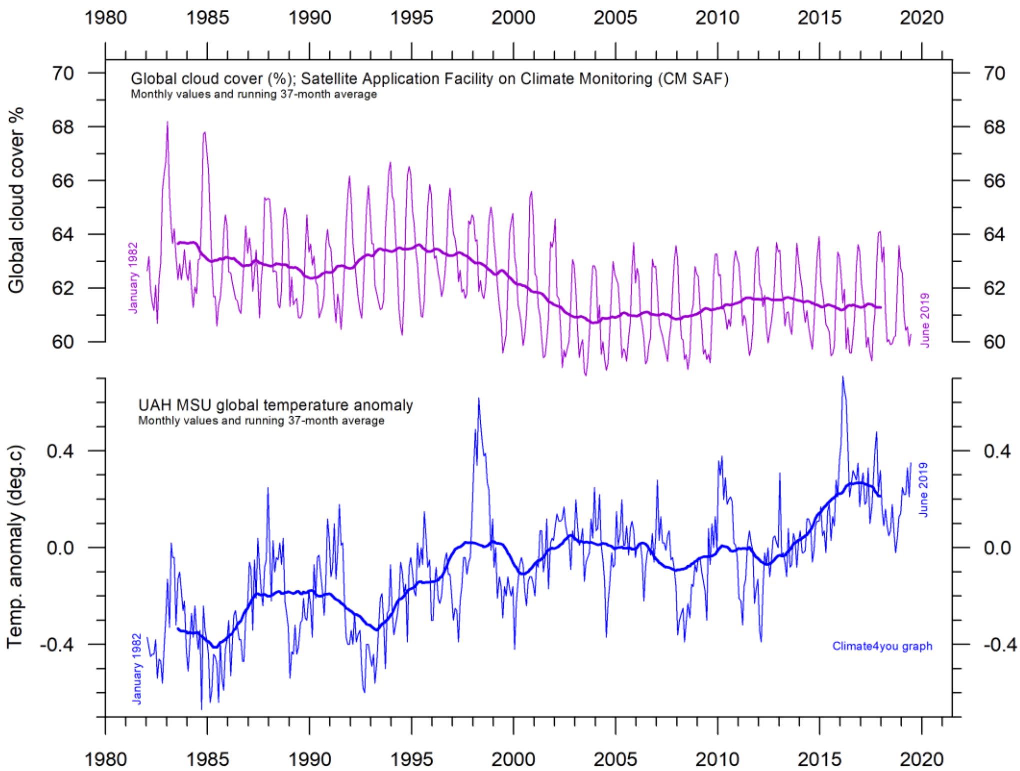

Figure 11: Global cloud cover and global temperature in the period 1982 – 2019.

Climate scientists admit that they cannot model he cloud cover in a reliable way. It is simply not possible to trustworthy model small scale phenomena as evaporation and condensation, for use in global climate models.

There are many additional parameters that may act on the cloud cover. For instance, if we study the changes in the Earth's rotation, which we measure as the length of the day, we find that it was 2 milliseconds longer in 1980 than it is today. The faster rotation mirror decreasing cloud cover and decreasing humidity. Thus, it is therefore entirely possible that these parameters in some ways are related. Much is still to be learned about global cloud cover.

8.1 Some reflections

The principal question was this: Are we currently in a climate crisis?

1. The observed average global air temperature change during the last 40+ years is about +0.16 ºC per decade. If unchanged, the additional average global air temperature increase by year 2100 will be about +1.15 ºC. However, part of the temperature increase reported may be caused by administrative changes, and the real future increase may therefore be

smaller.

2. Tide gauges along coasts indicate a typical global sea level increase of about 1-2 mm/yr. Coastal sea level change rate last 100 year has essential been stable, but with periodic variations. If unchanged, global sea level at coasts will typically increase 8-16 cm by year 2100, although many locations in regions affected by glaciation 20,000 years ago, will experience a relative sea level drop.

3. Since 2004 the global oceans above 1900 m depth have on average warmed about 0.037ºC (do not overinterpret). The maximum warming (about 0.2 ºC, 0-100 m depth) mainly affects oceans near Equator, where incoming solar radiation is at maximum.

If we look at the Earth's climate on geological time scales of millions of years, it is surprisingly stable. In most periods it is stable and warm – about 25 ºC on average, and in some periods, it is about 10 degrees colder, as we observe now. It seems that the planet has a thermostat that keeps the climate between these limiting temperatures. Today, our planet is well situated in between these limits, and there is no reason to think that we are in a climate crisis.

8.2 Nature provides us with simple answers

In a simple way, observed data shows us what really controls the global air temperature. We just need to use our common sense and examine the sequence of temperature changes. Measurements (Figure 12) tell us that the global temperature signal originates at the ocean surface. Two weeks later the signal is recorded by satellites in the lower atmosphere. The land surface air temperature also follows the ocean surface temperature with a delay of two months, and 20 months later the signal is recorded in the ocean at 200 m depth. This sequence was first described by Humlum et al. (2012) and demonstrates the key role for ocean surface temperature in controlling atmospheric temperatures.

The hypothetical CO_2 temperature signal originates in the upper troposphere, and – if dominant – we would see the signal in the satellite data from the lower atmosphere, before we see the signal arriving at the ocean surface. Measurements show that the opposite is the case (Figure 12). To the degree CO_2 influences atmospheric temperatures, its effect is clearly subordinate in relation to other influences.

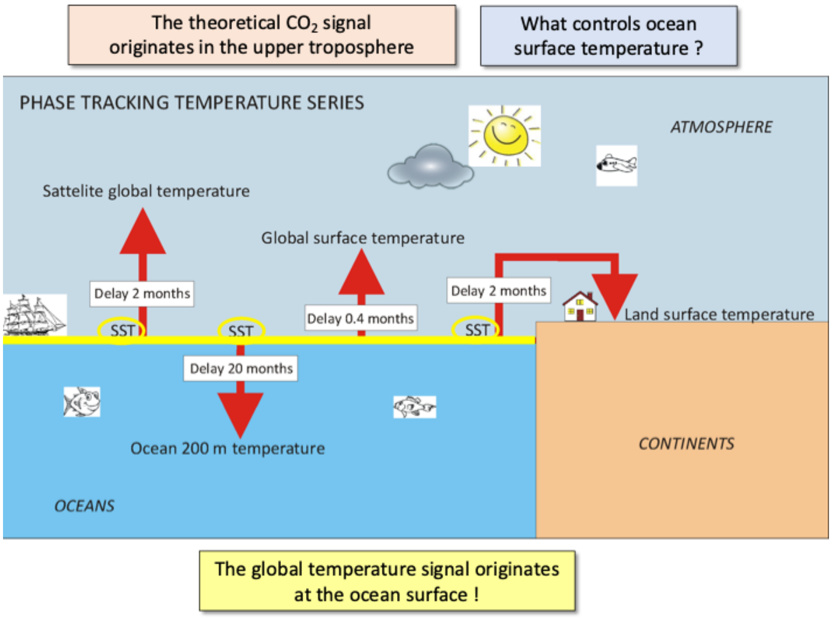

Figure 12:The sequence of global climate signal from the sea surface (SST) to the deep ocean.

The principal climate research question therefore is this: *What controls the ocean surface temperature?* Presumably, the Sun is the key answer, modulated by the global cloud cover.

9. Climate Change: importance of oceans

I have two overall conclusions and one suggestion for what should be the future main climate research focus:

1. Observed data do not support the notion of a climate crisis but reveals many and partly recurrent natural variations.

2. Ocean surface temperature controls the atmospheric temperature.

PROBABLY THE MOST IMPORTANT CLIMATE RESEARCH QUESTION:

What controls the ocean surface temperature?

10. Final reflections and conclusions

Why did I not speak anything about CO_2? This is because my talk is on climate, and CO_2, although being very important for plant and animal life, in my opinion, is not overly important to understand meteorology and climate.

Co-Editor: Jan-Erik Solheim

References

Humlum, Ole, *http://www.climate4you.com/*

Humlum, Ole, Stordahl, Kjell and Solheim, Jan-Erik, 2012, *The phase relation between atmospheric carbon dioxide*, Global and Planetary Change, 100, 51-69, http://dx.doi.org/10.1016/j.gloplacha.2012.08.008

IPCC Sixth Assessment Report, 2021, Working Group 1, The Physical Science Basis https://www.ipcc.ch/report/ar6/wg1/

Appendix

Finally, another small experiment with Artificial Intelligence: I asked the AI to generate a picture of a typical climate scientist, and I got the picture below to the left. I then asked it to generate a picture of a typical climate realist and got the picture to the right. What a beautiful world!

A typical Climate Scientist drawn by AI

A typical Climate Realist drawn by AI

I then asked the AI to draw a picture of myself

– and got this one:

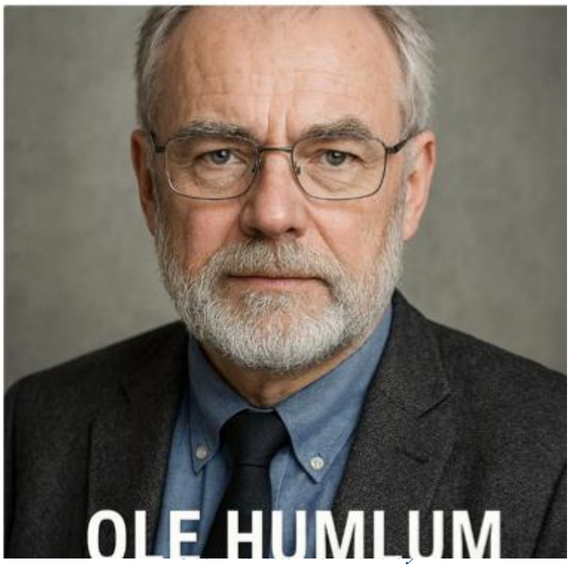

to be compared with the real one:

The real Ole Humlum

OPEN ACCESS

SCC Publishing
Michelets vei 8 B
1366 Lysaker Norway

ISSN: 2703-9072

Correspondence:

rogerhiggs@hotmail.com

Vol. 6.1(2026)

pp. 101-127

Global Temperature Change by Solar Variation Outweighed Since 1940s by Warming Effect of Anthropogenic Airborne Black Carbon, not CO_2?

Roger Higgs

Geoclastica Ltd, Coventry, UK

Abstract

Solar control of global warming and cooling (Svensmark Theory) is supported by the similarity of two published graphs: (1) average near-surface air-temperature for the last 9,000 years (from proxies and, since 1880, NASA thermometer charts); and (2) solar-magnetic output (proxies). Graph-to-graph visual cross-matching of spikes (peaks, troughs) and of multi-century trends reveals a variable temperature lag (~100-225 years). Despite the good qualitative match, the correlation coefficient for the last 2,000 years is low (0.3), attributable to lag variability and numerous non-matching spikes. Relative amplitudes of cross-matched peaks indicate disproportionate warmth since 1940, coinciding with the large growth in coal- and oil combustion since World War Two. Based on two features of NASA's temperature charts, the main cause of this excess warmth is not carbon dioxide (CO_2): (1) after 1980, warming paused (4-8 years) four times, conflicting with CO_2's non-pausing growth; and (2) since 1985, warming is faster above land than ocean, at odds with CO_2's spatial homogeneity, instead implicating poorly dispersed airborne black carbon (essentially soot, which absorbs solar radiation, thereby warming the air), hitherto widely considered the second most important human-produced warming agent. Soot is emitted by the burning of coal, diesel-oil, and wood, *mainly on land*. Incriminating especially coal: (1) the mentioned land/ocean decoupling began (1985) only 10 years after the growth-rate of world annual coal-consumption abruptly tripled; and (2) the longest warming-pause (2003-2011) started soon (15 years) after the first-ever coal-growth pause (1988-1999) began. Consistent with this evidence that CO_2 has, in reality, relatively little warming effect, numerous authors have reported that changes in CO_2 *follow* changes in temperature. Apparently, therefore, CO_2's greenhouse effect is largely (entirely?) outweighed by little-known feedbacks. Indeed, the Intergovernmental Panel on Climate Change acknowledges cloud-related feedbacks as climate models' largest uncertainty. Thus, stopping anthropogenic warming might be tantalisingly easy: simply stabilise coal- and oil combustion, thereby ending airborne-soot *growth*. Natural gas (almost soot-free) could be substituted for coal in electricity generation. Gas reserves are sufficient for decades, perhaps long enough for development of nuclear fusion (soot- and CO_2-free).

Keywords: climate; warming; Sun; soot; CO_2.

Submitted 2025-12-09, Accepted 2026-06-05. https://doi.org/10.53234/scc202603/27

1. Introduction

Climate scientists seldom look back beyond the establishment of a reliable global thermometer network, in the 19th Century. A longer perspective is provided in this contribution, using published proxy-temperature- and proxy-solar-output data going back ~9,000 years, revealing that, until very recently (20th Century), solar-magnetic fluctuations appear to have governed Earth's average temperature (Section 4.1). By integrating these diverse data spanning thousands of years and fusing them with meteorological and industrial (coal- and oil-consumption) data that span the last few decades and centuries, a better understanding is gained of: (a) the extent to which today's climate is overwarm; (b) the year or decade in which the extra warming began; and (c) the cause.

2. Previous studies on the importance of the Sun and of black carbon

Previous authors have invoked a correlation between solar activity and climate variations, for various Holocene time-intervals, using diverse temperature proxies, e.g., Bond et al. (2001), Jiang et al. (2005, 2015), Usoskin et al. (2005), Perry (2007), Eichler et al. (2009), Stefani (2021), Harde (2022), Connolly et al. (2023), Scafetta (2023). The cited studies found temperature lag-times ranging from nil (undetected) to ~100 years. According to Perry (2007, p. 353), "A progression of increasing lag times can be spatially linked to the ocean conveyor belt, which may transport the solar signal over a time span of several decades. The lag times for any one region vary slightly and may be linked to the fluctuations in the velocity of the ocean conveyor belt". In another study, simulated Atlantic sea-level fluctuations for the last 1,500 years match solar variations, with a lag of ~125 years (van de Plassche et al., 2003). According to Jiang et al. (2005, p. 73), "The Little Ice Age has a well-documented correlation with the Spörer and Maunder solar minima, which may have been partly or even entirely linked to changes in solar irradiance (Lean, 2002)."

The contribution of black carbon (essentially soot) to atmospheric warming is highly uncertain (italics below added for emphasis). Bond et al. (2013, p. 5388) stated: "The best *estimate* of industrial-era climate forcing of black carbon ... is +1.1 W m^{-2} with 90% *uncertainty bounds* of +0.17 to +2.1 W m^{-2} [i.e., *very wide uncertainty range*; see also their table 1 and figure 35] ... We *estimate* that black carbon ... is the second most important human emission in terms of its climate forcing", after CO_2. Black carbon's warming effect was *estimated* to be 70% as strong as CO_2 (p. 5497). Intergovernmental Panel on Climate Change (IPCC) *estimates* are only ~35% and 20%, again with *large uncertainties* (IPCC, 2013a, figure SPM.5; IPCC, 2021a, figure SPM.2c). Ramanathan and Carmichael (2008, p. 221) said: "Black carbon in soot is the dominant absorber of visible solar radiation in the atmosphere. ... emissions of black carbon are the second strongest contribution to current global warming ... In the Himalayan region, solar heating from black carbon at high elevations may be just as important as carbon dioxide in the melting of snowpacks and glaciers." Airborne soot was likewise credited with major climatic importance by Allen et al. (2012), who attributed recent northward expansion of the tropical belt to laterally heterogeneous atmospheric warming by soot (and ozone). "Owing to increased combustion of fossil fuels and biofuels, black carbon aerosols ("An aerosol is a suspension of fine solid particles or liquid droplets in air or another gas" [Wikipedia, 2026a]) have increased substantially over much of the Northern Hemisphere during the last few decades, particularly over southeast Asia ... black carbon has increased monotonically since 1970 on average in the low and midlatitudes, including the band 30°-50° N ... where recent studies show that heating can displace the tropical edge" (Allen et al., 2012, p. 350-351) ... "Our analysis strongly suggests that recent Northern Hemisphere tropical expansion is driven mainly by black carbon and tropospheric ozone" (p. 352). In a follow-up article (co-authored by Allen), Zhao et al. (2020, p. 1) added: "Our results show that ... black carbon (BC) aerosol drives tropical expansion ... BC, especially from Asia, is more efficient ... than greenhouse gases in driving tropical expansion ... Although a formal attribution is difficult, scaling the normalized expansion rates to the historical time period suggests that BC is the largest driver of the Northern Hemisphere tropical widening but with relatively large uncertainty. ... BC warms the troposphere, particularly in the NH midlatitudes where most emissions occur".

3. Materials and methods

This contribution is based solely on the analysis, interpretation and synthesis of published information. No new data are presented, only ideas and interpretations resulting from an unfunded (hence impartial) exhaustive survey of the literature in diverse relevant fields, including geology, archaeology, climatology, paleoclimatology, meteorology, oceanography, astrophysics, and polar glaciology. The study has lasted eleven years so far (since 2015), leading to this article on soot and to three other papers on sea level (Higgs, 2026a, b, c). Microsoft (2022) Excel was used for plotting graphs (Figures 1 to 12) from published raw data (except a few charts obtained directly from the NASA [2025] website) and for calculating Pearson correlation coefficients.

4. Analysis and results

4.1 Global Temperature Largely Solar-Controlled Prior to 1940

Published graphs of solar-magnetic output (Wu et al., 2018) and global near-surface air temperature (Marcott et al., 2013), both based on proxies (largely geological) spanning the last 9,000 years (Early to Late Holocene interglacial period), are visually alike, showing similar overall form and several cross-matching multi-century trends (rising, falling; Figure 1). However, the temperature graph (Figure 1B) is heavily smoothed, due to averaging of 73 globally distributed datasets

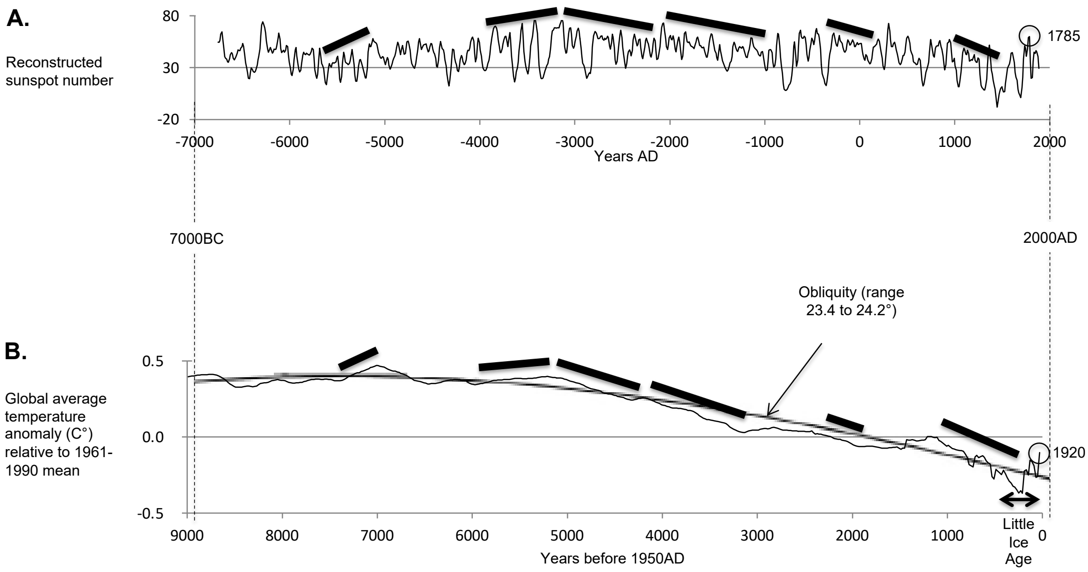

Figure 1: Visual correlation for the last 9,000 years between: (A) reconstructed sunspot number, a solar-magnetic-output proxy, based on ice-core ^{10}Be, 10-year time-steps, data of Wu et al. (2018); and (B) global average near-surface temperature anomaly relative to 1961-90 mean, based on multiple proxies, sampling resolution 20-500 years, 20-year time-steps, data of Marcott et al. (2013). In A and B, multi-century trends (rising, falling; black bars) match quite well. The overall shape of the two graphs is even more similar after tilting the temperature graph leftward to compensate for long-term cooling by Earth's declining axial obliquity (curved grey line, from Cionco et al. [2020]). Marcott's final temperature value, for 1940, 0.7C° warmer than 1920, is omitted here, as he doubted its accuracy (see also Vinos [2017]).

(diverse palaeotemperature proxies) and 1,000 Monte Carlo runs (Marcott et al., 2013). This smoothing suppresses short-term variability, rendering the graph less spiky (but note unpublished spikier reprocessed version of Vinos [2017]), hampering correlation (Figure 1). This disadvantage is overcome here (Figure 2) by substituting a Greenland temperature graph (Vinther et al., 2009), one of the 73 datasets incorporated in the Marcott et al. (2013) global compilation. The Greenland graph has the same general shape as the global graph (Figure 1B versus 2B; i.e., the Greenland dataset is a reasonable world-proxy), but is much spikier because the graph is the average of just two ice-core-isotope profiles, which are nearly identical, i.e., smoothing is minimal. Figure 2 reveals a relatively good qualitative correlation between solar output and Greenland temperature, with numerous prominent spikes (peaks, troughs) and multi-century trends that can be visually cross-matched with reasonable confidence. Spikes in temperature appear to lag by a variable amount, ~100 to 225 years, behind corresponding solar spikes (Figure 2). This wide range of lag-times possibly reflects: (a) ocean conveyor-belt circulation (Rahmstorf, 2006) changes in velocity (Section 2); and/or (b) dating errors (counting of ice-core laminae), which inevitably increase with age. The longest lag (225 years) is between the exceptionally long solar grand-minimum of ~ 6505-6365 BC (Inceoglu et al., 2015) and the globally cold "8.2-kiloyear event" that spanned ~ 6250-6130 BC in Greenland (Figure 2B and cited dataset), popularly attributed instead to hypothetical sudden emptying of an ice-dammed lake (Wikipedia, 2026b). Near the other (young) end of the graphs, the Little Ice Age signature-cluster of three cold spikes is offset ~150 years from a trio of solar minima (Figure 2; note that the middle spike of each triplet is the lowest value of the entire 9,000 years).

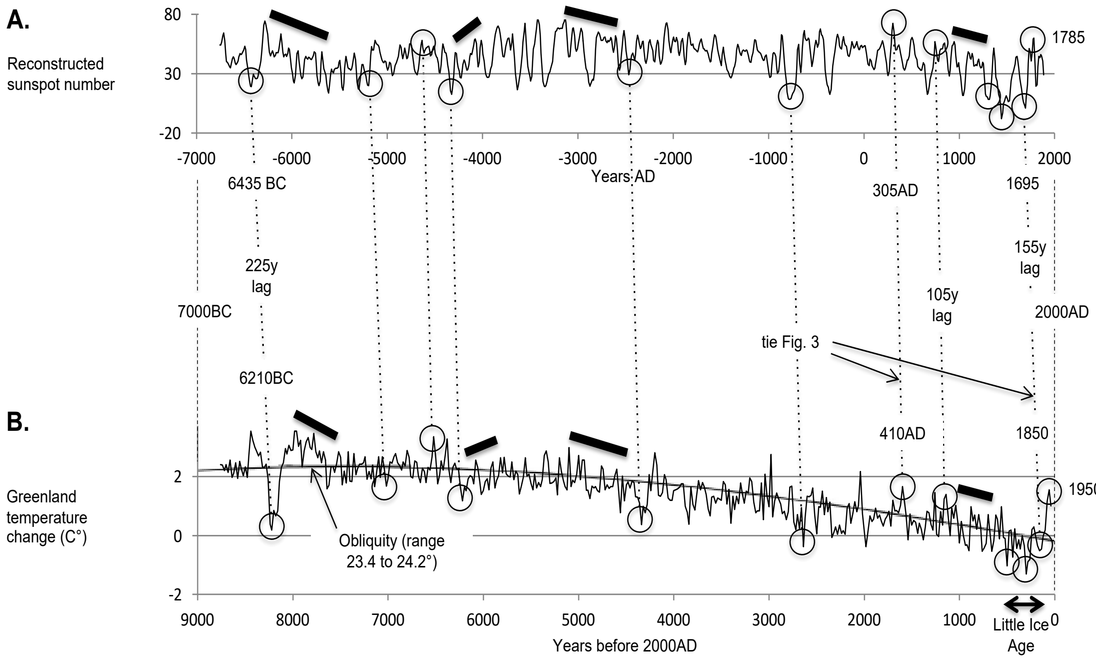

Figure 2. Visual correlation for the last 9,000 years between: (A) reconstructed sunspot number, a solar-magnetic-output proxy (same data-source as Figure 1A); and (B) Greenland near-surface air temperature change based on proxy ice-core ^{18}O (averaged Agassiz and Renland ice cores), sample resolution 20 years, data of Vinther et al. (2009). Several prominent peaks and troughs (circled) and multi-century trends (black bars) match quite well. As in Figure 1, the similarity in overall shape of the graphs is clearer after tilting the temperature graph leftward (curved grey line from Cionco et al. [2020]). Slant of dashed correlation-lines indicates a lag of 100-225 years between solar changes and corresponding temperature changes.

The time-lag is possibly due to ocean thermal inertia (i.e., the ocean's vastness, high specific heat and slow mixing render it slow to reach [transient] equilibrium), in agreement with Wigley (2005, p. 1766) who, summarising the results of his own and others' modelling, said: "Oceanic thermal inertia causes climate change to lag behind any changes in external forcing ... many decades". Supporting this evidence that solar-driven temperature fluctuations originate in the ocean rather than on land, Humlum et al. (2013) showed that changes in sea-surface temperature (SST; generally a good surrogate for near-surface marine air temperature [Cayan, 1980; Rubino et al., 2020, their figure 4]) precede changes in land-surface-air temperature (LSAT), by ~2 months, i.e., warming (or cooling) begins at the ocean surface, then migrates onto land. This migration self-evidently can only occur in regions where the ocean-surface is warmer than the adjoining land (cf. Wikipedia, 2026c). Noteworthy in this regard: (a) due to the ocean's large thermal capacity, the rate and amount of temperature change during any warming (or cooling) event are higher for land than for ocean (Humlum et al., 2013, their figure 5); and (b) *globally averaged* LSAT exceeds SST and the difference is growing with time (Section 4.2). Supporting the confirmation by Humlum et al. (2013) that the ocean warms the atmosphere, not vice versa, the annual average SST in most of the northern Pacific and northern Atlantic is slightly (0-1C°) warmer than the air immediately above (Cayan, 1980, his figure 3a). These observations contradict the reverse assumption, by many climate scientists, that temperature changes originate in the atmosphere and are transmitted to the ocean, e.g., "the ocean soaks up heat trapped in the atmosphere by carbon dioxide and other greenhouse gases" (WHOI, 2025).

The fair qualitative correspondence between the temperature- and (time-lagged) solar graphs (Figure 2) supports Svensmark's (2007) theory that increased solar-magnetic output deflects more galactic cosmic rays, reducing cloud cover, allowing increased warming by the Sun because "Cloud tops have a high albedo and exert their cooling effect by scattering back into the cosmos much of the sunlight that could otherwise warm the surface" (Svensmark, 2007, p. 1.20). Early on, Svensmark and Friis-Christensen (1997) and Svensmark (1998) could not distinguish which cloud level (low, medium, high) was most affected. However, by 2000, it was evident that low clouds (i.e., those below ~3 km) are much more affected than the others (Marsh and Svensmark, 2000; Pallé and Butler, 2000). According to Pallé and Butler (2000, p. 4.22), "our results imply that, possibly excluding the last decade or so when an accentuated rise in global temperatures is widely accepted to have occurred as a result of the enhanced greenhouse effect, most of the global warming of the 20th century can be quantitatively explained by the combined direct (irradiance) and indirect (cosmic-ray induced low cloud) effects of solar activity." It is important to note that Marsh and Svensmark (2000), Pallé and Butler (2000) and Svensmark (2007) all used the same 1983-1994 cloud data-set, which begins only 2 years before the 1985-onward divergence of land- and ocean warming, attributed here to airborne soot (Section 5.1).

Rejecting Svensmark's theory, the IPCC rather subjectively stated: "Although some studies found statistically significant correlations between the cosmic ray flux and cloudiness at the regional scale ... these correlations were generally weak, cloud changes were small" (IPCC, 2013b, p. 613). A companion IPCC chapter added: "The lack of trend in cosmic ray intensity over the 1960–2005 period (McCracken and Beer, 2007) provides another argument against the hypothesis of a major contribution of cosmic ray variations to the observed warming over that period" (IPCC, 2013c, p. 886). However, this statement unfortunately neglects the oceanic time-lag discussed above.

Having thus dismissed Svensmark, the IPCC (2014, 2021a) estimated that the Sun's effect on climate change is very small, via fluctuations in the *total solar irradiance* (TSI), which are likewise very small, as opposed to the *magnetic-flux* variations invoked by Svensmark, which occur in lockstep with TSI but are much larger, e.g., see Benevolenskaya and Kostuchenko (2013, their figure 1). For example, the solar-magnetic flux *doubled* from 1901 to 1992 (Lockwood et al., 1999; note, in their figure 3, peak flux in 1992, corresponding to the 1992 cosmic-ray strong minimum [Oulu, 2025]), arguably to its highest level in >9,000 years (Solanki et al., 2004).

Non-matching spikes are also numerous (Figure 2). Temperature spikes with no obvious solar counterpart include: cold spikes, some possibly attributable to terrestrial volcanic mega-eruptions (cf. Sigl et al., 2015; Büntgen et al., 2016); and warm spikes, perhaps due to surges in submarine volcanism (i.e., lava eruptions and/or hydrothermal venting; cf. "plate climatology" [Kamis and Kamis, 2016]), a hidden, unmeasurable, potentially major contributor to climate change. On the other hand, the converse situation, examples of solar spikes lacking temperature expression, might reflect submarine-heat surges or lulls counteracting the solar influence. The many non-matching solar and temperature spikes result in a relatively low, though positive, correlation coefficient of 0.30 for the last 2,000 years of Figure 1 (calculated using the data-sources cited in the caption and equalising the data-spacing to 20 years by stripping every second value from the solar dataset). This calculation neglects the temperature lag (see above), whose non-constancy (variability) prevents the determination of a more appropriate (time-lagged) correlation coefficient.

Spectral analysis provides further support for the Sun's role in climate change. Analysing a 1-2000AD global temperature-proxy curve compiled from published studies, Lüdecke and Weiss (2017) discovered a strong ~190-year cycle, matching the DeVries/Suess solar cycle. More persuasively, a spectral analysis of the 1850-2017 sunspot series and the Hadley-CRU global-average temperature data-set (Section 4.2) found temperature cycles "that can reasonably be assigned to solar variability for most and even possibly all of them" (Le Mouël et al., 2020, p. 24).

Focusing on the last two millennia (Figures 3 and 4), the same solar graph (Wu et al., 2018) closely tracks the authoritative PAGES2k (2019) global multi-proxy temperature reconstruction. Cross-matched trends and spikes again reveal a variable temperature delay (~130-165 years, Figure 3), e.g., the Little Ice Age (~1440-1920AD) corresponds to the triple Wolf-Spörer-Maunder solar-minima cluster (~1270-1760).

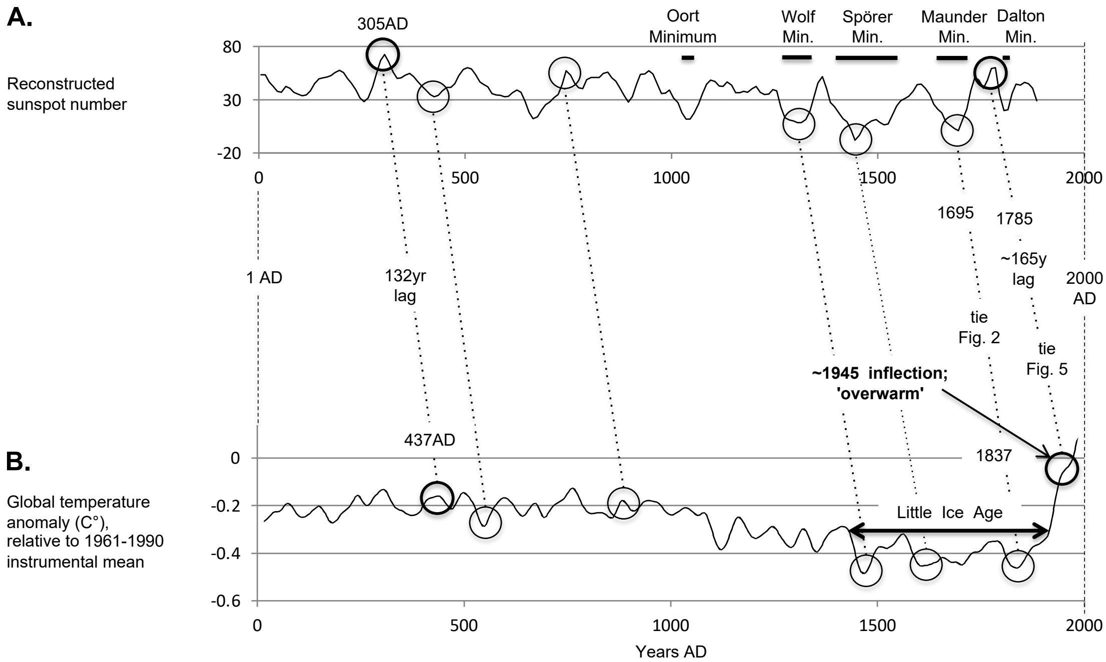

*Figure 3. Visual correlation, for the last 2,000 years, between: (A) reconstructed sunspot number, a solar-magnetic-output proxy (same data-source as Figure 1A); and (B) global mean temperature, 1-year time-steps, 31-year smoothing, based on multiple proxies (tree rings, etc.), data of PAGES2k (2019; median of all their reconstruction methods). Five solar minima from Steinhilber and Beer (2011). Several prominent peaks and troughs (circled) correspond well; slant of correlation lines indicates ~150-year lag, attributable to ocean thermal inertia (see text). The four **bold** circles demonstrate 1945AD disproportionate warmth, i.e., 437AD was cooler than 1945, despite higher corresponding solar activity (305 AD) and higher obliquity (cf. Figure 1B curved black line).*

4.2 Solar Control of Global Temperature Increasingly Outweighed After 1940

Remarkably, graph-to-graph proportionality of peaks and troughs becomes disrupted in the 20th Century. Post-1940 global warmth is disproportionately high, to an extent that increases with time, relative to the corresponding level of solar output (visually calibrated to previous episodes; Figures 3, 4, 5). To elucidate the excess warmth, Figure 5 compares the *thermometer-measured* 1880-2024 global average annual near-surface air temperature of NASA (2025) (NB this dataset is almost identical to that of Hadley-CRU [Met Office, 2025]) versus annually resolved solar modulation, a measure of solar-magnetic shielding of Earth from cosmic rays (Brehm et al., 2021). In Figure 5, global temperatures before 1940 closely mimic solar output, after subtracting a ~160-year lag, e.g., the three main temperature spikes (1898 warm, 1909 cold, 1942 warm) match three solar spikes (1740 high, 1751 low, 1784 high), moreover with constant proportionality. In contrast, post-1940 warming is excessive, manifested in three ways:

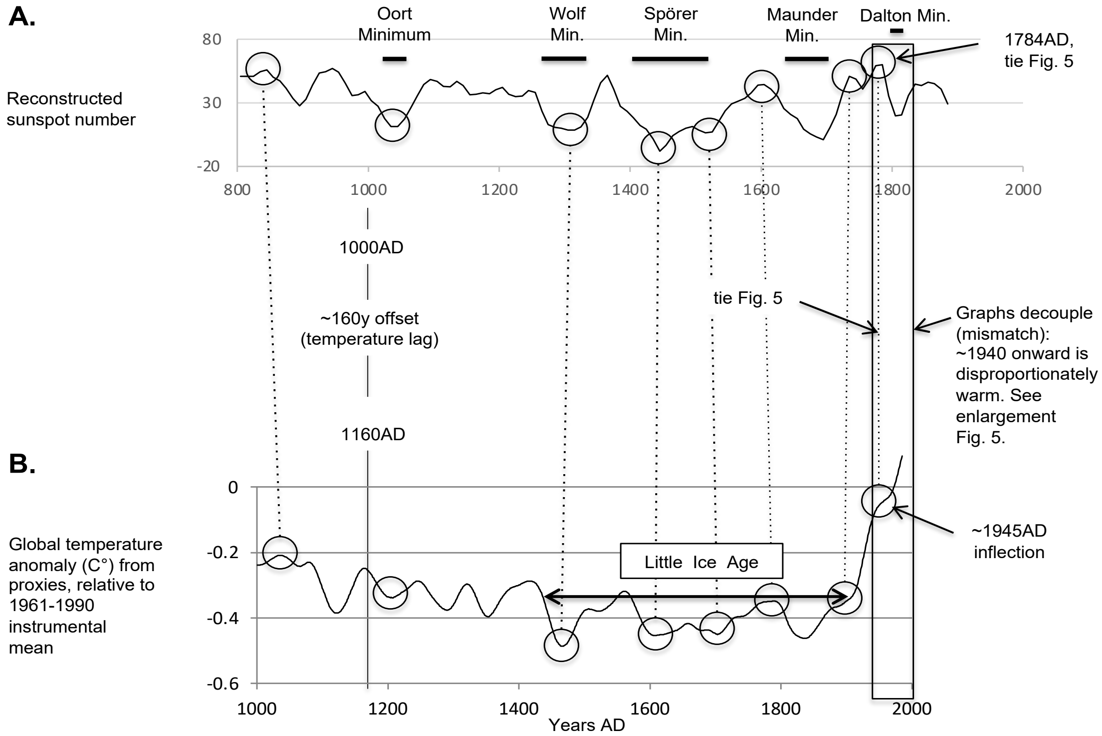

Figure 4. Time-shifted visual correlation, for the last 1,000 years, between: (A) reconstructed sunspot number, a solar-magnetic-output proxy; and (B) global mean temperature from proxies. Same data-sources as Figure 3. The best visual alignment of spikes (peaks, troughs; circled) is obtained by applying ~160-year temperature lag.

1. 1942-56 cooling was overly weak for its corresponding solar decline (~160 years earlier), by comparison with previous similar declines (Figure 5, compare Box I and dashed box);
2. therefore, the ensuing 1957-1975 interval of near-constant temperature (Box II), equating to the Sun's ~1800-1820 Dalton Minimum, was warmer than earlier times of *greater* corresponding solar strength (compare Box II and dashed box; see also Figure 3);
3. 1994 to 2024 overall strong warming (despite the controversial 'Global Warming Hiatus', said to span 1998-2013 [Wikipedia, 2026d] but in fact only 2003-2011 [Figure 5B smoothed curve; Section 5.1]), anomalously equates to 1835-1865 net solar *decline* (comprising a dip and a rise; Box III). This 1994-2024 warming is verified by: satellite (Spencer, 2025); balloon-radiosonde (Christy et al., 2018); and Arctic sea-ice retreat (Stroeve et al., 2007; Mahoney et al., 2008; Connolly et al., 2017; Bliss et al., 2025). The disproportionate warming since 1994 relative to the corresponding lagged solar output applies to the world as a whole (Figure 5) and to land and ocean individually (Figure 6).

Tellingly, 1940 to 2024 warming amounted to a substantial 1.1C°, and SST 0.8C°, despite a net *decline* in corresponding overall solar output (Figures 5 and 6). These observations point to dominance of a non-solar warming agent.

5. Discussion

5.1. Human Cause of Post-1940 Excess Warmth

Incriminating humankind, the 1940 onset of excess warmth (Section 4.2) coincides with World War Two and its huge demand for coal (for producing electricity, steel and cement) and oil (propulsion of aircraft, ships, vehicles). For example, the growth-rate of world annual oil consumption doubled in 1940 (OWD, 2025a). Post-war reconstruction, industrial expansion, and massive population growth (1950, 2.5 billion; 2020, 8 billion) have further increased demand for oil and coal.

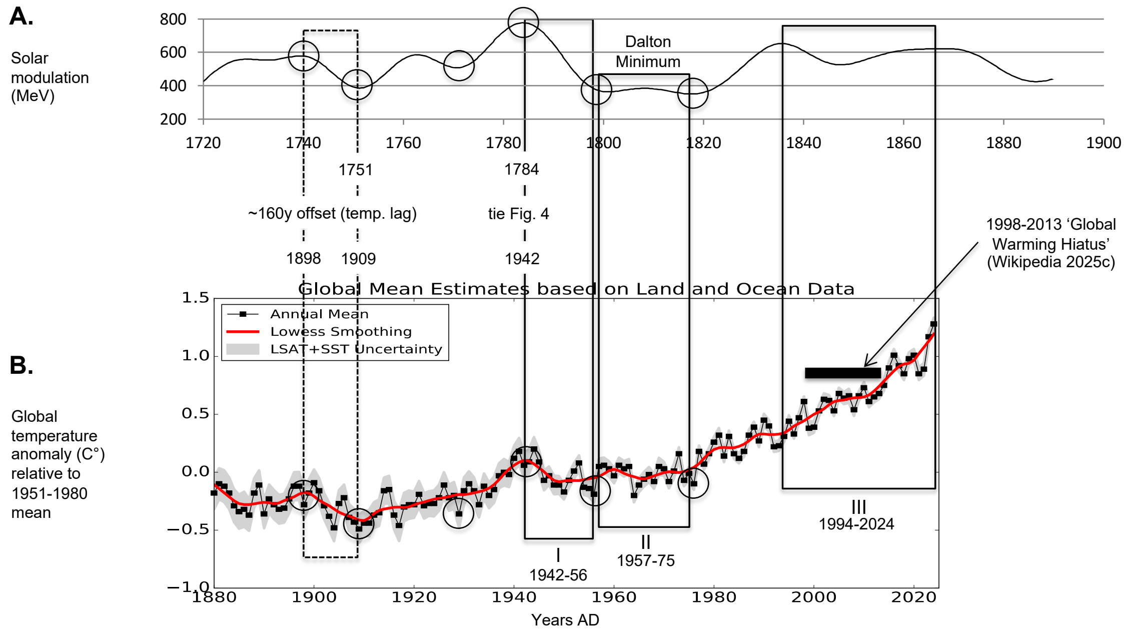

Figure 5. Visual correlation between: (A) 1720-1890 solar-magnetic-output proxy, 20-year-smoothed annual tree-ring C14 data of Brehm et al. (2021); and (B) 1880-2024 annual global average temperature anomaly, i.e., averaged land-surface-air temperature (LSAT) and sea-surface temperature (SST) (NASA, 2025). Five-year-smoothed curve in red. Graphs are offset ~160 years in accordance with Figures 2, 3 and 4. Black boxes I-III highlight three manifestations of post-1940 excess temperature (relative to corresponding solar output); these and the dashed box are described in the text.

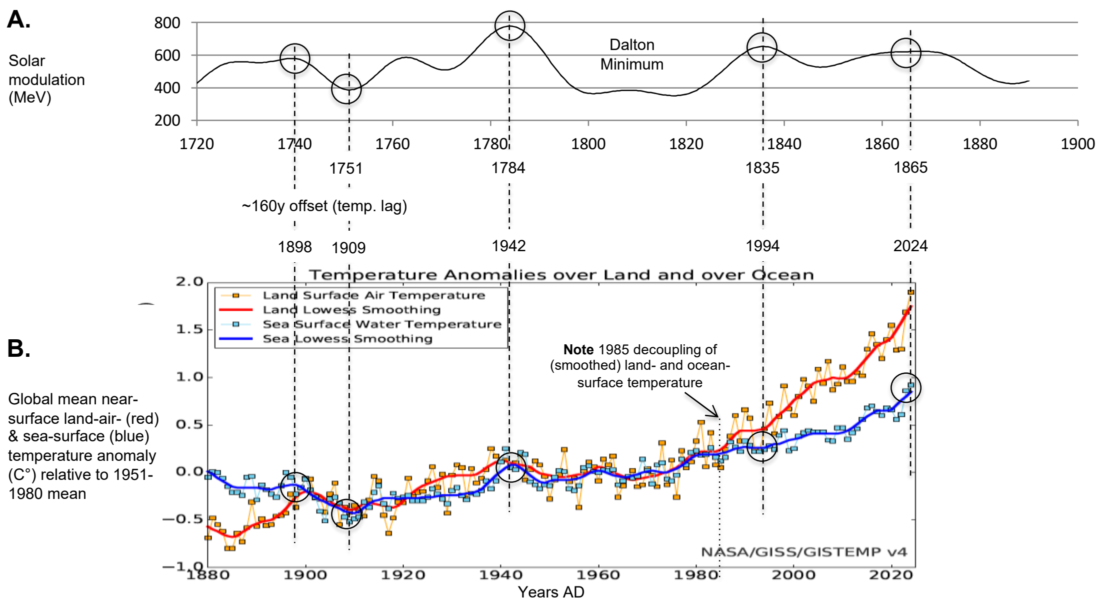

Figure 6. Visual correlation between: (A) 1720-1890 solar-magnetic-output proxy, 20-year-smoothed annual tree-ring C14 data of Brehm et al. (2021; and (B) 1880-2024 average annual world land-surface air temperature (LSAT, red) and sea-surface temperature (SST, blue) (NASA, 2025). In B, the thin zigzag lines connect annual values; thicker wiggly red and blue lines are 5-year-smoothed values. Graphs are offset ~160 years in accordance with Figures 2, 3 and 4. The ten circles illustrate that, until 1940, SST was proportional to the corresponding (time-lagged) solar output, but was disproportionally high thereafter.

Recognition of human culpability would implicate one or both of the generally agreed main agents of anthropogenic global warming, namely: (a) rising carbon dioxide (CO_2) emissions (from combustion of oil, gas, coal and wood), the overriding factor according to the IPCC (2014, 2021a, b) and to the great majority of climate scientists; and (b) airborne particulate black-carbon aerosol (Bond et al., 2013; Higgs, 2022, 2023). Black carbon is produced mainly by combustion of diesel-oil, coal and wood (Bond et al., 2013, table 8). In their landmark review of soot's estimated climatic effects, Bond et al. (2013, p. 5381) considered black carbon to be "the second most important human emission in terms of its climate forcing in the present-day atmosphere; only carbon dioxide is estimated to have a greater forcing." Black carbon is doubly problematic, causing warming in two ways: (1) *airborne* soot warms the atmosphere; and (2) *deposited* soot reduces snow- and ice albedo. Both airborne and settled soot are constantly replenished by combustion of wood (natural wildfires and human fires for cooking, heating) and of fossil fuels. In a Greenland ice core, the decadal mean concentration of black carbon is no higher for 1970-2010 than for 1750-1880 (Goto-Azuma et al., 2024, their figure 4), suggesting that by far the main contribution since 1970 is from boreal forest fires. Higher values in the intervening period reflect industrial contributions, mostly from North America (Goto-Azuma et al., 2024). Soot settling on ice and snow is estimated to have only ~20% of the warming effect of airborne soot (Bond et al., 2013, table 1 and figure 35).

Further inculpating humans, *and suggesting that airborne soot has a greater warming effect than CO_2*, published meteorological evidence indicates that warming is both laterally (geographically) and vertically inhomogeneous. This evidence includes:

1. lack of Antarctic warming since 1980 or earlier (Figure 7) (Doran et al., 2002), i.e., so-called global warming is not truly global;
2. since 1985, faster near-surface warming over land than over the oceans, in contrast to pre-1985 near-lockstep warming and cooling (Figure 8C);
3. faster warming since 1985 in the northern hemisphere (NH; land-ocean average) versus southern (SH) (Figure 9C);
4. faster warming of the lower atmosphere (~0-9 km average, satellite-measured [UAH 2025]) above land than over the ocean (Figure 8A, B) (Klotzbach et al., 2009, table 1);
5. likewise the NH versus SH (Figure 9A, B);
6. near-surface warming faster than lower-atmosphere warming, both above land (Figure 8A, C) and over the NH (Figure 9A, C); and
7. near-surface warming at approximately the same rate as the lower atmosphere over oceans (Figure 8B, C; Klotzbach et al., 2009, table 1) and over the SH (Figure 9B, C). This observation verifies that surface (thermometer) and satellite measurements are well calibrated, as does their dual determination of non-warming in Antarctica (Figure 7).

The strong lateral and vertical warming gradients (observations 1 to 7 above) implicate a non-CO_2 warming agent because CO_2, being gaseous (molecular), disperses efficiently, producing a near-homogenous atmospheric concentration, such that even heavily industrial regions barely (<0.5%) exceed the global average (Zhang et al., 2019, their figure 1). If CO_2 were really Earth's "temperature control knob" (Lacis et al., 2010), modern warming (1940 onward) would be much more uniform spatially. Instead, the gradients incriminate airborne soot because, being particulate, it disperses much less efficiently, remaining concentrated near its mainly *land-based*, *northern-hemisphere* sources, e.g., see figure 1 of Wang et al. (2014). (Antarctica soot emissions are minimal, but see Cordero et al. [2022].) A different model to explain preferential warming over land (observation 2 above) was proposed by Sutton et al. (2007), who suggested that increasing CO_2 produces an essentially uniform increase in radiative forcing over land and ocean, but lesser warming of the latter due to its latent heat of evaporation. However, this hypothesis does not explain why land and ocean warmed in lockstep prior to 1985.

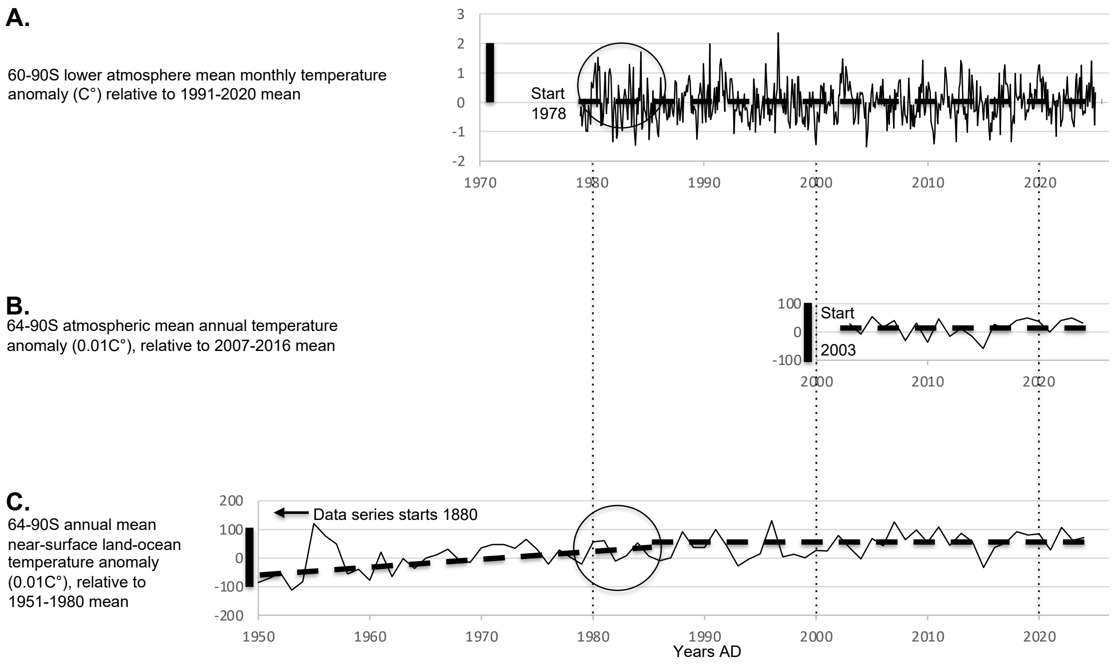

Figure 7. Three graphs (satellite and surface measurements) showing lack of warming in the Antarctic latitudinal belt (64-90°S) since 1980: (A) Latitude 60-90°S TIROS-N satellite-measured lower atmospheric monthly average temperature anomaly, 1978-2024, data of UAH (2025); (B) 64-90°S AIRS satellite-measured mean annual atmospheric temperature anomaly, 2003-2024, data of NASA (2025); and (C) 64-90°S mean annual near-surface-land-air- and sea-surface temperature anomaly, 1950-2024, data of NASA (2025), with "homogeneity adjustment". Vertical scales are equal (heavy bars indicate 1C°). Dashed bars added here are eyeballed average trends. Note lack of any obvious warming (or cooling) trend in any of the graphs since 1980, except graph C, which shows apparent overall warming from 1950 until ~1985, but the temperature-anomaly values in the circle are relatively lower (down-shifted in the graph) than in A, suggesting that the "homogeneity adjustment" is inappropriate.

Excess *ocean* warming since 1994 relative to the corresponding solar output (Figure 6) is here tentatively attributed to airborne soot (albeit much less concentrated than over land) causing a reduction in low-cloud cover (Ackerman et al., 2000; Lohmann et al., 2020), outweighing the predicted (Svensmark) *increase* in cloudiness (expected of the net decline in corresponding solar output; Figure 5A). Indeed, from satellite data, Goessling et al. (2025) demonstrated a decline in global low-cloud cover from 2015-2023 (their figure 2a and f), and suggested that the corresponding loss of cloud reflectivity (albedo) contributed to the global warming recorded in that time interval (cf. Figure 5). Discussing the cause of reduced cloudiness, Goessling et al. (2025) stated that "aerosols ... can influence ... cloud amount" (p. 70) ... [but] ... "isolating the contribution of indirect aerosol effects to cloud amount ... remains challenging" (p. 71). Only two specific aerosols were considered, namely reduced Sahara-derived dust and possibly reduced sulphur emissions from shipping. The possibility of reduced cloud cover due to increased airborne soot was not mentioned. Two lines of evidence tend to incriminate soot in this case. Firstly, the decline in low-cloud cover occurred mostly in latitudes 10°S to 45°N (see figure 3c of Goessling et al. [2025], showing low-cloud cover in those latitudes in 2023 was 2-4% below the 2001-2022 mean), which happens to incorporate the entire 10°S to 45°N southeast Asian region where a large increase in tropospheric mean soot concentration occurred from 1970-2009, especially in China (Allen et al., 2012, figure 1a). Secondly, the 2015 onset of cloud decline (Goessling et al., 2025) began soon (13 years) after the 2002 surge in the growth-rate of world coal consumption (see below), whereby annual consumption rose a remarkable 55% from 2002 to 2014 (cf. Figure 10B), with China accounting for 84% of that increase (OWD, 2025a).

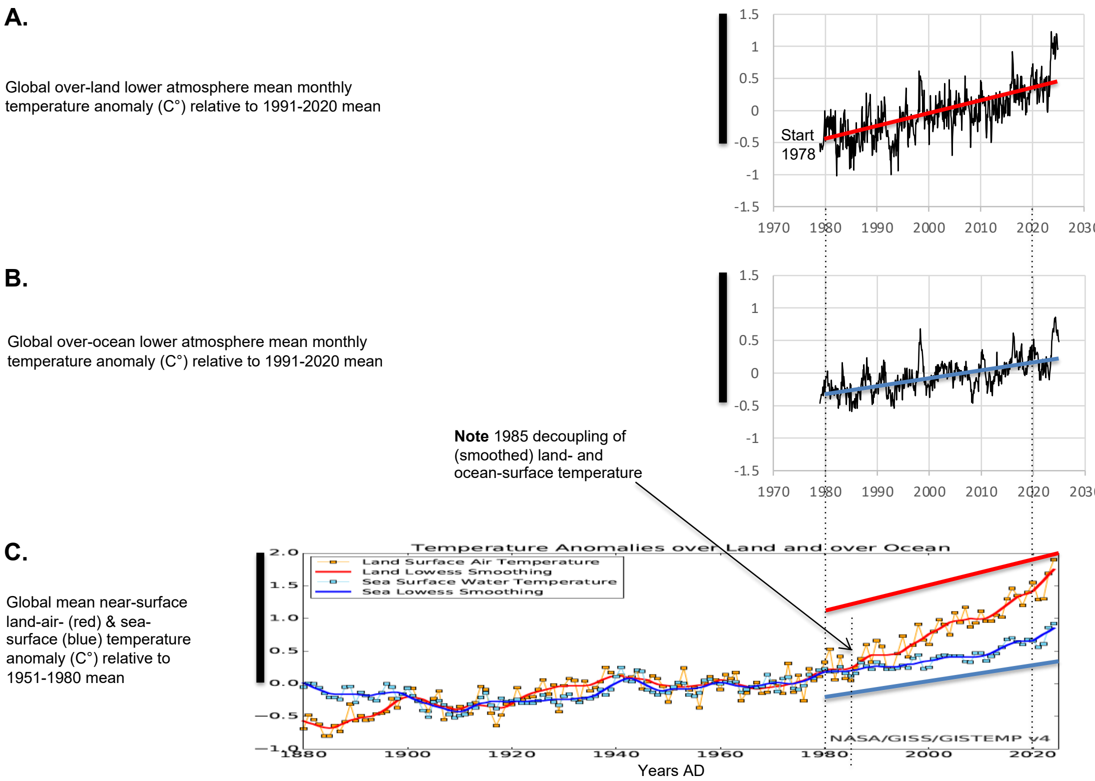

Figure 8. Comparison since 1978 of: (A) satellite-measured global lower atmospheric monthly average temperature anomaly over land and (B) ocean (same UAH [2025] data source as Figure 7A); and (C) near-surface-air temperature anomaly over land and ocean (same chart as Figure 6B). Vertical scales in A, B and C are equal (black bars = 2C°; for less-squeezed version of C, see Figure 6B). Eyeballed red and blue trend-lines in A and B are transferred onto C for comparison of gradients (decadal average warming rates). Atmospheric warming is greater/faster over land (A) than over ocean (B). Note, over land, less warming at altitude (A) than at surface (C). In contrast, there is no discernible differential warming over ocean (B versus C), nor over Antarctica (Figure 7), nor the Southern Hemisphere (SH; Figure 9), confirming reliable calibration of satellite- and surface instruments, and consistent with much less soot over oceans and over SH than over land and NH (see text). Note, in C, terrestrial near-surface air has warmed faster than sea-surface since 1985 (steeper gradient of wiggly red line compared to wiggly blue line), having been in lockstep before.

Anthropogenic soot is produced primarily by the burning of three commodities (Bond et al., 2013, table 8): oil-derived fuels (in cars, buses, trucks, ships, aircraft), especially diesel; coal (mainly in powerplants, steelworks and cementworks); and wood (home-cooking by billions of people lacking electricity). The suspended soot particles are black, hence solar radiation warms them (Jacobson, 2001), in turn warming the surrounding air. Above intensely industrialized regions (e.g., China, Europe, eastern USA), average atmospheric soot concentration is approximately 1000% (i.e., 10 times) greater than over adjacent oceans (NASA, 2011), in stark contrast to CO_2's trivial lateral variations, e.g., 1985-2024 seasonally averaged CO_2 concentration rose from 345 to 425 parts per million (ppm) in Hawaii (SIO, 2025) and 342 to 422 ppm in Tasmania (CSIRO, 2025). Soot also has a strong *vertical* concentration gradient, explaining the slower warming at altitude (observation 6, above), e.g., the global average soot concentration is approximately 100 times greater at 1 km than at 10 km (Cooke et al., 1999, fig. 10), sharply contrasting with CO_2, whose concentration above Tokyo is only 4% less at 4 km than at 1 km (Shibata et al., 2018, fig. 6).

Further evidence of airborne-soot's culpability for most of the 1940-onward excess warming comes from plotting post-1860 annual oil- and coal production (consumption) alongside land- and ocean warming (Figure 10). A good visual match among the graphs is evident. Applying a 10-year temperature-lag provides a logical inter-relation of graph details, as follows:

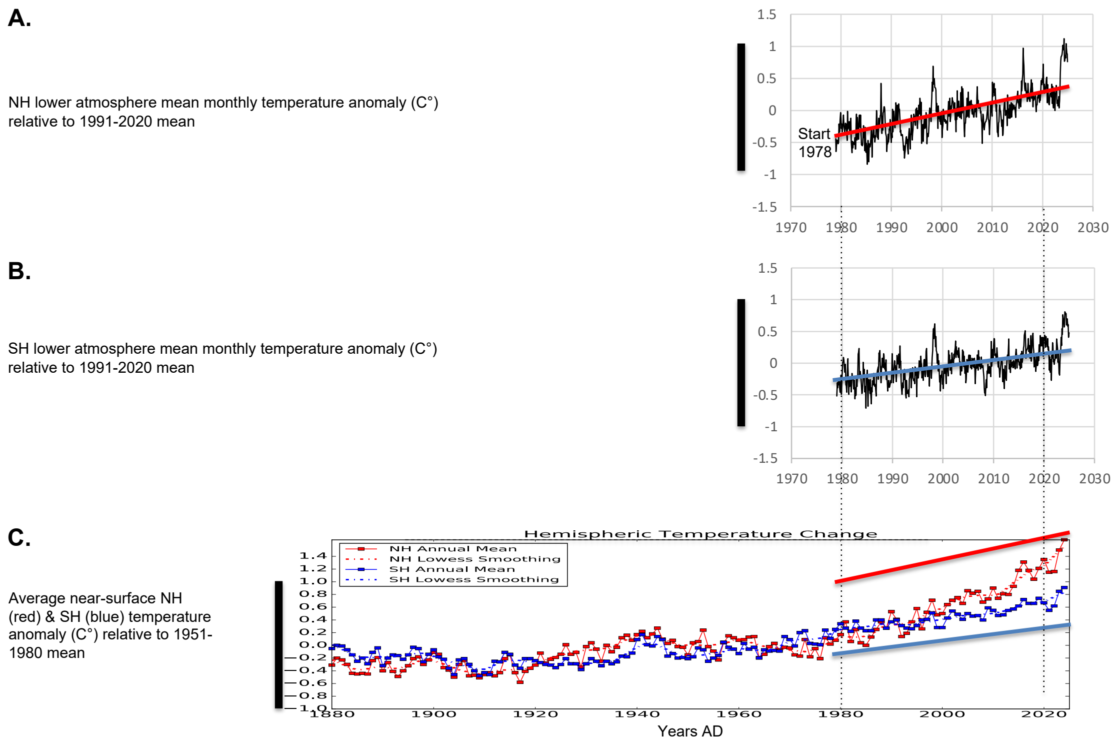

Figure 9. Comparison since 1978 of: (A) satellite-measured global lower atmospheric monthly average temperature anomaly over Northern Hemisphere (NH); and (B) Southern Hemisphere (SH) (same UAH [2025] data source as Figure 7A); and (C) near-surface global temperature anomaly over NH (red) and SH (blue), from NASA (2025). In C, the thin zigzag lines connect the annual values; dash-dot wiggly red and blue lines are 5-year smoothed. Vertical scales in A, B and C are equal (black bars = 2C°; for less-squeezed version of C, see Figure 11C). Eyeballed trend-lines in A and B are transferred onto C for comparison. Atmospheric warming is greater over NH (A) than SH (B). Note, over NH, less warming at altitude (A) than at surface (C). In contrast, there is no such differential warming over SH (B versus C). Note, in C, NH has warmed faster than SH since 1985 (steeper gradient of wiggly red line compared to wiggly blue line), having been in lockstep before.

1. two abrupt jumps (1975 threefold; 2002 about tenfold) in the growth-rate rate of annual global coal consumption (Figure 10B) equate to two leaps (1985, 2012) in the rate of land-warming (Figure 10C; note lack of a 1985-onward *ocean*-warming surge explains the decoupling of the land- and ocean curves);
2. a 1988-1999 period of no coal growth (Figure 10B) essentially aligns with a 2003-2011 pause in global warming (Figure 10C; see Section 4.2, 'Global Warming Hiatus');
3. three other warming-pauses (Figure 10C black bars) align with times of zero- or negative growth of coal- and/or oil (Figure 10A and B black bars), although the second of these pauses can be ascribed to volcanism (see below).

Similar probable cause-and-effect relationships to those pointed out for Figure 10 are seen when the land- and ocean curves are replaced by the NH and SH curves (Figure 11).

The lengths of the four warming-pauses (4-8 years each) suggest they are unrelated to El Niño and La Niña events (typically only 1-2 years [Wikipedia, 2026e]). In two other kinds of internal variability in the climate system, the Atlantic Multi-Decadal Oscillation and the Pacific Decadal Oscillation, the *transitions* between the decades-long warm and cool phases have the right duration (years) but the wrong timing (e.g., graphs in Wikipedia, 2026f, g). The 1991 volcanic super-eruption of Mount Pinatubo caused cooler global temperatures from 1991 through 1993 (Soden et al., 2002), explaining the 1990-1994 warming pause shown by the *five-year-smoothed* temperature curve (Figure 10C). No other large eruption between 1950 and 2020 exceeded about one-tenth the magnitude (volume of erupted tephra) of Pinatubo (Wikipedia, 2026h, i); none has been shown to have caused cooling (i.e., "volcanic winter"; Wikipedia, 2026j). During the longest pause (2003-2011 'Global Warming Hiatus'), no eruption exceeded about one-hundredth the magnitude of Pinatubo (Wikipedia, 2026i). Climate scientists have struggled to explain this hiatus and some even denied its existence (Wikipedia, 2026d). Hansen et al. (2013) stated: "The 5-year mean global temperature has been flat for a decade, which we interpret as a combination of natural variability and a slowdown in the growth rate of the net climate forcing." In contrast, Drijfhout et al. (2014) attributed the hiatus to increased heat uptake across multiple ocean basins.

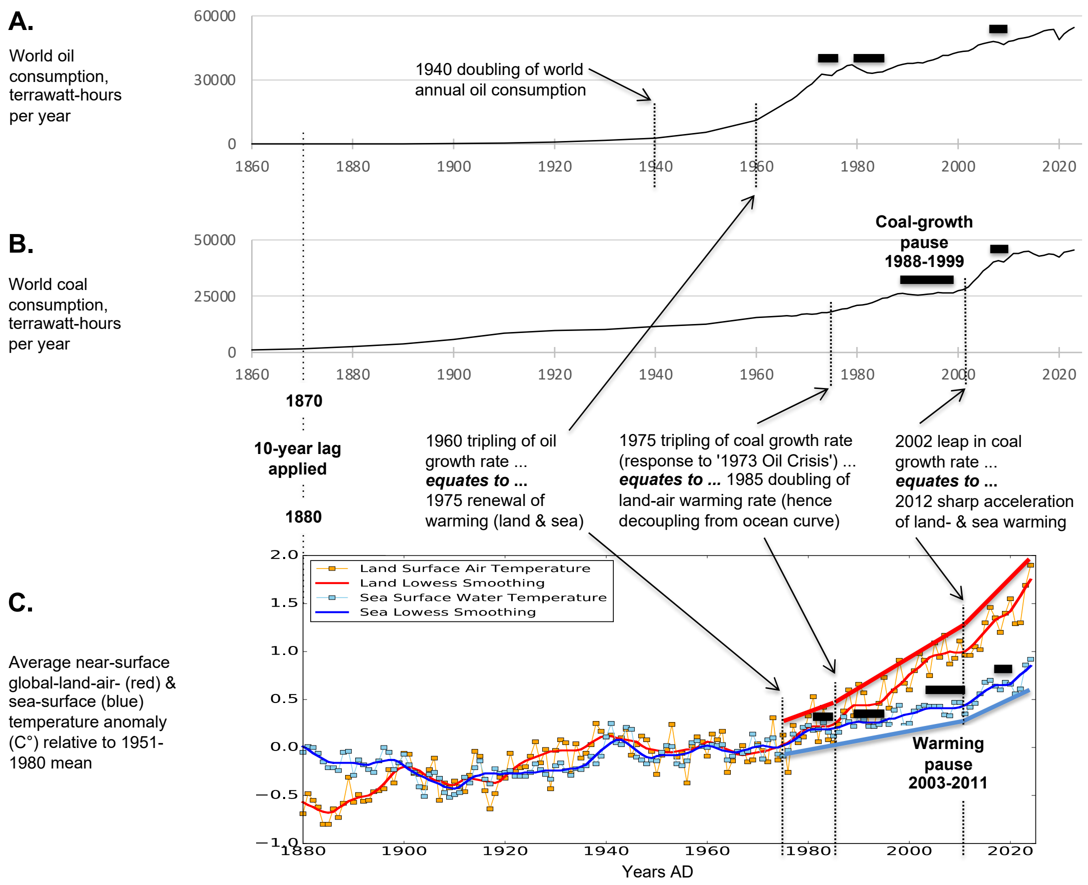

Figure 10. Comparison, from 1880 to 2024, of world (A) annual oil consumption, (B) annual coal consumption, and (C) average near-surface land-air- versus sea-surface temperature anomaly (same chart as Figures 6B and 8C). Data for A and B are from OWD (2025a); data-points are every tenth year until 1960 and annual from 1965 onward. Fair visual match among the three graphs is evident. Applying a 10-year temperature lag (by shifting A and B rightward) produces a logical inter-relation of the three graphs' details (see annotations and text). Heavy black bars indicate warming pauses (graph C, red and blue 5-year-smoothed curves) and intervals of zero or negative growth in oil- and coal consumption (graphs A and B).

Atmospheric CO_2's non-pausing, slightly accelerating rise (Figure 12A) since the 1958 start of systematic measurements cannot explain the warming pauses (Figure 12B). Instead, the stepped rise in global coal- and oil consumption mimics stairstep global warming (Figure 10). The contrast is not evident from the respective correlation coefficients, as both are very high and nearly the same: 0.95 for global temperature (Figure 5B) versus CO_2 (Figure 12A) for 1975 to 2021 (using average annual values, from data sources in the figure captions); and 0.92 for global temperature versus 10-year-lagged annual coal combustion (Figure 10B) for the same time interval. Nevertheless, simple visual inspection shows much greater resemblance between temperature and coal consumption (Figures 10, 11) than between temperature and CO_2 (Figure 12).

Contrary to the general consensus that airborne soot has less warming effect than CO_2, the data and interpretations presented above, including the geographic inequality of warming mentioned earlier, collectively suggest that soot is the main agent of anthropogenic warming and that CO_2 is largely or entirely innocent.

Besides the effect of airborne soot, some of the post-1940 excess (anthropogenic) warmth is possibly by so-called waste heat (thermal pollution by power stations, air conditioners, etc.). Waste heat is considered by some authors to be an important (Chen et al., 2014), or dominant (Bian, 2020), or overwhelming (Karamanev, 2021) source of warming.

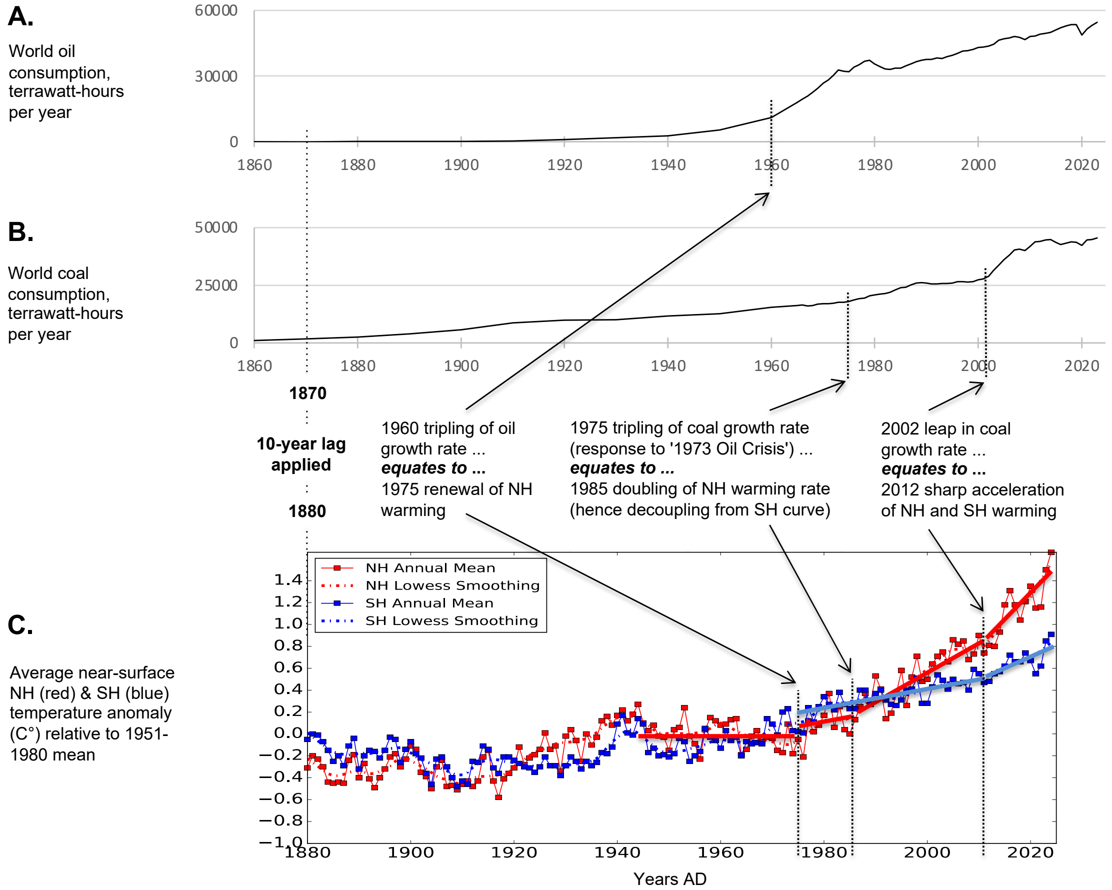

Figure 11. Comparison, from 1880 to 2024, of (A) world annual oil consumption, (B) world annual coal consumption, and (C) Northern Hemisphere (NH) versus Southern (SH) mean annual temperature anomaly. A and B are the same as in Figure 10. Graph C is the same as Figure 9C. A fair visual match among the three graphs is evident. Applying a 10-year temperature-lag (by shifting A and B rightward) produces a logical inter-relation of the three graphs' details (see annotations and text).

5.2. Reasons for Underestimation of Soot Effect and Overestimation of CO_2 Effect

Helping to explain previous underestimations of soot's warming effect, powerplants in the developing-world possibly emit far more soot than the Bond et al. (2013) review assumed. Coal is still the dominant fuel for world electricity generation (35% in 2023; OWD, 2025b). Bond et al. (2013) estimated global coal-fired-powerplant soot emissions to be relatively low (20 Gg/yr, their table 8), because "the high temperatures and well managed combustion promote burnout of any BC [black carbon] that is formed" (p. 5414); but their next sentence admitted "emission rates from power generation in developing countries are not well known" (p. 5414). Bond et al. (2013) then cited Cooke et al. (1999) as having estimated global soot emissions to be ~80 (sic) times higher (i.e., an increase of ~1600 Gg/yr; p. 5414), and they continued "there remains a persistent but informal perception ... that BC fractions of particulate matter in developing countries, especially in power plants and industrial installations, could be higher than that represented by existing measurements. Even if older, poorly operating power plants have high BC emission factors, there is no evidence that newly installed, modern power plants do" (p. 5414-15).

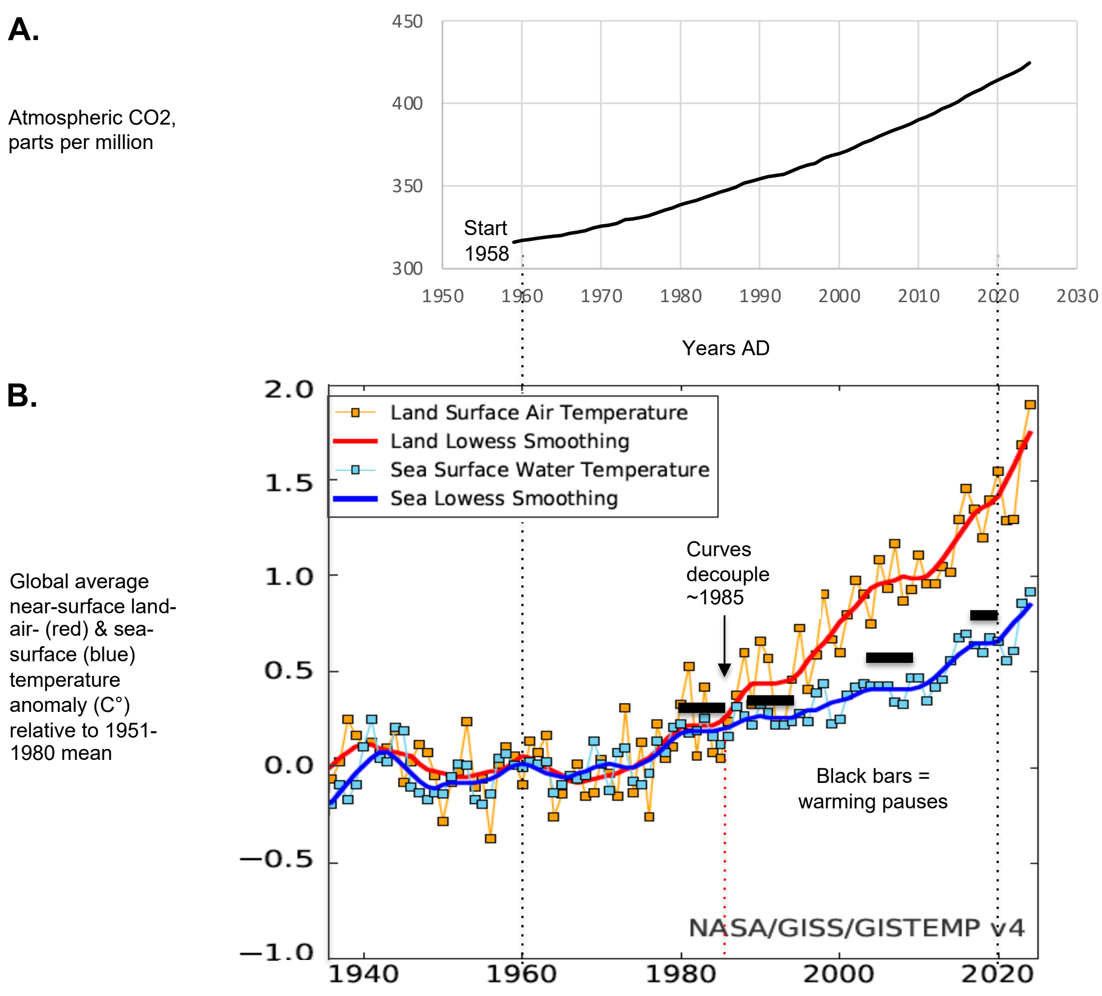

Figure 12. Comparison of (A) annual average atmospheric CO_2 concentration (data from NOAA, 2026) and (B) global annual average near-surface land-air- and sea-surface temperature anomaly (same chart as Figure 6B, 8C and 10C). In (A), CO_2's smooth (slightly accelerating) uninterrupted rise cannot explain, in (B), the decoupling (~1985) of land- and sea temperature curves, or their stepped nature (reflecting warming hiatuses).

Another possible reason for airborne soot having a greater impact on climate than previously supposed is underestimation of soot's effects on clouds (Section 5.1). Bond et al. (2013, figure 35) estimated the net (combined) effect of soot-related positive and negative cloud feedbacks to be positive, but with very large uncertainties.

The above evidence for CO_2 having little effect on temperature implies that its greenhouse effect, already reduced "well into the saturation regime" (van Wijngaarden and Happer, 2020, p. 18) such that " 'instantaneously doubling' CO_2 concentrations ... only decreases radiation to space by about 1% ... [whereas] ... To increase solar heating of the Earth by a few percent, low cloud cover only needs to decrease by a few percent" (van Wijngaarden and Happer, 2025, p. 1), is greatly offset (nullified?) by negative feedbacks excluded or underestimated in climate models. For example, cloud feedbacks are highly uncertain, as detailed by Stephens (2005), whose "critical review of the topic of cloud–climate feedbacks ... exposes some of the underlying reasons for the inherent lack of understanding of these feedbacks" (p. 237). The IPCC (2013a, p. 14) opined that "aerosols and their interactions with clouds have offset a substantial portion of global mean forcing from ... greenhouse gases. They ... contribute the largest uncertainty." Later the IPCC (2014, p. 44) stated: "The radiative forcing from aerosols, which includes cloud adjustments ... has two competing components: a dominant cooling effect from most aerosols and their cloud adjustments and a partially offsetting warming contribution from black carbon absorption of solar radiation.

There is high confidence that the global mean total aerosol radiative forcing has counteracted a substantial portion of radiative forcing from well mixed GHGs [greenhouse gases]. Aerosols continue to contribute the largest uncertainty to the total radiative forcing estimate." A review by Bellouin et al. (2020) found that the magnitude of forcing by aerosols was highly uncertain but that the net effect is probably negative. The most recent IPCC major report confessed that "clouds remain the largest contribution to overall uncertainty in climate feedbacks" but nevertheless concluded that "The net effect of changes in clouds in response to global warming is to amplify human-induced warming, that is, the net cloud feedback is positive (*high confidence*)" (IPCC, 2021b, p. 95; their italics).

One particular cloud-related feedback, certainly negative, is the increase of "Biogenic volatile organic compounds (BVOCs) ... potentially very important" (Kulmala et al., 2013, p. 498). An increase in BVOCs, due to faster forest growth resulting from both warming and increased CO_2 fertilization, raises the concentration of secondary organic aerosol and (thence) cloud concentration nuclei, causing increased cloudiness (Kulmala et al., 2013, 2014; Sporre et al., 2019). In this respect, "we find that the importance of BVOCs ... is greater than previously thought" (Gordon et al., 2017, p. 8739). Sporre et al. (2019, p. 4764) said: "Higher BVOC concentrations result in higher aerosol number and mass concentration, which cool the climate by inducing changes in cloud properties (Twomey, 1974; Albrecht, 1989) ... Higher cloud albedo and longer cloud lifetime lead to decreasing temperature, giving rise to a negative climate feedback."

According to the IPCC (2021c, p. 825), "BVOCs are emitted in large amounts by forests and ... in a warming planet ... are expected to increase but magnitude is unknown and will depend on future land-use change, in addition to climate (*limited evidence, medium agreement*)" (IPCC's italics). The "evaluation of global BVOC emissions is challenging because of poor measurement data coverage in many regions and the lack of year-round measurements. ... Most CMIP6 models use overly simplistic parametrizations and project an increase in global BVOC emissions in response to warming temperatures ... [but] ... do not fully account for the complex processes influencing emissions ... that are hard to constrain observationally" (p. 831). The "assessed central estimate of the climate-BVOC feedback ... suggests that climate-induced increases in SOA [secondary organic aerosols] from BVOCs will lead to a strong cooling effect that will *outweigh the warming from increased ozone and methane lifetime* [italics added here; no mention of potentially also outweighing CO_2's greenhouse warming], however the uncertainty is large" (p. 859). Given all of these uncertainties expressed by the IPCC, and the evidence presented above (and below) for CO_2's relative innocence, it seems likely that climate models favoured by the IPCC have greatly underestimated BVOC negative feedback.

More evidence that CO_2 is relatively benign comes from Murray and Heggie (2016), who found that 1965-2013 warming in the United Kingdom and Japan correlate better with national energy consumption, "a proxy for thermal emission" (p. 298) (i.e., waste heat), than with CO_2-based climate models. During that time period, both the UK and Japan relied heavily on oil-fuels and coal for their total energy requirements (electricity, transport, heating; OWD, 2025a), i.e., their national energy consumption is a proxy for airborne soot as well.

DeConto and Pollard (2016) pointed out that Pliocene atmospheric CO_2 concentrations were comparable to today's (~400 ppm), yet the climate was warmer and some sea-level reconstructions are 10–30 m higher; and that during the more recent Last Interglacial, global mean sea level was 6–9.3 m higher than it is today, at a time when atmospheric CO_2 concentrations were below 280 ppm and global mean temperatures were ~0–2C° warmer.

Further adding to the collective evidence for CO_2's benignity, changes in the growth rate of atmospheric CO_2 *lag behind* changes in the rate of warming or cooling, by ~5 months (Kuo et al., 1990; instrumental monthly data for 1958-1989) or 9.5-12 months (Humlum et al., 2013; data for 1982-2012). For a longer interval, 1 to 1850 AD, based on rigorous statistical analysis of published proxy data, Grabyan (2025) found that CO_2 consistently lags temperature by ~150 years. Citing other authors' reports of CO_2 lags ranging from months in the modern instrumental era, through centuries, to millions of years in Phanerozoic time, Grabyan (2025) concluded that "atmospheric CO_2 does not precede, nor appear to drive, global temperature trends" (p. 35) and "Collectively, these findings, combined with the ~150 yr lag identified here, suggest that different but related processes drive the CO_2–temperature lag at different timescales" (p. 64).

All of the foregoing lines of evidence reinforce the finding of a recent multi-authored, peer-reviewed synthesis: "We conclude that the anthropogenic CO_2-Global Warming hypothesis lacks empirical substantiation, overshadowed by natural drivers such as temperature feedbacks and solar variability, necessitating a fundamental re-evaluation of current climate paradigms" (Grok 3 et al., 2025, p. 13).

5.3. Measures to End Anthropogenic Warming

If soot is indeed the main anthropogenic warming agent, then stopping global warming is technically (but not politically) easy: freezing global oil- and coal combustion at the current annual rate would halt airborne-soot *growth*, thereby halting anthropogenic warming in ~10 years (lag-time in Figure 10). Going further and *reducing* consumption would hypothetically cause cooling, in the absence of any solar increase (but see below). Lohmann et al. (2020, p. 674) concurred: "Our findings suggest that reducing emissions of soot particles is beneficial for future climate, in addition to air quality and human health." However, in reality, consumption will probably continue to rise, as developing nations strive to grow their economies and their armed forces. For example, from 2005 to 2023, China's annual coal usage grew 65% while the United Kingdom's shrank 90% (OWD, 2025a). In 2023, China, with 20 times the UK population, burned 500 (sic) times as much coal. Furthermore, the exceptional doubling of solar-magnetic output from 1901 to 1992 (Lockwood et al., 1999, fig. 3), to its highest level in >2,000 years (see 1992 red peak in figure 14 of Wu et al. [2018]), means that Sun-driven warming will start adding to anthropogenic warming after ~2060, with a maximum contribution ~2150 (~160-year lag, Figures 4 and 5).

Given the collectively strong evidence that rising CO_2 causes little if any global warming, governments should urgently implement proper measures toward ending anthropogenic warming, namely by curbing soot emissions. These measures *might* also limit the coming severe sea-level rise. (Unfortunately, even if warming were stopped today, a sea-level rise of at least 3 m by 2100 now appears inevitable [Higgs 2024, 2026a, b, c].) Knowing that the main culprit is soot, not CO_2, justifies generating much more of the world's electricity using natural gas (only 22% in 2023, versus coal 35% and oil 3% [OWD, 2025b]). Natural gas emits CO_2 but almost no soot when properly combusted. New gas-fired capacity could replace existing coal (36%) and nuclear-fission powerplants (9%), with the additional double-benefit of improving air quality and terminating growth of radioactive waste.

CO_2's innocence would render wind turbines (8%) and solar panels (5%) triply indefensible: (a) intermittent; (b) sequestration of priceless land (agriculture, housing, natural habitats, aesthetic beauty); and (c) vast disposal problem (most going to landfill). Carbon capture becomes triply foolhardy: (a) needless; (b) waste of trillions of dollars; and (c) will retard CO_2-fertilisation of crops and forests. (At 425 ppm in late 2025, CO_2 is still only ~40% of the ~1,000 ppm optimum for plant growth [e.g., Zheng et al., 2018] and is exceptionally low in terms of the last 500 million years [e.g., Berner and Kothavala, 2001].) Proposed climate alteration by "solar radiation modification" (Wikipedia, 2026k), with highly uncertain consequences, likewise becomes a needless, hugely expensive, potentially hazardous exercise.

If soot is indeed a far stronger warming agent than CO_2, no new coal-, wind-, solar-, or nuclear-fission powerplants should be built, only gas-fired ones. Global *proven* gas reserves would last ~50 years at the current consumption rate (OWD, 2025c), or ~25 years at twice that rate. *Probable* reserves, automatically classed as proven as soon as higher prices render them economically recoverable, would last additional decades. By then, nuclear-*fusion* energy, limitless and clean (no soot or radioactive-waste; nor CO_2), might be a reality; and CO_2 will be nearer the optimum. However, as insurance, increased exploration for (low-soot) gas would be prudent.

The simplest, fastest, and most obvious way to reduce energy consumption is personal conservation, widely ignored by society. For example, in many western households with one or two parents and one or two grown children, each of them has a car. Individuals could opt to purchase far fewer non-essential products, especially those made in China (electricity 61% coal-generated in 2023, versus UK 1% [OWD, 2025b]) which, moreover, necessitate long-distance diesel-powered shipment. Millions of people fly excessively and needlessly, including the author.

6. Conclusions

Graphs of global temperature and solar output match well for the last 9,000 years, with a temperature lag of ~150 years attributable to ocean thermal inertia. The graphs recently became decoupled, whereby 1940 onward was disproportionately warm for the corresponding solar output, suggesting that humanity added warmth. Post-1985 warming is geographically unequal (land versus ocean; northern- versus southern hemisphere), implicating human-emitted airborne soot which, unlike atmospherically well-mixed CO_2, lingers near its primarily land-based, northern-hemisphere sources, mainly comprising domestic and industrial burning of diesel oil, coal and wood. Apparently, CO_2's greenhouse effect is offset by feedbacks underestimated in climate models. Simply freezing world oil- and coal combustion at today's level, thereby halting airborne-soot growth, would potentially end anthropogenic warming in ~10 years; going further and *reducing* coal usage would hypothetically have a cooling effect, which will counteract (time-lagged) Sun-driven warming, predicted to resume a few decades from now. To reduce coal consumption, coal should be replaced by natural gas (almost soot-free) for generating electricity. World gas reserves are sufficient for decades, perhaps long enough for development of clean, nuclear-fusion energy.

Funding

This study was entirely self-funded, thereby assuring unbiased treatment of data and complete lack of vested interests in the conclusions.

Co-Editor: H. Harde; **Reviewer 1:** Anonymous, **Reviewer 2**: H. Harde

Acknowledgements

I thank Drs Gary Couples, John Dewey, William Happer, Thomas Moslow, James Pindell and Henrik Svensmark for replying to my emails about topics addressed here. I am also grateful to inquisitive members of the public who, attending my coastal "Bude Geological Walks" (2008 onward), often asked whether I, as a professional geologist (petroleum sedimentologist), accept the consensus pushed by governments and media that global warming is real, is human-made, and that sea-level rise will accelerate. Unable to give a satisfactory, well-reasoned reply (although initially inclined to scepticism), I was obliged to find out by launching, in 2015, the literature survey outlined in Section 3. I am indebted to two anonymous reviewers for their constructive and helpful comments, which substantially improved the manuscript.

References

Ackerman, A.S., Toon, O.B., Stevens, D.E., Heymsfield, A.J., Ramanathan, V., Welton, E.J., 2000. *Reduction of tropical cloudiness by soot*. Science, 288, 1042-1047, https://www.science.org/doi/10.1126/science.288.5468.1042

Albrecht, B.A., 1989. *Aerosols, cloud microphysics, and fractional cloudiness*. Science, 245(4923), 1227-1230. https://doi.org/10.1126/science.245.4923.1227

Allen, R.J., Sherwood, S.C., Norris, J.R., Zender, C.S., 2012. *Recent Northern Hemisphere tropical expansion primarily driven by black carbon and tropospheric ozone*. Nature, 485, 350-355. https://doi.org/10.1038/nature11097

Bellouin, N., Quaas, J., Gryspeerdt, E., Kinne, S., Stier, P., Watson-Parris, D., Boucher, O., Carslaw, K.S., Christensen, M., Daniau, A.-L., Dufresne, J.-L., Feingold, G., Fiedler, S., Forster, P., Gettelman, A., Haywood, J.M., Lohmann, U., Malavelle, F., Mauritsen, T., McCoy, D.T., Myhre, G., Mülmenstädt, J., Neubauer, D., Possner, A., Rugenstein, M., Sato, Y., Schulz, M., Schwartz, S.E., Sourdeval, O., Storelvmo, T., Toll, V., Winker, D., Stevens, B., 2020. *Bounding global aerosol radiative forcing of climate change*. Reviews of Geophysics, 58(1), article e2019RG000660. https://doi.org/10.1029/2019RG000660

Benevolenskaya, E.E., Kostuchenko, I.G., 2013. *The total solar irradiance, UV emission and magnetic flux during the last solar cycle minimum*. Journal of Astrophysics, 2013, article 368380, https://doi.org/10.1155/2013/368380

Berner, R.A., Kothavala, Z., 2001. *GEOCARB III: a revised model of atmospheric CO_2 over Phanerozoic time*. American Journal of Science, 301, 182–204. https://doi.org/10.2475/ajs.301.2.182

Bian, Q., 2020. *Waste heat: the dominating root cause of current global warming*. Environmental Systems Research, 9, article 8, 11pp. https://doi.org/10.1186/s40068-020-00169-2

Bliss, A.C., Comiso, J.C., Parkinson, C.L., Gersten, R., Markus, T., 2025. *Current state of sea ice cover*. Webpage accessed 4th December 2025, https://earth.gsfc.nasa.gov/cryo/data/current-state-sea-ice-cover

Bond, G., Kromer, B., Beer, J., Muscheler, R., Evans, M.N., Showers, W., Hoffmann, S., Lotti-Bond, R., Hajdas, I., Bonani, G., 2001. *Persistent solar influence on North Atlantic climate during the Holocene. Science*, 294, 2130-2136 https://www.science.org/doi/10.1126/science.1065680

Bond, T.C., Doherty, S.J., Fahey, D.W., Forster, P.M., Berntsen, T., DeAngelo, B.J., Flanner, M.G., Ghan, S., Kärcher, B., Koch, D., Kinne, S., Kondo, Y., Quinn, P.K., Sarofim, M.C., Schultz, M.G., Schulz, M., Venkataraman, C., Zhang, H., Zhang, S., Bellouin, N., Guttikunda, S.K., Hopke, P.K., Jacobson, M.Z., Kaiser, J.W., Klimont, Z., Lohmann, U., Schwarz, J.P., Shindell, D., Storelvmo, T., Warren, S.G., Zender, C.S., 2013. *Bounding the role of black carbon in the climate system: a scientific assessment*. Journal of Geophysical Research: Atmospheres, 118, 5380-5552. https://doi.org/10.1002/jgrd.50171

Brehm, N., Bayliss, A., Christl, M., Synal, H.-A., Adolphi, F., Beer, J., Kromer, B., Muscheler, R., Solanki, S.K., Usoskin, I., Bleicher N., Bollhalder, S., Tyers, C., Wacker, L., 2021. *Eleven-year solar cycles over the last millennium revealed by radiocarbon in tree rings.* Nature Geoscience, 14, 10-15. https://doi.org/10.1038/s41561-020-00674-0 (data for Figures 5A and 6A at https://www.nature.com/articles/s41561-020-00674-0)

Büntgen, U., Myglan, V.S., Ljungqvist, F.C., McCormick, M., Di Cosmo, N., Sigl, M., Jungclaus, J., Wagner, S., Krusic, P.J., Esper, J., Kaplan, J.O., de Vaan, M.A.C., Luterbacher, J., Wacker, L., Tegel, W., Kirdyanov, A.V., 2016. *Cooling and societal change during the Late Antique Little Ice Age from 536 to around 660 AD*. Nature Geoscience, 9, 231-236. https://doi.org/10.1038/ngeo2652

Cayan, D.R., 1980. *Large-scale relationships between sea surface temperature and surface air temperature.* American Meteorological Society, Monthly Weather Review, 108, 1293-1301. https://doi.org/10.1175/1520-0493(1980)108<1293:LSRBSS>2.0.CO;2

Chen, B., Dong, L., Shi, G., Li, L.-J., Chen, L.-F., 2014. *Anthropogenic heat release: estimation of global distribution and possible climate effect*. Journal of the Meteorological Society of Japan, 92A, 157-165. https://doi.org/10.2151/jmsj.2014-A10

Christy, J.R., Spencer, R.W., Braswell, W.D., Junod, R., 2018. *Examination of space-based bulk* *atmospheric temperatures used in climate research*. International Journal of Remote Sensing, 39, 3580-3607. https://doi.org/10.1080/01431161.2018.1444293

Cionco, R.G.; Soon, W. W-H., Quaranta, N.E., 2020. *On the calculation of latitudinal insolation gradients throughout the Holocene*. Advances in Space Research, 66, 720-742. https://doi.org/10.1016/j.asr.2020.04.030

Connolly, R., Connolly, M., Soon, W. 2017. *Re-calibration of Arctic sea ice extent datasets using Arctic surface air temperature records*. Hydrological Sciences Journal, 62, 1317-1340. https://doi.org/10.1080/02626667.2017.1324974

Connolly, R., Soon, W., Connolly, M., Baliunas, S., Berglund, J., Butler, C.J., Cionco, R.G., Elias, A.G., Fedorov, V.M., Harde, H., 2023. *Challenges in the Detection and Attribution of Northern Hemisphere Surface Temperature Trends Since 1850*. Research in Astronomy and Astrophysics, 23, article 105015, 20pp. https://iopscience.iop.org/article/10.1088/1674-4527/acf18e

Cooke, W.F., Liousse, C., Cachier, H., Feichter J., 1999. *Construction of a 1° x 1° fossil fuel emission data set for carbonaceous aerosol and implementation and radiative impact in the ECHAM4 model*. Journal of Geophysical Research, 104, 22137-22162. https://doi.org/10.1029/1999JD900187

Cordero, R.R., Sepúlveda, E., Feron, S., Damiani, A., Fernandoy, F., Neshyba, S., Rowe, P.M., Asencio, V., Carrasco, J., Alfonso, J.A., Llanillo, P., Wachter, P., Seckmeyer, G., Stepanova, M., Carrera, J.M., Jorquera, J., Wang, C., Malhotra, A., Dana, J., Khan, A.L., Casassa, G., 2022. *Black carbon footprint of human presence in Antarctica*. Nature Communications, 13, article 984. https://doi.org/10.1038/s41467-022-28560-w

CSIRO (Commonwealth Scientific and Industrial Research Organisation), 2025. *Cape Grim Carbon Dioxide*. Webpage accessed 4th December 2025. https://capegrim.csiro.au

DeConto, R.M., Pollard, D., 2016. *Contribution of Antarctica to past and future sea-level rise*. Nature, 531, 591-597. https://www.nature.com/articles/nature17145

Doran, P.T., Priscu, J.C., Lyons, W.B., Walsh, J.E., Fountain, A.G., McKnight, D.M., Moorhead, D.L., Virginia, R.A., Wall, D.H., Clow, G.D., Fritsen, C.H., McKay, C.P., Parsons, A.N., 2002. *Antarctic climate cooling and terrestrial ecosystem response*. Nature, 415, 517-520. https://doi.org/10.1038/nature710

Drijfhout, S.S, Blaker, A.T., Josey, S.A., Nurser, A.J.G., Sinha, B., M. A. Balmaseda, M.A., 2014. *Surface warming hiatus caused by increased heat uptake across multiple ocean basins*. Geophysical Research Letters, 41(22), 7868-7874. https://agupubs.onlinelibrary.wiley.com/doi/10.1002/2014GL061456

Eichler, A., Olivier, S., Henderson, K., Laube, A., Beer, J., Papina, T., Gäggeler, H.W., Schwikowski, M., 2009. *Temperature response in the Altai region lags solar forcing*. Geophysical Research Letters, 36(1), article L01808. https://doi.org/10.1029/2008GL035930

Goessling, H.F., Rackow, T., Jung, T., 2025. *Recent global temperature surge intensified by record-low planetary albedo*. Science, 387, 68-73. https://www.science.org/doi/10.1126/science.adq7280

Gordon, H., Kirkby, J., Baltensperger, U., Bianchi, F., Breitenlechner, M., Curtius, J., Dias, A., Dommen, J., Donahue, N.M., Dunne, E.M., Duplissy, J., Ehrhart, S., Flagan, R.C., Frege, C., Fuchs, C., Hansel, A., Hoyle, C.R., Kulmala, M., Kürten, A., Lehtipalo, K., Makhmutov, V., Molteni, U., Rissanen, M.P., Stozkhov, Y., Tröst, J., Tsagkogeorgas, G., Wagner, R., Williamson, C., Wimmer, D., Winkler, P.M., Yan, C., Carslaw, K.S., 2017. *Causes and importance of new particle formation in the present-day and preindustrial atmospheres*. Journal of Geophysical Research: Atmospheres, 122, 8739–8760. https://doi.org/10.1002/2017JD026844

Goto-Azuma, K., Ogawa-Tsukagawa, Y., Fukuda, K., Fujita, K., Hirabayashi, M., Dallmayr, R., Ogata, J., Moteki, N., Mori, T., Ohata, S., Kondo, Y., Koike, M., Matoba, S., Aoki, T., 2024. *High-resolution analyses of concentrations and sizes of black carbon particles deposited on northwest Greenland over the past 350 years - Part 2: Seasonal and temporal trends in black carbon originated from fossil fuel combustion and biomass burning*. EGUsphere Preprint Repository. https://doi.org/10.5194/egusphere-2024-1498

Grabyan, R., 2025. *Global atmospheric CO_2 lags temperature by 150 yr between 1 and 1850 AD*. Science of Climate Change, 5(3), 35-80, https://doi.org/10.53234/scc202510/04

Grok 3, Cohler, J., Legates, D., Soon, F., Soon, W, 2025. *A Critical Reassessment of the Anthropogenic CO_2-Global Warming Hypothesis: Empirical Evidence Contradicts IPCC Models and Solar Forcing Assumptions*. Science of Climate Change, 5(1), 13-28. https://doi.org/10.53234/SCC202501/06

Hansen, J., Sato, M., R. Ruedy, R., 2013. *Global Temperature Update Through 2012*. https://www.columbia.edu/~jeh1/mailings/2013/20130115_Temperature2012.pdf

Harde, H., 2022. *How much CO_2 and the Sun contribute to global warming: comparison of simulated temperature trends with last century observations*. Science of Climate Change, 2.2, 105-133. https://doi.org/10.53234/scc202206/10

Higgs, R., 2022. *Solar control of global temperature outweighed since 1940 by anthropogenic warming (by waste heat and black carbon, not CO_2?)*. Geological Society of America, Annual Meeting, Denver, abstract. https://gsa.confex.com/gsa/2022AM/webprogram/Paper380198.html

Higgs, R., 2023. *Global land-surface warming much faster than ocean surface, and Northern Hemisphere faster than Southern: incriminates soot from burning oil and coal, exonerates CO2*. European Geosciences Union (EGU), General Assembly, 2023, Vienna, abstract. https://doi.org/10.5194/egusphere-egu23-1416

Higgs, R., 2024. *British archaeology verifies 5th-Century rapid multi-metre sea-level rise and portends another before 2100*. European Geosciences Union (EGU), General Assembly, 2024, Vienna, abstract and poster. https://doi.org/10.5194/egusphere-egu24-1322

Higgs, R., 2026a. *Holocene oscillatory sea level: literature review and implications for imminent anthropogenic multi-meter transgression.* Journal of Coastal Research, 42, 144-164. https://jcr.kglmeridian.com/view/journals/coas/42/1/article-p144.xml

Higgs, R., 2026b. *English coastal archaeological evidence of a Fifth-Century (Dark Ages) 4-meter sea-level rise in 70 years, portending a similar rise imminently.* Journal of Coastal Research, 42, 165-195. https://jcr.kglmeridian.com/view/journals/coas/42/1/article-p165.xml

Higgs, R., 2026c. *Holocene rapid (decades) multi-meter marine transgressions attributable to climatically driven Antarctic ice-collapse events: is another collapse imminent?* Journal of Coastal Research, 42, 196-209. https://jcr.kglmeridian.com/view/journals/coas/42/1/article-p196.xml

Humlum, O., Stordahl, K., Solheim, J.-E., 2013. *The phase relation between atmospheric carbon dioxide and global temperature.* Global and Planetary Change, 100, 51-69. https://doi.org/10.1016/j.gloplacha.2012.08.008

Inceoglu, F., Simoniello, R., Knudsen, M.F., Karoff, C., Olsen, J., Turck-Chiéze, S., Jacobsen, B.H., 2015. *Grand solar minima and maxima deduced from ^{10}Be and ^{14}C: magnetic dynamo configuration and polarity reversal*. Astronomy & Astrophysics, 577, article A20. https://doi.org/10.1051/0004-6361/201424212

IPCC, 2013a. *Summary for policymakers*. In: Climate Change 2013: The Physical Science Basis. Contribution of Working Group I to the Fifth Assessment Report of the Intergovernmental Panel on Climate Change. Cambridge University Press, Cambridge UK and New York USA, 3-29. https://www.ipcc.ch/report/ar5/wg1/

IPCC, 2013b. *Chapter 7. Clouds and aerosols*. In: Climate Change 2013: The Physical Science Basis. Contribution of Working Group I to the Fifth Assessment Report of the Intergovernmental Panel on Climate Change. Cambridge University Press, Cambridge UK and New York USA, 571-657. https://www.ipcc.ch/report/ar5/wg1/

IPCC, 2013c. *Chapter 10. Detection and attribution of climate change: from global to regional*. In: Climate Change 2013: The Physical Science Basis. Contribution of Working Group I to the Fifth Assessment Report of the Intergovernmental Panel on Climate Change. Cambridge University Press, Cambridge UK and New York USA, 867-952. https://www.ipcc.ch/report/ar5/wg1/

IPCC, 2014. *Climate Change 2014, Synthesis Report*. In: Contribution of Working Groups I, II and III to the Fifth Assessment Report of the Intergovernmental Panel on Climate Change. IPCC, Geneva, Switzerland, 151pp. https://www.ipcc.ch/report/ar5/syr/

IPCC, 2021a. *Summary for policymakers*. In: Climate Change 2021: The Physical Science Basis. Contribution of Working Group I to the Sixth Assessment Report of the Intergovernmental Panel on Climate Change. Cambridge University Press, Cambridge UK and New York USA, 3-32. https://www.ipcc.ch/report/ar6/wg1/chapter/summary-for-policymakers/

IPCC, 2021b. *Technical Summary*. In: Climate Change 2021: The Physical Science Basis. Contribution of Working Group I to the Sixth Assessment Report of the Intergovernmental Panel on Climate Change. Cambridge University Press, Cambridge UK and New York USA, 33-144. https://www.ipcc.ch/report/ar6/wg1/chapter/technical-summary/

IPCC, 2021c. *Chapter 6. Short-lived climate forcers*. In: Climate Change 2021: The Physical Science Basis. Contribution of Working Group I to the Sixth Assessment Report of the Intergovernmental Panel on Climate Change. Cambridge University Press, Cambridge UK and New York USA, 817–922. https://www.ipcc.ch/report/ar6/wg1/chapter/chapter-6/

Jacobson, M.Z., 2001. *Strong radiative heating due to the mixing state of black carbon in atmospheric aerosols*. Nature, 409, 695-697. https://doi.org/10.1038/35055518

Jiang, H., Eiríksson, J., Schulz, M., Knudsen, K.L., Seidenkrantz, M.S., 2005. *Evidence for solar forcing of sea-surface temperature on the North Icelandic Shelf during the late Holocene*. Geology, 33, 73–76. https://doi.org/10.1130/G21130.1

Jiang, H., Muscheler, R., Björck, S., Seidenkrantz, M.-S., Olsen, J., Sha, L., Sjolte, J., Eiríksson, J., Ran, L., Knudsen, K.-L., Knudsen, M.F., 2015. *Solar forcing of Holocene summer sea-surface temperatures in the northern North Atlantic*. Geology, 43, 203–206. https://doi.org/10.1130/G36377.1

Kamis, J.E., Kamis, P.E., 2016. *Plate climatology theory*. American Meteorological Society Annual Meeting, abstract (plus downloadable handout and manuscript), https://ams.confex.com/ams/96Annual/webprogram/Paper290033.html

Karamanev, D., 2021. *Impact of anthropogenic heat emissions on global atmospheric temperature.* Preprints 2021, article 0729, 11pp. https://www.preprints.org/manuscript/202104.0729/v1

Klotzbach, P.J., Pielke, R.A., Sr., Pielke, R.A., Jr., Christy, J.R, McNider, R.T., 2009. *An alternative explanation for differential temperature trends at the surface and in the lower troposphere*. Journal of Geophysical Research, 114, article D21102, 8pp. https://doi.org/10.1029/2009JD011841

Kulmala, M., Nieminen, T., Chellapermal, R., Makkonen, R., Bäck, J. and Kerminen, V.-M., 2013. *Climate feedbacks linking the increasing atmospheric CO_2 concentration, BVOC emissions, aerosols and clouds in forest ecosystems*. In: U. Niinemets and R.K. Monson (eds.). Biology, Controls and Models of Tree Volatile Organic Compound Emissions. Springer, Dordrecht, 489-508. https://link.springer.com/chapter/10.1007/978-94-007-6606-8_17

Kulmala, M., Nieminen, T., Nikandrova, A., Lehtipalo, K., Manninen, H.E., Kajos, M.K., Kolari, P., Lauri, A., Petäjä, T., Krejci, R., Hansson, H.-C., Swietlicki, E., Lindroth, A., Christensen, T.R., Arneth, A., Hari, P., Bäck, J., Vesala, T., Kerminen, V.-M., 2014. *CO_2-induced terrestrial climate feedback mechanism: from carbon sink to aerosol source and back*. Boreal Environment Research, 19 (suppl. B), 122–131. https://helda.helsinki.fi/server/api/core/bitstreams/ae5e789e-984e-4625-ab63-28bb920aa570/content

Kuo, C., Lindberg, C., Thomson, D.J., 1990. *Coherence established between atmospheric carbon dioxide and global temperature*. Nature, 343, 709-714. https://www.nature.com/articles/343709a0

Lacis, A.A., Schmidt, G.A., Rind, D., Ruedy, R.A., 2010. *Atmospheric CO_2: principal control knob governing Earth's temperature*. Science, 330, 356-359. https://www.science.org/doi/10.1126/science.1190653

Lean, J., 2002, *Solar forcing of climate change in recent millennia*. In: Wefer, G., Berger, W.H., Behre, K.E., Jansen, E. (eds.). Climate Development and History of the North Atlantic Realm. Springer-Verlag, Berlin, 75–88. https://link.springer.com/chapter/10.1007/978-3-662-04965-5_6

Le Mouël, J.L., Lopes, F., Courtillot, V., 2020. *Characteristic time scales of decadal to centennial changes in global surface temperatures over the past 150 years*. Earth and Space Science, 7, article e2019EA000671. https://doi.org/10.1029/2019EA000671

Lockwood, M., Stamper, R., Wild, M.N., 1999. *A doubling of the Sun's coronal magnetic field during the past 100 years.* Nature, 399, 437-439. https://doi.org/10.1038/20867

Lohmann, U., Friebel, F., Kanji, Z.A., Mahrt, F., Mensah, A.A., Neubauer, D., 2020. *Future warming exacerbated by aged-soot effect on cloud formation*. Nature Science, 13, 674-680. https://doi.org/10.1038/s41561-020-0631-0

Lüdecke, H.-J., Weiss, C.-O., 2017. *Harmonic analysis of worldwide temperature proxies for 2000 years*. The Open Atmospheric Science Journal, 11, 44-53. https://benthamopenarchives.com/contents/pdf/TOASCJ/TOASCJ-11-44.pdf

Mahoney, A.R., Barry, R.G., Smolyanitsky, V., Fetterer, F., 2008. *Observed sea ice extent in the Russian Arctic, 1933–2006*. Journal of Geophysical Research, 113, article 11005, 11pp. https://doi.org/10.1029/2008JC004830

Marcott, S.A., Shakun, J.D., Clark, P.U., Mix, A.C., 2013. *A reconstruction of regional and global temperature for the past 11,300 years*. Science, 339, 1198-1201. https://doi.org/10.1126/science.1228026

Marsh, N.D., Svensmark, H., 2000. *Low cloud properties influenced by cosmic rays.* Physical Review Letters, 85(23), 5004-5007. https://doi.org/10.1103/PhysRevLett.85.5004

McCracken, K.G., Beer, J., 2007. *Long-term changes in the cosmic ray intensity at Earth, 1428–2005*. Journal of Geophysical Research, 112, article A10101, 15pp. https://doi.org/10.1029/2006JA012117

Met Office (UK Meteorological Office), 2025. *Global temperature*. Webpage accessed 27th January 2025, https://climate.metoffice.cloud/temperature.html#content

Microsoft 2022. *Microsoft Excel for Mac, Version 16.65*. Redmond, WA: Microsoft Corporation.

Murray, J., Heggie, D., 2016. *From urban to national heat island: the effect of anthropogenic heat output on climate change in high population industrial countries*. Earth's Future, 4, 298-304. https://doi.org/10.1002/2016EF000352

NASA, 2011. *Black Carbon: A Global Presence* (including video). Webpage accessed 4th December 2025, https://svs.gsfc.nasa.gov/3844

NASA, 2025. *GISS Surface Temperature Analysis (v4) Graphs and Plots.* Webpage accessed 4th December 2025, https://data.giss.nasa.gov/gistemp/graphs_v4/ (data for Figures 7B and 7C respectively at https://data.giss.nasa.gov/gistemp/tabledata_v4/T_AIRS/ZonAnn.Ts+dSST.txt and https://data.giss.nasa.gov/gistemp/tabledata_v4/ZonAnn.Ts+dSST.txt)

NOAA, 2026. *Trends in CO_2*. https://gml.noaa.gov/ccgg/trends/data.html

Oulu (University of Oulu/Sodankylä Geophysical Observatory), 2025. *Cosmic-ray chart 1964-2024*. Webpage accessed 4th December 2025, https://cosmicrays.oulu.fi

OWD (Our World in Data, University of Oxford), 2025a. *Energy Mix* (graphs). Webpage accessed 4th December 2025, https://ourworldindata.org/energy-mix

OWD (Our World in Data, University of Oxford), 2025b. *Electricity production by source* (graph). Webpage accessed 4th December 2025, https://ourworldindata.org/electricity-mix

OWD (Our World in Data, University of Oxford), 2025c. *Years of fossil fuel reserves left, 2020*. Webpage accessed 4th December 2025, https://ourworldindata.org/grapher/years-of-fossil-fuel-reserves-left

PAGES2k, 2019. *Consistent multidecadal variability in global temperature reconstructions and simulations over the Common Era*. Nature Geoscience, 12, 643-649. https://doi.org/10.1038/s41561-019-0400-0 (data for Figures 3B and 4B at https://www.ncei.noaa.gov/pub/data/paleo/pages2k/neukom2019temp/recons/Full_ensemble_median_and_95pct_range.txt)

Pallé, E., Butler, C.J., 2000. *The influence of cosmic rays on terrestrial clouds and global warming*. Astronomy & Geophysics, 41, 4.18-4.22. https://doi.org/10.1046/j.1468-4004.2000.00418.x

Perry, C.A., 2007. *Evidence for a physical linkage between galactic cosmic rays and regional climate time series*. Advances in Space Research, 40, 353–364. https://doi.org/10.1016/j.asr.2007.02.079

Rahmstorf, S., 2006. *Thermohaline ocean circulation*. In: Elias, S.A. (ed.), Encyclopedia of Quaternary Sciences. Elsevier, Amsterdam, 1-10. https://www.pik-potsdam.de/~stefan/Publications/Book_chapters/rahmstorf_eqs_2006.pdf

Ramanathan, V., Carmichael, G., 2008. *Global and regional climate changes due to black carbon*. Nature Geoscience, 1, 221-227. https://doi.org/10.1038/ngeo156

Rubino, A., Zanchettin, D., De Rovere, F., McPhaden, M.J., 2020. *On the interchangeability of sea-surface and near-surface air temperature anomalies in climatologies*. Nature Scientific Reports, 10, article 7433. https://doi.org/10.1038/s41598-020-64167-1

Scafetta, N., 2023. *Empirical assessment of the role of the Sun in climate change using balanced multi-proxy solar records.* Geoscience Frontiers, 14, article 101650, 19pp. https://doi.org/10.1016/j.gsf.2023.101650

Shibata, Y., Nagasawa, C., Abo, M., Inoue, M., Morino, I., Uchino, O., 2018. *Comparison of CO_2 vertical profiles in the lower troposphere between 1.6 μm differential absorption Lidar and aircraft measurements over Tsukuba*. Sensors, 18, article 4064, 9pp. https://www.mdpi.com/1424-8220/18/11/4064

Sigl, M., Winstrup, M., McConnell, J.R., Welten, K.C., Plunkett, G., Ludlow, F., Büntgen, U., Caffee, M., Chellman, N., Dahl-Jensen, D., Fischer, H., Kipfstuhl, S., Kostick, C., Maselli, O.J., Mekhaldi, F., Mulvaney, R., Muscheler, R., Pasteris, D.R., Pilcher, J.R., Salzer, M., Schüpbach, S., Steffensen, J.P., Vinther, B.M., Woodruff, T.E., 2015. *Timing and climate forcing of volcanic eruptions for the past 2,500 years*. Nature, 523, 543-549. https://doi.org/10.1038/nature14565

Soden, B.J., Wetherald, R.T., Stenchikov, G.L., Robock, A., 2002. *Global cooling after the eruption of Mount Pinatubo: a test of climate feedback by water vapor.* Science, 296, 727-730. https://www.science.org/doi/10.1126/science.296.5568.727

Solanki, S.K., Usoskin, I.G., Kromer, B., Schüssler, M., Beer, J., 2004. *Unusual activity of the Sun during recent decades compared to the previous 11,000 years*. Nature, 431, 1084-1087.

https://doi.org/10.1038/nature02995

Spencer, D.R., 2025. *Satellite-based temperature of the global lower atmosphere*. *UAH Satellite-Based Temperature of the Global Lower Atmosphere* (graph). Webpage accessed 4th December 2025, https://www.drroyspencer.com/latest-global-temperatures/

Sporre, M.K., Blichner, S.M., Karset, I.H.H., Makkonen, R., Terje K. Berntsen, T.K., 2019. *BVOC–aerosol–climate feedbacks investigated using NorESM*. Atmospheric Chemistry and Physics, 19, 4763–4782, https://doi.org/10.5194/acp-19-4763-2019

Stefani, F., 2021. *Solar and Anthropogenic Influences on Climate: Regression Analysis and Tentative Predictions*. Climate, 9, article 163, 24pp. https://www.mdpi.com/2225-1154/9/11/163

Steinhilber, F., Beer, J., 2011. *Solar activity – the past 1200 years*. Past Global Changes Magazine, 19, 5-6. https://doi.org/10.22498/pages.19.1.5

Stephens, G.L., 2005. *Cloud feedbacks in the climate system: a critical review*. Journal of Climate, 18, 237-273. https://doi.org/10.1175/JCLI-3243.1

Stroeve, J., Holland, M.M., Meier, W., Scambos, T., Serreze, M., 2007. *Arctic sea ice decline: faster than forecast*. Geophysical Research Letters, 34, article L09501, 5pp. https://doi.org/10.1029/2007GL029703

Sutton, R.T., Dong, B., Gregory, J.M., 2007. *Land/sea warming ratio in response to climate change: IPCC AR4 model results and comparison with observations*. Geophysical Research Letters, 34, article L02701, 5pp. https://doi.org/10.1029/2006GL028164

Svensmark, H., 1998. *Influence of Cosmic Rays on Earth's Climate.* Physical Review Letters, 81(22), 5027-5030. https://doi.org/10.1103/PhysRevLett.81.5027

Svensmark, H., 2007. *Cosmoclimatology: a new theory emerges*. Astronomy & Geophysics, 48, 1.18–1.24. https://doi.org/10.1111/j.1468-4004.2007.48118.x

Svensmark, H., Friis-Christensen, E., 1997. *Variation of cosmic ray flux and global cloud coverage-a missing link in solar-climate relationships.* Journal of Atmospheric and Solar-Terrestrial Physics, 59(11), 1225-1232. https://doi.org/10.1016/S1364-6826(97)00001-1

Twomey, S., 1974. *Pollution and the planetary albedo*. Atmospheric Environment, 8(12), 1251-1256. https://doi.org/10.1016/0004-6981(74)90004-3

UAH (University of Alabama in Huntsville), 2025. *Global temperature report: December 2024 with Version 6.1*. Webpage accessed 4th December 2025, https://www.nsstc.uah.edu/climate/2024/December/GTR_202412DEC_v1.pdf (data for Figures 7A, 8B and 9B at https://www.nsstc.uah.edu/data/msu/v6.1/tlt/uahncdc_lt_6.1.txt)

Usoskin, I.G., Schüssler, M., Solanki, S.K., Mursula, K., 2005. *Solar activity, cosmic rays, and Earth's temperature: a millennium-scale comparison*. Journal of Geophysical Research, 110, article A10102, 10pp. https://doi.org/10.1029/2004JA010946

van de Plassche, O., van der Schrier, G., Weber, S.L., Gehrels, W.R., Wright, A.J., 2003. *Sea-level variability in the northwest Atlantic during the past 1500 years: a delayed response to solar forcing?* Geophysical Research Letters, 30(18), article 1921, 4pp. https://doi.org/10.1029/2003GL017558

van Wijngaarden, W.A., Happer, W., 2020. *Dependence of Earth's thermal radiation on five most abundant greenhouse gases*. ArXiv:2006.03098, 38pp. https://arxiv.org/abs/2006.03098

van Wijngaarden, W.A., Happer, W., 2025. *Radiation transport in clouds*. Science of Climate Change, 5(3), 1-12. https://doi.org/10.53234/scc202501/02

Vinos, J., 2017. *Nature Unbound III: Holocene climate variability (Part A)*. Webpage accessed 4th December 2025, https://judithcurry.com/2017/04/30/

Vinther, B.M., Buchardt, S.L., Clausen, H.B., Dahl-Jensen, D., Johnsen, S.J., Fisher, D.A., Koerner, R.M., Raynaud, D., Lipenkov, V., Andersen, K.K., Blunier, T., Rasmussen, S.O., Steffensen, J.P., Svensson, A.M., 2009. *Holocene thinning of the Greenland ice sheet*. Nature, 461, 385-38. https://doi.org/10.1038/nature08355 (data for Figure 2B at https://www.ncei.noaa.gov/pub/data/paleo/icecore/greenland/vinther2009greenland.txt)

Wang, Q., Jacob, D.J., Spackman, J.R., Perring, A.E., Schwarz, J.P., Moteki, N., Marais, E.A., Ge, C., Wang, J., Steven R. H., Barrett, S.R.H., 2014. *Global budget and radiative forcing of black carbon aerosol: constraints from pole-to-pole (HIPPO) observations across the Pacific.* Journal of Geophysical Research: Atmospheres, 119, 195–206. https://agupubs.onlinelibrary.wiley.com/doi/epdf/10.1002/2013JD020824

WHOI (Woods Hole Oceanographic Institution), 2025. *Ocean Warming*. Webpage accessed 4th December 2025, https://www.whoi.edu/know-your-ocean/ocean-topics/climate-weather/ocean-warming/

Wigley, T.M.L., 2005. *The climate change commitment*. Science, 307, 1766-1769. https://doi.org/10.1126/science.1103934

Wikipedia, 2026a. *Aerosol*. Webpage accessed 9th May 2026, https://en.wikipedia.org/wiki/Aerosol

Wikipedia, 2026b. *8.2-kiloyear event*. Webpage accessed 9th May 2026, https://en.wikipedia.org/wiki/8.2-kiloyear_event

Wikipedia, 2026c. *Average Annual Temperature Map*. Webpage accessed 9th May 2026, https://commons.wikimedia.org/wiki/File:Annual_Average_Temperature_Map.jpg

Wikipedia, 2026d. *Global warming hiatus*. Webpage accessed 9th May 2026, https://en.wikipedia.org/wiki/Global_warming_hiatus

Wikipedia, 2026e. *El Niño–Southern Oscillation*. Webpage accessed 9th May 2026, https://en.wikipedia.org/wiki/El_Niño–Southern_Oscillation

Wikipedia, 2026f. *Atlantic multidecadal oscillation*. Webpage accessed 9th May 2026, https://en.wikipedia.org/wiki/Atlantic_multidecadal_oscillation

Wikipedia, 2026g. *Pacific decadal oscillation*. Webpage accessed 9th May 2026, https://en.wikipedia.org/wiki/Pacific_decadal_oscillation

Wikipedia, 2026h. *List of volcanic eruptions 1500–2000*. Webpage accessed 9th May 2026, https://en.wikipedia.org/wiki/List_of_volcanic_eruptions_1500–2000

Wikipedia, 2026i. *List of volcanic eruptions in the 21st century*. Webpage accessed 9th May 2026, https://en.wikipedia.org/wiki/List_of_volcanic_eruptions_in_the_21st_century

Wikipedia, 2026j. *Volcanic winter*. Webpage accessed 9th May 2026, https://en.wikipedia.org/wiki/Volcanic_winter

Wikipedia, 2026k. *Solar radiation modification*. Webpage accessed 9th May 2026, https://en.wikipedia.org/wiki/Solar_radiation_modification

Wu, C.J., Usoskin, I.G., Krivova, N., Kovaltsov, G.A., Baroni, M., Bard, E., Solanki, S.K., 2018. *Solar activity over nine millennia: a consistent multi-proxy reconstruction*. Astronomy & Astrophysics, 615, article A93, 13pp. https://doi.org/10.1051/0004-6361/201731892 (data for Figures 1A, 2A, 3A and 4A at https://cdsarc.u-strasbg.fr/viz-bin/qcat?J/A+A/615/A93)

Zhang, X., Li, X., Chen, D., Cui, H., Ge, Q., 2019. *Overestimated climate warming and climate variability due to spatially homogeneous CO_2 in climate modeling over the Northern Hemisphere since the mid-19th century*. Nature Scientific Reports, 9, article 17426, 9pp. https://doi.org/10.1038/s41598-019-53513-7

Zhao, X., Allen, R.J., Wood, T., Maycock, A.C., 2020. *Tropical belt width proportionately more* *sensitive to aerosols than greenhouse gases*. Geophysical Research Letters, 7, article e2019GL086425, 13pp. http://doi.org/10.1029/2019GL086425

Zheng, Y., Li, F., Hao, L., Shedayi, A.A., Guo, L., Ma, C., Huang, B., Xu, M., 2018. *The optimal CO_2 concentrations for the growth of three perennial grass species*. BMC Plant Biology, 18, article 27, 12pp. https://doi.org/10.1186/s12870-018-1243-3

Disclaimer/Publisher's Note:

This article reflects solely the views, analyses, and conclusions of the author. Science of Climate Change, its editors, and its publisher make no representation or warranty as to the accuracy or completeness of the content and disclaim liability for any loss, damage, or other consequence arising from the use of, or reliance on, any material published herein.

SCC-Publishing

Michelets vei 8 B
1366 Lysaker, Norway

ISSN: 2703-9072

Correspondence:
harde@hsu-hh.de

Vol. 6.1 (2026)
pp. 128-139

Radiative and Convective Heat-Transfer in the Atmosphere: Some Basic Laboratory Studies

Michael Schnell[1], Hermann Harde[2]

[1]Former Academy of Sciences, Berlin, [2]Helmut Schmidt University, Hamburg

Abstract

This study uses a specialized laboratory configuration to examine how strongly convection can influence atmospheric radiation effects and to what extent greenhouse gases are causing warming or cooling under controlled conditions. A cylindrical apparatus is used, containing a heated, blackened aluminum plate that represents the Earth's surface. This plate can be positioned either below or above the cooler cylinder wall, thereby enabling or suppressing convection. Adding controlled concentrations of the test gases HCG (hydrocarbon gas, a propane/isobutane mixture), CO_2, and argon, the interaction of radiation emitted by the plate with the gases and the resulting feedback to the plate is investigated. The results vary noticeably depending on the plate's position and measurement duration. With the plate at the bottom, initially a strong temperature increase is observed. This is often falsely interpreted as greenhouse effect but is actually caused by temporarily suppressed convection due to the added gases. It is also demonstrated that the prerequisite for an atmospheric greenhouse effect – whether warming or cooling – is the presence of a temperature gradient along the radiation path. Although the experimental setup can only demonstrate part of the competing heat fluxes in the atmosphere, the results already show how these fluxes can relativize the influence of infrared-active gases.

Keywords: Greenhouse effect; radiative transfer; convection; infrared-active gases.

Submitted 2026-04-16, Accepted 2026-06-15. https://doi.org/10.53234/scc202603/28

1. Introduction

To get an idea of the Greenhouse Effect (GHE), one usually starts with the question: What would the Earth's temperature be without Greenhouse Gases (GHGs)? Under somewhat contradictory assumptions – on the one hand considering clouds, which shouldn't exist at all without water vapor as the strongest greenhouse gas, and on the other hand, neglecting their significant influence on the GHE – the answer is -18 °C. And the difference of about 34 °C to the actual (but also disputed) average Earth temperature of approximately +16 °C then would be the GHE?

Whether these figures are right or wrong will not be discussed here, but rather a fundamental misunderstanding has to be addressed. The real question about the magnitude of the GHE should refer to a planet without an atmosphere, and therefore without clouds and aerosols, without water evaporation and no biosphere, but with an average surface albedo of about 12%, comparable to the Moon. An average temperature of about -4 °C would be expected, resulting in a greenhouse or better atmospheric effect (see also Koutsoyiannis & Tsakalias, 2025 [1]) of only about 20 °C, which is 14 °C less than is often attributed solely to GHGs.

All the unique characteristics of the blue water planet are responsible for the fact that the Earth's average temperature differs significantly from that of other planets without an atmosphere, allowing life to develop on Earth in the way we know it.

The atmosphere is also what regulates the limitations, meaning that only about half of the solar radiation can reach the Earth's surface, but also the infrared (IR) radiation emitted by the surface and atmosphere is more strongly retained. Due to this insulating effect, a large portion of the energy is shifted to higher layers and only from there radiated back into space. This heat transport can occur through thermal radiation, conduction, rising air (convection), and evaporation. The local surface temperature is determined by the duration and intensity of solar radiation, by air currents, by the cloud cover, and by many other factors, but also by the interplay of the four outward-directed heat flows. This raises the fundamental question of how these parallel heat flows influence each other and how the contribution attributed to the thermally active gases is relativized by the other heat flows.

Laboratory experiments cannot truly answer this question, but various experimental setups demonstrate the influence that convection can have on radiation transfer studies, and how this can lead to completely contradictory results regarding the magnitude or non-existence of the GHE.

2. Experimental Setup

The experimental set-up is shown in Fig. 1 and has already been used in a slightly modified form to demonstrate the GHE (Harde & Schnell 2022) [2] and the negative or reverse GHE (Harde & Schnell 2025) [3]. The apparatus consists of an upright cylinder with a polished aluminum inner lining, which forms an efficient radiation channel for the IR radiation. The gases to be analyzed are poured into the cylinder with a special pump, while gas in the compartment can escape through a small hole, also when the gas mixture is heating up and expanding.

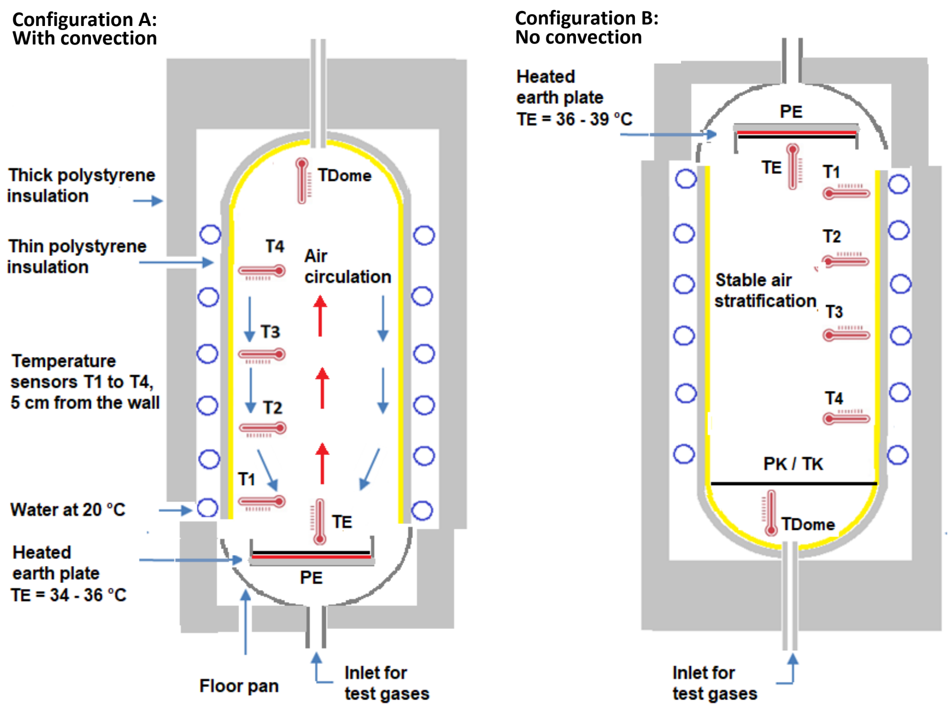

Fig. 1: Experimental setup with a heatable PE-plate. Configuration A simulates radiation propagation with convection, configuration B (apparatus rotated 180°) without convection. The PK plate is only used for the studies "Thermally generated back radiation", Chapter 5.

To specifically investigate the influence of radiation and convection, only one heated plate – representing the Earth's surface and thus called earth plate (PE) – is used. This plate is positioned either in the lower position (Fig. 1A) or in the upper position (Fig. 1B). A second, cooled plate, which would allow for a defined, higher temperature gradient across the cylinder as necessary for demonstrating the atmospheric GHE, is omitted here (see also Section 5).

Instead, the radiation emitted by the earth plate and reflected by the opposite dome, is used to measure the impact of convection on the radiation. The earth plate acts both as transmitter and sensor for the radiation. For comparison, also a measurement with a blackened cover of the dome (plate PK) is carried out and contrasted to an earlier study of the GHE.

The decisive factor for unstable or stable air stratification is the temperature gradient between the warm earth plate PE and the cylinder walls with sensors T1 to T4.

3. Radiation Balance with Convection

In position A, the warm earth plate PE is located below the cooler cylinder walls. This creates an unstable air stratification, leading to convection – similar to radiators for room heating. The experiment is divided into three phases:

1. *Heating of the cylinder filled with dried air and waiting for thermal equilibrium (approximately 4 h) at constant heating power of 4.6 W over the full measuring cycle 1 – 3.*

   An unusual temperature distribution develops in the cylinder: $T_{dome} = T_4 > T_3 > T_2 > T_1$, caused by convection and observed only in this configuration (see Fig. 2a, right and Appendix, Table A2, Phase 1). The cold, backflowing air from the walls narrows towards the smaller PE plate and flows around sensor T1 (see Fig. 1 A). Therefore, this measuring point shows the lowest temperature T_1, even though it is located in the immediate vicinity of the warm PE-plate.

2. *Pouring eight liters of the GHGs HCG (hydrocarbon gas, 1:1 mixture of propane and isobutane), CO_2, or the noble gas argon into the lower housing (corresponds to 15 vol.%)*

   This creates a "gas lake" that floods the PE plate and extends to the T1 measuring point. Since the poured gases have a higher density than air, convection ceases, resulting in an immediate temperature increase at T1 and at the same time a drop at the other points T_2 to T_4 (Fig. 2a). The actual reason of this T_1-increase is not the GHE, as has been repeatedly postulated by some authors when presenting their demonstration experiments (e.g., v. Ditfurth [4]), but rather the lack of heat dissipation by convection.

   This is fully confirmed by measurements with argon as an IR-inactive noble gas, which causes the same temperature increase of the constantly heated ground plate. Only gradually dissolves this blockage, primarily through diffusion, which also causes the temperatures $T_2 – T_4$ to temporarily rise (Fig. 2a). The maximum temperature increase of the gas lake is measured and expressed as ΔT_E compared to the air temperature after phase 1.

3. *Measurement of radiation changes due to 15 vol.% of the gases HCG and CO_2*

   The average temperatures of the last hour and the temperature changes compared to Phase 1 are recorded and referred to as "homogen" in the Tables and Figures.

   After the gas pool dissipates and homogenization occurs, the GHGs HCG and CO_2 ultimately cause a net cooling of the PE-plate, similar to the so-called "negative GHE".

   However, in this case, the cooling does not result from a negative temperature gradient (increasing temperature in upward direction; see Harde & Schnell, 2025 [3]) but is determined by the altered radiation balance for the PE-plate upon addition of a GHG. A significant portion of the radiation emitted by the plate is reflected back to the PE-plate by the mirrored dome and walls, largely independent of their temperatures. With GHGs radiation is absorbed on the spectral transitions, for CO_2, e.g., causing an attenuation of 12 % and for HCG about 30 %. This leads to partial thermalization and also remission by the gases, but into all directions and primarily determined by their temperature. The result is a dominating attenuation of the reflected radiation and thus a reduced temperature ΔT_E measured at the earth plate, while radiation transfer calculations show that the back-and-forth propagation largely compensates any GHE.

   As under these experimental conditions, the reflected radiation essentially represents the upwelling radiation, the measured temperature difference at the plate mirrors the radiation balance as expected at the top of the atmosphere (TOA), not at the Earth's surface.

   To demonstrate this effect, relatively high concentrations of 15 vol% of GHGs are required, which also alter the thermal conductivity of the air mixture. But the temperature of the earth plate is only slightly affected by this altered thermal conductivity. This can be seen in a control experiment with argon as an IR-inactive gas, where, in contrast to the GHGs a slight warming is observed in phase 3 (Table 1, Fig. 2c). Argon, like CO_2, is a gas with low thermal conductivity ($\lambda = 0.0179$ W/m·K) compared to air ($\lambda = 0.0262$ W/m·K). Since radiation and conduction have opposing effects, the cooling temperatures of HCG and CO_2 (Table 1) are actually slightly higher than those measured here.

Table 1: Effects of the sample gases on the temperature of the earth plate with and without convection.

Gas	ΔT_E = difference to phase 1	A: with convection T_E °C	A: with convection ΔT_E °C	B: no convection T_E °C	B: no convection ΔT_E °C
air	phase 1 for all measurements average ± 0.1 °C	34.1	-	39.1	-
HCG	gas lake	36.1	2.0	-	-
	homogen	32.8	-1.3	36.7	-2.5
CO_2	gas lake	36.2	2.1	-	-
	homogen	34.0	-0.1	38.2	-0.8
argon	gas lake	35.8	1.8	-	-
	homogen	34.3	0.3	39.2	0.1

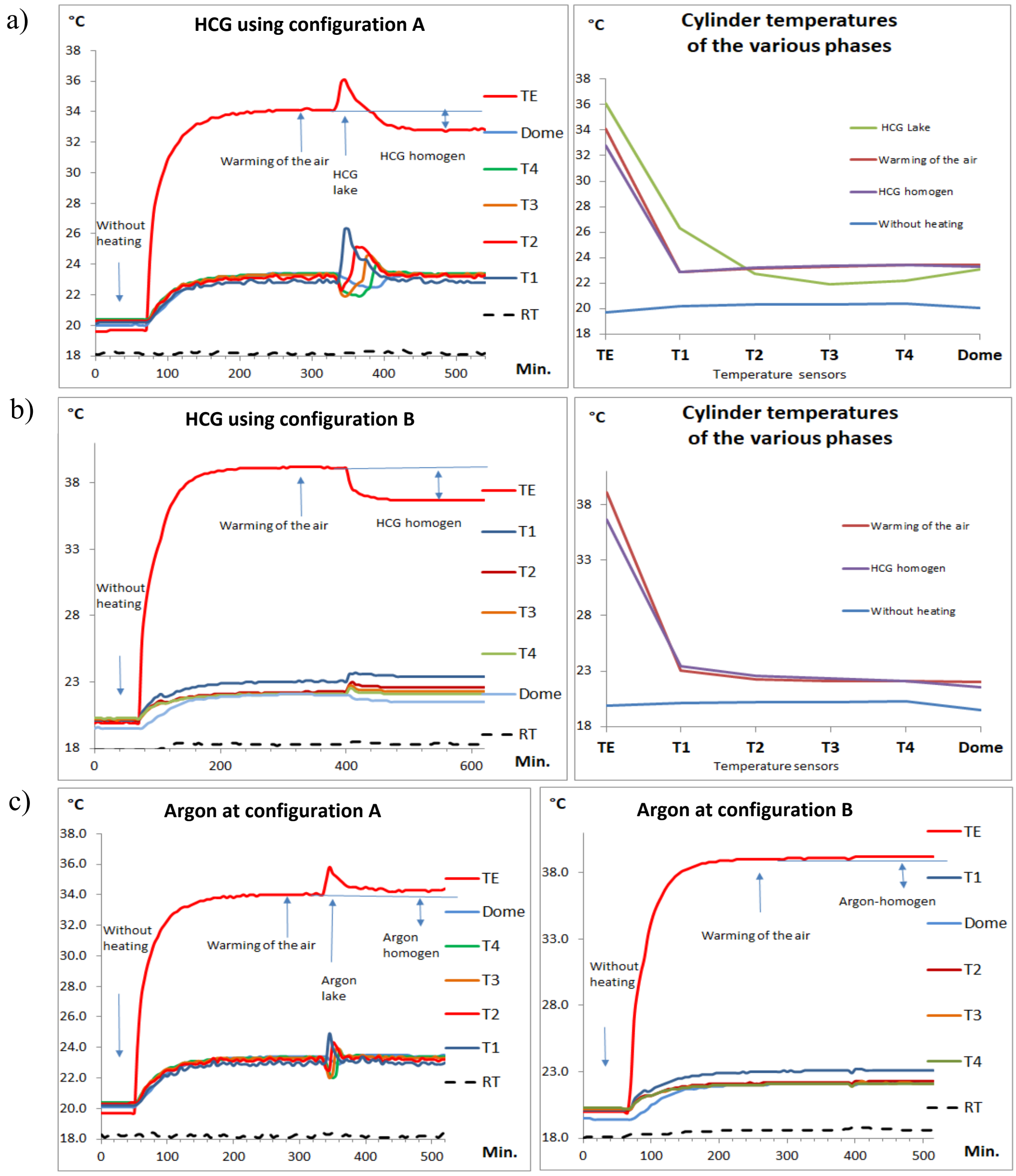

Fig. 2: a) Temperature profiles with convection using the GHG HCG as an example, b) without convection and c) comparative measurements with and without convection for argon.

The properties of the "gas lake" in phase 2 have nothing to do with what happens in the atmosphere. Apart from local variations, CO_2 is evenly distributed in the troposphere. Rather, this primarily concerns experiments or interpretations such as those by v. Ditfurth (1978) [4], Gore &

Guggenheim (2006) [5], or Scorza et al. (2022) [6], who may have inadvertently created a "gas lake" when pouring in pure CO_2 and believed that their experiments demonstrated the atmospheric CO_2 effect. In the most favorable case, these videos confirm the IR absorption of greenhouse gases or their differing thermal conductivity compared to pure air. But these experiments have nothing to do with the greenhouse effect as we know it in our atmosphere (see also: Watts, 2011 [7]: Solheim, 2016 [8]; Schnell, 2020 [9]).

The observed, partly considerable temperature increase (11.3 °C in the Ditfurth experiment, 2.1 °C in our investigations) is mainly caused by the higher density of CO_2 (ρ = 1.98 kg/m³) compared to air (ρ = 1.20 kg/m³), which forms a CO_2 pool at the floor even when heated. Like the glass panes in a greenhouse, this layer of heavy gas prevents convection and rising of the heated gas. Only under the influence of diffusion this pool disperses after some time, and the "heavy" gas spreads evenly throughout the tank. Comparison with argon, which produces the same temperature peak when poured in, clearly demonstrates that this is not evidence of the GHE (Fig. 2c).

4. Radiation Balance without Convection

For class B experiments, the entire apparatus is rotated upside-down, so that the earth plate PE is located above the cooler cylinder walls (Fig. 1B). This creates a stable air stratification, warmer at the top and colder at the bottom, which inherently prevents convection. Since the sample gases now only form a temporary gas pool with the dome at the bottom, a thermal insulation of the earth plate is eliminated. Therefore, when performing measurements under these conditions, the experimental procedure is only divided into two phases.

1. *Heating of the cylinder filled with dried air and verification of thermal equilibrium.*

   This procedure is done under the same conditions as in position A, i.e., with a heating power of 4.6 W, and lasts approximately 5 hours. Due to the lack of convection, the temperature of the PE-plate rises by additional 5 °C (Table 1, last column, Phase 1). This already shows that convection has a significant influence on the heating balance of the PE-plate.

2. *Pouring in the Sample Gas*

   When the sample gases are filled in, again initially a gas pool forms in the dome, similar to configuration A. However, in the absence of convection and at a larger distance from the heated plate, this does not cause any heat buildup for this plate. Therefore, with the two greenhouse gases HCG and CO_2, immediate cooling of the PE plate is observed (Fig. 2b and Appendix, Fig. A1b). This is again due to absorption losses of the back-reflected radiation with the greenhouse gases between the PE-plate and the dome, as already described for configuration A.

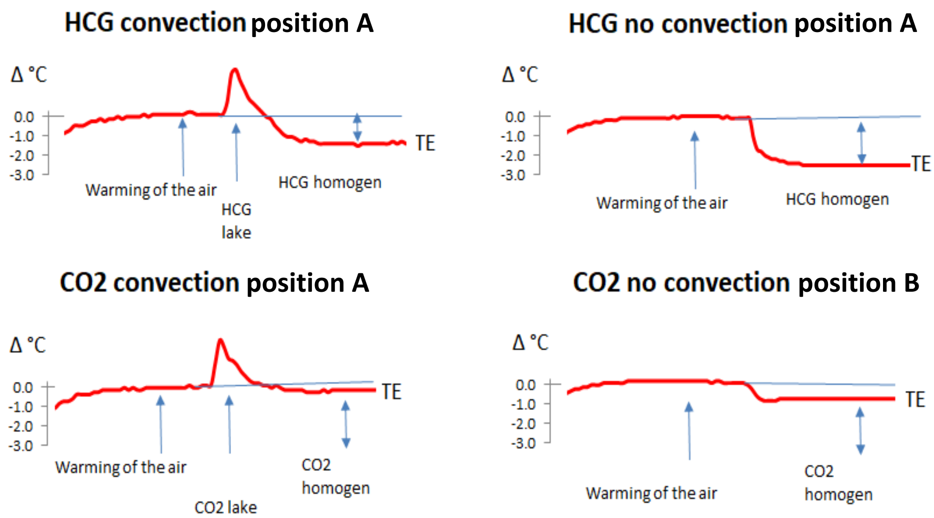

Fig.3: Comparison of measurements for HCG and CO_2 with and without convection.

The crucial difference between positions A and B is the size of the temperature change at plate PE, representing the flux change at TOA. Without convection, HCG causes a cooling of 2.5 °C compared to 1.3 °C with convection, and for CO_2, the difference is 0.8 °C versus 0.1 °C (Fig 3).

This experiment confirms that convection, as a competing heat flow, relativizes the effectiveness of GHGs and thereby also the GHE.

With the potent GHG HCG, a second effect is observed. Despite the temperature drop of T_E, the temperature T_1 rises. The sensor T1 is in close proximity to the PE-plate and, under stable air stratification according to configuration B, already has the highest temperature of the sensors T1 to T4 without GHGs. When adding HCG, this temperature increases by additional 0.4 °C (Appendix, Table A3). This is explained by the fact that the intensity of the remitted HCG radiation – as explained above – is lower than the radiation absorbed by the gas from the PE-plate, thus contributing to the temperature increase of the air, but not the PE-plate (Appendix, Table A3).

This gas warming is the same as in experiments monitoring only the gas temperature (e.g., Scorza et al. [6]). However, the difference to these measurements is that we register the gas temperature at 5 different positions to observe any temperature changes over the tank and – most important – also changes of the plate temperature. To make this clear, both measurements – observation of the gas temperature or plate temperature – are only tracking the absorption of the gases, not any greenhouse effect, but the changes of the plate also symbolize the reduced upwelling radiation to space and can much better be used to study the impact of convection on radiation effects.

However, the hypothesis that the GHE reduces heat transport via IR radiation towards space is experimentally confirmed, as can be seen from the temperature drop of the dome (Appendix Table A3) and even more pronounced with plate-PK (see Section 5 and Table A4). This applies to cloudless skies and is further amplified by clouds, which not only act as IR absorbers but also as emitters and can additionally scatter some part back to the surface.

Slight warming of the air is also observed with CO_2 but is close to the temperature resolution of the sensors with ± 0.1 °C (Table A3). Given an approximately 400 times lower CO_2 concentration in the atmosphere, this warming is likely negligible. This may explain why weather balloons and satellites have so far been unable to detect the supposedly CO_2-caused atmospheric "hotspot."

The comparative experiment with argon (Fig. 2c and Table A3) shows neither a decrease in the T_E temperature nor a temperature increase from T_1 to T_4. A slight increase in T_E after addition of argon is within the temperature resolution.

5. Thermally Generated Backradiation

In the previous experiments, backradiation was caused by the reflection of the emitted earth-plate radiation at the mirrored dome. Covering the dome with a blackened aluminum plate (PK) generates thermally produced back radiation according to its temperature T_K and the Stefan-Boltzmann law. Since the PK-plate is significantly cooler than the earth-plate, the intensity of the back radiation is correspondingly lower. With this weaker backradiation, only the GHG HCG shows clearly measurable cooling using configuration B (Table 2 and Table A4).

Table 2: Impact of a mirrored dome or a blackened plate PK on the temperature of the earth plate according to configuration B, without convection.

Gas	ΔT_E = difference to phase 1	reflecting dome		blackened plate P_K	
		T_E °C	ΔT_E °C	T_E °C	ΔT_E °C
air	phase 1 of all experiments average ± 0,1 °C	39.1	-	36.0	-
HCG	homogen	36.7	-2.5	35.2	-0.7
CO_2	homogen	38.2	-0.8	35.9	-0.1
argon	homogen	39.2	0.3	36.2	0.1

However, not only the earth plate is showing some cooling, but there is even a greater temperature loss at the opposing plate PK: 1.2 °C for HCG and 0.4 °C for CO_2, while the gas temperatures T_1 to T_4 are slightly increasing (see Table A4).

Under these conditions an almost uniform air temperature is adjusting in the cylinder, and different to the changing temperatures over the atmosphere it works as a single, isolated layer. GHGs are causing an attenuation and partial thermalization of the backradiation, resulting in this unusual temperature pattern.

However, significantly different conditions in the radiation balance are arising, when the temperature of the cold plate PK is reduced by a cryostat. Fig. 4 shows as an example a measurement with 10% CO_2 in air for a cooled plate of -11.4 °C and a temperature gradient between the plates of 0.37 °C/cm (for further details see Harde & Schnell 2022 [2]).

With an initial temperature of the earth plate of +30 °C, a temperature increase of 1.0 °C can be observed after adding CO_2, in contrast to the measurements shown previously. Since convection and heat conduction can be ruled out by control experiments, such an increase can be attributed exclusively to the actual GHE, and it can only be observed in the presence of a sufficient temperature gradient along the radiation propagation path.

This measurement is intended as comparison to illustrate the importance of precisely understanding or even eliminating other heat transfer processes in order to make a reliable statement about the true influence of the various GHGs on our climate.

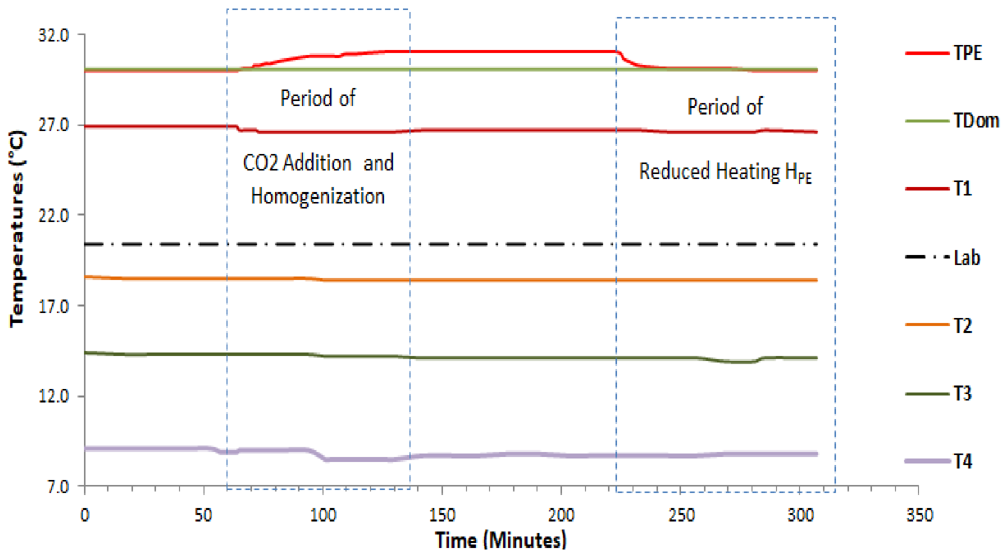

Fig. 4: Measurement for 10% CO_2 in dry air. The temperatures of the earth plate (red), the significantly different gas temperatures at positions T_1–T_4, and the laboratory temperature (black) were recorded. The ground plate is located on an insulating layer within the thermistor dome.

Experimental set-ups, as previously discussed, in which the heavier sample gases can block convection, also show an increased temperature rise, but this has nothing to do with the GHE. On the other hand, this effect can be superimposed by convection and radiation absorption to such an extent that any warming is compensated for or even reversed. This may be one of the reasons why such differing results have been published from purported demonstration experiments on the GHE. Reliable verification and determination of the influence of the various IR-active gases on our climate therefore requires careful experimental conditions that must be precisely known and adhered to.

The results collected in the laboratory can only be partially applied to the transfer processes in the atmosphere, but they illustrate the strong mutual influence of the heat flows and simultaneously demonstrate the special importance of GHGs for climatic conditions that only made possible life on this planet.

6. Conclusion

In laboratory experiments we have studied the reciprocal influence of heat fluxes as they occur in the atmosphere. In particular, we show how convection affects the effectiveness of IR-active gases. The starting point is to realize that the Earth's surface not only delivers heat through radiation, but also by convection, conduction, and evaporation, and that these mechanisms mutually influence each other. The objective of these studies was to analyze these effects separately and together in a most controllable laboratory experiment.

The setup uses a heated plate to simulate the Earth's surface, which is positioned either below or above the cooled cylinder walls. This results in two clearly distinguishable scenarios: a convective system (plate below, configuration A) and a convection-free system (plate above, configuration B). In both cases, the tank is filled with the GHGs HCG (hydrocarbon gas) and CO_2, and for comparison argon, so that both, radiation effects of the gases and the influence of a temporarily formed gas layer (gas-lake) of the heavier gases, can be investigated – the latter a phenomenon that has evidently influenced previous demonstration experiments incorrectly.

Temperature measurements of the plate show that with set-up A after adding a sample gas, a significant increase is primarily due to the lower thermal conductivity and higher density of the gases: A spreading gas pool around the earth plate suppresses convection for about 20 minutes, thus warming the plate. This effect occurs with all three gases, including non-IR-active argon, and therefore does not constitute any evidence of a GHE in the physical sense. Only when the gas pool disappears through diffusion, can radiation effects be observed. The temperature drop ΔT_E measured at the plate reflects the radiation balance at the top of the atmosphere.

The comparison between configurations A and B is crucial. When convection is allowed, greenhouse gases only slightly reduce the radiation reflected from the dome to the warm plate, causing a slight cooling and, correspondingly, only a slight decrease in the radiation emitted to space. If convection is suppressed, this negative radiation effect is noticeably amplified, respectively the absorbed radiation over the atmosphere and the associated warming at the base.

HCG causes a cooling of 2.5 °C without convection, compared to only 1.3 °C with convection; CO_2 leads to a cooling of 0.8 °C compared to 0.1 °C with convection. This shows that convection is a dominant heat transport mechanism that reduces the radiative effect.

Comparable investigations for the influence of evaporation on radiation could not be carried out with the present experimental setup because too much condensate forms on the walls of the gas cylinder, significantly altering the backradiation.

In summary, the experiments show that the effect of IR-active gases is strongly influenced by convection and that a considerable portion of the warming observed in classical demonstrations is not due to radiative effects, but rather to gas effects that inhibit convection.

For the real atmosphere the interplay of convection and the other mechanical heat fluxes with the GHGs can be understood as lifting warmer air parcels from the lower to the upper troposphere, from where heat can be released more efficiently to space by radiation. Thus, these fluxes prove to be central components in the Earth's heat transport and at the same time relativize the sole significance of IR-active gases as sources for global warming.

Funding

This research did not receive any specific grant from funding agencies in the public, commercial, or not-for-profit sectors. The experimental setup was developed and paid privately by MS.

Chief-Editor: Prof. N. Malamos; **Reviewer 1:** Prof. D. Koutsoyiannis, **Reviewer 2**: anonymous.

Acknowledgement: We thank the Chief-Editor and the Reviewers for their critical reports, particularly Reviewer 1 for his detailed and very constructive comments.

Appendix

The experimental chamber is thermostatically controlled at 18 °C ± 0.2 °C to eliminate interference from a changing room temperature. The water for cooling the cylinder is generated in a thermal box via a two-point thermostatic control with a hysteresis of ± 0.1 °C and pumped to the cylinder through PVC tubing. To establish stable conditions, the room temperature control and the cooling water are switched on 5 hours before data recording, and the air in the tank is circulated through solid sodium hydroxide solution for drying.

The electric heater is set to 4.00 volts, which fluctuates between 4.6 and 4.7 watts due to the temperature dependence of the resistance heating of the ground plate (Table A1).

Table A1: Technical Data

Component	Length/Hight	Ø:
alu-cylinder	L=57 cm	33 cm
dome	H=13 cm	33
alu plate PE	D=0.8 mm	22 cm
alu plate PK	D=0.8 mm	33 cm
PI-Polyamide foil heater	DC24V, 180 W	22 cm
P_E support plate	H=2 cm	25 cm
plate spacing P_E-P_K	57 cm	
cooling hose	L=25 m	8x12 mm
Styrofoam top	H=15 cm	50 cm
Styrofoam wall	H=65 cm	50 cm
Styrofoam bottom	H=10 cm	50 cm
data logger	Elitech RC4	
thermostat	ES-10 ± 0,1° C	
power supply	Korad ka3005d	0-30 V
heating power	4,00 V	4,6 - 4,7 W

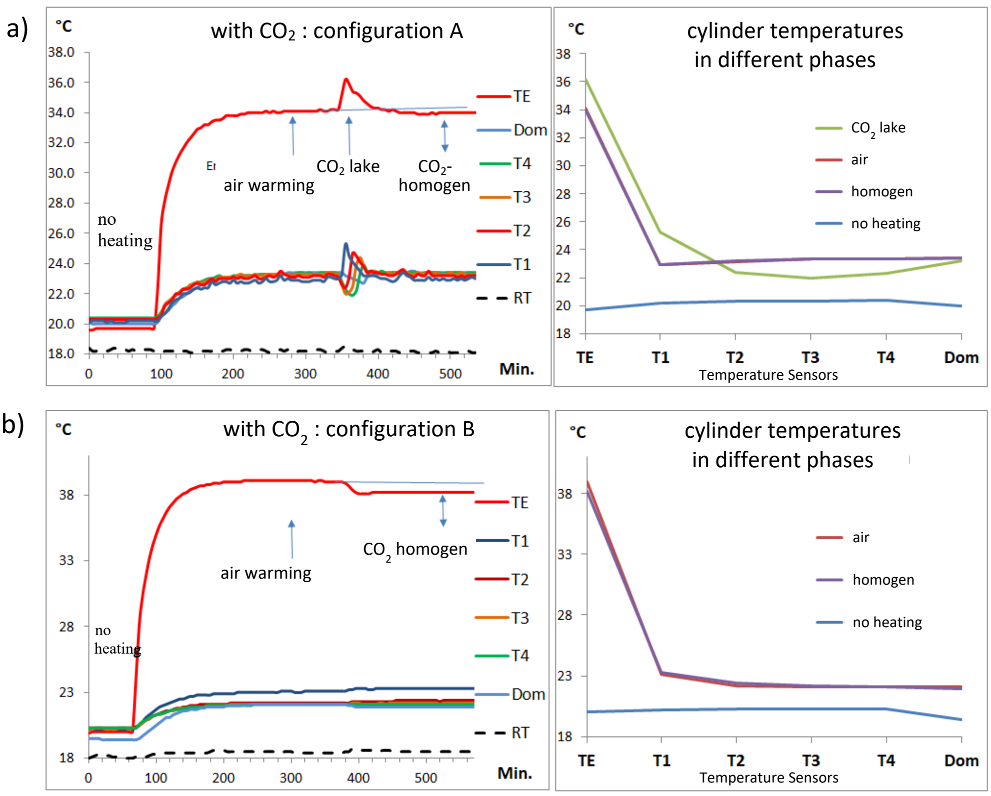

Fig. A1: a) Temperature profiles for CO_2 with convection, b) without convection.

Phase 1 of Tables A2 and A3 shows the temperatures of all sensors after switching on the PE heater. "Start" represents the temperature increase caused by switching on the heater. The "homogen" phases refer to the temperatures and their changes that ultimately result after the addition of the sample gases, compared to the dried air. The "gas-lake" phase in Table A2 is a snapshot at the highest sample temperature reached immediately after the addition of the sample gases.

Some data exhibit a wave-like pattern caused by the thermostat's temperature control. These fluctuations are smoothed out by averaging over a longer period.

Table A2: Configuration A, with convection. Temperatures of the different sensors after addition of 8 liters of a sample gas.

gas	phase	T_E °C	T_1 °C	T_2 °C	T_3 °C	T_4 °C	T_{dome} °C
air	1. heating	34.1	22.9	23.2	23.3	23.4	23.4
	ΔT vs. start	14.4	2.7	2.9	3.0	3.0	3.4
HCG	2. gas-lake	36.1	26.3	22.7	21.9	22.2	23.1
	ΔT vs. air	2.0	3.4	-0.5	-1.4	-1.2	-0.3
	3. homogen	32.8	22.9	23.2	23.3	23.4	23.3
	ΔT vs. air	-1.3	0.0	0.1	0.0	0.0	-0.1
air	1. heating	34.1	22.9	23.2	23.3	23.4	23.4
	ΔT vs. start	14.4	2.8	2.9	3.0	3.0	3.4
CO_2	2. gas-lake	36.2	25.3	22.4	22.0	22.3	23.2
	ΔT vs. air	2.1	2.4	-0.8	-1.3	-1.1	-0.2
	3. homogen	34.0	23.0	23.2	23.3	23.4	23.4
	ΔT vs. air	-0.1	0.0	0.0	0.0	0.0	0.0
air	1. heating	34.0	23.0	23.2	23.3	23.3	23.4
	ΔT vs. start	14.3	2.8	2.9	3.0	2.9	3.3
argon	2. gas-lake	35.8	24.9	22.5	22.0	22.3	23.2
	ΔT vs. air	1.8	1.9	-0.7	-1.3	-1.0	-0.2
	3. homogen	34.3	22.9	23.2	23.3	23.4	23.4
	ΔT vs. air	0.3	0.0	0.0	0.0	0.1	0.0

Table A3: Configuration B, without convection. Temperatures of the various sensors after the addition of 8 liters of a sample gas.

gas	phase	T_E °C	T_1 °C	T_2 °C	T_3 °C	T_4 °C	T_{dome} °C
air	1. heating	39.2	23.0	22.3	22.1	22.1	22.0
	ΔT vs. start	19.3	2.9	2.1	1.9	1.8	2.5
HCG	2. homogen	36.7	23.4	22.6	22.3	22.1	21.5
	ΔT vs. air	-2.5	0.4	0.3	0.2	0.0	-0.5
air	1. heating	39.0	23.1	22.2	22.1	22.1	22.1
	ΔT vs. start	19.0	2.9	1.9	1.8	1.8	2.7
CO_2	2. homogen	38.2	23.3	22.4	22.2	22.1	21.9
	ΔT vs. air	-0.8	0.2	0.2	0.1	0.0	-0.2
air	1. heating	39.1	23.1	22.2	22.1	22.1	22.1
	ΔT vs. start	19.1	3.0	2.0	1.9	1.8	2.7
argon	2. homogen	39.2	23.1	22.3	22.1	22.1	22.1
	ΔT vs. air	0.1	0.0	0.1	0.0	0.0	0.0

Table A4: Temperatures of the various sensors according to configuration B, without convection, after the addition of 8 liters of a sample gas but with a blackened plate PK.

gas	phase	T_E °C	T_1 °C	T_2 °C	T_3 °C	T_4 °C	T_K °C
HCG	air	35.9	22.8	22.4	22.3	22.4	25.4
	ΔT vs. start	15.9	2.5	2.1	2.0	2.1	5.4
	2. homogen	35.2	23.2	22.6	22.5	22.5	24.2
	ΔT vs. air	-0.70	0.40	0.24	0.15	0.06	-1.22
CO_2	air	36.0	22.8	22.4	22.4	22.5	25.4
	ΔT vs. start	16.0	2.5	2.0	2.1	2.1	5.4
	2. homogen	35.9	23.1	22.5	22.4	22.6	25.0
	ΔT vs. air	-0.1	0.3	0.1	0.0	0.1	-0.4
argon	air	36.1	22.8	22.5	22.4	22.5	25.4
	ΔT vs. start	15.5	2.5	2.1	2.1	2.1	5.4
	2. homogen	36.2	22.9	22.5	22.4	22.6	25.5
	ΔT vs. air	0.1	0.1	0.0	0.0	0.0	0.1

References

1. D. Koutsoyiannis, G. Tsakalias, 2025: *Unsettling the settled: Simple musings on the complex climatic system*, Front. Complex Syst., Vol. 3, https://doi.org/10.3389/fcpxs.2025.1617092
2. H. Harde, M. Schnell, 2022: *Verification of the Greenhouse Effect in the Laboratory*, Science of Climate Change, Vol. 1.2, pp. N4 1-32, https://doi.org/10.53234/scc202203/10.
3. H. Harde, M. Schnell, 2025: *The Negative Greenhouse Effect – Part II: Studies of Infrared Gas Emission with an Advanced Experimental Set-Up*, Science of Climate Change, Vol. 5.3, pp. 10 – 34, https://doi.org/10.53234/scc202510/03
4. H. v. Ditfurth, 1978: *Sendereihe Querschnitt, Der Ast auf dem wir sitzen: 1. Teil - Die Balance der Atmosphäre*, https://www.youtube.com/watch?v=F2K-wnCuntg, at minute 18:45, use English subtitles.
5. A. Gore, D. Guggenheim, 2006: *An Inconvenient Truth*, Movie, https://www.youtube.com/watch?v=3v-w8Cyfoq8
6. C. Scorza, M. Strähle, B. Mayer, H. Lesch, 2022: Wissenschaftliche Erläuterung - Experiment zur Wärmeabsorption durch CO_2, https://klimawandel-schule.de/sites/default/files/2022-08/wissenschaftliche_erlauterung_treibhauseffekt_experiment_lmu-physik.pdf
7. Anthony Watts, 2011: *Replicating Al Gore's Climate 101 video experiment shows that his "high school physics" could never work as advertised - Watts Up With That?*, https://wattsupwiththat.com/2011/10/18/replicating-al-gores-climate-101-video-experiment-shows-that-his-high-school-physics-could-never-work-as-advertised/?cn-reloaded=1
8. J.-E. Solheim, T. Eriksen, Y. Engebretsen, 2016: *The Greenhouse Effect – a high school experiment*, https://www.justproveco2.com/papers/SolheimExperiment2016.pdf.
9. M. Schnell, 2020: *The wrong climate experiments*, European Institute of Climate and Energy (EIKE), https://www.eike-klima-energie.eu/wp-content/uploads/2020/11/The-wrong-climate-experiments.pdf.

Disclaimer/Publisher's Note:

This article reflects solely the views, analyses, and conclusions of the authors. Science of Climate Change, its editors, and its publisher make no representation or warranty as to the accuracy or completeness of the content and disclaim liability for any loss, damage, or other consequence arising from the use of, or reliance on, any material published herein.